universität wien

DISSERTATION

Titel der Dissertation

„Exploring dental morphological variability using virtual techniques“

Verfasserin

Cinzia Fornai

angestrebter akademischer Grad

Doctor of Philosophy (PhD)

Wien, 2015

Studienkennzahl lt. Studienblatt:	A 094 437
Dissertationsgebiet lt. Studienblatt:	Anthropologie
Betreuer:	a.o. Univ.-Prof. Dr. Gerhard W. Weber

Table of contents

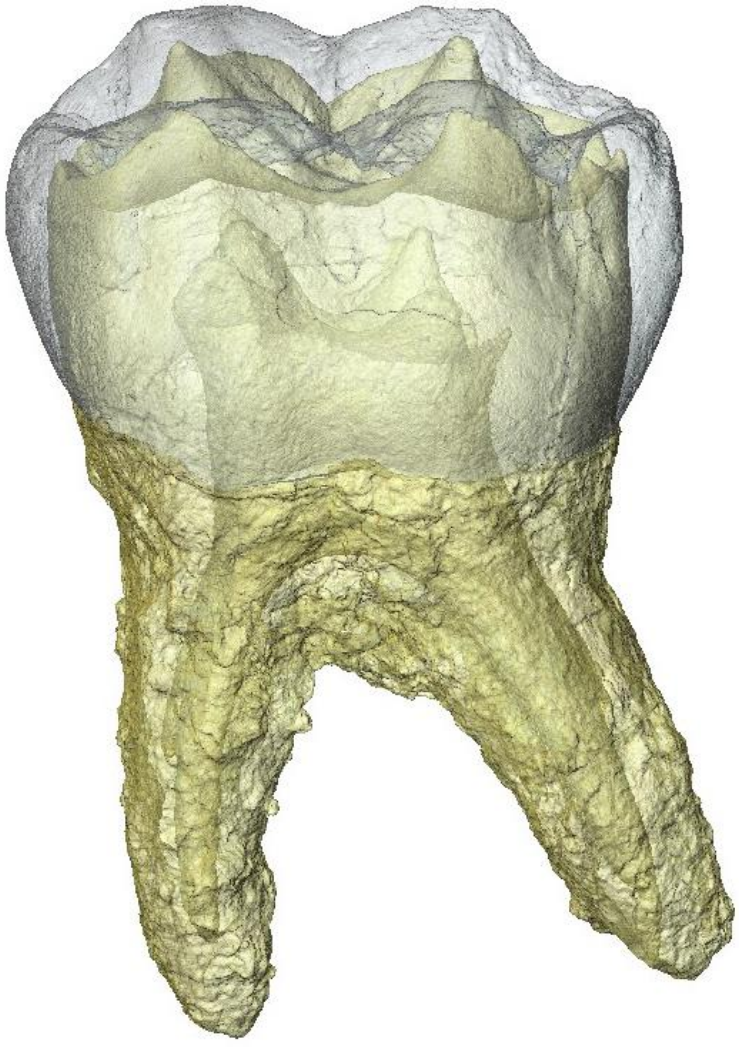

Abstract (English)

In the study of extinct hominin forms, teeth play key role due to their abundance. Teeth possess a primary role in mastication, thus their morphology reflects dietary adaptation. Owing to functional constraints, the shape of the teeth is rather conservative among primates. Dental morphogenesis is regulated genetically by a complex signaling pattern, and once teeth are formed, they do not remodel as bones do under biomechanical stimulation.

The investigation of dental remains presents several challenges owing to the small size of teeth, their geometric complexity, as well as the effects of wear, damage and incompleteness in paleontological settings. The introduction of virtual imaging techniques in dental anthropology has fundamentally changed the way teeth are studied. These techniques enable non-destructive access to dental inner structures through high-resolution three-dimensional visualization. As a result, teeth can be handled as virtual models which can be used to substitute the traditional morphometric approaches with protocols combining these imaging techniques with statistical tools such as geometric morphometrics, an approach suitable for the quantification of biological shapes.

In this thesis, several studies using imaging techniques for the investigation of enamel thickness and the creation of surface models as a basis for geometric morphometric analysis are presented. These works investigate the morphology of both deciduous and permanent teeth belonging to various hominin clades, with threefold aims: to provide a morphological characterization of unknown specimens, and, if possible, achieve a taxonomic assessment; to explore the intra- and inter-specific variability of various dental features; and to design new protocols for the study of dental crown morphology.

The outcomes of the research conducted have contributed to our knowledge on hominin dental variability and to the morphological description or taxonomic (re)assessment of dental specimens from different times and places of human evolution. The methods used have shown suitability for addressing different biological questions and to be accurate and adaptable to different tooth types or degrees of dental wear. At the same time, these contributions highlighted the problems and limitations in the study of fossil teeth, despite the use of state-of-the-art techniques.

In conclusion, considering the paucity of fossils, and the rarity in paleontological settings of other biological evidence other than dental and skeletal remains, it is crucial that as much information as possible should be gathered from each (dental) remain. However, a careful interpretation of the results of the morphological and morphometric investigation should integrate the information from any other evidence available. The exploration of the intra- and interspecific variation and the creation of new methods for the investigation of dental morphology are pivotal elements in the study of dental remains from extinct species.

Abstract (German)

Bei der Erforschung unserer Vorfahren spielen Zähne seit jeher eine entscheidende Rolle, weil sie relativ häufig fossile Elemente darstellen. Zähne spielen auch eine dominante Rolle beim Kauvorgang und ihre Morphologie spiegelt deshalb Ernährungsadaptationen wider. Aufgrund der funktionellen Randbedingungen ist die Gestalt von Zähnen bei Primaten eher konservativ. Die Zahnmorphogenese unterliegt einer komplexen genetischen Regulierung. Nach ihrer Entstehung werden Zähne jedoch nicht mehr umgeformt, so wie es bei Knochen durch biomechanische Stimulation passiert.

Die Untersuchung von Zähnen und deren Fragmenten birgt zahlreiche Schwierigkeiten. Zähne sind kleine und komplexe Objekte, die üblicherweise der Abnutzung unterliegen, oder, im paläontologischen Kontext, oft beschädigt und inkomplett sind. Die Einführung von virtuellen Techniken in der Zahnanthropologie hat nachhaltig die Art und Weise verändert, in der Zähne untersucht werden. Nun werden auch die inneren Strukturen zerstörungsfrei zugänglich. Für die Quantifizierung der biologischen Form und Gestalt können die traditionellen morphometrischen Abläufe ersetzt oder kombiniert werden mit neuen statistischen Werkzeugen wie der Geometrischen Morphometrie.

Diese Doktorarbeit hat zahlreiche Studien zum Gegenstand, die virtuelle Techniken für die Untersuchung von Zahnschmelzdicken und die geometrisch morphometrische Analyse von Zahn-Oberflächenmodellen nutzen. Die Arbeiten beziehen sich sowohl auf das Milchgebiss als auch auf die permanente Bezahnung von verschiedenen hominin Kladen hinsichtlich dreier verschiedener Zielrichtungen: die morphologische Charakterisierung von bisher unbekannten Fundstücken und deren mögliche taxonomische Einordnung; die Exploration der inner- und zwischenartlichen Variation von dentalen Merkmalen; die Erstellung von neuen Protokollen für die Untersuchung der dentalen Kronenmorphologie.

Die Ergebnisse der Forschung konnten wesentlich zu unserem derzeitigen Wissenstand über die hominine Variabilität von Zähnen und zur morphologischen Beschreibung und taxonomischen (Wieder)Einordnung von Fundstücken aus verschiedensten Epochen und Orten der menschlichen Evolution beitragen. Es konnte auch demonstriert werden, dass die verwendeten Werkzeuge tauglich und akkurat sind, um verschiedenste biologische Fragestellungen zu beantworten, und ebenfalls an unterschiedliche Zahntypen und Stadien der Zahnabnutzung angepasst werden können. Gleichzeitig heben die Beiträge aber auch die Grenzen und Probleme bei der Untersuchung fossiler Zähne hervor, die trotz Einsatz modernster Technologie bleiben.

Wenn man die äußerst limitierte Anzahl an verfügbaren Fossilien bedenkt, muss man zum Schluss kommen, dass so viel Information als möglich aus jedem noch so kleinen (Zahn)Fundstück gewonnen werden muss. Natürlich muss die sorgfältige Interpretation der morphologischen und morphometrischen Ergebnisse integriert werden mit anderen verfügbaren Informationen. Die Exploration der inner- und zwischenartlichen Variation und die Schaffung neuer Methoden für die Untersuchung der dentalen Morphologie sind jedenfalls Eckpfeiler für die Untersuchung von Zahnfossilen ausgestorbener Spezies.

1. Introduction

1.1. Teeth in the human fossil record and their importance for taxonomy

Teeth have long been the subject of anthropological and paleoanthropological studies since they are durable and are the most abundant remains in archeological and fossil sites. Dental development and morphology are under a tight genetic control (Jernvall and Thesleff, 2000; Kangas et al., 2004; Kavanagh et al., 2007). The dental crown is already fully formed in the crypt before it comes into function. The dental tissues are highly mineralized, and contrary to bony structures, enamel does not reshape in response to biomechanical demands. In non-pathological conditions, the alteration of the dental crown after eruption occurs only by erosion (chemical dissolution of hard tissues), or by physical removal of material through abrasion (tooth to food contact) and attrition (tooth to tooth contact) (Lucas, 2004). In addition, taphonomic agents may alter the original shape of the teeth post-mortem, causing further erosion, cracks, or fractures.

Owing to the crucial importance of their function, teeth have been mostly studied to gather information about the feeding adaptation, para masticatory functions and social behavior, as well as for the pathologies they might present. Dental eruption time and dental wear have been traditionally used as means for the estimation of age at death for modern populations. Dental microscopic accretion rate has been recently evaluated for the estimation of age at death of extinct hominin (Guatelli-Steinberg et al., 2014; Smith et al., 2014). Several aspects of the dental tissues can be investigated since they store information useful for the reconstruction of life history in extinct taxa (Tafforeau and Smith, 2008; Smith, 2013; Smith and Alemseged, 2013).

Hominoid teeth share a similar general pattern and do not differ substantially in their overall appearance (Butler, 1986; Robinson, 1956). The dental morphology is rather conservative in hominins and primates in general. Dental traits are subject to the same selective processes than other body variables, and are the outcome of evolutionary processes and population history; they vary in number and expression as populations are in isolation or interbreed. Owing to their complex morphology and the slow rate of changes in the course of evolution, the dentition has long been studied to gather insight about the taxonomy and phylogeny of extinct hominins. A number of dental features have been proved suitable for taxonomic purposes, including dental gross morphology and size (Lavelle, 1977; Wood and Zuckerman, 1981; Sharma, 1985; Calcagno et al., 1997, 1999; Moggi-Cecchi, 2003; Scott and Lockwood, 2004; Moggi-Cecchi and Boccone, 2007; Skinner et al., 2009a; Liu et al., 2010; Prado et al., 2012; Bailey et al., 2014), dental tissue proportions (Gantt, 1983; Martin, 1985; Beynon and Wood, 1986; Beynon et al., 1991; Zilberman et al., 1992; Gantt and Rafter, 1998; Shellis et al., 1998; Martin et al., 2003; Smith et al., 2005; Macchiarelli et al., 2006; Kupczik and Hublin, 2010; Benazzi et al., 2011b, 2012; Fornai et al., 2011, 2012, 2014), discrete traits such as accessory cusps, number of roots, fissure pattern and ridges (e.g., Kovacs, 1971; Turner et al., 1991; Scott and Turner, 1997; Kupczik et al., 2005; Harris, 2007; Kupczik and Hublin, 2010; Ortiz et al., 2012; Carter et al., 2014) and other aspects such as the relative dimension of teeth and their degree of rotation along the tooth row, the shape of the dental arch, and the dimension of the canines (Robinson, 1956; Lavelle, 1977; Kieser, 1990; Aiello and Dean, 2002).

1.2. Variability and the different concepts of species

The definition of extinct taxa presents several limitations owing to the nature of the fossil material itself. Information about diet and behavior, for example, can be inferred thought indirect evidence such as isotopic composition of the hard tissues, paleoecology, and material culture. The preservation of soft tissues or other organic evidence are indeed very rare in archeological and paleontological settings (Seidler et al., 1992; Henry et al., 2012; Keeling and Berger, 2013), and nuclear or mitochondrial DNA can be only occasionally found in fossils (Green et al., 2006; Keller et al., 2012; Fu et al., 2014; Meyer et al., 2014; Lari et al., 2015). Appearance, physiology, ecology, reproductive strategies, geographic distribution, possible interbreeding, mode of speciation, and causes of extinction have to be inferred from the hard evidence and the paleontological or archeological contexts in which the remains were found.

Mayr's biological definition of a species (Mayr, 1942) cannot be applied in paleontology. Since the morphology of the hard tissues is the predominant evidence that paleontologists can consider, the taxonomy of extinct species is based on quite specific and limited diagnostic traits (Eldredge and Cracraft, 1980; Nixon and Wheeler, 1990; Wiley and Lieberman, 2011). Species are considered entities with a clear historical identity (Ghiselin, 1974; Hull, 1974, 1976, 1978). Cracraft (1989, pp. 34-35) has defined the phylogenetic species as "an irreducible cluster of organisms, diagnosably distinct from other such clusters, and within which there is a parental pattern of ancestry and descent". Nonetheless, the fossil record is usually scant and incomplete, probably not representative of the population variability, and in the majority of cases is constituted by only particular anatomical regions of an organism. Given the inherent limitations in paleoanthropology, setting boundaries between extinct species is obviously a difficult task. Following Hennig's work (Hennig, 1950, 1966) paleoanthropologists as other biologists recognize branching of species lineages from shared, derived characters (Beutel et al., 2009). Resolving independent acquisition of traits from real homology is possible using genomic data, but, as noted earlier, fossils containing DNA are rare.

Paleosystematics mainly uses the shape and size of hard tissue components, but these vary between species as well as within the same species. The morphological variability of a species is mostly unknown along with the diagnostic value of the features to consider, or the polarity of certain traits in evolution (Bailey, 2002; Bailey and Hublin, 2007; Schroer and Wood, 2013; Carter et al., 2014). For instance, Wiens and Servedio (2000) have postulated that samples of hundreds or even thousands of individuals might be needed to detect polymorphisms in diagnostic traits, while a paleoanthropological hypodigm might be composed of a handful of remains. These difficulties and limitations in the interpretation of the fossil record might lead different scholars to different conclusions, situations well represented by the long-standing debate between lumpers and splitters (Simpson, 1945; Leakey et al., 2012; Carstens et al., 2013; White, 2014). In paleoanthropology this has resulted in the proliferation of hominin taxa (White, 2014).

One of the aims in dental anthropology is to investigate the form and the structure of dental remains in order to gather information about the biology and taxonomy of extinct species. The morphological characterization of the dental remains has three main aims:

- exploring the morphological variability of a particular clade,

- allocating taxonomically undetermined specimens, and

- investigating diet and feeding adaptations.

The characterization of a species' variation is built upon the sample available; in turn, the interpretation of traits presented by an unknown individual is influenced by the current knowledge of dental variation in potential populations to which this individual might belong. Using extant or well-represented extinct species as benchmark to evaluate the observed variation in other taxa might be misleading because it would imply that the degree of variability is similar in all of those species. Using extinct species might generate a circular problem, for the range of variability of those groups might also be uncertain. Under these premises one might fail to detect multiple species in a sample, as simulation studies have already shown (Cope, 1993; Cope and Lacy, 1992; Kelley and Plavcan, 1998). Conversely, one might underestimate the degree of variation of an extinct taxon by assuming that the upper limit of variation possible in extinct species is comparable to that of the most sexual dimorphic extant species (Scott and Lockwood, 2004; Skinner et al., 2006). Moreover, a fossil assemblage usually incorporates considerable depth in time, while an extant sample might integrate geographical variation. Also, we cannot assume that evolutionary processes affect simultaneously and at similar rates various anatomical regions, since some features are more conservative than others. As mentioned above, teeth can be regarded as rather conservative structures in the process of evolution, which might be due to their functional role, their highly mineralized structures, and their ontogenesis. Indeed, the dentition is also subject to morphological variation, with different manifestation and level of expression of the dental traits (Dahlberg, 1971; Gingerich and Schoeninger, 1979). In hominins, the mandibular teeth, for instance, are known to be more complex and variable than the maxillary teeth. The anterior teeth are simpler in shape than the postcanine dentition, with an increasing complexity towards the distal side of the dental row. Within the same tooth type, aspects such as the metacone, the hypocone, the Carabelli's trait and the parastyle are highly variable (Robinson, 1956; Dahlberg, 1971; Scott and Turner, 1997). The enamel-dentine junction (EDJ) is regarded to be more conservative than the enamel cap (Korenhof, 1960; Butler, 1986; Corruccini, 1987). Interestingly, studying both the enamel cap and the EDJ, Corruccini (1987) found a decoupling of the morphology of these two dental surfaces in modern humans, e.g., with some features appearing on the EDJ but not on the enamel, or to the contrary, a feature developed only at the enamel cap. Nonetheless, considering various variables such as the slope and direction of dentine horns and cusps, Guy et al. (2013) reported a various expression of the topography of EDJ and OES in different primates.

1.3. What makes up tooth diversity

1.3.1. The genetics of morphogenesis

The study of evolution and biodiversity is based on comparative observations of those dental traits that can be described and quantified in their appearance and degree of expression. The dental traits are genetically determined, and are mostly of polygenetic nature, and their degree of expression depends on developmental factors (Jernvall and Thesleff, 2000; Tucker and Sharpe, 2004; Bei, 2009; Tummers and Thesleff, 2009). In primates, as in all mammals, teeth form as distinct organs from the dental lamina by cells migrated from the cranial neural crest and the oral cavity to what will become the alveolar margin (Lumsden, 1988; Chai et al., 2000). Each of the dental types originates from specific regions of the dental lamina. The determination of the dental type, as well as the morphogenesis of the single tooth, are under a rigorous genetic control, and are orchestrated by complex receptor-signaling pathways (Tucker and Sharpe, 2004). Tooth morphogenesis is initiated by diffusible growth factors secreted by the oral epithelium that activate transcription factors in the underlying mesenchyme (Thesleff and Sharpe, 1997; Bei and Maas, 1998; Tucker and Sharpe, 2004; Bei, 2009; Tummers and Thesleff, 2009). The regulation of

each tooth organ occurs by reiterative interaction between the opposing epithelial and mesenchymal tissues, and involves several classes of homeobox genes (fig. 1; Jernvall and Thesleff, 2000). The genetics of tooth morphogenesis is known through the study of genetic defects that alter it. For instance, early developmental disturbances leading to tooth agenesis or supernumerary teeth can be caused by modification of transcription factors, or alterations of signaling pathways (Kere et al., 1996; Vastardis et al., 1996; Bayes et al., 1998; Stockton et al., 2000; Nieminen, 2009; Wang et al., 2009).

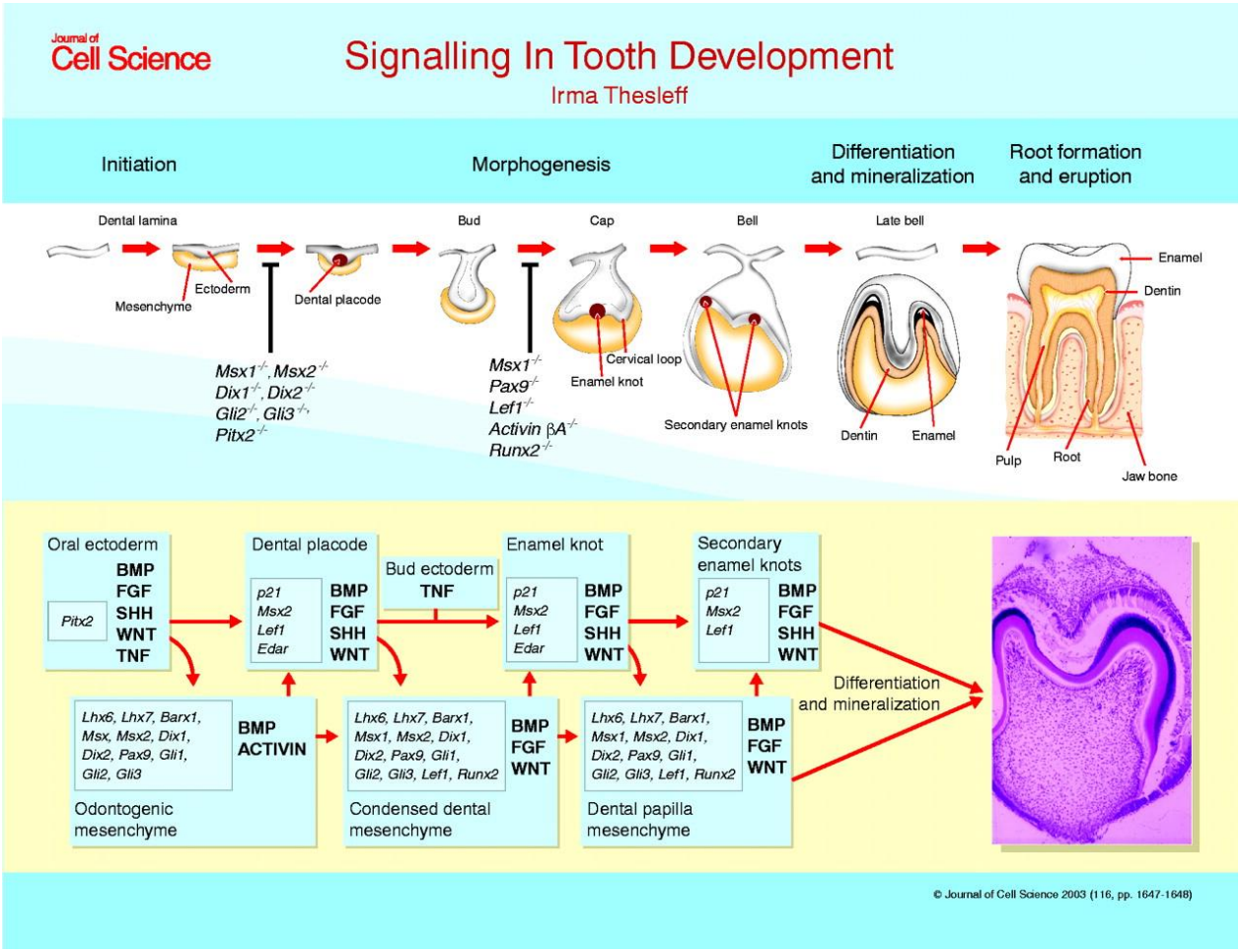

Fig. 1 – Illustration of various phases of tooth development and of the signaling networks regulating them (from Thesleff 2003).

Following initiation, the bud stage occurs, where an outgrowth of the epithelial tissue forms. The bud represents the primordial stage of what will become the dental crown. In the following phase, known as cap stage, the dental crown starts shaping. The transition from bud to cap is orchestrated by the interaction of various signaling pathways. An enamel knot forms at the tip of the tooth and the mesenchyme condense around it. The enamel knot acts as signaling center, is formed by non-dividing cells, and leads to the proliferation of surrounding cells. The growth proceeds from mesial to distal and the downward folding of the epithelial tissues results in the cervical loop (Jernvall et al., 1998). Once the activity of the primary knot is terminated, it disappears apoptotically and secondary knots form (Jernvall et al., 1994). The secondary knots act in the same way as primary knots; however, their activation is species-specific and must be under accurate genetic control for a correct determination of cusp size and

position (Jernvall and Thesleff, 2000). During the bell stage, the final shape of the tooth crown is achieved, before the process of biomineralization starts. In the process of mineralization, epithelium and mesenchyme cells differentiate. The ameloblasts form from the epithelium and produce enamel matrix; the odontoblasts originate from the mesenchyme and produce dentine matrix.

The epithelium-mesenchyme boundary will be preserved as the enamel-dentine junction. The cervical margin corresponds to the boundary where inner and outer layers of the epithelium fuse and form the Hertwig's sheath, which grows into the outer surface of the root. The Hertwig's sheath grows apically forming the basal surface of the pulp chamber and the surfaces of the roots. Usually, Hertwig's sheath folds beneath the cervical margin and meets at the pole, where it then divides to form the individual Hertwig's sheath for each branch of the root. This folding results in a constriction of the crown at the cervical area. The rate at which the cells of the Hertwig's sheath divide determines the shape of the cervical third of the root (Kovacs, 1971). If the cells proliferate at a slow rate, the constriction and therefore the pulp chamber will be low, giving rise to an enlarged pulp chamber and short roots (Kovacs, 1967, 1971). This condition is known as taurodontism (Keith, 1913). Taurodontism might be associated with certain syndromes or diseases, but might occur also in non-pathological individuals (Constant and Grine, 2001; Jafarzadeh et al., 2008; Saini and Wilson, 1990), and is highly prevalent in Neanderthals (e.g., Jafarzadeh et al., 2008; Kupczik and Hublin, 2010; Benazzi et al., 2015).

Simmer et al. (2010) illustrated the factors regulating the growth of the enamel crown and ultimately determined its thickness and shape. They included (Simmer et al., 2010, p. 1026): "the (1) appositional growth rate, (2) duration of appositional growth (at the cusp tip), (3) ameloblast extension rate, (4) duration of ameloblast extension, and (5) spreading rate of appositional termination". In other words, the final enamel thickness results from the rate of appositional growth (increase of enamel thickness per day) multiplied by the growth duration (namely the number of days in which the ameloblasts are in the appositional phase). The appositional growth rate varies within the same crown at different locations. The enamel thickness at the various locations, and ultimately the shape of the dental crown, depend on the rate of differentiation of the epithelial cells into ameloblasts, the duration of the ameloblast extension, and the ameloblast secretory-stage termination.

1.3.2. Dental gross morphology

Regardless of the genetics underlying the expression of the dental traits, the latter have been used to assess biological distances. The protocol for the description and evaluation of the main discrete dental traits has been summarized and standardized in the ASUDAS (Turner et al., 1991; Scott and Turner, 1997), which indicates the nomenclature and the evaluation criteria for several features of the dental crown and roots, such as Carabelli's trait, the degree of shoveling of the anterior teeth, the number of roots, and the presence of additional molar cusps. Another illustrative example of a discrete trait is the midtrigonid crest, a crest located between the mesial cusps of the molar teeth, which can show various shapes and diverse degrees of expression, from very marked to absent, and might appear on both the enamel cap and the enamel dentine junction (Bailey et al., 2011; Martínez de Pinillos et al., 2014). In addition to non-metric traits, the gross morphology of crown and roots and the dental tissue proportions are usually considered in the investigation of primate dental variation.

Teeth are grouped according to their shape and functional role into different dental types which have specific positions within the dental arch. Mammalian teeth are heteromorphic, and four main dental types are known, namely, incisor and canine (anterior teeth), and premolar and molar (posterior teeth).

In particular, hominoids have two incisors, one canine, two premolars and three molars per hemi-arcade. Within each of the dental types, the shape of both crown and root(s) defines the gross morphology of the tooth. For example, in posterior teeth the relative position, size, and height of the dental cusps, the occlusal space that occurs between the cusps, the tilting of the cusps and the steepness of the lateral walls are variably expressed. These features are genetically determined and depend on the time and rate of cell proliferation before the tissues begin to calcify, and the time and rate of mineralization (Butler, 1967, 1971; Simmer et al., 2010). For example, Butler (1967, 1971) showed that the growth of the basal area and the tilting of the cusps stop when the first bridges of calcified tissues appear. Therefore, he claimed that final shape and relative position of the cusps depend on the time and position of the first bridges formed. Tooth morphogenesis is known in more detail today, as discussed in section 1.2.3.

Roots also vary in their number, length, and width among primates (e.g., Abbott, 1984; Wood et al., 1988; Kupczik et al., 2005; Kupczik and Dean, 2008; Kupczik and Hublin, 2010; Emonet et al., 2012). The final morphology of the crown is the result of genetic heritage and the developmental process. Their shape and size also reflect functional adaptations. The molar roots are mostly monomorphic, while the most variable tooth group in terms of root number is the premolar (Sperber, 1974; Wood et al., 1988; Tobias, 1995). The plesiomorphic condition for this tooth is two-rooted mandibular premolars and three-rooted maxillary premolars. This root pattern is observed in australopithecines, while modern humans show mostly a reduced number of roots. It has been argued that the root attachment surface offers biomechanical resistance to masticatory stress (e.g., Kovacs, 1971; Kupczik and Dean, 2008), thus, an increased root surface might be favorable for feeding on hard food items. Nonetheless, Kupczik et al. (2005) found that root surface is uncorrelated to root number, as a variation of the root attachment area can be achieved also by root lengthening, or widening of root girth. Conversely, the root number is more likely to reflect a polymorphism (Sperber, 1974; Tobias, 1995), and might not strictly depend on functional demands.

1.3.3. Enamel thickness

The relative thickness of the enamel with respect to the underlying dentine is a further characteristic that has attracted the interest of scholars because of its functional implications. It has also been extensively studied for its taxonomic significance (Kay, 1981; Gantt, 1983; Martin, 1985; Gantt and Rafter, 1998; Martin et al., 2003). Enamel thickness variation represents a basis for delineating evolutionary relationships. Martin (1985) and Gantt and Rafter (1998) concluded that the primitive condition in hominoids is thin and fast-formed enamel. The common ancestor to hominins and great apes had thick and fast-forming enamel, which was maintained in both orangutans and hominins, while the great apes reverted to thin enamel via a reduction of the secretory rate. An alternative view is that the ancestral condition in hominins and *Pongo* was initially thin or intermediate thick enamel, and later a derived condition of thick enamel evolved in parallel in both groups (Beynon et al., 1991; Shellis et al., 1998).

Thick molar enamel, which produces blunt and bulging cusps, is regarded as an adaptation to feeding on hard food items such as seeds and nuts, while thin enamel creates sharp edges closely resembling the topography of the enamel-dentine junction and is more favorable for processing tough and fibrous vegetation (Butler, 1956; Gantt and Rafter, 1998; Lucas, 2004). The enamel distribution pattern reflects a functional adaptation for breaking down food stuffs possessing different mechanical properties. This adaptation results in an occlusal topography well suited to process the food items that constitute an animal's diet. For example, even though both *Gorilla* and *Pan* are regarded as thin-enameled apes,

Schwartz (2000) demonstrated how their teeth are structurally dissimilar, and explained the differences in enamel distribution patterns by the different functional demands originating from their varying diets (where *Gorilla* feeds mostly on leaves and pith, while *Pan* feeds on a great variety of food items, including small animals, eggs, and insects). Likewise, the quite similar relative enamel thicknesses in *Pongo* and *Homo* do not represent a developmental synapomorphy since their final amount of enamel and its distribution is achieved through different patterns of enamel deposition. Strait et al. 2013 substantiated the hypothesis that enamel thickness and other dental and facial characteristics might represent an adaptation to feeding on fallback food rather than to the food items prevalent in the diet. Furthermore, they claimed these features may be preserved in successive phylogenetic lineages if no selective pressure occurs to eliminate them.

The topography of the dental crowns changes throughout the lifetime of an individual owing to wear. Wear has been interpreted in an evolutionary perspective as a physiological phenomenon (Kay, 1975; Kaifu et al., 2003; Ulhaas et al., 2007; Kaidonis, 2008) and an adaptation to mechanical stress (Benazzi et al., 2013b). Dental and occlusal features such as fissures and crests have thus been regarded as functional adaptations withstanding loading forces (Benazzi et al., 2011c, 2013a).

1.4. Virtual imaging techniques in dental anthropology

Classical dental studies have mostly been based on the external aspect of the teeth (outer enamel and root surfaces). Any investigations on the internal structure required the use of partially destructive techniques such as the chemical dissolution of the enamel cap to expose the underlying dentine (e.g., Korenhof, 1960, 1961; Sakai et al., 1965, 1967a,b, 1969, 2002; Sakai and Hanamura, 1971, 1973a,b; Corruccini, 1987; Kono et al., 2002; Skinner et al., 2008b), or the production of physical sections (Martin, 1985) in cases where the teeth did not present natural fractures.

In the last three decades, the advent of virtual image techniques has opened new perspective in the various fields of anthropology, including dental anthropology (for recent summaries see Weber, 2015; Weber and Bookstein, 2011). Several kinds of tools can be used to obtain 3D virtual representations of the teeth. 3D surface scanners can produce 3D models of the outer aspect of dental specimens, while Computed Tomography (CT) devices can non-destructively image the inner structure of teeth or of any other object composed of materials that feature different degrees of X-rays attenuation (fig. 2; Tafforeau et al., 2014; Weber, 2015). Producing virtual data for (dental) specimens accounts for several other advantages since, once produced, they remain available for further studies, can be shared, and represent an accurate replica of the original specimen (Weber, 2001, 2015). CT scanning devices have become increasingly sophisticated and accessible to researchers, providing high resolution data for detailed study of the inner structure and even microstructure of teeth (Tafforeau, 2004; Suwa et al., 2007; Kono and Suwa, 2008; Olejniczak et al., 2008b,c,d; Skinner et al., 2008b, 2009; Tafforeau and Smith, 2008; Smith, 2013; Smith and Alemseged, 2013; Smith et al., 2014; Tafforeau et al., 2012).

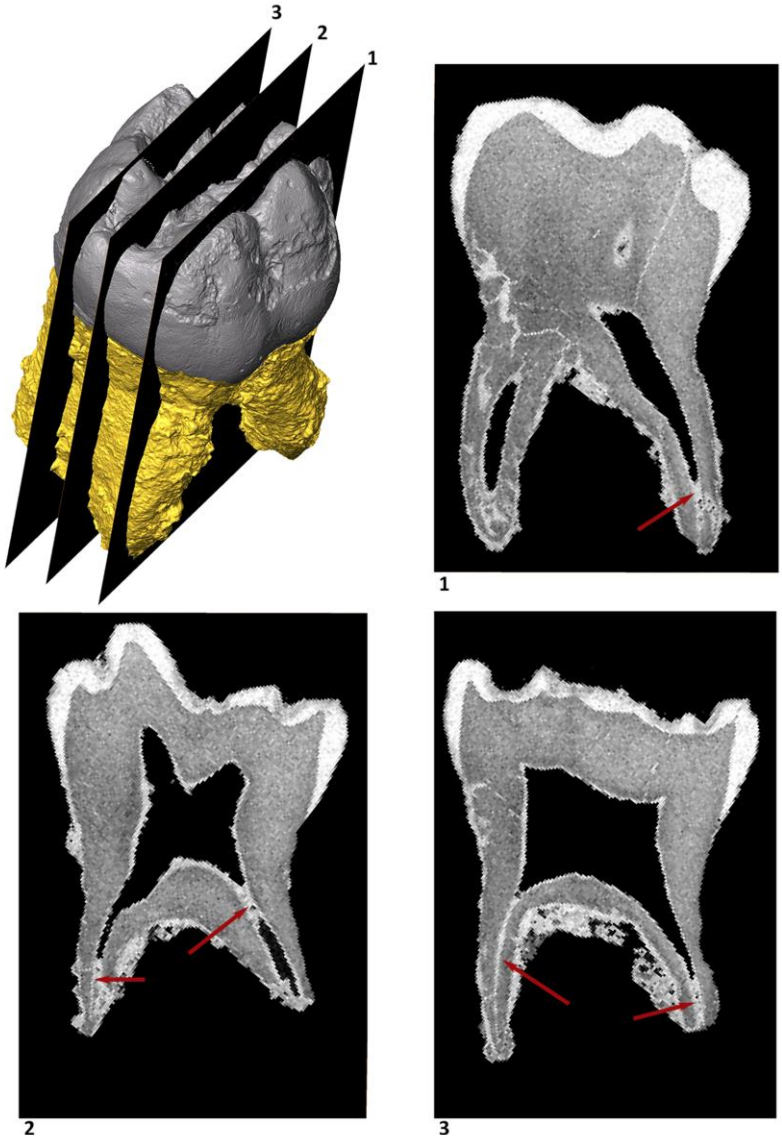

Fig. 2 – The internal structure of the Qesem Cave deciduous lower second molar dm2-QC2 is visible at three chosen slices showing the taurodontic pulp chamber and sediments obstructing the root channels (red arrows) (from Fornai et al., in preparation).

Olejniczak and Grine (2006) have estimated that the resolution needed to confidently detect the enamel-dentine junction is at about 50 µm. This resolution can be achieved using an industrial CT scanner (micro-CT, or µCT), while a clinical, whole-body CT would be inadequate. Conversely, a synchrotron facility can produce extremely high-resolution images (up to 0.7 µm) from which even the micro-structure of teeth can be detected (e.g., Tafforeau and Smith, 2008; Tafforeau et al., 2012). However, before volumetric data can be explored, the 3D image data needs to be processed in order to reconstruct the dental surfaces and eventually collect morphometric variables. The process of attributing particular voxels to specific materials, with the goal to separate the materials from each other, is called segmentation (fig. 3). Through segmentation, for instance, a tooth can be separated from the adjacent teeth and supportive tissues, and its various components (i.e., enamel, dentine, pulp chamber and root canals) can be

differentiated from one other. Segmentation is necessary for volume or surface area estimation of tissue, and of course for the extraction of the 3D surface models.

In turn, the latter can be further processed for the acquisition of different sorts of variables (such as landmark coordinates, curves, lengths, angles). These procedures usually require dedicated software (e.g., Amira or VGStudioMAX) and specialized technical skills. The manipulation of virtual surface models can be carried out by means of CAD software that allow, among other things, for the realignment of the surface on the bases of given axes or planes, for their cropping, for the extraction of silhouettes, or for the production of constructed landmarks (i.e., pseudolandmarks). All of the Methods sections in the research works presented here, namely chapters 2.1 to 2.8, describe the use of CAD software for at least part of the protocol of data collection. This approach is advantageous since information about the 3D morphology of the tooth can be gathered, and standardized and reproducible protocols for data collection can be established. Moreover, this approach overcomes or reduces the intra-observer error in acquiring variables from such small and complex objects as teeth.

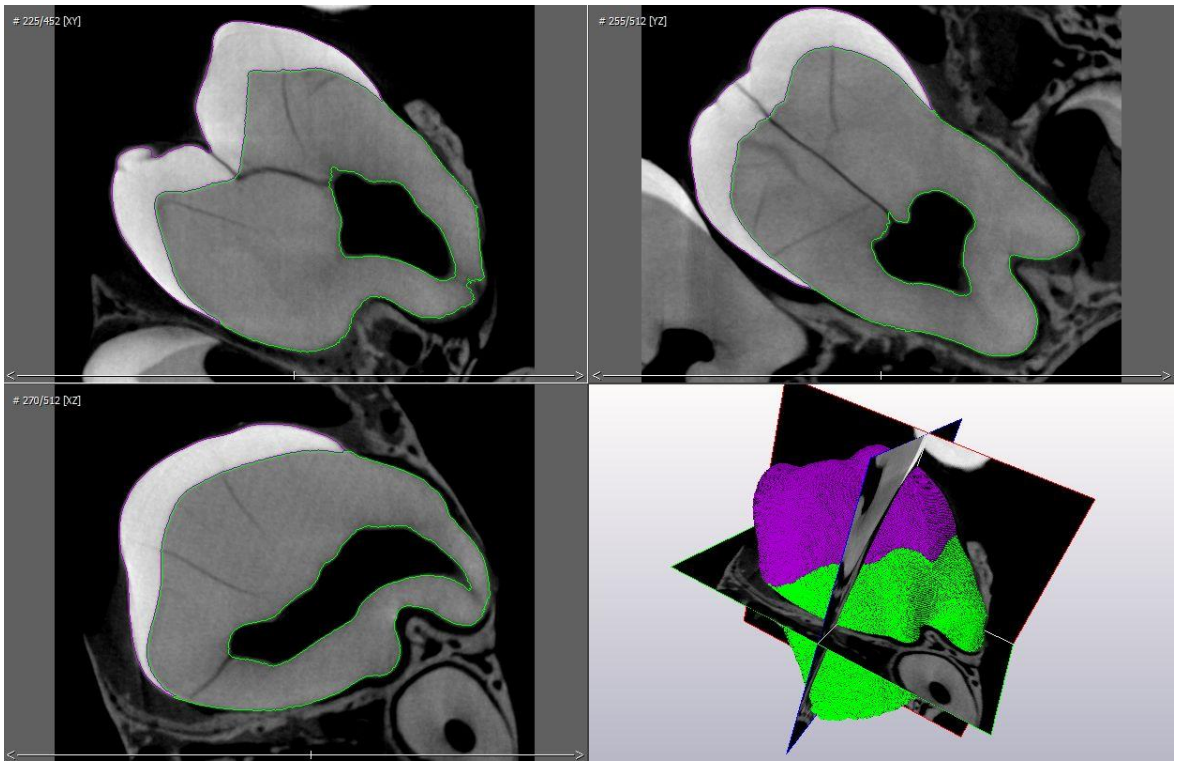

Fig. 3 – Various views showing the image data for an upper second human molar. Dentine (green) and enamel (violet) are segmented from the air, alveolar bone, and adjacent teeth.

1.4.1. Analysis of the enamel thickness and dental tissue proportions

Enamel thickness of extant and extinct primates has been extensively investigated for its taxonomic, phylogenetic, and dietary implications (e.g., Martin, 1985; Grine, 2002, 2005; Schwartz, 2000; Martin et al., 2003; Tafforeau and Smith, 2008). Traditionally, the study of the enamel thickness required the use of a single physical cross section of the tooth. Although this procedure has been successfully used to investigate the enamel thickness and dental tissue proportions in hominoids (Martin, 1985; Beynon et

al., 1991; Gantt and Rafter, 1998; Schwartz, 2000; Smith et al., 2012a) and hominins (Beynon and Wood, 1986; Grine, 2005; Mahoney, 2010; Mahoney, 2013), it suffers some inherent limitations such as the irreversible destruction of the tooth, a loss of dental material caused by the act of sawing, and the problem of maintaining homology of the sections (Suwa and Kono, 2005). Based on Martin's classical approach (1985) for measuring enamel thickness on mesial sections (namely the section passing through the mesial cusps), various non-destructive methods based on both synchrotron and standard µCT have been proposed to enhance the analysis of 2D enamel thickness, as measured on defined sections (fig. 4; Chaimanee et al., 2003; Martin et al., 2003; Olejniczak et al., 2008a; Feeney et al., 2010b; Smith et al., 2012b). In addition, the use of image data have given way to a number of studies investigating both the 3D enamel thickness (fig. 5; Kono, 2004; Macchiarelli et al., 2006; Kono and Suwa, 2008; Olejniczak et al., 2008a,b,c,d; Kono et al., 2014), specifically considering the volume of the dental tissues for the entire dental crown, or 2D enamel thickness measured on multiple sections (Smith et al., 2005; chapter 2.5). However, there is a cogent need to establish standardized protocols which account for the particular morphology of each dental type and provide accuracy, reproducible, and less subjectivity. This topic is treated in detail in chapters 2.1 and 2.4.

In chapter 2.1, we tested the discriminant power of several variables for the purposes of discriminating between Neanderthal and modern human lower second deciduous molars, using also the lateral enamel thickness (introduced by Toussaint et al., 2010), a feature considering only the lateral aspect of the dental crown that remains present despite moderate occlusal wear.

In chapter 2.4, we proposed new guidelines for the analysis of enamel thickness in unworn or slightly worn teeth, and evaluated them against previously established methods (Tafforeau, 2004; Olejniczak, 2006; Feeney et al., 2010a).

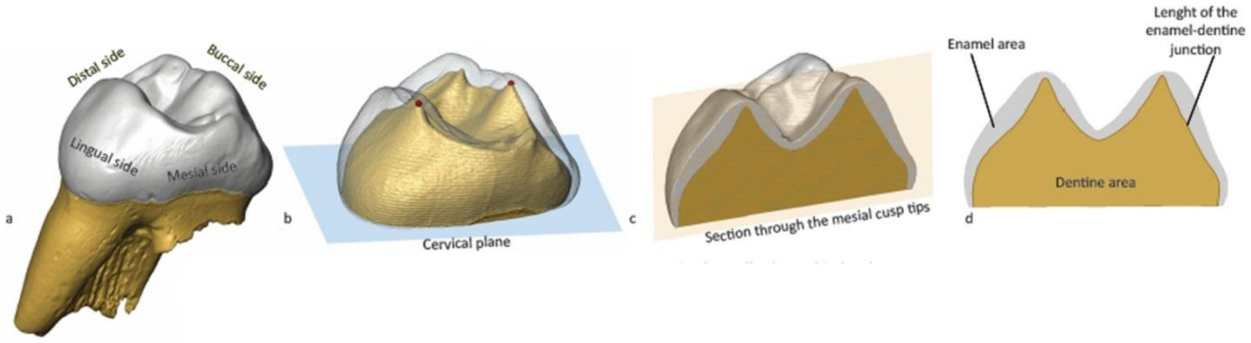

Fig. 4 – Identification of the mesial section on a 3D dataset from (a.) modern human upper first deciduous molar. b. Computation of the best-fit plane of the cervical line. Two landmarks (red dots) are located on the mesial dentine horn tips. c. A plane perpendicular to the cervical plane and passing through the two landmarks identifies the section to analyze. d. The enamel area, the dentine area and the length of the enamel-dentine junction for each section are used as basis to calculate both the average enamel thickness (AET= Enamel area/EDJ length) and the relative enamel thickness (RET= AET/square root(Dentine_area)), the latter being a unitless, scale-invariant measurement (from Fornai et al., 2012.)

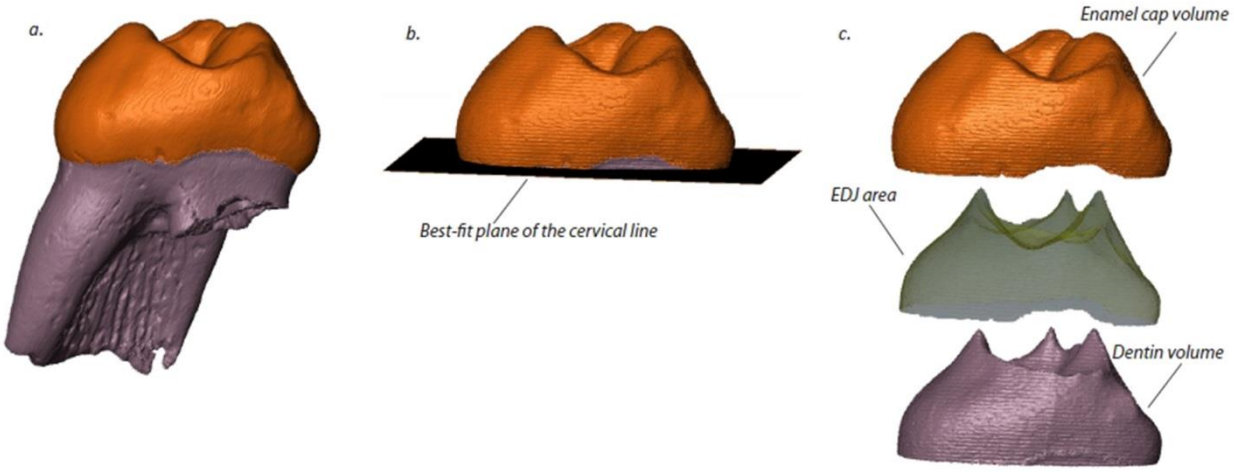

Fig. 5 - (a.) 3D model of a modern human upper first deciduous molar. (b.)The crown is separated from the rest of the tooth at the best-fit plane of the cervical margin. (c.) The enamel volume, the dentine volume (including the pulp chamber) and the EDJ area of the portion of the crown above the best-fit plane of the cervical line were gathered in order to calculate the average enamel thickness (enamel volume/EDJ surface area) and the relative enamel thickness (average enamel thickness/cube root(Dentine_volume) x 100) (from Fornai et al., 2011.)

The approach described in chapter 2.4 was used in chapters 2.2, 2.5, and 2.8 (and in Fornai et al., in preparation). The aims of these studies were diverse. In chapter 2.2, the 2D enamel thickness was performed in addition to a morphometric investigation of the dental crowns of two deciduous molars from Grotta del Cavallo, Apulia, Italy. The classification was reconsidered in the light of the results obtained, with important implications for the contextual Uluzzian culture and the European population history.

In chapter 2.5, the enamel thickness and dental tissue proportions were assessed in modern human and Neanderthal upper deciduous teeth to investigate the variability of the component values of enamel thickness in these *Homo* taxa. These aspects were still unexplored for deciduous teeth, the latter being underrepresented in the literature with respect to permanent dentition. Furthermore, the protocol was integrated in order to apply it to teeth whose dentine is affected by wear. Such condition in fact is ubiquitous in dental samples. In addition to the mesial section, in chapter 2.5 we considered the section passing from the buccal cusps for the deciduous upper second molar and compared the outcomes for both sections (see also, chapter 2.2; and Fornai et al. [2012]).

In chapter 2.8, the analysis of the enamel thickness was performed for comparative purposes in order to evaluate the effects of congenital syphilis in the dentition of a pathological individual from the XVI century Croatia.

Additionally, Fornai et al. (in preparation) investigated the enamel thickness on the mesial section together with other features of the crown in order to assess morphologically the Middle Pleistocene lower deciduous second molar from Qesem Cave, Israel, a specimen whose taxonomy is still unresolved.

1.4.2. Geometric morphometrics (GMM)

One of the fields of research in dental anthropology focuses on the morphometric characterization of teeth in order to describe their within- and between-species shape and size variation. Traditional

techniques are based on the analysis of the linear dimensions of the teeth such as the bucco-lingual and mesio-distal diameters, and the crown height. The following citations are examples of the vast literature produced using this traditional approach: Robinson, 1956; Garn et al., 1966; Wood and Abbott, 1983; Wood et al., 1983; Wood and Zuckerman, 1981; Wood and Engleman, 1988; Rightmire, 1993; Calcagno et al., 1997; 1999; Liu et al., 2000; Belmaker et al., 2002; Moggi-Cecchi, 2003; Manthi et al., 2012; Schroer and Wood, 2015. Using linear distances, angles and surface measurements, also 2D images of teeth, such as photos of the occlusal aspect, have been extensively exploited in order to gather information about the occlusal polygon and the relative position and size of the dental cusps (e.g., Wood and Abbott, 1983; Wood et al., 1983; Wood and Engleman, 1988; Moggi-Cecchi and Boccone, 2007). The aforementioned methods have several advantages since they exploit rather simple techniques and allow using large dental samples (see discussion in Benazzi, 2007). At the same time, the main drawback of linear measurements is that they do not preserve the spatial relation of the anatomical points they sample. Therefore, they are not ideal to represent the morphology of complex objects, which limits the outcomes of studies employing them (Sharma, 1985; Bernal, 2007). Moreover, size and shape cannot be separated easily. Furthermore, since the orientation of a tooth is not a trivial task owing to its irregular morphology, reproducibility of the outcomes in studies based on photos might be an issue (but see also Bailey et al., 2014 for another point of view).

Traditionally, physical anthropology has used linear distances, distance ratios, and angles based on anatomical landmarks as quantitative information to assess shape variation (Martin and Saller, 1957; Howells, 1973, 1989, 1995). In the last decades, the investigation of biological shapes has gone through major changes since new methods for the investigation of Cartesian coordinates from anatomical landmarks have been introduced. These methods, collectively known as Geometric Morphometrics (Bookstein, 1991, 1998, 2013; Corti, 1993; Adams et al., 2004; Slice, 2005, 2007) have been extensively applied in biology and anthropology (see the reviews by, Bookstein, 1996; James Rohlf and Marcus, 1993; O'Higgins, 2000; Lawing and Polly, 2010; Weber and Bookstein, 2011; Weber, 2015).

The anatomical landmarks used in GMM must comply with the rule of homology (Weber and Bookstein, 2011). The concept of homology in GMM is not as strict as in theoretical biology, but it remains a prerequisite of any GM analysis which studies sample variation based on the spatial relationship of structures. Weber and Bookstein (2011) described six landmark types, according to the geometry of the anatomical structure on which they are located. Landmarks are fix (types 1 – 3) if they can be identified on specific anatomical structures. A further category of landmarks include those points that are not fixed but can be slid along a tangent of a curve (i.e., curve semilandmarks, type 4) or across a tangent plane (i.e., surface semilandmarks, type 5) (Gunz et al., 2005; Gunz and Mitteroecker, 2013). Semilandmarks are used to explore inter-landmark morphology and through the sliding process acquire the property of geometric homology. Landmarks geometrically constructed (type 6) are determined through projections or other geometric constructions, and can be referred to as pseudolandmarks.

One of the points of strength of GMM is that it allows retaining the whole 3D geometry of the object as represented by the landmark configuration used to resample it. Other spatial information such as distances and angles are inherently included in the Cartesian coordinate data and can also be produced during the workflow. The landmark configuration must be designed in order to address the pending biological question. Landmark coordinates convey information about the position and orientation of the object in space. In addition, they incorporate information about size. Therefore they have to be normalized before they can be analyzed as shape variables through standard multivariate approaches.

Several registration methods have been proposed to eliminate unwanted information, including interlandmark distances (Bookstein et al., 1985; Lele and Richtsmeier, 2001), or registration on a common baseline (Bookstein, 1986, 1991). Today, broadly employed methods are the Procrustes superimpositions (Gower, 1975; Rohlf and Slice, 1990; Dryden and Mardia, 1998). Among them, the Generalized Procrustes analysis (GPA) brings all landmark configurations into a common coordinate system where the differences between homologous landmarks reflect differences in shape. In GPA, the conversion of the landmark coordinates into shape variables is based on the minimization of the Pythagorean distances between homologous points via translation and rotation, with reference to an iteratively computed mean configuration (consensus). In addition, the configurations are scaled to the same unitary size (the Centroid Size, Bookstein, 1991), so that the differences between the landmark configurations reflect only differences in shape. Size might be relevant to the biological issue to address, therefore the information about size can be brought back into the analysis, as explained by Mitteroecker and Gunz (2009), by adding the column of natural logarithm Centroid Sizes to the matrix of Procrustes shape coordinates. Landmark coordinates result in shape coordinates after their registration. Shape coordinates induce the mathematical, non-linear Kendall shape space (Kendall, 1984). A Euclidean tangent space approximates locally Kendall's shape space, which allows shape coordinates to be analyzed through multivariate approaches.

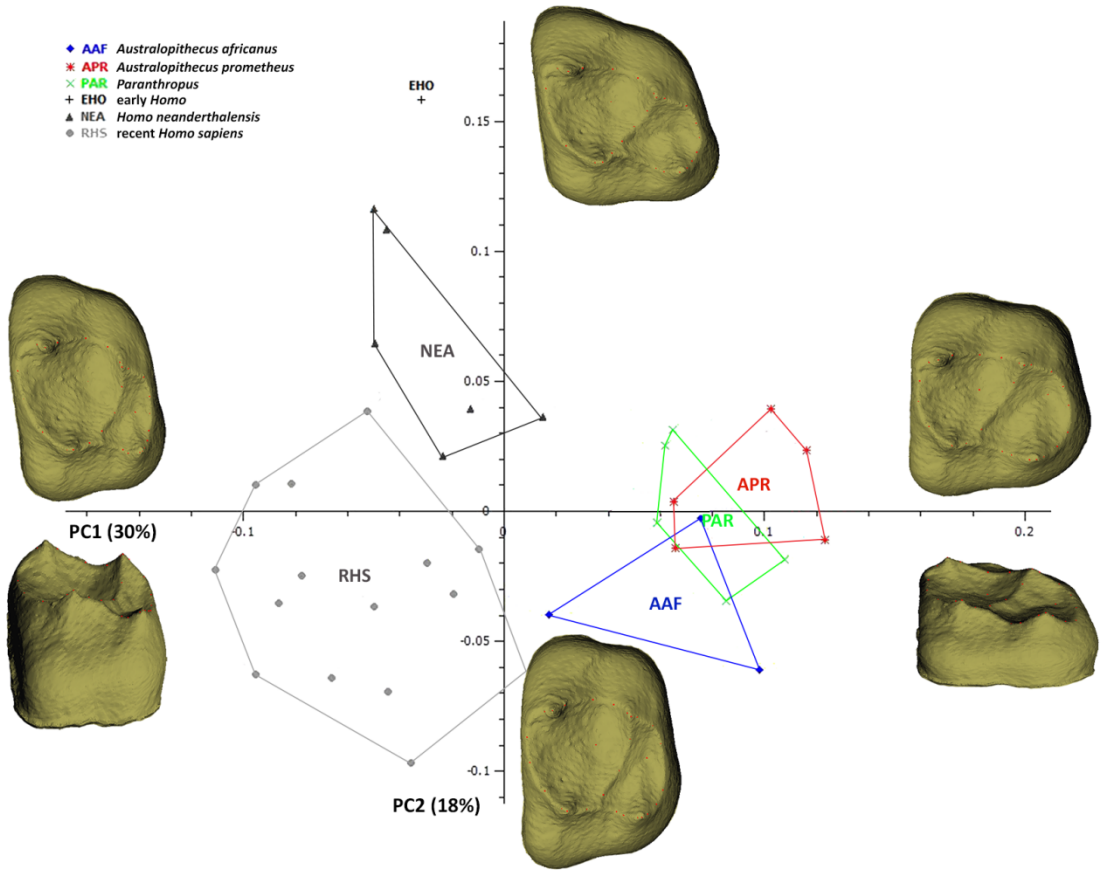

Since the spatial arrangement of the landmark points is retained throughout the analysis, a further

Fig. 6 – Example of warped surfaces (from chapter 2.6, modified) showing the deformation of the enamel-dentine junction at the extremes of the range of variability along PC1 and PC2 of a sample of hominin maxillary second molars. The *Australopithecus* specimen Sts 8 is warped.

advantage of GMM is that the statistical results can be converted into visualizations of the shape changes occurring, for instance, between individuals or between group means. This can be achieved by means of vector diagrams (Slice, 2005, 2007), in which the shape differences are visualized trough vectors originating at each landmark position and ending at the position of the homologous landmark of the compared configuration. Such vectorial changes can also be visualized using a thin-plate spline graphical device (fig. 6; Bookstein, 1989, 1991). This provides a mapping of one landmark configuration, which can then be warped into another configuration using a minimal bending energy algorithm, meaning that the space between landmarks undergoes the smoothest interpolation.

As mentioned above, the distances between homologous Procrustes shape coordinates are a measure of the shape differences between specimens. Therefore, the full Procrustes distance, equal to the sum of root mean square distances between homologous points, represents a direct measure of such shape differences. Furthermore, mean shapes and covariance of the sample around the mean derive from GPA. Patterns of covariation across sets of variables can be explored using a partial least-squares analysis (PLS). In morphometrics, PLS (Bookstein, 1991; Rohlf and Corti, 2000) can be used to investigate the relationship between two landmark configuration sets, e.g. the face and the braincase, or the third and the fourth premolar. Using the mean shape and shape covariance, group differences can be investigated. Furthermore, through a regression analysis shape can be related to intrinsic (e.g., sex or size) or extrinsic (e.g., time, developmental environmental) variables.

In GM investigations, principal component analysis (PCA) is most widely used as a means for the estimation of parametric structures proper of the sample. PCA is a statistical tool for dimension-reduction that identifies the orthogonal linear combinations of the original variables that best reproduce the variability of the sample. When combined with visualization techniques, PCA is of particular use for revealing factors of covariation among the shape variables.

Recently, scholars have contemplated the opportunity to use the statistical results from GM analysis for phylogenetic studies (Fink and Zelditch, 1995; Zelditch et al., 1995; Swiderski et al., 1998; Macleod and Forey, 2002; González-José et al., 2008). However, there are cogent reasons to consider shape variables such as partial warps unsuitable for cladistic analysis (Bookstein, 1994; Adams and Rosenberg, 1998; Rohlf, 1998; Monteiro, 2000; Adams et al., 2011). For parsimony analysis in cladistics, a reduction through different rotations of a multivariate set of variables into sets of single dimensions is required. The single characters used must have biological significance, but in fact partial warps do not (Rohlf, 1998; Bookstein, 2015). Although GMM preserve spatial relationships between specimens in the multivariate space, the ordination of the taxa in such space is not consistent for all shape variables (Bookstein, 1980, 1994). Monteiro (2000) and Adams et al. (2011) explained with illustrative examples that shape variables are not suitable for phylogenetic analysis since rank-ordering techniques and the rotations they cause do not preserve the distances among the objects. Different sample compositions would cause different rotations of the datasets, leading to unstable parsimony trees.

However, GMM remains a useful tool for the exploration of biological shapes and forms. The morphological information obtained for the specimens allow inferring about taxonomy provided that the observations are carried out in a robust comparative setting. Dental evolution is subject to parallelism, convergence and reversals; therefore, it is important to consider that the outcome of a morphometric analysis, even if sophisticated, must be interpreted cautiously since morphological affinities might not necessarily imply taxonomic alliance. Moreover, taxonomic classification based solely on dentition might lead to inconclusive results, particularly when the species did not accumulated clear synapomorphies

(Corruccini, 1987; and chapter2.6). Moreover, it has been long argued that phylogeny inferred on the bases of a single factor is mainly biased (Butler, 1986). It is therefore beneficial to consider different aspects of a tooth at once and assess the diagnostic value of those features in a comparative context.

1.4.3. GMM applied on teeth: studying a three-dimensional object in 3D

Teeth feature complex geometries, making them an ideal application area for landmark based techniques.

GM studies using 2D representations of teeth (usually, but not exclusively, photos taken in occlusal view) are abundant (e.g., Robinson et al., 2001; Bailey, 2004; Bailey and Lynch, 2005; Bernal, 2007; Gómez-Robles et al., 2007, 2008, 2011, 2012; Kieser et al., 2007; White, 2009; Liu et al., 2010; Bailey et al., 2014) since they present several advantages. 2D images are more likely to allow for larger sample sizes since they can be acquired more easily and faster than 3D datasets, and the equipment required is generally available to all research institutions.

3D GM studies have the advantage of taking into account the complex morphology of the tooth, which is irregular and asymmetric (e.g., Skinner et al., 2008a, 2009a,b; Morita et al., 2014; and chapters 2.6, 2.7). In conjunction to different kinds of imaging techniques, GMM has also found several applications for the investigation of the 3D morphology of the various dental regions, including the outer and inner aspects of the crown, and the roots (Bailey, 2004; Bailey and Lynch, 2005; Skinner et al., 2008a, 2009a,b; Bailey et al., 2011, 2014; Chaimanee et al., 2011; Emonet et al., 2012; Morita et al., 2014; Fornai et al., in preparation; Krenn et al., in preparation; and chapters 2.2, 2.3, 2.6, 2.7). However, 3D imaging devices are not always easy to access; likewise, handling 3D images requires dedicated software and specialized technical skills.

Challenges in the use of 3D GMM for the assessment of dental morphology arise from the shape and nature of teeth themselves. One of the rules of GMM (Weber and Bookstein, 2011) is that the landmark points used must be homologous throughout the sample. There are several conditions in teeth that challenge the rule of homology. Wear is a one of them, and impedes the morphological comparison of teeth, either when it occurs on the occlusal surface, or in the proximal areas of contact between adjacent teeth. Several solutions can be found to circumvent the problem of wear. For instance, a dental sample composed of teeth showing similar degrees of wear can be chosen. But since fossil samples are usually small, this might not be a suitable option. Alternatively, the protocol for data collection can be designed in order to gather information from the region still present. For example, the enamel-dentine junction could be accessed via 3D imaging technics and used instead of the outer enamel surface (Skinner et al., 2008a, 2009a,b; Skinner et al., 2008b; Fornai et al., in preparation; Krenn et al., in preparation; and chapters 2.6, 2.7.) In fact, a high co-variation of the occlusal curve in molar teeth at the enamel-dentine junction and outer enamel surface was found in Buchegger et al. (2014), Morita et al. (2014), Krenn et al. (in preparation) and in chapters 2.6 (fig. 7).

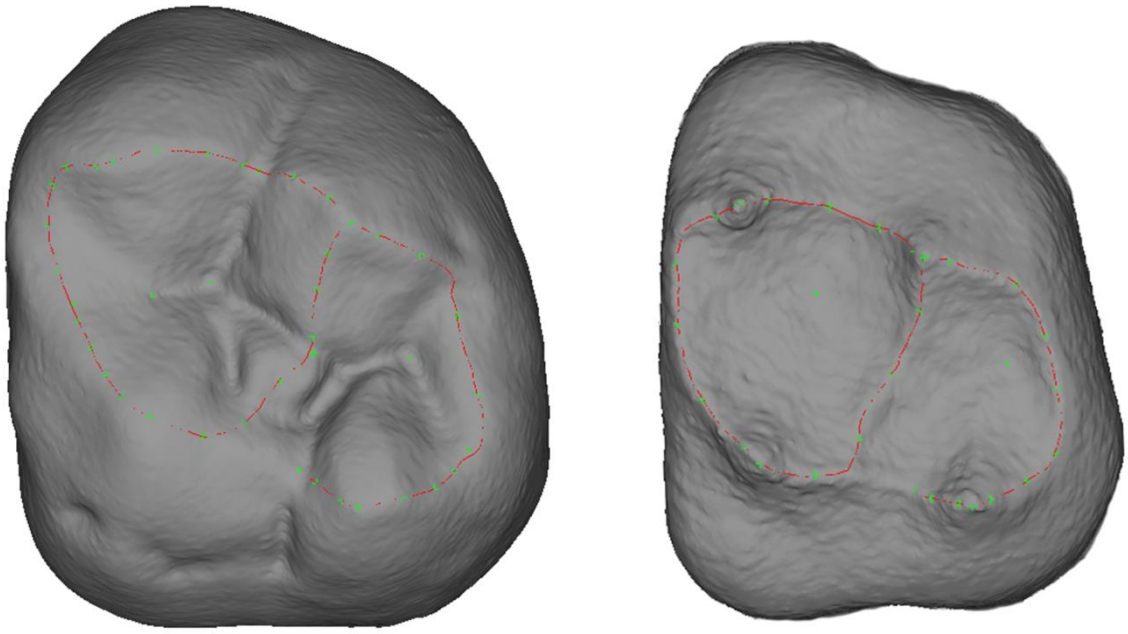

Fig. 7 – Landmarks (green crosses) resampling the occlusal curve (in red) at both the outer enamel surface (left) and enamel-dentine junction of the same dental specimen (i.e., upper second molar Sts 8 *Australopithecus africanus*)

Otherwise, the crown outline can still be gathered from a moderately worn tooth and the cervical outline is still available even in case of heavy wear (fig. 8). Nonetheless, one might need to correct for interproximal wear using interpolating curves as done on outlines gathered either from photos or 3D virtual models (e.g., Wood and Engleman, 1988; Bailey, 2004; Bailey et al., 2014; Fornai et al., in preparation; Krenn et al., in preparation; and chapters 2.2, 2.3, 2.6, 2.7.) If the unworn condition is to be studied, a light wear of the dentine horns can be virtually reconstructed by following the contour of the horn still present and interpolating the selection at a few slice intervals (this solution was used for the works presented in chapter 2.7; Fornai et al., in preparation; and Krenn et al., in preparation). This approach is helpful only to correct for minor loss of dental material, but it would require too much approximation for high degrees of dental wear (i.e., higher than wear stage 3 of Molnar [1971]). Conversely, unworn teeth could be virtually worn down to match the degree of wear from the rest of the sample, but this procedure is complicated to achieve virtually since teeth do not wear down uniformly. Other complex techniques have been applied to wear down mechanically physical models of the teeth using an articulator, where the occlusal relationships are known (Benazzi et al., 2013a).

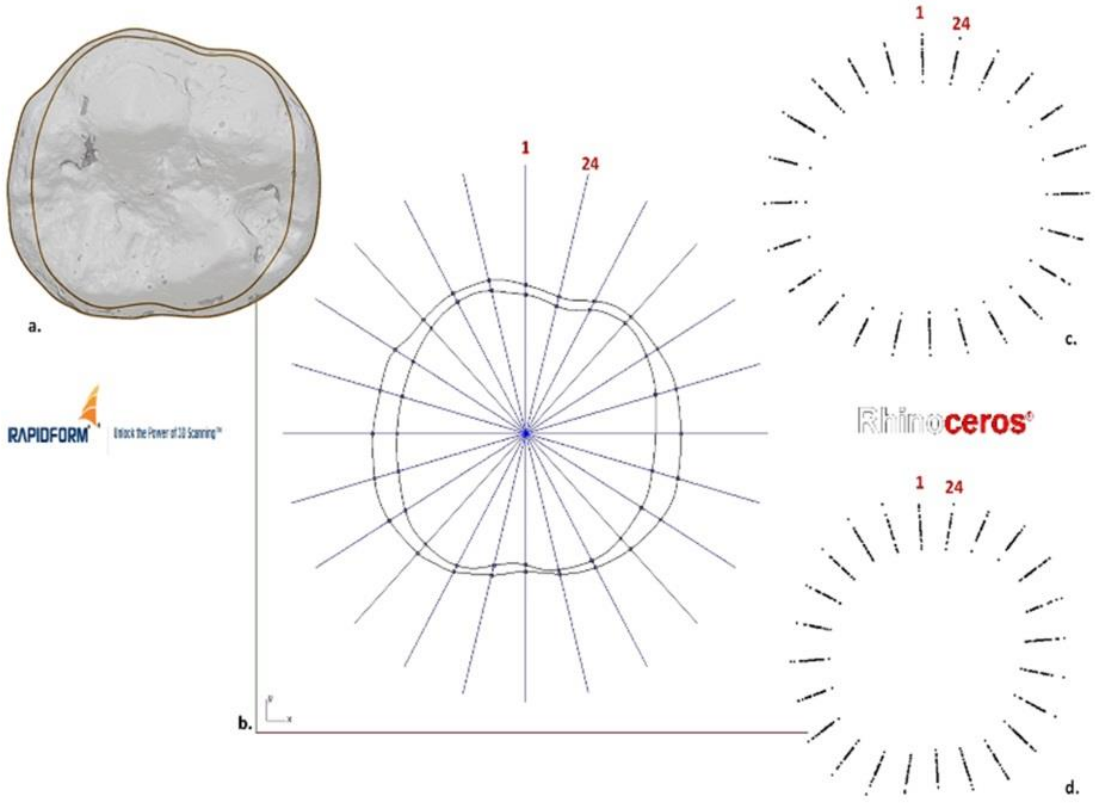

Fig. 8 - Cervical and crown outlines are gather from the Middle Pleistocene deciduous lower second molar dm2-QC2 from Qesem Cave, Israel. Each of the outlines is then resampled using 24 pseudolandmarks (from Fornai et al., in preparation.)

Similarly to wear, the existence of discrete traits that are inconsistently present throughout the sample, such as additional cusps or the Carabelli's trait, makes it difficult to comply with the rule of homology. In the case of additional horn tips in the distal aspect of the lower molars, Skinner et al. (2008a, 2009a,b) collected landmarks from the marginal edge considering only the main horns. Similarly, in chapters 2.7 and Fornai et al. (in preparation), we did not place landmarks on additional distal horns, and traced the marginal edge interpolating the curve at the base of the additional horns to avoid that the position of the semilandmarks would reflect non-homologous features.

Studies using various GM approaches based on 3D images are illustrated in chapters 2.2, 2.3, 2.6, and 2.7. These studies are focused on various dental types, including both deciduous and permanent teeth, and were conceived for the morphological characterization of specimens. The latter was then interpreted for the purposes of taxonomic assessment and exploration of morphological variability. In particular, the protocols gathered the shape of the dental crown using four of its features, namely, the occlusal aspect of the outer enamel surface and of the enamel-dentine junction, using landmarks and semilandmarks sliding along the marginal edge (fig. 7), and the crown and the cervical outlines, resampled by geometrically constructed landmarks (or pseudolandmarks) (fig. 8).

While the crown outline and the outer enamel surface are accessible also using 2D representations of the teeth, the cervical outline and the 3D aspect of the enamel-dentine junction are better gathered using 3D image data.

In chapter 2.2 the crown and cervical outlines were used for the taxonomic assessment of the deciduous upper molars from Grotta del Cavallo, Italy.

In chapter 2.3 the variability of Neanderthal and modern human upper deciduous molars in terms of crown and the cervical outlines is explored, and a classification of the Bondi 1 (Western Georgia), and Lagar Vehlo 1 (Portugal) is attempted.

Chapter 2.6 reports a study exploring the variability of the *Australopithecus africanus* upper second molars in comparison to a sample of *Paranthropus* and *Homo* specimens, in order to test the hypothesis of the occurrence of multiple species in the South African fossil site Sterkfontein Member 4. For this investigation a comprehensive study of the dental crown was undertaken, including the occlusal curves at both the outer and inner aspects of the crown, and the crown and cervical outlines.

Finally, chapter 2.7 exploits the crown and cervical outline and the enamel-dentine junction to investigate the morphological variability of Middle Pleistocene Levantine lower premolars and second molar from Qesem Cave (Israel).

In summary, the chapters to follow illustrate eight works based on various virtual techniques for the investigation of dental morphology and enamel thickness. These studies are presented in chronological order, from the oldest published in 2011 (chapter 2.1) to the most recent still in revision while I write (chapter 2.8).

These papers aimed at investigating the within and between groups variability of different dental types, belonging to different taxa (chapters 2.2-2.3, 2.5-2.8). The investigation of dental variation served in some cases as background information for the taxonomic assessment of undetermined specimens (chapters 2.2, 2.3, 2.6, 2.7). Chapters 2.1 and 2.4 are merely methodological.

2. Research works

2.1. Comparison of dental measurement systems for taxonomic assignment of Neanderthal and modern human lower second deciduous molars.

Benazzi, S., Fornai, C., Bayle, P., Coquerelle, M., Kullmer, O., Mallegni, F., Weber, G.W.

Journal of Human Evolution 2011; 61, 320-326.

Synopsis

The study reported in this chapter was designed for the evaluation of the discriminant power of various dental features gathered from the lateral aspect of the crown of Neanderthal and modern human lower deciduous second molars (dm_2s). This paper followed a contribution by Toussaint et al. (2010) who suggested the relative enamel thickness of the lateral crown could be used for the taxonomic assessment of unknown dm_2 specimens when the occlusal aspect of the tooth is worn away. In our study, we produced 3D surface models derived from µCT images of the teeth and extracted features of the lateral aspect of the crown. We found that the height of the lateral wall of the crown and the volume of the coronal pulp chamber provided a higher correct classification of the Neanderthal and modern human dm_2s in comparison to the relative enamel thickness of the lateral crown.

The impact of our study is that it assesses the diagnostic power of several features for worn teeth, which are abundant in paleontological settings. Furthermore, our study is focused on deciduous teeth, which are underrepresented in the literature with respect to permanent teeth.

Contribution

Participation in the data collection and editing of the manuscript.

Journal of Human Evolution 61 (2011) 320e326

Contents lists available at ScienceDirect

Journal of Human Evolution

journal homepage: www.elsevier.com/locate/jhevol

Comparison of dental measurement systems for taxonomic assignment of Neanderthal and modern human lower second deciduous molars

Stefano Benazzi [a,*], Cinzia Fornai [a], Priscilla Bayle [b,c], Michael Coquerelle [a], Ottmar Kullmer [d], Francesco Mallegni [e], Gerhard W. Weber [a]

[a] Department of Anthropology, University of Vienna, Althanstrasse 14, 1090 Vienna, Austria
[b] UMR 5199 PACEA, Université Bordeaux 1, avenue des Facultés, 33405 Talence, France
[c] Research Department of Cell and Developmental Biology, University College London, London WC1E 6BT, United Kingdom
[d] Department of Palaeoanthropology and Messel Research, Senckenberg Research Institute, Senckenberganlage 25, D-60325 Frankfurt am Main, Germany
[e] Department of Biology, University of Pisa, Via S. Maria 53, 56126 Pisa, Italy

a r t i c l e i n f o

Article history:
Received 14 September 2010
Accepted 11 April 2011

Keywords:
Neanderthals
Dental tissue proportions
Deciduous teeth
Micro-CT
Morphometrics

a b s t r a c t

Traditional morphometric approaches for taxonomic assignment of Neanderthal and modern human dental remains are mainly characterized by caliper measurements of tooth crowns. Several studies have recently described differences in dental tissue proportions and enamel thickness between Neanderthal and modern human teeth. At least for the lower second deciduous molar (dm_2), a three-dimensional lateral relative enamel thickness index has been proposed for separating the two taxa. This index has the advantage over other measurements of being applicable to worn teeth because it ignores the occlusal aspect of the crown. Nevertheless, a comparative evaluation of traditional crown dimensions and lateral dental tissue proportion measurements for taxonomic assignment of Neanderthal and modern human dm_2s has not yet been performed.

In this study, we compare various parameters gathered from the lateral aspects of the crown. These parameters include crown diameters, height of the lateral wall of the crown (lateral crown height ¼ LCH), lateral enamel thickness, and dentine volume of the lateral wall, including the volume of the coronal pulp chamber (lateral dentine plus pulp volume ¼ LDPV), in a 3D digital sample of Neanderthal and modern human dm_2s to evaluate their utility in separating the two taxa.

The LDPV and the LCH allow us to discriminate between Neanderthals and modern humans with 88.5% and 92.3% accuracy, respectively. Though our results confirm that Neanderthal dm_2s have lower relative enamel thickness (RET) index compared with modern humans (p ¼ 0.005), only 70% of the specimens were correctly classified on the basis of the RET index. We also emphasize that results of the lateral enamel thickness method depend on the magnitude of the interproximal wear. Accordingly, we suggest using the LCH or the LDPV to discriminate between Neanderthal and modern human dm_2s. These parameters are more independent of interproximal wear and loss of lateral enamel.

Introduction

High-resolution micro-tomographic investigation and three-dimensional (3D) digital visualization have recently been used to quantify and describe the internal structure of Neanderthal and modern human dentition (e.g., Macchiarelli et al., 2006, 2007, 2008; Smith et al., 2007a,b, 2010; Olejniczak et al., 2008). The 3D approach improves the results obtained by previous contributions based on two-dimensional (2D) enamel thickness measurements that were successfully used to discriminate between the two taxa (e.g., Zilberman and Smith, 1992; Zilberman et al., 1992; Smith and Zilberman, 1994; Ramirez Rozzi, 1996). Compared with modern humans, Neanderthals show a similar enamel volume but deposited over a greater, more complex enamel-dentine junction surface and larger dentine volume, resulting in lower average and relative enamel thicknesses (Macchiarelli et al., 2006, 2008; Smith et al., 2007b; Olejniczak et al., 2008; Bayle et al., 2009a). Nevertheless, the quantification of 3D enamel thickness requires a completely unworn or only slightly worn crown. In practice, however, occlusal wear processes reduce the enamel volume of many specimens, thereby affecting further computation of the dental tissue proportions.

* Corresponding author.
E-mail address: stefano.benazzi@univie.ac.at (S. Benazzi).

0047-2484/$ e see front matter © 2011 Elsevier Ltd. All rights reserved.
doi:10.1016/j.jhevol.2011.04.008

To overcome this problem, Toussaint et al. (2010) suggested the measurement of lateral enamel thickness to assess the taxonomy of the lower second deciduous molar (dm_2) from the cave of Trou de l'Abîme (Couvin, Belgium). The Couvin specimen was found in association with archaeological material that was, at the time of the discovery, interpreted as a transitional facies between the Middle and Upper Paleolithic. The tooth shows occlusal wear, preventing an evaluation of the complete tooth crown for dental tissue proportions analysis. Because analysis of the buccolingual (BL) and mesiodistal (MD) crown diameters did not allow for taxonomic assessment, the authors compared the thickness of the lateral aspect of the enamel cap of the Couvin specimen with three Neanderthals and six modern humans, which strengthened its classification as a Neanderthal. In particular, the authors suggested that the lateral relative enamel thickness index of dm_2 (see below) effectively separates the two taxa. Nevertheless, a comparative evaluation of several morphometric parameters to distinguish between Neanderthal and modern human isolated dm_2 has not yet been performed.

In this study we compare various measurements (the crown diameters, the height of the lateral wall of the crown, the lateral enamel thickness and the dentine volume, which includes the volume of the coronal pulp chamber) of Neanderthal and modern human dm_2s in order to test their discriminating power in taxonomic problems. In addition, we carry out an experimental test to quantify the effect that the interproximal wear could produce on the lateral enamel thickness evaluation.

Materials and methods

Sample

The dental sample consists of a total of 28 dm_2s, including 10 Neanderthals (N), two Upper Paleolithic modern humans (UPMH), and 16 extant human teeth from Medieval and contemporary samples. Only specimens with well-preserved enamel surfaces were selected. Provenance details, laterality and wear stage (based on Smith, 1984) are provided in Table 1. For the statistical analysis (see below), the UPMH specimens were combined with the extant humans in the modern human (MH) sample, but they were plotted with distinct labels for clarity.

Scanning of the specimens

Scans of all of the specimens were undertaken by means of industrial micro-tomography scanners at isotropic voxel length between 16 and 55 μm. The exceptions to this are the Abri Suard and Roc de Marsal Neanderthal specimens, which were scanned by means of synchrotron radiation micro-tomography at the beamline ID17 of the European Synchrotron Radiation Facility of Grenoble, France (ESRF) at a voxel size of 45.5 × 45.5 × 45.7 μm. The original specimens used in this study were scanned at the Vienna Micro-CT Lab, Department of Anthropology, University of Vienna, with a Viscom X8060 μCT scanner using the following scan parameters: 130 kV, 100 mA, voxel size ¼ 25 μm^3. Details about the scanning procedure of the other specimens can be found in Macchiarelli et al. (2006), Bayle et al. (2009a,b, 2010), Toussaint et al. (2010), and the NESPOS (Neanderthal Studies Professional Online Service) digital internet archive (www.nespos.org) (Table 1).

Segmentation and 3D reconstruction

The extant human sample, Cavallo A and the Krapina sample were segmented ex novo for this project. For the Abri Suard sample, Roc de Marsal and the UPMH sample, we used a previously segmented and reconstructed digital record (Bayle et al., 2009a,b, 2010).

For the segmentation process, we used a well-established protocol in virtual dental paleoanthropology (e.g., Kono, 2004; Olejniczak et al., 2008; Smith et al., 2010). The half-maximum height (HMH) protocol (Spoor et al., 1993) was used to reconstruct 3D digital surface models for the dentine and the enamel of each CT-scanned tooth using the software package Amira 5.2 (Mercury Computer Systems, Chelmsford, MA). This protocol samples the Hounsfield values on either side of the transition between two adjacent tissues and takes the value halfway between them as the threshold value. When voxels were located on the boundary between two tissues with similar Hounsfield values and the automatic threshold could not distinguish the differences, manual corrections were conducted. For each specimen, the HMH protocol was measured on 12 selected slices (Bayle, 2008). The segmentation process and the parameter measurements were carried out by two of us (CF and PB). The interobserver error was evaluated for the enamel and dentine volume of two extant human specimens of our sample, and did not exceed 3% in each case.

Table 1
List of fossil and extant human dm_2s.

Taxon	Specimen	Country	Side	Source	Wear stage[d]
Neanderthals	Abri Suard S14-5	France	R	Bayle et al. (2010), available in NESPOS[a]	2
	Abri Suard S37	France	R	Bayle et al. (2010), available in NESPOS[a]	1
	Abri Suard S42	France	R	Bayle et al. (2010), available in NESPOS[a]	1
	Cavallo A	Italy	L	Original data	5
	Couvin	Belgium	R	Toussaint et al. (2010)	3
	Engis 2	Belgium	R	Toussaint et al. (2010)	3
	Krapina d62	Croatia	L	Available in Nespos[a]	2
	Krapina d63	Croatia	L	Available in Nespos[a]	3
	Krapina d64	Croatia	L	Available in Nespos[a]	3
	Roc de Marsal 1	France	L	Bayle et al. (2009a), available in NESPOS[a]	1
UPMH[b]	Lagar Velho 1	Portugal	R	Bayle et al. (2010), available in NESPOS[a]	2
	La Madeleine 4	France	L	Bayle et al. (2009b), available in NESPOS[a]	1
Extant humans	From Medieval and contemporary samples[c]	Austria ¼ 1	L	From Bayle et al. (2010), NESPOS[a], and original data	Wear stage 1 ¼ 10
		France ¼ 7	L		Wear stage 2 ¼ 4
		Italy ¼ 8	L		Wear stage 3 ¼ 2

[a] NESPOS Database/www.nespos.org.
[b] UPMH ¼ Upper Paleolithic Modern Humans.
[c] Hosted at the Department of Anthropology (University of Vienna, Austria), the University of Bordeaux, the Institut d'Anatomie of Strasbourg (France), and the Department of History and Method for the Conservation of Cultural Heritage, University of Bologna (Ravenna, Italy).
[d] Based on Smith (1984).

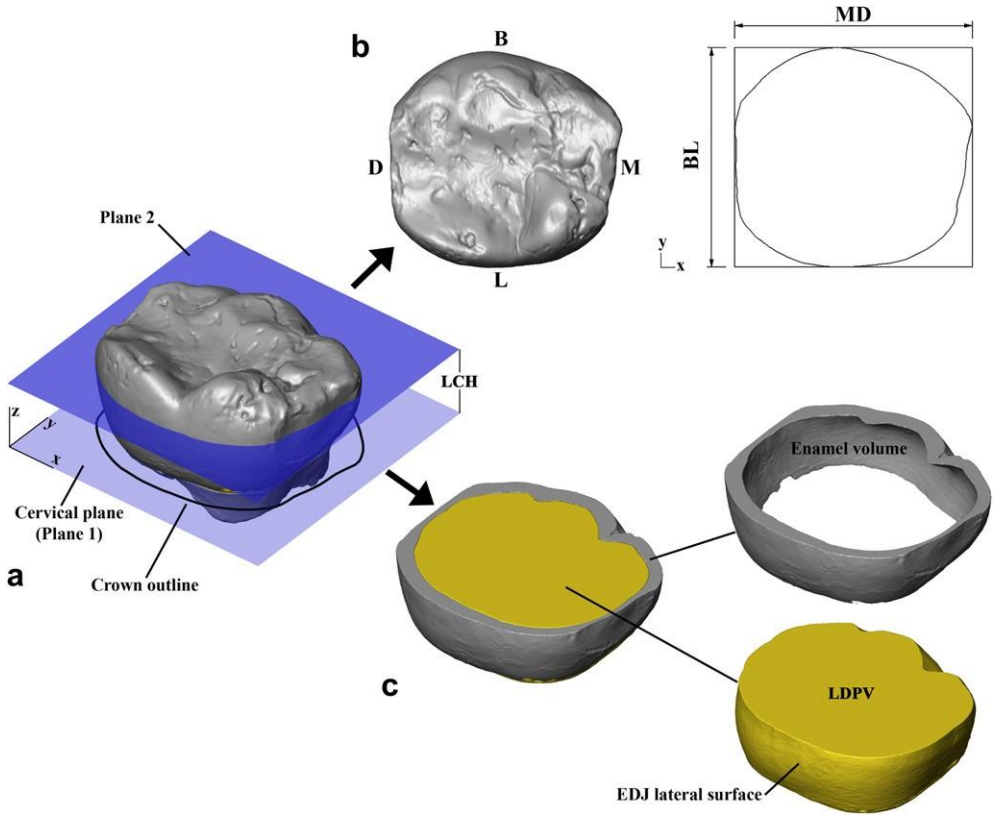

Figure 1. a) The Neanderthal specimen Cavallo A (Grotta del Cavallo, Puglia, Italy; Palma di Cesnola and Messeri, 1967; Palma di Cesnola, 2001) was aligned with the cervical plane (Plane 1) parallel to the *xy*-plane of the Cartesian coordinate system and with the mesiodistal groove parallel to the *x*-axis. To identify the portion of the crown for lateral enamel thickness analysis, a second plane (Plane 2) was created parallel to Plane 1, passing through the lowest point of the enamel-dentine junction in the mid-occlusal basin (Toussaint et al., 2010). To measure the crown diameters, the crown outline was projected in the cervical plane and (b) inscribed in a bounding box, the sides of which provide the buccolingual (BL) and mesiodistal (MD) diameters. (c) Enamel volume, lateral dentine plus pulp volume (LDPV) and enamel-dentine junction (EDJ) lateral surface, used for lateral enamel thickness measurement. LCH ¼ lateral crown height.

Morphometric analysis

A morphometric analysis of the dm_2 sample based on traditional BL and MD diameters was carried out to evaluate the variability of the sample studied compared with a larger Neanderthal and UPMH sample of diameters acquired from the supplementary material provided by Toussaint et al. (2010).

The BL and MD diameters were obtained digitally and measured at the level of the crown outline, as follows. The cervical lines of the teeth were manually digitized by a polyline in the IMEdit module of PolyWorks® 10 (InnovMetric Software Inc.). Vertices were selected within ±0.2 mm of the cervical polyline and a best-fit plane through those selected vertex points was computed (cervical plane ∈ Plane 1 in Fig. 1a). Each tooth was then rotated until the cervical plane was parallel to the *xy*-plane of the Cartesian coordinate system. In order to align the teeth, each model was rotated along the *z*-axis until the mesiodistal groove was parallel to the *x*-axis. The crown outline was projected onto the cervical plane in Rhino 4.0 Beta CAD environment (Robert McNeel & Associates, Seattle, WA) (Fig. 1a). To identify the MD and BL diameters, the crown outline was inscribed in a bounding box tangential to the most extreme points of the crown sides (Fig. 1b).

Enamel thickness analysis

The best-fit plane at the cervix (plane 1 in Fig. 1a) of every tooth was imported into Amira. In order to follow the method of Toussaint et al. (2010) (but see also Olejniczak, 2006), this plane was used to re-align the micro-tomographic image stacks. To evaluate only the lateral aspect of the enamel thickness, another plane (plane 2) was drawn parallel to plane 1, which passed through the lowest point of the enamel-dentine junction in the mid-occlusal basin (Toussaint et al., 2010) (Fig. 1a). Only the region of the tooth between these two planes was used to measure lateral enamel thickness (for standard 3D enamel thickness measurements, see, e.g., Kono, 2004; Macchiarelli et al., 2006; Olejniczak, 2006; Olejniczak et al., 2008). Fig. 1c shows the three measurements derived from this portion of the crown: the enamel volume (mm^3), the lateral dentine plus pulp

Table 2
Enamel thickness of the Neanderthal dm_2 Abri Suard S14-5.

Specimen		Enamel volume (mm^3)	LDPV[a] (mm^3)	EDJ lateral surface (mm^2)	AET[b] (mm)	RET[c] (scale-free)
Abri Suard S14-5	Current results	34.41	196.25	92.17	0.37	6.42
	Toussaint et al. (2010)	33.87	194.82	91.48	0.37	6.39

[a] Lateral dentine plus pulp volume.
[b] Average enamel thickness index.
[c] Relative enamel thickness index.

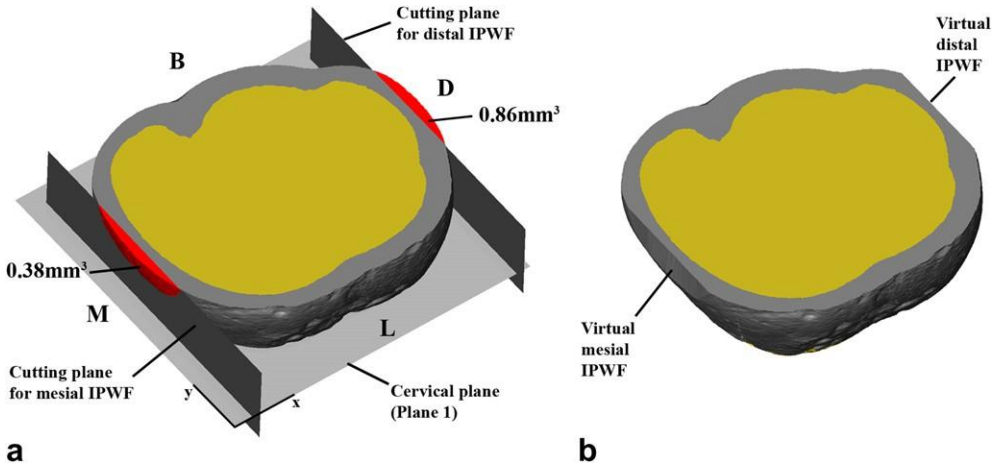

Figure 2. Artificial creation of interproximal wear facets (IPWF) in an unworn modern human dm_2 (ID ¼ Casalmoro T85, from Medieval Italy). (a) Two planes orthogonal to the cervical plane and parallel to the *y*-axis were used to simulate IPWF (cut enamel in red). (b) The new crown with artificial IPWF. (For interpretation of the references to color in this figure legend, the reader is referred to the web version of this article.)

volume (LDPV in mm^3; called "dentine volume" in Toussaint et al., 2010), and the enamel-dentine junction (EDJ) lateral surface (mm^2). These measurements were used for the computation of both the lateral average enamel thickness index (AET ¼ volume of lateral enamel divided by the EDJ lateral surface. This index is in millimeters) and the lateral relative enamel thickness index (RET ¼ AET divided by the cubic root of LDPV. This index is scale-free) (Martin,1985; see also Olejniczak et al., 2008). Finally, for each specimen, except the Couvin and Engis 2 specimens for which this dimension is not available, the distance between the two planes (lateral crown height ¼ LCH) was measured (Fig. 1a).

To verify whether our results are comparable with those obtained by Toussaint et al. (2010), the lateral enamel thickness from the Neanderthal Abri Suard S14-5 specimen was evaluated independently and compared with the results published by Toussaint and colleagues (Table 2).

To evaluate the significance of the differences between Neanderthals and modern humans for all the variables (crown diameters, LCH, LDPV, AET and RET indices), a permutation test (n ¼ 1000) on group mean and variance differences was used. The Quadratic Discriminant Analyses (QDA's) of the same variables were used to classify the specimens. We used QDA because for some of our measurements the within-group variances are different between our two taxonomic groups. When the standard deviations are different, the corresponding log likelihood ratio is in fact a quadratic function (a function of x^2 as well as of x) hence we use a "quadratic" discrimination (e.g., Benazzi et al., 2011a). We used a cross validation approach (leave-one-out method) to assign each of the specimens to the group with the higher posterior probability. For the diameters, the LDPV and the indices the cross-validation QDA was carried out with and without the Couvin and Engis 2 specimens. For data processing and analyses, we used software routines written in "R" software (R Development Core Team, 2008).

Quantification of the effect of IPWF

The lateral aspect of the enamel thickness is usually affected by interproximal wear. To show the effect of interproximal wear facets (IPWF) on the enamel thickness volume, and consequently on the AET and RET indices, we artificially created two IPWFs in an unworn modern human specimen from our sample (ID ¼ Casalmoro T85, from Medieval Italy) (Fig. 2).

With the crown in occlusal view, two planes orthogonal to the cervical plane (Plane 1 of Fig. 1a) and parallel to the *y*-axis were subsequently created. These cutting planes slice the enamel thickness in half at the most mesial and distal regions of the crown in order to create two artificial IPWF (cut enamel in red in Fig. 2a): the mesial worn-out volume is 0.38 mm^3, while the distal one is 0.86 mm^3 (total volume removed ¼ 1.24 mm^3). The height of the mesial and distal artificial IPWF is 1.1 mm and 1.7 mm, respectively, while the maximal buccolingual extension is 3.7 mm for the mesial IPWF and 3.2 mm for the distal IPWF. The mesial IPWF of Cavallo A (Fig. 1c; Palma di Cesnola and Messeri, 1967; Palma di Cesnola, 2001) is 1.73 mm high and 4.12 mm wide in the buccolingual direction, and the distal IPWF is 2 mm high and 4.69 mm wide in the buccolingual direction. Since our aim was to give an indication of the effect of interproximal wear in the computation of AET and RET indices, we purposely avoided exaggerating the size of the artificial IPWFs.

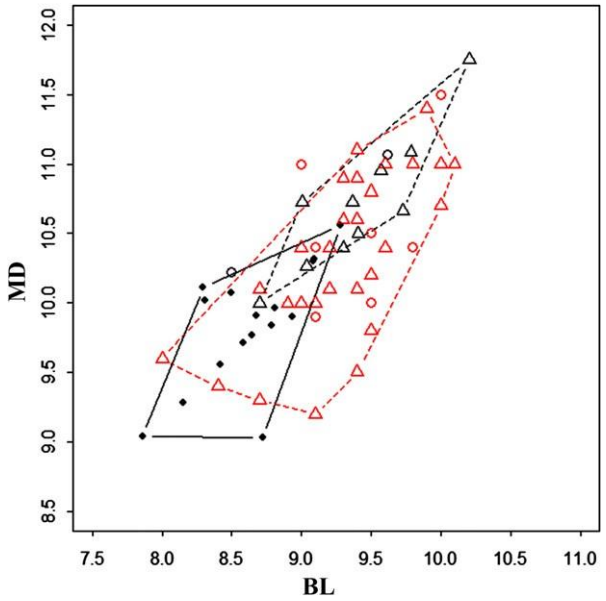

Figure 3. Scatter-plot of the buccolingual (BL) and mesiodistal (MD) diameters (in millimeters). Our sample (black labels) is plotted with a more comprehensive sample (red labels). Extant humans, black circles; Neanderthals, triangles; UPMH, white circles. (For interpretation of the references to color in this figure legend, the reader is referred to the web version of this article.)

Table 3
Descriptive statistics and permutation test of group mean and variance difference of Neanderthal (N) and modern human (MH) dm_2 crown diameters, LCH, LDPV, AET and RET indexes (significant values ($p<0.05$) are presented in bold).

	MH[a]					N					*p*-value
	n	Mean	S.D.	Min	Max	*n*	Mean	S.D.	Min	Max	
BL diameter (mm)	18	8.68	0.42	7.86	9.62	10	9.41	0.44	8.70	10.20	<0.001
MD diameter (mm)	18	9.93	0.51	9.03	11.07	10	10.71	0.49	10.00	11.75	<0.001
LCH[b]	18	2.58	0.22	2.20	2.88	8	3.03	0.23	2.56	3.24	<0.001
LDPV[c]	18	138.20	19.49	103.70	168.50	10	183.70	28.22	132.80	227.20	<0.001
AET[d]	18	0.41	0.05	0.33	0.50	10	0.37	0.07	0.27	0.49	0.095
RET[e]	18	7.91	0.85	6.00	9.18	10	6.54	1.17	4.89	8.09	0.005

[a] Extant humans and UPMH.
[b] Lateral crown height (mm).
[c] Lateral dentine plus pulp volume (mm^3).
[d] Average enamel thickness index (in mm).
[e] Relative enamel thickness index (scale-free).

Results

The BL and MD diameters of our sample, characterized by black labels, were combined with data from Neanderthal (n ¼ 28) and UPMH (n ¼ 7) specimens provided by Toussaint et al. (2010: Supplementary Tables 1 and 2), that appear as red labels in Fig. 3. The Neanderthal specimens in our sample (black triangles) have large diameters and are not representative of the Neanderthal variability (red triangles). Even though our modern human sample (black circles) has smaller diameters, it is well imbedded in the Neanderthal range. Accordingly, Fig. 3 emphasizes two aspects: (1) as generally admitted, the crown diameters are not useful for separating the two taxa, and (2) a sampling bias affects our sample.

Table 3 provides the descriptive statistics of the Neanderthal and modern human dm_2 sample. The result of the permutation test emphasizes the significant difference between the means of the diameters, the LCH (see also Fig. 4a), the LDPV (Fig. 4b) and the RET index (Fig. 4c) for the two taxa. The AET index is not significantly different between the two taxa (Table 3, Fig. 4d).

The results of the cross-validation QDA without the Couvin and Engis 2 specimens (26 specimens considered in the analysis) show that between 84.6% and 92.3% of the Neanderthals and modern humans are correctly classified based on crown dimensions (diameters and LCH, respectively). The LDPV allows a correct classification of 88.5% of the specimens, while a high misclassification is obtained for both the AET and RET index (Table 4). The values of

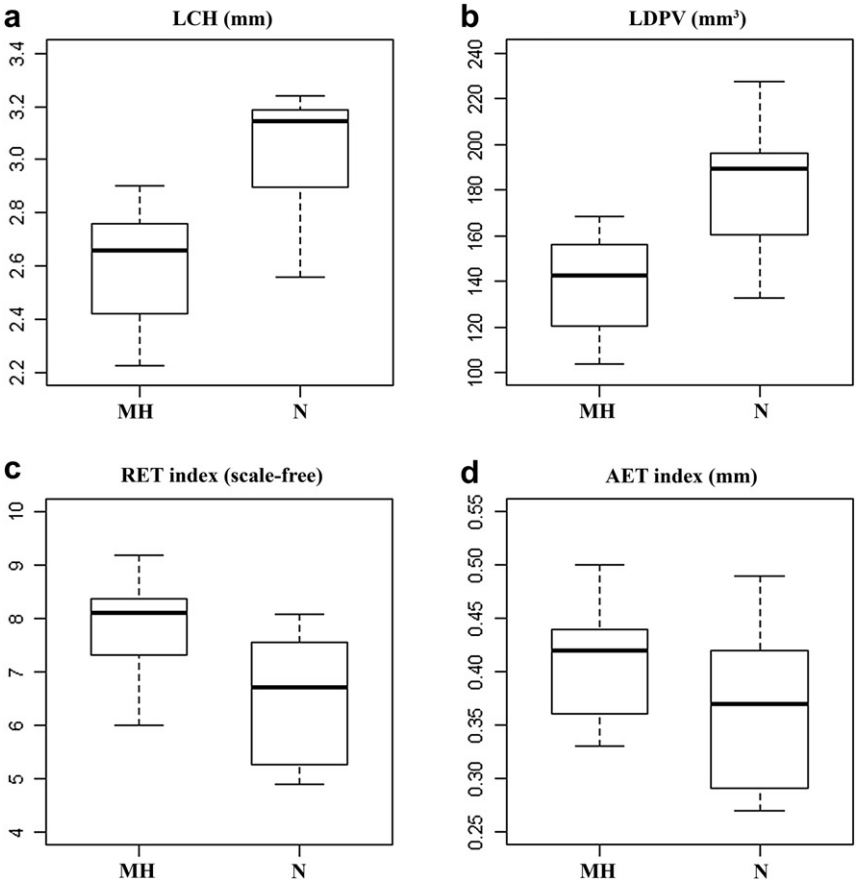

Figure 4. Box-plot of the LCH e lateral crown height (a), LDPV e lateral dentine plus pulp volume (b), RET index (c) and AET index (d). MH ¼ modern human; N ¼ Neanderthal.

Table 4
Results of the cross-validation QDA for the dm_2 with (n ¼ 28) and without Couvin and Engis 2 specimens (n ¼ 26).

Dental measurements	Misclassified			Total misclassified	Correctly classified (%)	Misclassified			Total misclassified	Correctly classified (%)
	n	MH[a]	N[b]			n[c]	MH[a]	N[b]		
Diameters[d]	26	2	2	4	84.6%	28	3	3	6	78.6%
LCH[e]	26	0	2	2	92.3%					
LDPV[f]	26	1	2	3	88.5%	28	1	3	4	85.7%
AET[g]	26	1	8	9	65.4%	28	1	7	8	71.4%
RET[h]	26	3	5	8	69.2%	28	3	5	8	71.4%

[a] Extant humans and UPMH.
[b] Neanderthals.
[c] Couvin and Engis 2 are included in the cross-validation QDA.
[d] Both the diameters (MD and BL) are considered.
[e] Lateral crown height (mm).
[f] Lateral dentine plus pulp volume (mm^3).
[g] Average enamel thickness index (in mm).
[h] Relative enamel thickness index (scale-free).

the AET and RET indices do not change importantly when the Couvin and Engis 2 specimens are included in the analysis. Despite the QDA shows a decrease in the number of correctly classified teeth by the LDPV (85.7%) and the diameters (78.6%), these parameters remain preferable to the AET and RET indices (Table 4).

Table 5 shows the effect that IPWF can produce on the AET and RET indices. As the dentine volume is not affected by interproximal wear, an increase in IPWF size produces a reduction of the RET index. When the tooth used for exemplification purposes is virtually worn out (Casalmore T85) its RET index drops from 6.82 to a value close to the Neanderthal mean (6.47) (Tables 3 and 5).

Discussion

In a number of publications, efforts have been made to characterize Neanderthal teeth derived from size measurements and assessment of occlusal morphology (e.g., Bailey, 2002, 2004). Additionally, dental tissue proportions and enamel thickness distribution have been used (e.g., Olejniczak and Grine, 2005; Macchiarelli et al., 2006; Olejniczak et al., 2008). Compared with modern humans, Neanderthal molars are generally characterized by similar absolute enamel volumes, but deposited over a topographically more complex enamel-dentine junction surface and larger volumes of dentine, thus resulting in lower average and relative enamel thickness values (Macchiarelli et al., 2006; Olejniczak et al., 2008; Bayle et al., 2009a), which provides an additional diagnostic feature for separating taxa (Olejniczak et al., 2008). The use of the enamel of the lateral walls of a tooth has been suggested for taxonomic purposes when dealing with heavily worn dm_2 (Toussaint et al., 2010).

Since several morphometric approaches have been proposed for dental analyses, it is of importance to evaluate their reliability for taxonomic assignment of Neanderthal and modern human teeth.

The results of our analysis on dm_2 show that the lateral average enamel thickness (AET) index is not significantly different between Neanderthals and modern humans. Conversely, we confirm that Neanderthal dm_2s have a statistically significant lower lateral relative enamel thickness (RET) index, but only 70% of the specimens in our sample were correctly classified (Table 4).

The Neanderthal dm_2 sample studied has significantly longer BL and MD diameters compared with those of modern humans. Therefore, a correct taxonomic classification of our specimens is possible by using only these two linear measurements (Table 4). However, as aforementioned, our sample is biased because we know that in a more comprehensive sample, Neanderthals and modern humans crown diameters should largely overlap (Fig. 3). In spite of this bias and of the wide chronological distribution of the fossil sample (OIS6-OIS3), the RET index fails to correctly classify the two groups.

Moreover, in many cases the IPWF alters the MD crown diameter as well as the AET and RET indices. For MD diameter measurements, the 2D crown outline can be reconstructed following Wood and Engleman (1988; see also Bailey, 2004). Nevertheless, we have verified that for three Neanderthals and two modern humans, for which an outline reconstruction can be conducted, differences between uncorrected and corrected MD diameters are less than 0.15 mm. The maximum difference was found in Cavallo A: uncorrected ¼ 10.51 mm; corrected ¼ 10.66 mm. Considering that for the Couvin and Engis 2 specimens only the uncorrected MD diameters are available, their 2D crown outlines were not reconstructed. On the contrary, a method for 3D virtual reconstruction of the IPWF has not been developed thus far. Therefore, since the RET index is a function of the enamel thickness, the values we obtained are certainly lower than if computed for the unworn teeth (see also Table 5). Interproximal tooth wear is produced by tooth-to-tooth contact and crown movements occurring during the chewing cycle (Picton, 1962; Kieser et al., 1985; Benazzi et al., 2011b). Since it is an age-related process (Kieser et al., 1985), we can assume that the amount of enamel lost by interproximal wear tends to be larger in advanced dental wear stages. The Neanderthal specimens of our sample show, on average, a higher wear stage compared with the modern humans (Table 1). Therefore, we assume that a larger IPWF affects the computation of the indices. As shown in our IPWF simulation, a decrease in enamel volume of 1.24 mm^3 (5.2% of the enamel volume) reduces the RET index from 6.82 to 6.47 (Table 5).

Table 5
Enamel thickness of a specimen from the extant human sample before and after artificial IPWF creation.

Specimen		Enamel volume (mm^3)	LDPV[a] (mm^3)	EDJ lateral surface (mm^2)	AET[b] (mm)	RET[c] (scale-free)
Casalmoro T85	Original crown	23.80	138.13	67.50	0.35	6.82
	Artificial IPWF	22.56	138.13	67.50	0.33	6.47

[a] Lateral dentine plus pulp volume.
[b] Average enamel thickness index.
[c] Relative enamel thickness index.

We agree that Neanderthals show larger dentine volumes and consequently lower RET indices compared with modern humans (e.g., Macchiarelli et al., 2006, 2008; Olejniczak et al., 2008; Toussaint et al., 2010). However, we have to emphasize that the lateral enamel thickness method has to be applied cautiously for taxonomic assessment purposes because it strongly depends on the magnitude of the interproximal wear and on the completeness of the preserved lateral crown surface (missing enamel portions reduce the RET index).

As we quantitatively stressed in our analysis, the lateral dentine plus the pulp volume (LDPV) and the height of the lateral wall of the crown (LCH), represent more stable measures in this context, independent of both occlusal and interproximal wear and missing enamel portions.

Conclusions

Our analysis of the lateral enamel thickness in Neanderthal and modern human dm_2s confirms that Neanderthals and modern humans do not differ in average enamel thickness index. On the other hand, Neanderthal dm_2s show a larger absolute lateral dentine plus pulp volume (LDPV) and have a consequently lower lateral RET index. While the lateral RET index e and, to a lower extent, the MD diameter as well e are influenced by the interproximal wear, the LCH and the LDPV are more often unaltered in dental remains. We thus propose using those parameters to discriminate between Neanderthals and modern humans in the case of isolated (and worn out) dm_2s.

Despite our intention to use a representative fossil sample, we are aware that our sample cannot account for the whole variability of Neanderthal and UPMH dm_2. Therefore, we emphasize that the results mentioned above are relevant for our dm_2 sample, and that further work on the subject with a larger sample is in progress.

Acknowledgments

Access to the fossil specimens was made possible by the Croatian Natural History Museum, the French Musée de Préhistoire, the Musée d'Angoulême, the Portuguese Ministério da Cultura, via the NESPOS database (https://www.nespos.org/display/openspace/Home). We acknowledge the Centre de Microtomographie at the Université de Poitiers (R. Macchiarelli, A. Mazurier, P. Sardini), the ESRF beamline ID17, Grenoble (A. Bravin, C. Nemoz, P. Tafforeau), and the NESPOS Society. The authors would like to thank G. Gruppioni for providing the modern human sample used in this work. We finally thank A.G. Drake and C.N. Shaw for their comments on the last draft of this manuscript and the English editing. This work was supported by NSF 01-120 Hominid Grant 2007, and the Fyssen Foundation.

References

Bailey, S.E., 2002. A closer look at Neanderthal postcanine dental morphology: the mandibular dentition. Anat. Rec. 269, 148e156.

Bailey, S.E., 2004. A morphometric analysis of maxillary molar crowns of Middle-Late Pleistocene hominins. J. Hum. Evol. 47, 183e198.

Bayle, P., 2008. Analyses quantitatives par imagerie à haute resolution des séquences de maturation dentaire et des proportions des tissus des dents déciduales chez les Néanderthaliens et les Hommes modernes. Ph.D. Dissertation, University Toulouse III e Paul Sabatier.

Bayle, P., Braga, J., Mazurier, A., Macchiarelli, R., 2009a. Dental developmental pattern of the Neanderthal child from Roc de Marsal: a high-resolution 3D analysis. J. Hum. Evol. 56, 66e75.

Bayle, P., Braga, J., Mazurier, A., Macchiarelli, R., 2009b. Brief communication: high-resolution assessment of the dental developmental pattern and characterization of tooth tissue proportions in the late Upper Paleolithic child from La Madeleine, France. Am. J. Phys. Anthropol. 138, 493e498.

Bayle, P., Macchiarelli, R., Trinkaus, E., Duarte, C., Mazurier, A., Zilhão, J., 2010. Dental maturational sequence and dental tissue proportions in the early Upper Paleolithic child from Abrigo do Lagar Velho. Portugal. Proc. Natl. Acad. Sci. 107, 1338e1342.

Benazzi, S., Coquerelle, M., Fiorenza, L., Bookstein, F., Katina, S., Kullmer, O., 2011a. Comparison of dental measurement systems for taxonomic assignment of first molars. Am. J. Phys. Anthropol. 144, 342e354.

Benazzi, S., Fiorenza, L., Katina, S., Bruner, E., Kullmer, O., 2011b. Quantitative assessment of interproximal wear facet outlines for the association of isolated molars. Am. J. Phys. Anthropol. 144, 309e316.

Kieser, J.A., Groeneveld, H.T., Preston, C.B., 1985. Patterns of dental wear in the Lengua Indians of Paraguay. Am. J. Phys. Anthropol. 66, 21e29.

Kono, R., 2004. Molar enamel thickness and distribution patterns in extant great apes and humans: new insights based on a 3-dimensional whole crown perspective. Anthropol. Sci. 112, 121e146.

Macchiarelli, R., Bondioli, L., Debénath, A., Mazurier, A., Tournepiche, J.-F., Birch, W., Dean, C., 2006. How Neanderthal molar teeth grew. Nature 444, 748e751.

Macchiarelli, R., Bondioli, L., Mazurier, A., 2008. Virtual dentitions: touching the hidden evidence. In: Irish, J.D., Nelson, G.C. (Eds.), Technique and Application in Dental Anthropology. Cambridge University Press, Cambridge, UK, pp. 426e448.

Macchiarelli, R., Mazurier, A., Volpato, V., 2007. L'apport des nouvelles technologies à l'étude des Néandertaliens. In: Vandermeersch, B., Maureille, B. (Eds.), Les Néandertaliens. Biologie et Cultures. CTHS, Paris, pp. 169e179.

Martin, L., 1985. Significance of enamel thickness in hominoid evolution. Nature 314, 260e263.

Olejniczak, A.J., 2006. Micro-Computed Tomography of Primate Molars. Ph.D. Dissertation, Stony Brook University.

Olejniczak, A.J., Grine, F.E., 2005. High-resolution measurement of Neanderthal tooth enamel thickness by micro-focal computed-tomography. S. Afr. J. Sci. 101, 219e220.

Olejniczak, A.J., Smith, T.M., Feeney, R.N.M., Macchiarelli, R., Mazurier, A., Bondioli, L., Rosas, A., Fortea, J., de la Rasilla, M., Garcia-Tabernero, A., Radovcic', J., Skinner, M.M., Toussaint, M., Hublin, J.J., 2008. Molar tissue proportions and enamel thickness distinguish Neanderthals from modern humans. J. Hum. Evol. 55, 12e23.

Palma di Cesnola, A., 2001. Il Paleolitico inferiore e medio in Italia. MILLENNI, Collana del Museo Fiorentino di Preistoria "Paolo Graziosi" Firenze.

Palma di Cesnola, A., Messeri, M.P., 1967. Quatre dents humaines paléolithiques trouvées dans des cavernes de l'Italie Méridionale. L'Anthropologie 71, 249e262.

Picton, D.C.A., 1962. Tilting movements of teeth during biting. Arch. Oral Biol. 7, 151e159.

R Development Core Team, 2008. R: a Language and Environment for Statistical Computing. R Foundation for Statistical Computing, Vienna, Austria, ISBN 3-900051-07-0. http://www.r-project.org.

Ramirez Rozzi, F., 1996. Comment on the causes of thin enamel in Neanderthals. Am. J. Phys. Anthropol. 99, 625e626.

Smith, B.H., 1984. Patterns of molar wear in hunter-gatherers and agriculturists. Am. J. Phys. Anthropol. 63, 39e56.

Smith, P., Zilberman, U., 1994. Thin enamel and other tooth components in Neanderthals and other hominids. Am. J. Phys. Anthropol. 95, 85e87.

Smith, T.M., Tafforeau, P., Reid, D.J., Grün, R., Eggins, S., Boutakiout, M., Hublin, J.J., 2007a. Earliest evidence of modern human life history in North African early *Homo sapiens*. Proc. Natl. Acad. Sci. 104, 6128e6133.

Smith, T.M., Tafforeau, P., Reid, D.J., Pouech, J., Lazzari, V., Zermeno, J.P., Guatelli-Steinberg, D., Olejniczak, A.J., Hoffman, A., Radovcic, J., Makaremi, M., Toussaint, M., Stringer, C., Hublin, J.J., 2010. Dental evidence for ontogenetic differences between modern humans and Neanderthals. Proc. Natl. Acad. Sci. 107, 20923e20928.

Smith, T.M., Toussaint, M., Reid, D.J., Olejniczak, A.J., Hublin, J.J., 2007b. Rapid dental development in a Middle Paleolithic Belgian Neanderthal. Proc. Natl. Acad. Sci. 104, 20220e20225.

Spoor, F., Zonneveld, F., Macho, G.A., 1993. Linear measurements of cortical bone and dental enamel by computed tomography: applications and problems. Am. J. Phys. Anthropol. 91, 469e484.

Toussaint, M., Olejniczak, A.J., El Zaatari, S., Cattelain, P., Flas, D., Letourneux, C., Pirson, S., 2010. The Neanderthal lower right deciduous second molar from Trou de l'Abîme at Couvin, Belgium. J. Hum. Evol. 58, 56e67.

Wood, B.A., Engleman, C.A., 1988. Analysis of the dental morphology of Plio-Pleistocene hominids: V. Maxillary postcanine tooth morphology. J. Anat. 161, 1e35.

Zilberman, U., Skinner, M., Smith, P., 1992. Tooth components of mandibular deciduous molars of Homo sapiens sapiens and Homo sapiens neanderthalensis: a radiographic study. Am. J. Phys. Anthropol. 87, 255e262.

Zilberman, U., Smith, P., 1992. A comparison of tooth structure in Neanderthals and early Homo sapiens sapiens: a radiographic study. J. Anat. 180, 387e393.

2.2. Early dispersal of modern humans in Europe and implications for Neanderthal behaviour

Benazzi, S., Douka, K., Fornai, C., Bauer, C.C., Kullmer, O., Svoboda, J., Pap, I., Mallegni, F., Bayle, P., Coquerelle, M., Condemi, S., Ronchitelli, A., Harvati, K., Weber, G.W.

Nature 2011; 479, 525-528.

Synopsis
This chapter reports the outcome of a project that combined state-of-the-art techniques from two different fields of research: dental morphometrics and radiocarbon dating. Two upper deciduous molars from the Uluzzian site Grotta del Cavallo, Apulia, Italy were investigated to assess their taxonomic attribution. Based on the analysis of the enamel thickness and the geometric morphometric investigation of crown and cervical outlines, these teeth, previously thought as belonging to Neanderthals, were re-classified as modern humans. This reassessment of the Cavallo teeth has had important implications for the interpretation of the Uluzzian culture and their makers. This evidence, together with a re-dating of the shell-beads associated with the teeth to an earlier date (about 45,000–43,000 calendar years), suggested that modern humans reached the European continent through a Mediterranean route prior to the Aurignacian.

Contribution
Participation in data collection, discussion of the data, and editing of the manuscript.

LETTER

doi:10.1038/nature10617

Early dispersal of modern humans in Europe and implications for Neanderthal behaviour

Stefano Benazzi[1], Katerina Douka[2], Cinzia Fornai[1], Catherine C. Bauer[3], Ottmar Kullmer[4], Jiří Svoboda[5,6], Ildikó Pap[7], Francesco Mallegni[8], Priscilla Bayle[9], Michael Coquerelle[10], Silvana Condemi[11], Annamaria Ronchitelli[12], Katerina Harvati[3,13] & Gerhard W. Weber[1]

The appearance of anatomically modern humans in Europe and the nature of the transition from the Middle to Upper Palaeolithic are matters of intense debate. Most researchers accept that before the arrival of anatomically modern humans, Neanderthals had adopted several 'transitional' technocomplexes. Two of these, the Uluzzian of southern Europe and the Châtelperronian of western Europe, are key to current interpretations regarding the timing of arrival of anatomically modern humans in the region and their potential interaction with Neanderthal populations. They are also central to current debates regarding the cognitive abilities of Neanderthals and the reasons behind their extinction[1–6]. However, the actual fossil evidence associated with these assemblages is scant and fragmentary[7–10], and recent work has questioned the attribution of the Châtelperronian to Neanderthals on the basis of taphonomic mixing and lithic analysis[11,12]. Here we reanalyse the deciduous molars from the Grotta del Cavallo (southern Italy), associated with the Uluzzian and originally classified as Neanderthal[13,14]. Using two independent morphometric methods based on microtomographic data, we show that the Cavallo specimens can be attributed to anatomically modern humans. The secure context of the teeth provides crucial evidence that the makers of the Uluzzian technocomplex were therefore not Neanderthals. In addition, new chronometric data for the Uluzzian layers of Grotta del Cavallo obtained from associated shell beads and included within a Bayesian age model show that the teeth must date to ~45,000–43,000 calendar years before present. The Cavallo human remains are therefore the oldest known European anatomically modern humans, confirming a rapid dispersal of modern humans across the continent before the Aurignacian and the disappearance of Neanderthals.

Two deciduous molars (Cavallo-B and Cavallo-C) were excavated in 1964 from the site of Grotta del Cavallo (Apulia, southern Italy; Supplementary Information). Cavallo is important as the type site of the Uluzzian technocomplex[15], one of the three main transitional industries alongside the Châtelperronian and Szeletian, in Cantabria and Central Europe, respectively. These are strongly suspected of being produced by Neanderthals, although the actual fossil evidence in association is scant[16].

Cavallo-B is a deciduous left upper first molar (dM^1), found in layer EIII (archaic Uluzzian). Cavallo-C is a deciduous left upper second molar (dM^2) found 15–20 cm above Cavallo-B, in layer EII-I (evolved Uluzzian)[13] (Supplementary Fig. 1 and Supplementary Table 1). The specimens (Fig. 1) were described in 1967 by Palma di Cesnola and

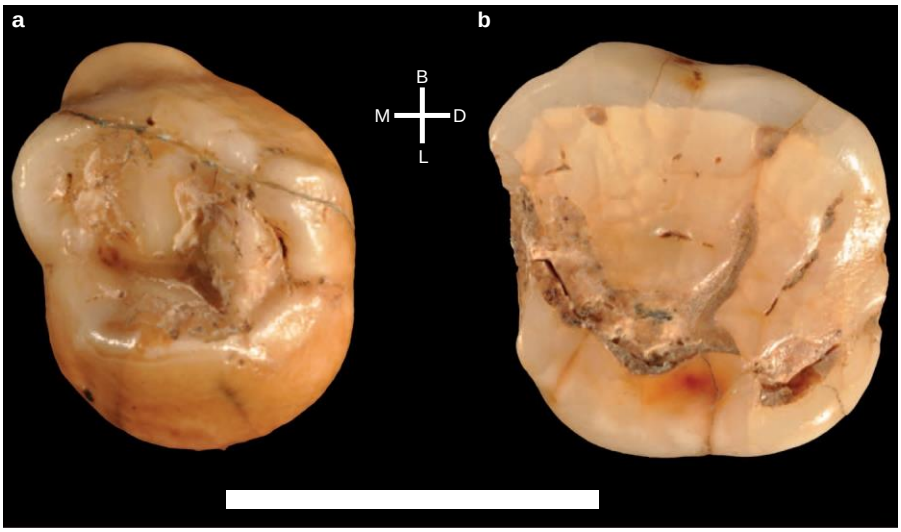

Figure 1 | Occlusal view of the deciduous molars from the Uluzzian layers of Grotta del Cavallo (Apulia, southern Italy). a, Cavallo-B (deciduous left upper first molar; dM^1). b, Cavallo-C (deciduous left upper second molar; dM^2). B, buccal; D, distal; L, lingual; M, mesial. Scale bar, 1 cm.

[1]Department of Anthropology, University of Vienna, Althanstrasse 14, 1090 Vienna, Austria. [2]Oxford Radiocarbon Accelerator Unit, Research Laboratory for Archaeology and the History of Art, University of Oxford, Dyson Perrins Building, South Parks Road, Oxford OX1 3QY, UK. [3]Paleoanthropology, Department of Early Prehistory and Quaternary Ecology, Eberhard Karls Universität Tübingen, Rümelinstrasse 23, Tübingen 72070, Germany. [4]Department of Paleoanthropology and Messel Research, Senckenberg Research Institute Frankfurt, Senckenberganlage 25, D-60325 Frankfurt, Germany. [5]Institute of Archaeology, Academy of Sciences of the Czech Republic, Královopolská 147, 612 00 Brno, Czech Republic. [6]Department of Anthropology, Faculty of Science, Masaryk University, Vinařská 5, 603 00 Brno, Czech Republic. [7]Department of Anthropology, Hungarian Natural History Museum, Ludovika tér 2-6, 1083 Budapest, Hungary. [8]Department of Biology, University of Pisa, Via S. Maria 53, 56126 Pisa, Italy. [9]UMR 5199 PACEA, Université Bordeaux 1, avenue des Facultés, 33405 Talence, France. [10]Paleoanthropology group, Department of Paleobiology Museo Nacional de Ciencias Naturales (MNCM-CSIC), C/ José Gutiérrez Abascal 2, 28006 Madrid, Spain. [11]UMR 6578 CNRS/Aix Marseille/EFS, Laboratoire d'Anthropologie Bioculturelle, Faculté de Médecine/Secteur Nord, CS80011 Bd Pierre Dramard 13344, Marseille Cedex 15, France. [12]Department of Environmental Sciences "G. Sarfatti", U.R. Prehistoric Ecology, University of Siena, via T. Pendola 62, 53100 Siena, Italy. [13]Senckenberg Center for Human Evolution and Paleoecology, Eberhard Karls Universität Tübingen, Rümelinstrasse 23, Tübingen 72070, Germany.

Messeri[13] who classified Cavallo-B as modern human and Cavallo-C as Neanderthal. On this basis, the authors suggested a persistence of Neanderthal populations in southern Italy after the appearance of modern humans[17].

Although information about these specimens is scarce and contradictory, most scholars accept that the deciduous molars from Grotta del Cavallo are attributable to Neanderthals, and therefore that Neanderthals produced the Uluzzian. This attribution was proposed by ref. 14 for Cavallo-B on the basis of the specimen's crown diameters

Neanderthals and anatomically modern humans). However, the Cavallo-B buccolingual and mesiodistal diameters used by ref. 14 appear to have been accidentally substituted for each other when compared to the crown diameters reported by ref. 13. The correct crown diameter values do not support Neanderthal affinities for Cavallo-B, neither does the crown morphology of the two specimens. Cavallo-B shows three dental cusps, typical of dM^1 (ref. 10) from anatomically modern humans, with the lingual cusps mesially oriented and separated from the buccal cusps by a well-defined sagittal sulcus. Conversely, the dM^1 of Neanderthals is more frequently four-cusped, with cusp tips compressed internally[10]. Cavallo-C has a sub-square crown outline, similar to dM^2 of anatomically modern humans and different from the typical rhomboid outline with distolingual hypocone expansion of Neanderthal dM^2s (ref. 10).

To establish firmly the taxonomic affinities of the Cavallo human remains, we re-analysed Cavallo-B and Cavallo-C with two independent morphometric methods, using a comparative sample of Neanderthal, Upper Palaeolithic modern human (UPMH) and recent modern human (RMH) dM^1 and dM^2 specimens (Supplementary Tables 2–4).

Our first approach is a geometric morphometric analysis of outlines obtained from the dental crown[18] (see Methods), for which the group shape variation was evaluated through a shape–space principal component analysis (PCA).

For the dM^1 crown outlines (Fig. 2a), the first two principal components (PCs) account for about 63% of the total variance. Neanderthals and modern humans separate along PC1 (42.7%), which characterizes size-independent shape variation ($r = 20.33$; $P = 0.06$). Neanderthal dM^1 specimens show an ovoid outline, whereas RMH and UPMH specimens are more irregularly shaped for the presence of well-expressed tuberculum molare (molar tubercle of Zuckerkandl) and metacone (buccodistal) cusp, and for a general distolingual constriction due to the reduction of the hypocone. Cavallo-B plots well within the range of variability of the anatomically modern human sample. The cross-validation quadratic discriminant analysis (QDA) of the PC1 scores classified Cavallo-B as modern human with a posterior probability (P_{post}) . 0.90 (Supplementary Table 4).

In the analysis of the dM^2 cervical outlines (Fig. 2b), the first two PCs account for about 84% of the total variance. Neanderthals and anatomically modern humans are even more clearly separated along PC1 (71.4%), which expresses size-dependent shape variation (static allometry, $r = 0.74$; P , 0.001). Neanderthal dM^2 specimens are characterized by a rhomboid cervical outline due to their large hypocone, whereas UPMH and RMH specimens have sub-square outlines. Cavallo-C plots unambiguously within the modern human range. The cross-validation QDA of the first two PC scores attributes Cavallo-C to modern human with a P_{post} . 0.90 (Supplementary Table 4).

The second morphometric method considers the internal structure of the teeth and consists of the two-dimensional enamel thickness and dental tissue proportions analysis (Fig. 3) (see Methods and Supplementary Tables 3 and 4). The average and relative enamel thickness (AET and RET, respectively) have been described as effective taxonomic discriminators between Neanderthals and modern humans because Neanderthal molars are characterized by significantly thinner enamel relative to dentine volume[19].

The dM^1 modern human samples (UPMH and RMH) shown in Table 1 have been divided into sub-groups on the basis of their degree

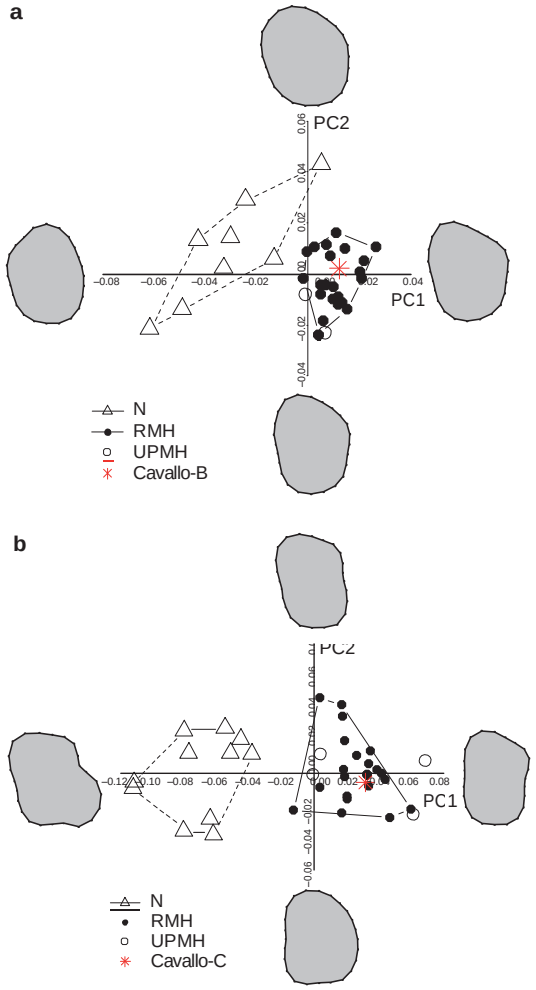

Figure 2 | Shape–space PCA plots of dM^1 crown outlines and dM^2 cervical outlines. a, dM^1 crown outline. b, dM^2 cervical outline. The deformed mean crown outline in the direction of the PC is drawn at the extremity of each axis. N, Neanderthal; RMH, recent modern human; UPMH, Upper Palaeolithic modern human.

of wear (unworn/wear stage 1 distinguished by wear stage 3; based on Smith[20]) to ease the comparison with the Neanderthal dM^1 samples, which is entirely affected by wear stage 3. The Neanderthal dM^1 RET indexes are significantly lower than those of RMH at similar wear stages (P , 0.001; permutation test, $n = 1{,}000$) on group mean and variance differences. The AET and RET indexes of Cavallo-B lie beyond the highest values computed so far for the unworn UPMH and RMH (Table 1). Considering that the RET index average difference from unworn to wear stage 3 for both RMH and UPMH is about 0.80, it is reasonable to assume that if Cavallo-B would have worn down to a wear stage 3, it would provide a RET index of approximately 11. This value is still completely outside the Neanderthal range of variation and near the highest values computed for the unworn RMH. The result further supports strongly the affiliation of Cavallo-B as anatomically modern human rather than Neanderthal.

With regard to the dM^2 specimens (Table 1), the Neanderthal RET indexes are significantly lower than those of RMH (P , 0.001). The UPMH specimens present the highest AET and RET indexes of the whole sample, RMH included. Cavallo-C is the most worn specimen within our dM^2 sample (wear stage 5), therefore the AET and RET indexes result in a rather lower value than could be expected for the unworn stage of the same tooth. Nonetheless, both indexes still rank among the highest values obtained (Table 1). The cross-validation

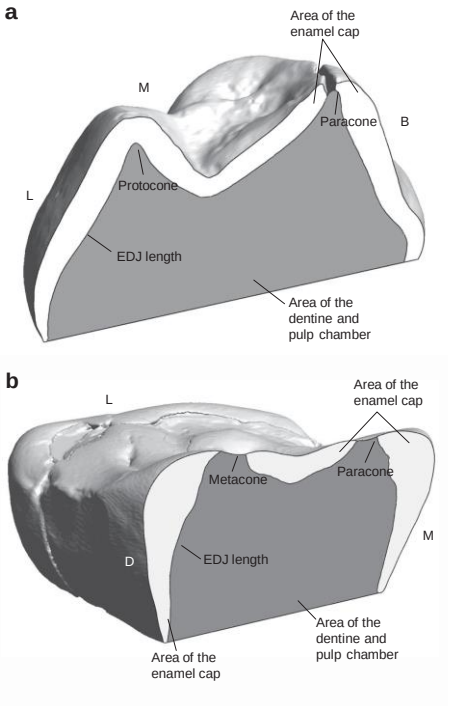

Figure 3 | Cross-sections of Cavallo-B and Cavallo-C for two-dimensional enamel thickness analysis. a, Buccolingual cross-section of Cavallo-B through the dentine horns of the protocone and paracone. b, Mesiodistal cross-section of Cavallo-C through the dentine horns of the paracone and metacone. B, buccal; D, distal; EDJ, enamel–dentin junction; L, lingual; M, mesial.

QDA of the dM^2 RET index classifies Cavallo-C as modern human with a P_{post} .0.90 (Supplementary Table 4).

New radiocarbon dating of the Uluzzian layers was undertaken to produce a more robust chronology. Previous dates from the site disclosed inconsistency due to incomplete decontamination and unsuitability of the dated samples (Supplementary Information). In the absence of collagen from bone at the site and the lack of charcoal samples collected at the time of the excavation, marine shell samples were the only alternative and were therefore selected for dating. In the Uluzzian layers of Cavallo, several shells were transformed into beads, by snapping or piercing to produce personal ornaments. These beads are generally held to be an indicator of symbolic and complex behaviour. Eight shells of *Dentalium* sp., *Nuculana* sp. and *Cyclope neritea* were dated by accelerator mass spectrometry (AMS) radiocarbon dating following a novel methodological approach (Supplementary Information and Supplementary Fig. 3). The new dates were incorporated into a Bayesian model using the OxCal program (Supplementary Information) and calibrated against the INTCAL09 calibration curve[21] (Supplementary Figs 4 and 5 and Supplementary Tables 5 and 6). Layer EIII was calculated by the model to date between 45,010—43,380 (68.2% probability) and 47,530—43,000 (95.4% probability) calendar years before present (where present 5 1950) (cal. yr BP). The distribution falls within Greenland Interstadial (GIS) 12, a long warm phase following Heinrich Event 5, and most likely towards its latter part. A decrease in temperature has been inferred based on the faunal assemblage from EIII (ref. 22). A likely initial arrival of anatomically modern humans during this post-HE5 interstadial has been suggested previously[23]. Layer EII-I, associated with a shell date of 40,000 ^{14}C yr BP, was modelled to date between 44,000—43,000 cal. yr BP (68.2% probability), a similar age to layer EIII. Comparable chronometric results were obtained from Grotta di Fumane, another Uluzzian site in the Italian pre-Alps and the only other with reliable chronometric information, where the technocomplex is dated at 44,800–43,900 cal. yr BP (95.4% probability) (or ,42,000–40,000 ^{14}C yr BP)[24].

The new chronometric results show that the two deciduous molars from Grotta del Cavallo are the earliest European anatomically modern human fossils currently known. Because the Uluzzian technocomplex stratigraphically underlies the earliest Aurignacian in all instances where the two co-occur (for example, Grotta di Castelcivita, Grotta della Cala, Grotta La Fabbrica and Grotta di Fumane)[5], the arrival of the earliest modern humans at these sites must pre-date the Aurignacian. Furthermore, considering that Neanderthals are likely to have survived in most of continental Europe until at least ,40,000 cal. yr BP (ref. 25), our results offer fossil evidence for a longer period of co-existence in Europe between Neanderthals and modern humans.

The re-attribution of the teeth of Grotta del Cavallo to anatomically modern human has implications for the interpretation of the Uluzzian technocomplex[14,16]. The presence of personal ornaments in the form of marine shell beads, worked bone and colorants—including ochre and limonites—in the Uluzzian layers of Grotta del Cavallo[5,6] has been used as direct evidence for Neanderthals reaching behavioural modernity independent of, and before, anatomically modern humans reaching Europe[1,26]. These attributes are all more typical of Upper Palaeolithic industries. This multiple species model for the origin of fully modern behaviour has been considered by some to be an impossible coincidence[27] and a fervent debate has ensued among prehistorians on the behavioural and cognitive capabilities of the makers of the transitional industries found across Europe and the Levant. Our results show that the Uluzzian is not a Neanderthal industry.

Stratigraphically, the Uluzzian is always separated from the final Mousterian by sterile layers, volcanic ash (as in Cavallo), erosional discontinuities or depositional hiatuses, which might suggest that a period of time has elapsed between the two phases. In southern Italy, economic and cultural behaviour of the Uluzzian suggests a greater affinity with the succeeding Aurignacian (with marginally backed tools) than with the final Mousterian[5,6,22]. These findings provide additional support for a modern human authorship of the Uluzzian. Although we cannot extrapolate our conclusions to other transitional industries, our findings indicate that caution should be applied when associating Neanderthals with them, particularly the Chatelperronian and Szeletian (see details of the ongoing debate on this topic[2–4,9,11,12]).

Table 1 | Two-dimensional enamel thickness of Cavallo-B and Cavallo-C compared with the indicated dM^1 and dM^2 samples.

Tooth	Taxon	Wear stage*	*n*	AET (mm)		RET (scale free)	
				Mean	Range	Mean	Range
dM^1	Neanderthal	3	6	0.40 (0.03)	0.37–0.45	7.17 (0.54)	6.61–7.93
dM^1	UPMH	3	2	0.51 (0.01)	0.50–0.52	9.56 (0.13)	9.47–9.66
dM^1	RMH	3	14	0.47 (0.03)	0.43–0.52	9.12 (0.67)	8.50–10.52
dM^1	UPMH	Unworn	1	0.56	– 0.41–	10.36	– 8.66–
dM^1	RMH	Unworn–stage 1	8	0.51 (0.06)	0.58	9.96 (0.96)	11.36
dM^1	Cavallo-B	Unworn	1	0.69	– 0.58–	11.80	– 9.60–
dM^2	Neanderthal	Unworn–stage 1	9	0.63 (0.04)	0.69	10.89 (0.84)	12.39
dM^2	UPMH	Stage 1–stage 2	2	0.97 (0.15)	0.86–1.07	17.93 (1.40)	16.94–18.92
dM^2	RMH	Unworn–stage 3	23	0.73 (0.08)	0.56–0.93	13.84 (1.53)	11.43–18.00
dM^2	Cavallo-C	Stage 5	1	0.74	–	14.28	–

Standard deviation is indicated in brackets. AET, average enamel thickness index; RET, relative enamel thickness index; RMH, recent modern human; UPMH, Upper Palaeolithic modern human.
*Based on ref. 20.

The association of the Uluzzian with anatomically modern humans implies much greater complexity and age depth to the movement of modern humans into Europe and may lend support to a southern Mediterranean route in their dispersal, similar to that identified previously[27] for the spread of the Aurignacian. Although it is during the Aurignacian that certain technological and behavioural innovations efflorescence, such as blade and bladelet-dominated lithic assemblages, bone and ivory tools, art and personal ornaments, the initial appearance of these traits in southern Europe clearly pre-dates this. This discovery has significant implications for our understanding of the earliest presence of anatomically modern humans in Europe, expands the period of overlap between modern humans and Neanderthals and makes it much less likely that Neanderthals developed their own Upper Palaeolithic suite of behaviours before the arrival of anatomically modern humans.

METHODS SUMMARY

The comparative dental sample for both the morphometric outline analyses and the two-dimensional enamel thickness and dental tissue proportions analysis is provided in Supplementary Table 2.

Scans of all the specimens were undertaken by means of industrial and synchrotron-based microtomographic scanners at isotropic voxel length between 15 and 55 mm. The microtomographic image stacks of each tooth were aligned with the cervical plane parallel to the x–y plane of the Cartesian coordinate system. The three-dimensional digital surface models were created semi-automatically by threshold-based segmentation, contour extraction and surface reconstruction.

For the outline analyses we considered the dM^1 crown outlines because Cavallo-B is unworn; conversely, we used the cervical outlines of the dM^2 samples, as Cavallo-C shows both occlusal and interproximal wear. To identify the crown outline and the cervical outline we followed the procedures described previously[18], with some adjustment for our specific case.

For the analyses of the two-dimensional enamel thickness and dental tissue proportions, the following measurements were recorded: the area of the enamel cap (mm^2), the area of the coronal dentine (which includes the coronal pulp; mm^2), the length of the enamel–dentine junction (EDJ; mm), the average enamel thickness (AET) index (the area of the enamel cap divided by the length of the EDJ; index in mm) and the RET index (the average enamel thickness divided by the square root of the coronal dentine area; scale free index)[19,28]. The data were analysed via software routines written in R[29] (Supplementary Information).

Full Methods and any associated references are available in the online version of the paper at www.nature.com/nature.

Received 30 August; accepted 5 October 2011.
Published online 2 November 2011.

1. d'Errico, F., Zilhão, J., Julien, M., Baffier, D. & Pélegrin, J. Neanderthal acculturation in Western Europe? A critical review of the evidence and its interpretation. *Curr. Anthropol.* 39, 1–44 (1998).
2. Gravina, B., Mellars, P. & Ramsey, C. B. Radiocarbon dating of interstratified Neanderthal and early modern human occupations at the Châtelperronian type-site. *Nature* 438, 51–56 (2005).
3. Mellars, P., Gravina, B. & Bronk Ramsey, C. Confirmation of Neanderthal/modern human interstratification at the Châtelperronian type-site. *Proc. Natl Acad. Sci. USA* 104, 3657–3662 (2006).
4. Zilhão, J. *et al.* Analysis of Aurignacian interstratification at the Châtelperronian-type site and implications for the behavioral modernity of Neandertals. *Proc. Natl Acad. Sci. USA* 103, 12643–12648 (2006).
5. Ronchitelli, A., Boscato, P. & Gambassini, P. in *La lunga storia di Neandertal. Biologia e comportamento* (eds Facchini, F. & Belcastro, G. M.) (Jaca Book, 2009).
6. d'Errico, F., Borgia, V. & Ronchitelli, A. Uluzzian bone technology and its implications for the origin of behavioural modernity. *Quat. Int.* doi:10.1016/j.quaint.2011.03.039 (in the press).
7. Lévêque, F. & Vandermeersch, B. M. Découverte de restes humains dans un niveau castelperronien à Saint-Césaire (Charente-Maritime). *CR Acad. Sci. Paris* 291, 187–189 (1980).
8. Hublin, J. J., Spoor, F., Braun, M., Zonneveld, F. & Condemi, S. A late Neanderthal associated with Upper Palaeolithic artefacts. *Nature* 381, 224–226 (1996).
9. Harvati, K., Panagopoulou, E. & Karkanas, P. First Neanderthal remains from Greece: the evidence from Lakonis. *J. Hum. Evol.* 45, 465–473 (2003).
10. Bailey, S. E. & Hublin, J. J. Dental remains from the Grotte du Renne at Arcy-sur-Cure (Yonne). *J. Hum. Evol.* 50, 485–508 (2006).
11. Bar-Yosef, O. & Bordes, J. G. Who were the makers of the Châtelperronian culture? *J. Hum. Evol.* 59, 586–593 (2010).
12. Higham, T. *et al.* Chronology of the Grotte du Renne (France) and implications for the context of ornaments and human remains within the Châtelperronian. *Proc. Natl Acad. Sci. USA* 107, 20234–20239 (2010).
13. Palma di Cesnola, A. & Messeri, M. P. Quatre dents humaines paléolithiques trouvées dans des cavernes de l'Italie Méridionale. *L'Anthropologie* 71, 249–262 (1967).
14. Churchill, S. E. & Smith, F. H. Makers of the early Aurignacian of Europe. *Am. J. Phys. Anthropol.* 113 (Suppl. 31), 61–115 (2000).
15. Palma di Cesnola, A. L'Uluzzien: faciès italien du leptolithique archaique. *L'Anthropologie* 93, 783–812 (1989).
16. Riel-Salvatore, J. in *Sourcebook of Paleolithic Transitions* (eds Camps, M. & Chauhan, P.) (Springer, 2009).
17. Messeri, P. & Palma di Cesnola, A. Contemporaneità di paleantropi e fanerantropi sulle coste dell'Italia meridionale. *Zephyrus* 26–27, 7–30 (1976).
18. Benazzi, S. *et al.* Comparison of dental measurement systems for taxonomic assignment of first molars. *Am. J. Phys. Anthropol.* 144, 342–354 (2011).
19. Olejniczak, A. J. *et al.* Dental tissue proportions and enamel thickness in Neandertal and modern human molars. *J. Hum. Evol.* 55, 12–23 (2008).
20. Smith, B. H. Patterns of molar wear in hunter-gatherers and agriculturists. *Am. J. Phys. Anthropol.* 63, 39–56 (1984).
21. Reimer, P. J. *et al.* IntCal09 and Marine09 radiocarbon age calibration curves, 0–50,000 years cal BP. *Radiocarbon* 51, 1111–1150 (2009).
22. Boscato, P. & Crezzini, J. Middle-Upper Palaeolithic transition in Southern Italy: Uluzzian macromammals from Grotta del Cavallo (Apulia). *Quat. Int.* doi:10.1016/j.quaint.2011.03.028 (in the press).
23. Müller, U. C. *et al.* The role of climate in the spread of modern humans into Europe. *Quat. Sci. Rev.* 30, 273–279 (2011).
24. Higham, T. European Middle and Upper Palaeolithic radiocarbon dates are often older than they look: problems with previous dates and some remedies. *Antiquity* 85, 235–249 (2011).
25. Pinhasi, R., Higham, T. F., Golovanova, L. V. & Doronichev, V. B. Revised age of late Neanderthal occupation and the end of the Middle Paleolithic in the northern Caucasus. *Proc. Natl Acad. Sci. USA* 108, 8611–8616 (2011).
26. Zilhão, J. in *Continuity and Discontinuity in the Peopling of Europe* (eds Condemi, S. & Weniger, G. C.) (Springer, 2011).
27. Mellars, P. The impossible coincidence: a single species model for the origins of modern human behavior in Europe. *Evol. Anthropol.* 14, 12–27 (2005).
28. Martin, L. B. Significance of enamel thickness in hominoid evolution. *Nature* 314, 260–263 (1985).
29. R Development Core Team. R: a language and environment for statistical computing. Æhttp://www.r-project.orgæ (2008).

Supplementary Information is linked to the online version of the paper at www.nature.com/nature.

Acknowledgements We thank the Soprintendenza per i Beni Archeologici della Puglia which facilitated the excavation of Grotta del Cavallo over the years. We also thank M. A. Gorgoglione who supported and helped in the collection of samples for ^{14}C dating and encouraged the collaboration with the University of Siena for the study of the archaeological remains. P. Boscato, H. Klempererova, F. Ranaldo and S. Ricci have all helped in aspects of the research and are especially thanked. We are grateful to G. Gruppioni for providing the Italian modern human sample used in this work. We thank M. Francken, B. Trautmann, I. Trautmann, H. Scherf, M. Dockner and R. Ginner for technical assistance. We thank F. L. Bookstein for suggestions on statistics. Access to the fossil specimens was made possible by the Croatian National History Museum, the French Musée National de Préhistoire, the French Musée um National d'Histoire Naturelle, Paleoanthropology, Eberhard Karls Universität Tübingen and the NESPOS Database 2011 (https://www.nespos.org/display/openspace/Home). We acknowledge the Centre de Microtomographie (Université de Poitiers), the Vienna micro-CT Laboratory (University of Vienna), VISCOM AG Hannover, the Paleoanthropology High Resolution Computing Tomography Laboratory (Eberhard Karls Universität Tübingen), the European Synchrotron Radiation Facility beamline ID17, the AST-RX platform (French Musée um National d'Histoire Naturelle) and the Oxford Radiocarbon Accelerator Unit (ORAU). The authors would like to thank T. Higham and R. E. M. Hedges for their input in the radiocarbon dating part of the project, for important comments and proofreading this manuscript. The radiocarbon dating was funded by the Natural Environment Research Council (NERC) NRCF programme. K.D. is part of the Ancient Human Occupation of Britain project, funded by the Leverhulme Trust. This work was supported by the NSF 01-120 Hominid Grant 2007, A.E.R.S. Dental Medicine Organisations GmbH FA547013, the Fondation Fyssen, the DFG INST 37/706-1 FUGG and the NERC Grant (NE/D014077/1).

Author Contributions S.B., F.M., K.H. and G.W.W. initiated and organized the project. S.B., C.C.B., P.B., J.S., I.P., K.H. and G.W.W. collected the fossils and modern human sample. S.B. and C.F. carried out the dental measurements. S.B. and M.C. analysed the data. K.D. initiated and performed the radiocarbon dating project. S.B., K.D., C.F., O.K., M.C., S.C., A.R., K.H. and G.W.W. discussed the results. S.B., K.D., C.F., M.C., S.C., A.R., K.H. and G.W.W. wrote and edited the manuscript.

Author Information Reprints and permissions information is available at www.nature.com/reprints. The authors declare no competing financial interests. Readers are welcome to comment on the online version of this article at www.nature.com/nature. Correspondence and requests for materials should be addressed to S.B. (stefano.benazzi@univie.ac.at).

METHODS

Scanning, segmentation and three-dimensional reconstruction of the specimens. Microtomographic scans of all the specimens (Supplementary Table 2) were undertaken by means of industrial and synchrotron-based microtomographic scanners at isotropic voxel length between 15 and 55 mm. The microtomographic image stacks of each tooth were aligned to the best-fit plane computed at the cervical line (cervical plane) through Amira 5.3 (Mercury Computer Systems), and then rotated up so that the cervical plane was parallel to the *x*–*y* plane of the Cartesian coordinate system. For the segmentation process, the half-maximum height (HMH) protocol was used to reconstruct three-dimensional digital surface models of each microtomography-scanned tooth using Amira 5.3 (Supplementary Information).

Outline data. A further orientation of the dM^1 and dM^2 digital models in the Cartesian coordinate system was required before the outline analysis. The dM^1 oriented digital models were rotated around the *z* axis to align the projection on the *x*–*y* plane of the intercept between the paracone and protocone cusp tips parallel to the *y* axis of the Cartesian coordinate system. The crown outlines were then projected onto the *x*–*y* plane. The dM^2 digital models were oriented with the lingual side parallel to the *x* axis. The best-fit plane of the cervical line identified the cervical outline. In one case (the Neanderthal specimen Engis 2), computer-aided design (CAD) techniques were used to restore the dM^1 crown outline (Supplementary Fig. 2).

All the outlines were represented by 24 landmarks obtained by equiangularly spaced radial vectors out of the centroid of their area[18]. These landmarks were superimposed through a generalized Procrustes analysis (GPA)[30]. Since the outlines were oriented and centred on the centroid of their area[18], GPA only entailed a uniform scaling of the landmark configurations to unit centroid size. This step removed size differences, except for static allometry.

Two-dimensional enamel thickness data. For the two-dimensional enamel thickness assessment we followed techniques developed previously[28], adapted to our specific case. A plane perpendicular to the cervical plane of the tooth and passing through two dentine horn tips was used for sectioning the dental crowns. The section passed through the dM^1s' paracone and protocone dentine horn tips, and through the dM^2s' paracone and metacone dentine horn tips (Fig. 3). The dentine horn tips were identified as the highest points of the dentine in the central mammelon by scrolling apically through the oriented slices. For Cavallo-C (wear stage 5; based on Smith[20]) and the comparative sample with wear stage 3, this approach was further verified by segmenting the whole crown dentine to check the continuity of the marginal ridges beside the dentine horns. For worn teeth, the EDJ length was truncated at the exposed edge of the occlusal dentine basins.

Cavallo-B shows a crack crossing the paracone mesiodistally (Fig. 3a). The area of the crack pertaining to the dentine was included in the dentine area, and the trait of the EDJ intersected by the crack was calculated in the EDJ length. On the contrary, the missing area of the enamel cap was not reconstructed. Therefore, the computed RET index for Cavallo-B is slightly underestimated.

The segmentation process and the parameter measurements were carried out by S.B. and C.F. The interobserver error was evaluated for the enamel and dentine area of three of the fossil specimens from our sample, and did not exceed 3% in each case.

The following measurements were recorded: the area of the enamel cap (mm^2), the area of the coronal dentine (which includes the coronal pulp; mm^2), the length of the enamel–dentine junction (EDJ; mm), the average enamel thickness (AET) index (the area of the enamel cap divided by the length of the EDJ; index in mm) and the RET index (the average enamel thickness divided by the square root of the coronal dentine area; scale free index)[19,28].

Statistical analysis. A Principal component analysis (PCA) of the matrix of Procrustes coordinates was carried out for the dM^1 crown outlines and dM^2 cervical outlines, separately. Because we aimed at assessing the dental outline shapes of the teeth from Grotta del Cavallo with respect to both the anatomically modern human and the Neanderthal outline shape variation, Cavallo-B and Cavallo-C spatial configurations were projected into the space built from the comparative sample only. In the Supplementary Information we show that the first PC of dM^1 crown outlines PCA and the first two PCs of dM^2 cervical outlines PCA are the only informative ones.

We did not regress the part of radial size correlated with the diameters, diagonals and area out of the crown and cervical outline data (as previously suggested[18] for the first permanent molars) because size information related to static allometry is an important factor for the separation of Neanderthal and anatomically modern human dM^2s.

The differences between the AET and RET indexes of Neanderthal and RMH were tested via a permutation test ($n = 1{,}000$) on group mean and variance.

Finally, we used leave-one-out cross-validation quadratic discriminant analysis (QDA) for the taxonomic classification of Cavallo-B and Cavallo-C. We built up QDA models leaving out the data from the Cavallo specimens. The computation of the posterior probabilities (P_{post}) was made with an equal prior probability (P_{prior}) of 0.5 for Neanderthal and anatomically modern human groups (UPMH plus RMH). The threshold for taxonomic determination was a $P_{post} \geq 0.90$. The taxonomic analyses are summarized in the Supplementary Information. The data were processed and analysed through software routines written in R[29].

30. Rohlf, F. J. & Slice, D. E. Extensions of the Procrustes method for the optimal superimposition of landmarks. *Syst. Zool.* 39, 40–59 (1990).

doi:10.1038/nature10617

Supplementary Methods

GROTTA DEL CAVALLO

Description of the site and history of excavations

Grotta del Cavallo (40°9'18.85"N, 17° 57' 37.27"E) is situated on the rocky coast of the Bay of Uluzzo, Nardò, around 90 km south of the town of Taranto in Apulia, SE Italy. It is located within a low Mesozoic limestone plateau, about 15m above the present day shore, with a large, 5 m wide by 2.5 m high opening facing NW and an approximately circular shape, about 9 m in diameter[31]. Cavallo was discovered in 1960 and was initially investigated in 1961 by A. Palma di Cesnola. Official excavations took place between 1963–1966[31-34], and again between 1986–2008 focusing on the Mousterian parts of the sequence[35,36]. In the interlude between the two series of excavations, looters severely disturbed the central part of the deposits, removing much of the Upper Palaeolithic layers. In the light of this damage, salvage excavations were conducted by the University of Siena (P. Gambassini and colleagues) for four seasons in the late 1970s/early 1980s and a metal gate was installed at the entrance of the cave. In the process of installing it, the standing sections were cleaned and some free-standing deposits at the entrance of the cave were carefully removed and correlated to the original stratigraphy.

Stratigraphy

The site preserves a long stratigraphic succession comprising about 7 m of archaeological deposits directly based on a marine interglacial beach conglomerate (layer N) (Fig. S1). The archaeological sequence of Cavallo is dominated by Middle Palaeolithic layers (MIV-F I),

capped by a thin layer of green volcanic ash (Fα), which separates Mousterian from the overlying Uluzzian layers (E-DIb) (Fig. S1).

The Uluzzian deposits, about 80-85 cm thick, were excavated both in the 1960s and in the late 1970s/early 1980s at separate sections of the site. A correlation is given in Table S1.

These layers are divided into Archaic Uluzzian (E III), Evolved Uluzzian (EII-I) and Final Uluzzian (D II – D Ib)[37-40]. They are separated from the upper part of the sequence by a stalagmitic crust (D Ia) and two sterile layers of volcanic ash (C II and C Ia-b). The tephra in layer C has been traditionally assigned to the Campanian Ignimbrite eruption[41] on empirical grounds and by comparison to other sequences (e.g. Castelcivita), but no geochemical characterisation has been attempted. Directly superimposed are Epigravettian horizons B II- B I (Romanellian and Epiromanellian *facies*), of much younger age (≈11,000 yr BP).

The Uluzzian layers of Cavallo comprise the most complete stratified sequence of the technocomplex ever revealed.

DENTAL MORPHOMETRIC ANALYSIS

Comparative sample

Table S2 shows the comparative sample used for the morphometric analyses. The whole corpus, except for the UPMH specimen Brillenhöhle, was used for outline analysis. For enamel thickness and dental tissue proportions, only individuals with wear stage equal or lower than 3 (based on Smith[42]) were selected. Nonetheless, the different wear stage of the fossil sample forced us to follow different solutions for dM^1 and dM^2. The fossil dM^1 sample is almost completely dominated by wear stage 3. Accordingly, a modern human comparative sample of similar wear stage was created. Additionally, since Cavallo-B is unworn, we

collected also an unworn modern human sample to figure out the hypothetical 2D AET and 2D RET indexes that Cavallo-B could have in wear stage 3. For the dM^2 Neanderthal sample, because almost all individuals are unworn or slightly worn, specimens with wear stage 3 were not considered to measure the enamel thickness and dental tissue proportions. Conversely, in the modern human sample specimens with wear stage 3 were included to create the worst scenario in support to the attribution of Cavallo specimen to *H. sapiens*. Namely, the AET and RET indexes obtained for the modern human sample are slightly underestimated.

Scanning of the specimens and segmentation

The original specimens used in this study were scanned at the Vienna Micro-CT Lab, Department of Anthropology, University of Vienna (Viscom X8060 µCT scanner using the following scan parameters: 130kV, 100mA, isotropic voxel size=25µm), at the Paleoanthropology High Resolution CT laboratory, Senckenberg Center for Human Evolution and Paleoecology, Eberhard Karls Universität Tübingen (v|tome|x s 240 µCT from GE Pheonix, using the following scan parameters: 130kV, 100mA, isotropic voxel size ranging from=15-26µm), and at the AST-RX platform (Accès Scientifique à la Tomographie à Rayons X) at the Muséum national d'Histoire naturelle (using the following scan parameters:150 kV, 220 mA, isotropic voxel size=33.62µm). Details about the scanning procedure of the other specimens can be found in NESPOS (Neanderthal Studies Professional Online Service) Database 2011.

For the segmentation process, the half-maximum height (HMH) protocol[43] was used to reconstruct 3D digital surface models for the dentine and the enamel of each CT-scanned tooth using the software package Amira 5.3 (Mercury Computer Systems, Chelmsford, MA). This protocol samples the Hounsfield values on either side of the transition between two

adjacent tissues and takes the value halfway between them as the threshold value. When voxels were located on the boundary between two tissues with similar Hounsfield values and the automatic threshold could not distinguish the differences (for example, for the presence of cracks or small decays), manual corrections were conducted.

Digital reconstruction of Engis 2 dM^1 crown outline

Computer-Aided Design (CAD) techniques in RapidForm XOR2 (INUS Technology, Inc.) were used to restore the dM^1 crown outline of the Neanderthal specimen Engis 2 (Fig. S2; the reconstructed regions in red). At the distal side, the small part of the outline missing was reconstructed by using a spline (namely, a curve interpolation). At the buccal side, the enamel is chipped away due to a post-mortem fracture, which reveals the dentine. This missing region of the enamel outline was restored virtually by offset of the corresponding dentine outline. In particular, the dentine outline exposed was duplicated and translated towards the enamel outline of 0.39 mm (length equal to the enamel thickness measured in the fracture). Finally, that segment was fused to the rest of the outline.

Statistical analysis

The data was analyzed via software routines written in R[44]. Table S3 shows the complete descriptive statistic for dM^1 and dM^2 enamel thickness and dental tissue proportions.

Principal Component Analysis (PCA)

The PCA of the matrix of Procrustes coordinates was carried out on the sample of the dM^1 crown and the dM^2 cervical outlines respectively. We applied Anderson's formula to test the

deviation from joint equality of any sequence of consecutive eigenvalues[45,46]. When the formula is applied to a single pair of consecutive eigenvalues, it states that the distribution of $2N \log(a/g)$ is that of an ordinary chi-square on two degrees of freedom. Here N is the sample size (Cavallo's teeth excluded), a is the arithmetic mean of the pair of consecutive eigenvalues, and g is the geometric mean of this same pair of eigenvalues. The expected value of the chi-square is two (its degrees of freedom), and so no PC (eigenvector) should be considered for interpretation if, when its eigenvalue is compared with the next eigenvalue, $2N \log(a/g)$ does not exceed two, as their ordination most probably accounts only for noise.

PCA of the dM^1 and dM^2 outlines

When applying Anderson's formula[45] to test PC2 and PC3 from the PCA of the dM^1s, of eigenvalues of 0.083 and 0.072, we obtain the value of 0.644 (N =32) — clearly below the expected value of a chi-square on two degree of freedom. Likewise for the PCA of the dM^2s, PC3 and PC4, of eigenvalues 0.083 and 0.070, Anderson's value is equal to 1.097 (N =38). The eigenvalues of PC2 and PC3 from the PCA of the dM^1s and those of PC3 and PC4 from the PCA of the dM^2s are nearly equal, and hence cannot be considered for either interpretation or further statistical analyses.

Quadratic Discriminant Analysis (QDA)

The leave-one-out cross-validation QDA was used for the taxonomic classification of Cavallo-B and Cavallo-C. We built up QDA models on RET, AET and subsets of PCs of the outline analysis, leaving out the data from the Cavallo specimens. The use of QDA is justified as the results show that the variances of the dental variables are significantly different between Neanderthals and modern humans. The computation of the posterior probabilities (P_{post}) was made with an equal prior probability ($P_{prior} = 0.5$) for the Neanderthal and modern

human groups (UPMH+RMH). Taxonomic determination is accepted with a P_{post} equal or superior to 0.90. The performance of the QDA models is defined by the percentage of specimens which taxon is determined with a $P_{post} \geq 0.90$ (correctly and incorrectly classified) and by the percentage of specimens correctly classified (accuracy). Cavallo's teeth have been tested through all the iterations of leave-one-out cross-validation QDAs. The accuracy of the classification was also computed as the number of iterations for which Cavallo's teeth were classified with a $P_{post} \geq 0.90$ either as modern human or Neanderthal.

QDA of dM^1 and dM^2 PCs, RET and AET

Table S4 summarizes the analysis. The performance of the QDA models is high for the tooth outlines (dM^1: PC1 scores, dM^2: PC1 and PC2 scores) and RET with a high accuracy ranging from 96.3% to 100% and percentage of specimens classified superior to 82%. For both dM^1 and dM^2, although the accuracy is high, the QDA models based on AET have a low power of classification when the threshold of decision $P_{post} \geq 0.90$. Therefore, they are not used for the classification of Cavallo-B and Cavallo-C. According to the QDA models based on outline and RET data, Cavallo-B and Cavallo-C are classified as modern humans with a $P_{post} > 0.90$ and with an accuracy of 100%.

RADIOCARBON DATING

Previous chronology

Since the first identification of the technocomplex in 1963 by Palma di Cesnola[33,34] and for four decades afterwards, the chronology of the Uluzzian of Cavallo was based on an infinite conventional radiocarbon date, RM-352: >31,000 ^{14}C yr bp (yr BP)[39]. The sample comprised a piece of charcoal recovered from layers E II-I excavated in 1966.

More recently, four new radiocarbon determinations (AA-66812: 34,900 ± 1900 yr BP, AA-66813: 32,300 ± 2700 yr BP, AA-66814: 36,510 ± 2300 yr BP, AA-66819: 36,600 ± 2300 yr BP) were reported by Ronchitelli et al.[47] and Kuhn et al.[48]. They belong to a series of ten AMS dates made on burnt bone from layer E III ranging from 21,000–36,000 yr BP with no age-depth consistency[49]. This is not surprising because burnt bone is an unreliable material for AMS dating[50]. It consists of pyrolysed collagen, often with sediment carbon and non-autochthonous material within it, and has a tendency to produce ages that often underestimate the true age, especially of Palaeolithic-aged samples.

These previous dates, therefore, can only serve as a minimum estimate of the real age of layer EIII, and should be set to one side.

New radiocarbon chronology

Material

More recent chronometric work has been undertaken by one of us (KD) as part of a D.Phil project at the University of Oxford[51], supervised by Prof. R.E.M. Hedges. Two shells from the uppermost layers D II and D I of the original 1963 excavations[31] were selected for dating from the *Soprintendenza per i Beni Archeologici della Puglia* in Taranto. In addition, six shells from the salvage fieldwork in the 1970s and 1980s were sampled from the collection housed at the University of Siena. All dated shells are shown in Fig. S3.

The *Dentalium* sp. shells (Cvl 3, 4, 5, 8, 11) are of smooth morphology and have been snapped transversely to create regular tube-shaped beads. The *Nuculana* sp. shell (Cvl 2) is a relatively uncommon species in Upper Palaeolithic ornamental assemblages and was one of eight similarly perforated small valves from the same context.

Pretreatment methods

All new radiocarbon dates in this paper were produced at the Oxford Radiocarbon Accelerator Unit (ORAU), University of Oxford. Ten determinations were obtained from eight shells –Cvl 10 and 5 were dated twice for methodological reasons or as internal laboratory checks.

Part of each shell was cleaned using an air-abrasive system with aluminum oxide until the surface was removed and the inner shell structure was exposed. A small fragment of the carbonate was sawn off and crushed in an agate mortar and pestle to a fine powder. Approximately 30mg of powdered sample was reacted with 5ml of 80% phosphoric acid (H_3PO_4) for 12h at 60^{o}C, under vacuum. The CO_2 evolved via this process was extracted through a manifold and cryogenically purified while passing through a liquid N_2–methanol cooled trap that removes less volatile impurities (H_2O and phosphoric acid vapour). The gas was injected through an automated elemental analyzer connected to a continuous flow isotope-ratio-monitoring mass spectrometer (EA-CF-IRMS) system where it was measured isotopically. The CO_2 remaining from the process was transferred to a graphitization rig and was reduced to graphite with H_2 at 560 °C for 6h, in the presence of ≈2 mg of a Fe^+ catalyst. The graphite was pressed into a target holder prior to accelerator mass spectrometry (AMS).

Results

The raw determinations and sample details are given in Table S5. The majority of the new radiocarbon dates (OxA-19242, OxA-19256, OxA-19258, OxA-20631, OxA-19255, OxA-19254) are consistent with respect to the stratigraphic position of the samples.

Only OxA-19257 from horizon D II is too old for its context. This is *not* an ornament but a small, indeterminate fragment of a bivalve shell (Fig. S3; Cvl 6). Its preservation state was poor and the sample surface showed alteration and a chalky appearance. Given that the rest of the shells are much better preserved and with a very low degree of fragmentation a possible

explanation may be that Cvl 6 is an old shell, either collected on purpose, or accidentally brought to the site. Bivalve shells are found in lower layers of Cavallo and the breaking pattern, the small dimensions and the old age of Cvl 6, in contrast with the rest of the shell Uluzzian assemblage, supports the suggestion of an old or redeposited specimen.

In contrast, OxA-21072 (and its duplicate) was obtained from a *Cyclope neritea* shell, discovered during the original excavation of Palma di Cesnola in 1963 in layer D I on the top of the Uluzzian sequence. The material was stored in Taranto since the 1960s separately from the other dated samples. These dates are surprising young, especially since there has been no other archaeological material of a similar age discovered in Cavallo Cave.

Infiltration of younger Epigravettian material to the uppermost Uluzzian layer D I would require passing through the stalagmitic crust and the volcanic ash layers (see Fig. S1). However, according to the excavator's observations the ash and the stalagmite crust formed a continuous layer. While we suspect several reasons might be responsible for this younger age, we cannot prove them. What is certain, however, is that the sample does not truly relate to the Uluzzian layers. Other similarly young material has not been discovered in the Uluzzian layers and the few Aurignacian-like elements observed at the uppermost Uluzzian layer D I were considered by Palma di Cesnola to belong to a transitional, Terminal Uluzzian phase, before the arrival of the Protoaurignacian in the region[40].

XRD analyses

Prior to chemical pretreatment, all samples were mineralogically characterized using X-Ray Diffraction (XRD), following the optimized methods described by Douka et al.[52] which allow detection and quantification of very low amounts of calcite in binary mixtures with aragonite. With the exception of Cvl 3, all shells appeared well-preserved and largely unaffected by

diagenesis (Table S5 shows the percentage of calcite present in the naturally aragonitic shell samples).

Cvl 3 contained large amounts of calcite (≈50%) in the originally aragonite structure. The sample was examined microscopically and no evidence of mineral overgrowth or other form of alteration was observed. It is very likely that the formation of calcite was caused by exposure to high temperature (over 230^{o}C) which readily alters biogenic aragonite to calcite. This would not incorporate a shift in the radiocarbon age. OxA-19242 is in very good agreement with the rest of the dates from overlying spits of layers E and D (see below).

Cvl 5 was also dated twice as part of an experimental project where the effect of surface cleaning (by abrasion) was examined. The results of the two methods are statistically indistinguishable, but the first determination (OxA-19256) is preferred over the second date (OxA-X-2280-16), given that the fraction used for the latter was not thoroughly cleaned.

Bayesian model

In an attempt to place the two human teeth, Cavallo-B and Cavallo-C, within their most likely age and palaeoclimatic context, the new radiocarbon determinations were incorporated into a Bayesian model built with OxCal 4.1.7[53] and calibrated using the INTCAL Marine09 curve[54]. This is an interim curve and will be refined as additional datasets become available and are incorporated into it.

The Bayesian model (Fig. S4) includes prior stratigraphic information as observed at the site during excavation, as well as the presence of the tephra on top of the Uluzzian sequence, here taken as the CI (≈39,300 ± 55 yr BP)[55]. This age estimate has been produced from an average of 36 ^{40}Ar/^{39}Ar measurements from twelve proximal deposits. Since there is no chemical identification of the tephra capping the Uluzzian deposits in Cavallo, the probability distribution for the CI is only tentatively placed on top of the Bayesian plot. An outlier

detection analysis was used to assess outliers in the model. This showed two outliers of significance: OxA-21072 and its duplicate date (not shown in Fig. S4) and OxA-19257.

The earliest Uluzzian phase of layer E III, in which Cavallo-B was found, was not dated directly due to the lack of suitable samples. Using the `Date` function in OxCal, however, we calculated a probability distribution function (PDF) for the likely age of the human fossil within this phase. This PDF corresponds to a range between 45,010—43,380 (68.2% prob.) and 47,530—43,000 (95.4% prob.) cal yr BP with respect to INTCAL Marine09 (Fig. S5). The longer tail of the distribution and wider uncertainty is caused because it is unconstrained by chronometric data below the Uluzzian layers. Further work is needed to refine this estimate for the age of the layer.

The oldest radiocarbon determination from the site comes from E II-I and places the evolved Uluzzian –and the age of Cavallo-C– at about 40,000 ^{14}C yr BP or 43,000 cal yr BP. This date also acts a *terminus ante quem* for Cavallo-B and the arrival of modern humans in the cave. The PDF for the age of Cavallo B determined using the `Date` function in OxCal ranges between 43,970—43,060 (68.2% prob.) and 44,910—42,660 (95.4% prob.) cal yr BP.

The two age estimates overlap significantly, although the PDF for EIII is by definition older than that of EII-I (Fig. S5).

We compare these data tentatively against the NGRIP δ^{18}O record[56,57] tuned with respect to the Hulu Cave U-series chronology (following Weninger and Jöris[58]) (Figs. S4, S5). The PDF for EIII fits within the latter part of GIS 12 on this timescale, while the PDF for EII-I is slightly later (Fig. S5). Overall, the radiocarbon determinations from Grotta del Cavallo agree with the stratigraphic position of the majority of the samples and the presence of the CI ash. This is the first time the Uluzzian of the type-site of Grotta del Cavallo has been dated reliably since its discovery in 1963.

Confirmation of the age of the La Rochette and Brillenhohle specimens

We checked the age of these two comparative human specimens by redating the samples to confirm their antiquity (Table S6).

Supplementary Figures

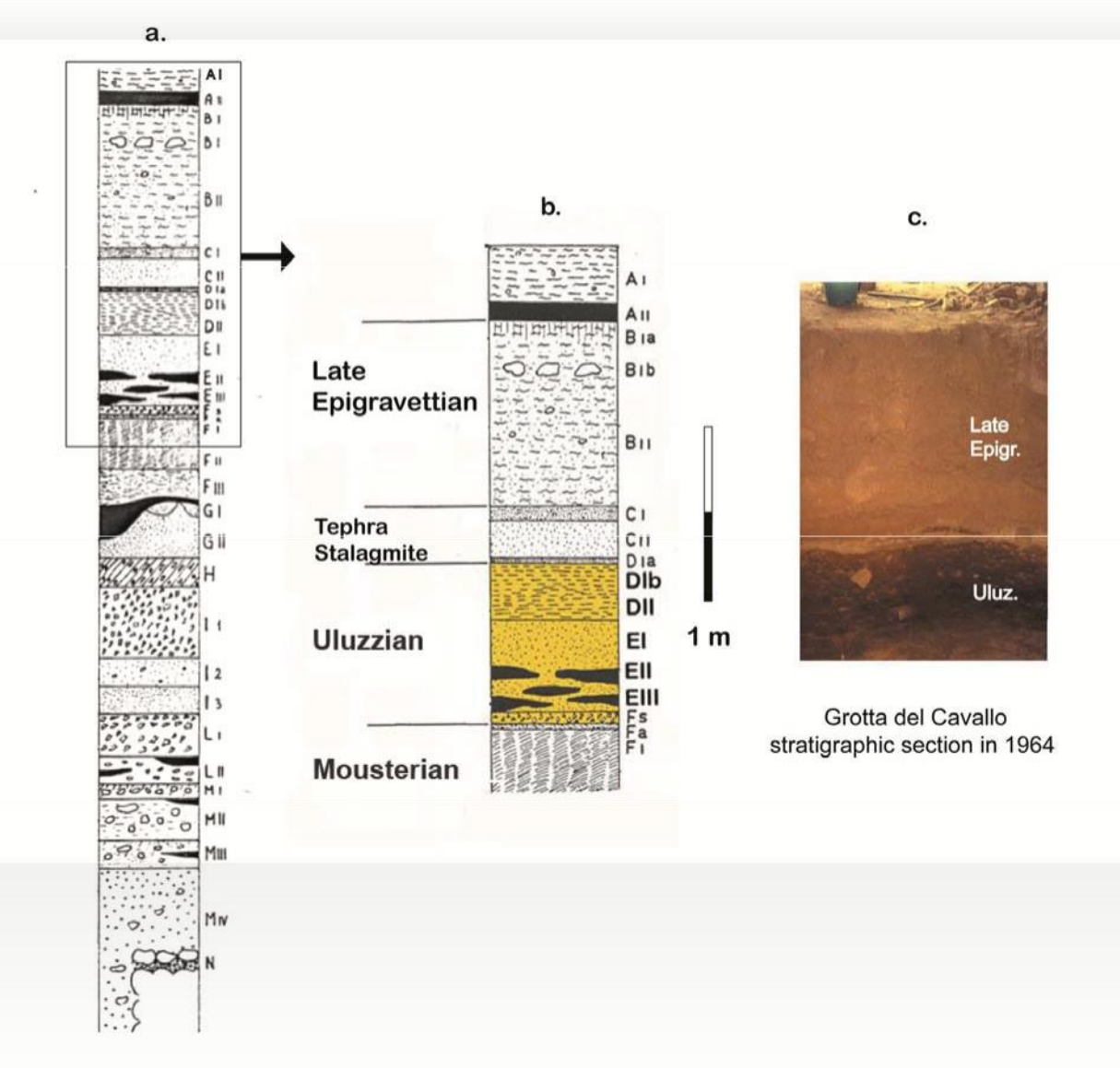

Figure S1: Section drawing of the Palaeolithic sequence of Grotta del Cavallo. **a**, The entire stratigraphic section of Cavallo Cave, after Palma di Cesnola[38]; **b**, detail of the section showing only the late Mousterian and UP layers; **c**, the section photograph illustrates the clear distinction between the very dark Uluzzian deposits from the lighter-coloured sediments of the later UP layers at the site.

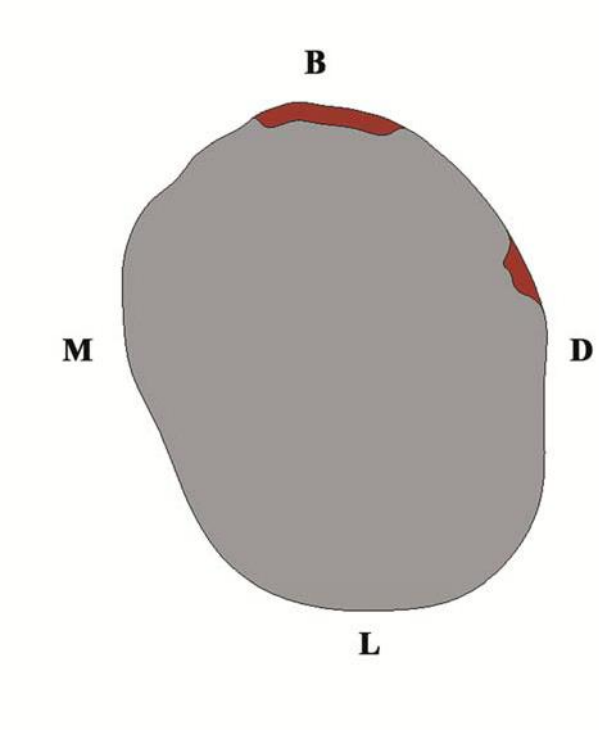

Figure S2: 2D virtual reconstruction of Engis 2 dM^1 crown outline. The crown outline of the original tooth is in grey; the reconstructed portions are shown in red. B=buccal; D=distal; L=lingual; M=mesial.

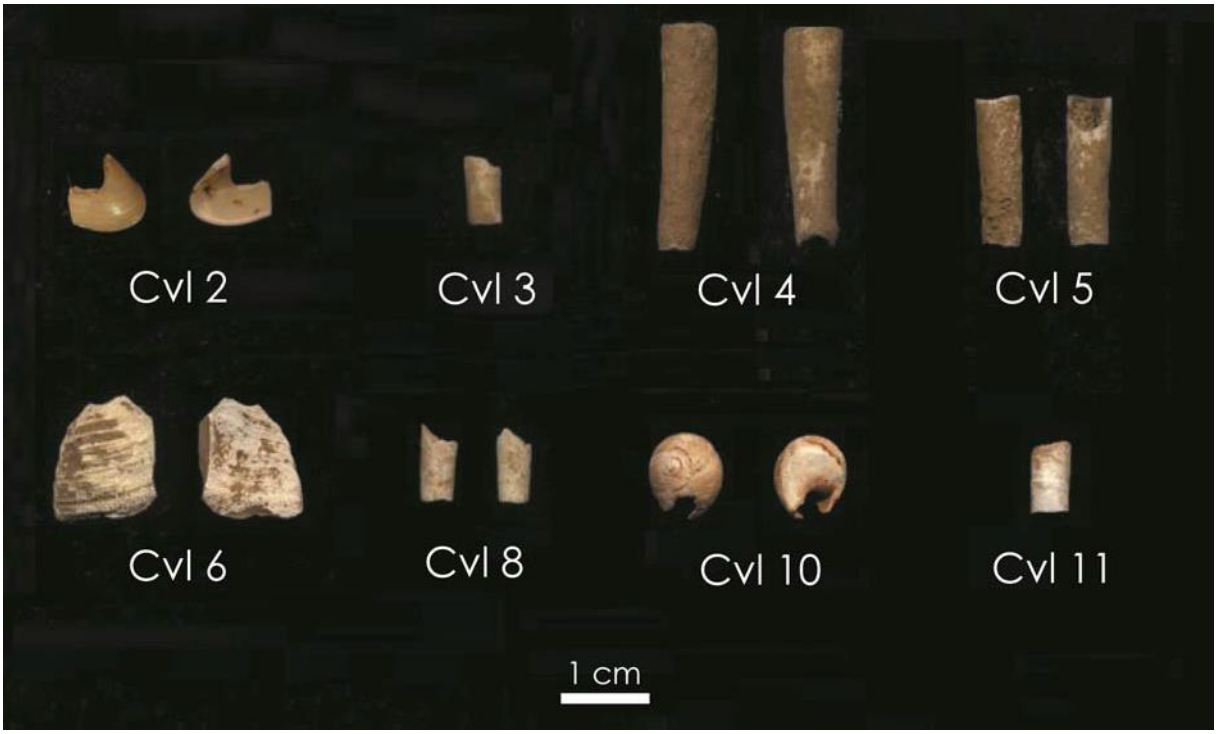

Figure S3: **Marine shells from the Uluzzian layers of Grotta del Cavallo used for AMS dating**. *Dentalium* sp. (Cvl 3, 4, 5, 8, 11), *Nuculana* sp. (Cvl 2), *Cyclope neritea* (Cvl 10) and bivalve fragment (Cvl 6).

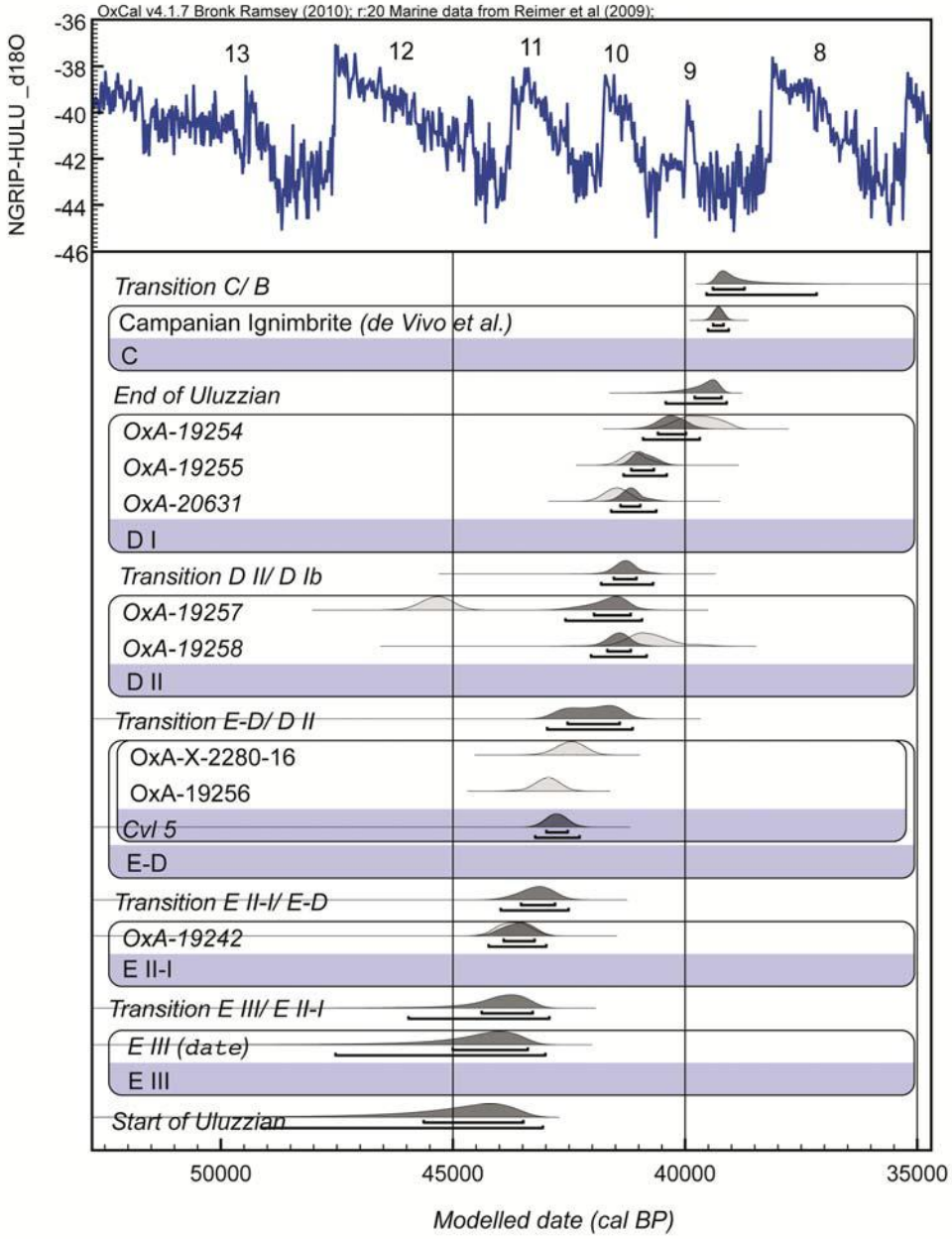

Figure S4: Bayesian model of the calibrated radiocarbon dates obtained on shell material from the Uluzzian layers of Cavallo. The radiocarbon dates are calibrated using the INTCAL Marine09 curve[54] with resolution set at 20. The NGRIP $\delta^{18}O$ record is shown[56,57] tuned with the U/Th chronology for the Hulu Cave speleothem[58]. Individual likelihoods are shown with lighter shaded distributions. Posterior probability distributions are in black outline. OxA-19257 is an outlier (100% chances for being an outlier) and most probably corresponds to an 'old' or redeposited shell (see text). The rest of the determinations demonstrate a consistent trend of decreasing age until the time of the inferred CI eruption.

OxA-19254 is in perfect agreement with this age. The very young dates from Cvl 10 (OxA-21072 and duplicate) are not included in the figure since they certainly do not relate to the Uluzzian occupation (see text). Cvl 5 was dated twice. Figure generated using OxCal 4.1.7[53].

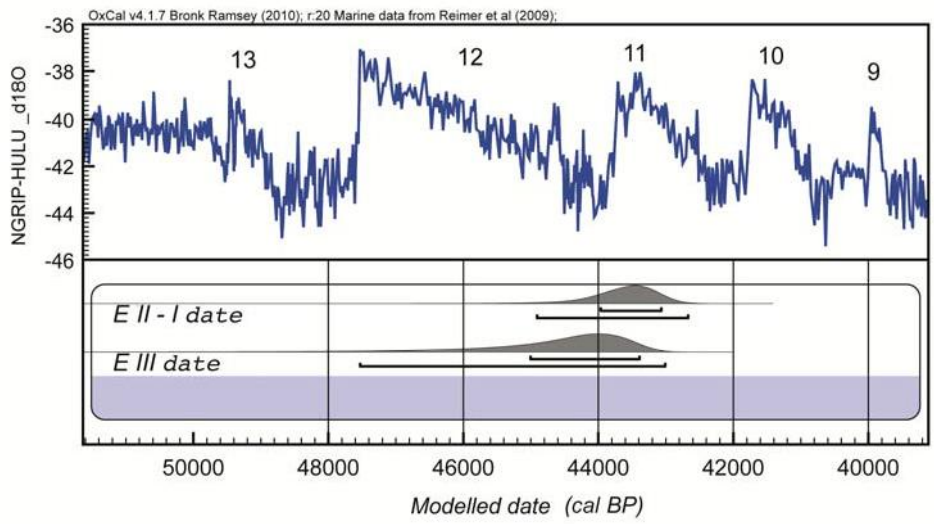

Figure S5: Age estimates for the human remains found in Cavallo layers **EIII and EII-I.** These ages are `Date` estimates, no direct measurements, which provide probability distribution functions (PDFs) for the likely age for the human teeth in layers EIII and EII-I. The NGRIP $\delta^{18}O$ record is shown[56,57], tuned with respect to the U/Th chronology for the Hulu Cave speleothem[58]. The relevant Greenland interstadials (GI) are given. Figure generated using OxCal 4.1.7[53].

Supplementary Tables

Table S1: Cross-correlation of Uluzzian layers at Cavallo, revealed in the original excavations of Palma di Cesnola (1963-1966) and in the subsequent rescue operations in the late 1970s and early 1980s.

Layers (1963-1966)	Spits (1978-1984)
DIb	D1–D2
DII	D3–D4
E-D	E 1
EII-I	E2–E4
EIII	E5–E7

Table S2: List of Neanderthal (N) and modern human (UPMH and RMH) dM^1s and dM^2s

	dM^1				dM^2			
Taxon	Specimen	Country	Source	Wear stage[d]	Specimen	Country	Source	Wear stage[d]
N	Engis 2[e]	Belgium	NESPOS[a]	stage 4	Krapina d185	Croatia	NESPOS[a]	unworn
	Krapina d181	Croatia	NESPOS[a]	stage 3	Krapina d186	Croatia	NESPOS[a]	unworn
	Krapina d183	Croatia	NESPOS[a]	stage 3	Krapina d187[g]	Croatia	NESPOS[a]	stage 3
	Pech-de-l'Azé I-R	France	Original data	stage 3	Krapina d188	Croatia	NESPOS[a]	unworn
	Pech-de-l'Azé I-L	France	Original data	stage 3	Krapina d189[g]	Croatia	NESPOS[a]	stage 3
	Roc de Marsal 1-R	France	NESPOS[a]	stage 3	Krapina d190	Croatia	NESPOS[a]	stage 1
	Roc de Marsal 1-L	France	NESPOS[a]	stage 3	Pech-de-l'Azé I-R	France	Original data	stage 1
	Subalyuk 2-R[e]	Hungary	Original data	stage 3	Pech-de-l'Azé I-L	France	Original data	stage 1
					Roc de Marsal 1-R	France	NESPOS[a]	unworn
					Roc de Marsal 1-L	France	NESPOS[a]	unworn
					Subalyuk 2-L	Hungary	Original data	stage 1
UPMH[b]	Brillenhöhle[f]	Germany	Original data	stage 3	Dolni Vestonice 36-3	Czech Republic	Original data	stage 1
	Dolni Vestonice 36-2	Czech Republic	Original data	unworn	La Rochette	France	Original data	stage 2
	La Rochette	France	Original data	stage 3	Pavlov 6[g]	Czech Republic	Original data	stage 4
					Pavlov 12[g]	Czech Republic	Original data	stage 6
RMH[c]	From Medieval and contemporary samples	France: 2 Germany: 11 Italy: 9	Original data	Unworn: 5 Stage 1: 3 Stage 2: 0 Stage 3: 14	From Medieval and contemporary samples	France: 2 Germany: 10 Italy: 11	Original data	Unworn: 5 Stage 1: 9 Stage 2: 6 Stage 3: 3

[a]NESPOS Database 2011/ www.nespos.org/display/openspace/Home; [b]UPMH= Upper Paleolithic modern human; [c]RMH= recent modern human; [d]based on Smith[42]; [e]used only for crown outline analysis; [f]used only for 2D enamel thickness and dental tissue proportions; [g]used only for cervical outline analysis

Table S3: 2D enamel thickness of Cavallo-B and Cavallo-C compared with Neanderthal (N), Upper Paleolithic modern human (UPMH), recent modern human (RMH) dM^1s and dM^2s (SD in brackets)

Tooth	Taxon	Wear stage[a]	n	Enamel area (mm^2)	Coronal dentine area (mm^2)	EDJ[b] length (mm)	AET[c] (mm)	RET[d] (scale free)
dM^1	N	3	6	7.02 (0.69)	31.76 (2.10)	17.36 (0.42)	0.40 (0.03)	7.17 (0.54)
	UPMH	3	2	7.26 (1.10)	28.16 (0.84)	14.28 (1.75)	0.51 (0.01)	9.56 (0.13)
	RMH	3	12	7.28 (0.65)	26.62 (1.51)	15.38 (0.78)	0.47 (0.03)	9.19 (0.70)
	UPMH	unworn	1	9.63	29.14	17.22	0.56	10.36
	RMH	unworn-stage 1	8	8.39 (1.26)	26.18 (1.73)	16.39 (0.73)	0.51 (0.06)	9.96 (0.96)
	Cavallo-B	unworn		12.64	34.14	18.33	0.69	11.80
dM^2	N	unworn-stage 1	9	12.14 (1.23)	33.85 (5.10)	19.25 (1.39)	0.63 (0.04)	10.89 (0.84)
	UPMH	stage 1-stage 2	2	16.75 (3.14)	28.93 (4.23)	17.30 (0.64)	0.97 (0.15)	17.93 (1.40)
	RMH	unworn-stage 3	20	12.33 (1.61)	28.36 (2.32)	16.83 (0.93)	0.73 (0.09)	13.78 (1.63)
	Cavallo-C	stage 5		13.4	34.59	15.96	0.84	14.28

[a]Based on Smith[42]; [b]EDJ= enamel-dentine junction; [c]AET = average enamel thickness index; [d]RET = relative enamel thickness index

Table S4: Summary of the leave-one-out cross validation Quadratic Discriminant Analysis (QDA)

Tooth	Parameter	n	Classified $P_{post} \geq 0.90$ MH	Classified $P_{post} \geq 0.90$ N	Indetermined $0.10 < P_{post} < 0.90$	Missclassified $P_{post} \geq 0.90$	Taxa %	Accuracy %
dM^1	Outline	32	20 (24)	7 (8)	5	1	84.4	96.3
	RET	31	23 (24)	4 (7)	4	0	87.1	100
	AET	31	14 (24)	3 (7)	14	0	54.8	100
	Cavallo-B		$P_{post} = 0.98$[a]					100[c]
dM^2	Outline	38	25 (27)	11 (11)	2	0	94.7	100
	RET	34	21 (25)	7 (9)	6	0	82.3	100
	AET	34	13 (25)	0 (9)	21	0	38.2	100
	Cavallo-C		$P_{post} = 0.99$[a]					100[c]
			$P_{post} = 0.99$[b]					100[c]

P_{post} = posterior probability; n = sample size; () = original group sample size; MH = modern human (UPMH and RMH); N = Neanderthal. AET = average enamel thickness index; RET = relative enamel thickness index; Species % = percentage of specimens for which a taxon is determined with $P_{post} \geq 0.90$ after cross validation; Accuracy % = percentage of specimens correctly classified after cross-validation; [a] P_{post} based on outline data; [b] P_{post} based on RET data; [c] Percentage of iterations (during cross validation) for which Cavallo's tooth is classified as modern human with a $P_{post} \geq 0.90$.

Table S5: New radiocarbon determinations for the Uluzzian layers in Grotta del Cavallo

Sample	OxA	^{14}C yr BP	±	Layer-Spit	Species	Calibrated (95.4%) yr BP from	Calibrated (95.4%) yr BP to	Aragonite-Calcite %
Cvl 10	21072	19,685	75	D I	*Cyclope neritea*	23,380	22,470	100-0
Cvl 10	Dupl.	19,235	75	D I	*Cyclope neritea*	23,220	22,060	100-0
Cvl 2	19254	35,080	230	D 1=DIb	*Nuculana* sp.?	40,450	38,860	100-0
Cvl 4	19255	36,260	250	D 2=DIb	*Dentalium* sp.	41,570	40,390	100-0
Cvl 11	20631	36,780	310	D II	*Dentalium* sp.	42,010	40,880	99.8-0.2
Cvl 6	19257	42,360	400	D 3=D II	Bivalve fragm.	45,990	44,640	100-0
Cvl 8	19258	36,000	400	D 8=DII?	*Dentalium* sp.	41,570	39,560	100-0
Cvl 5	19256	39,060	310	E 1=E-D	*Dentalium* sp.	43,510	42,350	99.7-0.3
Cvl 5	X-2280-16	38,300	400	E 1=E-D	*Dentalium* sp.	43,380	42,080	100-0
Cvl 3	19242	39,990	340	E 4=EII-I	*Dentalium* sp.	44,300	43,000	50-50

Conventional ages are expressed in ^{14}C years BP, after Stuiver and Polach[59]. Note that layer assignation for Cvl 10 and Cvl 11 follows that of the original excavations[31]. The rest of the shells were recovered during rescue excavations in subsequent years and follow different assignation system. The correlation of the two series is based on field documentation. Percentages of aragonite to calcite are listed in the right hand column based on high precision XRD analysis.

Table S6: Radiocarbon determinations from La Rochette and Brillenhöhle

Specimen	OxA	^{14}C yr BP	±	Used (mg)	Yield (mg)	%Yld	%C	d^{13}C (‰)	d^{15}N (‰)	C:N atomic ratio
La Rochette	11053	23,630	130	710	34.2	4.8	45.8	-17.1	11.7	3.3
	23413	23,400	110	na	23.84	3.4	42.9	-17.2	11.9	3.1
Brillenhöhle	11054	12,470	65	600	34.7	5.8	44.7	-19.2	8.5	3.3
	23414	12,535	50	na	22.67	3.8	42.5	-19.5	8.5	3.1

Conventional ages are expressed in years BP, after Stuiver and Polach[59]. Stable isotope ratios are expressed in ‰ relative to vPDB with a mass spectrometric precision of ±0.2‰. Gelatin yield represents the weight of gelatin or ultrafiltered gelatin in milligrams. %Yld is the percent yield of extracted collagen as a function of the starting weight of the bone analysed. %C is the carbon present in the combusted gelatin. CN is the atomic ratio of carbon to nitrogen and is acceptable if it ranges between 2.9—3.5. The new AMS dates are reultrafiltered gelatin sample extracted from the first pretreatment chemistries undertaken. This was done as a check on the original filtration chemistry. You can see that the results are statistically identical and confirm the original measurements.

Supplementary References

31. Palma Di Cesnola, A. Prima campagna di scavi nella Grotta del Cavallo presso Santa Caterina (Lecce). *Riv. Sc. Preist.* **18**, 41-74 (1963).

32. Palma di Cesnola, A. Seconda campagna di scavo nella grotta del Cavallo. *Riv. Sc. Preist.* **19**, 23-39 (1964).

33. Palma di Cesnola, A. Notizie preliminari sulla terza campagna di scavi nella Grotta del Cavallo (Lecce). *Riv. Sc. Preist.* **20**, 291-302 (1965a).

34. Palma di Cesnola, A. Gli scavi nella Grotta del Cavallo (Lecce) durante il 1966. *Riv. Sc. Preist.* **21**, 289-302 (1966a).

35. Sarti, L., Boscato, P. & Lo Monaco, M. Il Musteriano finale di Grotta del Cavallo nel Salento, studio preliminare. *Origini* **22**, 45-109 (1998-2000).

36. Sarti, L., Boscato, P., Martini, F. & Spagnoletti, A.P. Il Musteriano di Grotta del Cavallo - strati H e I : studio preliminare. *Riv. Sc. Preist.* **52**, 21-110 (2002).

37. Palma di Cesnola, A. Il Paleolitico superiore arcaico (facies uluzziana della Grotta del Cavallo, Lecce. *Riv. Sc. Preist.* **20**, 33-62 (1965b).

38. Palma di Cesnola, A. Il Paleolitico superiore arcaico (facies uluzziana) della Grotta del Cavallo, Lecce (continuazione). *Riv. Sc. Preist.* **21**, 3-59 (1966b).

39. Palma di Cesnola, A. Datazione dell'Uluzziano col Metodo del C–14. *Riv. Sc. Preist.* **24**, 341–348 (1989).

40. Palma di Cesnola, A. *Il Paleolitico superiore in Italia* (Garlatti e Razzai, 1993).

41. Giaccio, B., Hajdas, I., Peresani, M., Fedele, F.G. & Isaia, R. in *When Neanderthals and Modern Humans Met* (ed. Conard, N.J.) (Kerns Verlag, Tubingen, 2006).

42. Smith, B.H. Patterns of molar wear in hunter-gatherers and agriculturists. Am. J. Phys.

Anthropol. 63, 39-56 (1984)

43. Spoor, F., Zonneveld, F. & Macho, G.A. Linear measurements of cortical bone and dental enamel by computed tomography: applications and problems. *Am. J. Phys. Anthropol.* **91**, 469-484 (1993).

44. R Development Core Team. R: a language and environment for statistical computing. Vienna, Austria: R Foundation for Statistical Computing.http://www.r-project.org. (2008).

45. Anderson, T.W. Asymptotic Theory for Principal Component Analysis. *Ann. Math. Statist.* **34**, 122-148 (1963).

46. Coquerelle, M. et al. Sexual dimorphism of the human mandible and its association with dental development. *Am. J. Phys. Anthropol.* **145**, 192-202 (2011).

47. Ronchitelli, A., Boscato, P. & Gambassini, P. in La lunga storia di Neandertal. Biologia e comportamento (eds Facchini, F. & Belcastro, G.M.) (Jaca Book, 2009).

48. Kuhn, S.L. et al. Radiocarbon Dating Results for the Early Upper Paleolithic of Klissoura 1 Cave. *Euras. Prehist*. 7 (2), 37-46 (2010).

49. Riel-Salvatore, J. The Uluzzian and the Middle-Upper Paleolithic Transition in Southern Italy. Unpublished Ph.D. dissertation, School of Human Evolution and Social Change, Arizona State University (2007).

50. Van Strydonck, M., Boudin, M. & De Mulder, G. ^{14}C dating of cremated bones: the issue of sample contamination. *Radiocarbon* **51**, 553-568 (2009).

51. Douka, K. *Investigating the Chronology of the Middle to Upper Palaeolithic Transition in Mediterranean Europe by Improved Radiocarbon Dating of Shell Ornaments*. Unpublished D.Phil in Archaeological Science, University of Oxford (2011).

52. Douka, K., Hedges, R.E.M., Higham, T.F.G., 2010. Improved AMS ^{14}C dating of shell

carbonates using high-precision X-Ray Diffraction (XRD) and a novel density separation protocol (CarDS). *Radiocarbon* 52 (2): 735–751.

53. Bronk Ramsey, C. Bayesian analysis of radiocarbon dates. *Radiocarbon* **51**, 337-360 (2009).

54. Reimer, P.J. *et al*. IntCal09 and Marine09 radiocarbon age calibration curves, 0–50,000 years cal BP. *Radiocarbon* **51**, 1111-1150 (2009).

55. De Vivo, B., Rolandi, G., Gans, P.B., Calvert, A., Bohrson, W.A., Spera, F.J. & Belkin, H.E. New constraints on the pyroclastic eruptive history of the Campanian volcanic Plain (Italy). *Mineral. Petrol.* **73**, 47–65 (2001).

56. Andersen, K.K. *et al*. The Greenland ice core chronology 2005, 15-42 ka. Part 1: constructing the time scale. *Quat. Sci. Rev.* **25**, 3246-3257 (2006).

57. Svensson, A. *et al*. The Greenland ice core chronology 2005, 15-42ka. Part 2: Comparison to other records. *Quat. Sci. Rev.* **25**, 3258-3267 (2006).

58. Weninger, B., Jöris, O. A ^{14}C age calibration curve for the last 60 ka: the Greenland-Hulu U/Th timescale and its impact on understanding the Middle to Upper Paleolithic transition in Western Eurasia. *Journal of Human Evolution* **55**, 772–781 (2008).

59. Stuiver, M. & Polach, H.A. Discussion: Reporting of ^{14}C Data. *Radiocarbon* **19**, 355-363 (1977).

2.3. Cervical and crown outline analysis of worn Neanderthal and modern human lower second deciduous molars.

Benazzi, S., Fornai, C., Buti, L., Toussaint, M., Mallegni, F., Ricci, S., Gruppioni, G., Weber, G.W., Condemi, S., Ronchitelli, A.

American Journal of Physical Anthropology 2012; 149, 537-546.

Synopsis

This work was conceived for the investigation of Neanderthal and modern human worn lower second deciduous molars (dm_2s) using crown and cervical outlines gathered from 3D virtual models of the dental crown. The sample variability was explored by exploiting methods suitable for the investigation of teeth for which the occlusal aspect is obliterated. Based on the comparative sample used, we attempted an assessment of two specimens with uncertain taxonomic affiliation, namely, Bondi 1 (Western Georgia) and Lagar Vehlo 1 (Portugal), which were both found to possess morphological affinities to modern humans.
Moreover, this work suggested that the crown outline, a feature that can be easily gathered from published pictures (as in the case of Bondi 1), could be used to enable inclusion of a larger number of specimens.

Contribution

Participation in the data collection, discussion of the data, and editing of the manuscript.

Cervical and Crown Outline Analysis of Worn Neanderthal and Modern Human Lower Second Deciduous Molars

Stefano Benazzi,[1,2]* Cinzia Fornai,[2] Laura Buti,[3] Michel Toussaint,[4] Francesco Mallegni,[5] Stefano Ricci,[6] Giorgio Gruppioni,[3] Gerhard W. Weber,[2] Silvana Condemi,[7] and Annamaria Ronchitelli[6]

[1]*Department of Human Evolution, Max Planck Institute for Evolutionary Anthropology, Deutscher Platz 6, 04103 Leipzig, Germany*
[2]*Department of Anthropology, University of Vienna, Althanstrasse 14, 1090 Vienna, Austria*
[3]*Department of History and Methods for the Conservation of Cultural Heritage, University of Bologna, 48100 Ravenna, Italy*
[4]*Direction de l'Archéologie, Service Public de Wallonie, 1 rue des Brigades d'Irlande, B-5100 Namur, Belgium*
[5]*Department of Biology, University of Pisa, Via S. Maria 53, 56126 Pisa, Italy*
[6]*Department of Environmental Sciences "G. Sarfatti," U.R. Prehistoric Ecology, University of Siena, Via Laterina 8, 53100 Siena, Italy*
[7]*ADES, UMR 7268 CNRS/Université Aix Marseille/EFS, Faculté de Médecine/Secteur Nord, CS80011 Bd Pierre Dramard 13344, Marseille Cedex 15, France*

KEY WORDS deciduous teeth; crown and cervical outlines; geometric morphometrics; wear

ABSTRACT Despite the general increase in digital techniques for dental morphometric analyses, only a few methods are available to study worn teeth. Moreover, permanent dentitions are studied much more frequently than deciduous teeth. In this study, we address both issues by providing a taxonomic classification of Neanderthal and modern human (MH) lower second deciduous molars (dm_2s) through the analysis of crown and cervical outlines. Crown and cervical outlines were obtained from a three-dimensional (3D) digital sample of uniformly oriented dm_2s. Both outlines were centered on the centroid of their area and represented by 16 pseudolandmarks obtained by equiangularly spaced radial vectors out of the centroid. We removed size information from the oriented and centered outlines with a uniform scaling of the pseudolandmark configurations to unit Centroid Size. Group shape variation was evaluated separately for the dm_2 crown and cervical outlines through a shape–space principal component (PC) analysis. Finally, quadratic discriminant analysis of a subset of PCs was used to classify the specimens. Our results demonstrate that both outlines successfully separate the two groups. Neanderthals showed a buccodistal expansion and convex lingual outline shape, whilst MHs have buccodistal reduction and straight lingual outline shape. Therefore, we confirmed that the cervical outline represents an effective parameter for distinguishing between the two taxa when dealing with worn or damaged dm_2s. Am J Phys Anthropol 149:537–546, 2012.

Teeth are the most abundant remains in the fossil record and bear crucial biological and therefore taxonomical evidence. For this reason, much effort has been devoted in the development of methodologies to revealing information that teeth convey. To overcome the limitations linked to caliper measurements, two-dimensional (2D) and three-dimensional (3D) computer-based methods have been used to quantify and describe, for example, the crown shape, with particular emphasis to the occlusal surface (i.e., Wood et al., 1983; Peretz et al., 1998; Bailey, 2004; Kondo and Townsend, 2006; Martinón-Torres et al., 2006; Gómez-Robles et al., 2007; Benazzi et al., 2011a,b; Fiorenza et al., 2011a), the internal structure of the teeth (i.e., Smith et al., 2007; Olejniczak et al., 2008; Smith et al., 2010; Benazzi et al., 2011a,c,d), and the dental root morphology (Kupczik and Hublin, 2010; Emonet et al., 2012).

Despite the methodological advances of the last 30 years, we acknowledge an imbalance in dental research, because digital methods have generally been applied to permanent teeth (mainly to postcanine dentition), whereas very few contributions have focused on the deciduous dentition. Among the latter, Bayle e al. (2009a,b, 2010) have addressed this problem by studying the dental developmental pattern and tooth tissue proportions in a sample of Neanderthal and Upper Paleolithic modern human (UPMH) deciduous teeth. Toussaint et al. (2010) used the lateral enamel thickness to confirm the taxonomy of the Neanderthal lower second deciduous molar (dm_2) from the cave of Trou de l'Abîme (Couvin, Belgium). Benazzi et al. (2011c) provided the first comparison of dental measurement systems collected by digital models for taxonomic assignment of Neanderthal

Grant sponsor: Hominid Grant 2007; Grant number: NSF BCS 0725126; Grant sponsor: A.E.R.S. Dental Medicine Organisations GmbH; Grant number: FA547013.

*Correspondence to: Stefano Benazzi, Deutscher Platz 6, Leipzig 04103, Germany. E-mail: stefano_benazzi@eva.mpg.de

Received 7 June 2012; accepted 29 August 2012

DOI 10.1002/ajpa.22155
Published online 17 October 2012 in Wiley Online Library (wileyonlinelibrary.com).

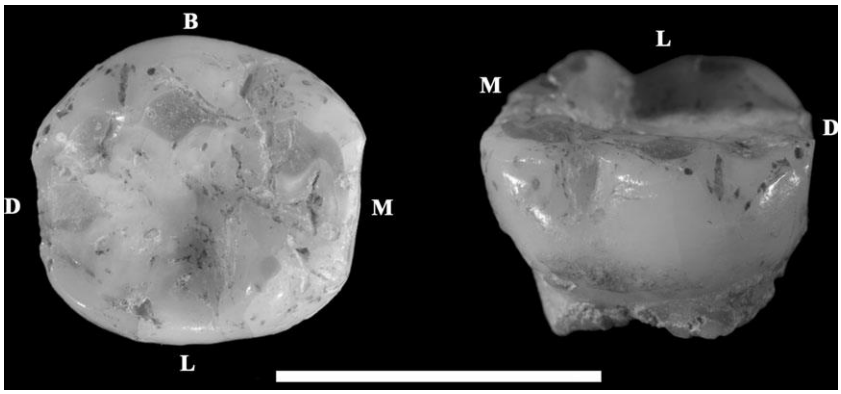

Fig. 1. Occlusal view (left) and buccal view (right) of Cavallo A, a Neanderthal lower left second deciduous molar (Ldm_2). B, buccal; D, distal; L, lingual; M, mesial. The white bar in the figure is equivalent to 1 cm.

and modern human (MH) dm_2s. In a recent contribution, Benazzi et al. (2011a) have applied geometric morphometric (GM) methods and investigated the dental tissue proportions for the taxonomic reassessment of two upper deciduous molars found in the Uluzzian ("transitional" cultural) levels of Grotta del Cavallo (Apulia, South Italy). The authors compared the crown (for the dm^1) and the cervical outline (for the dm^2), as well as the enamel thickness of the deciduous molars from Grotta del Cavallo, with those of large samples of MHs and Neanderthals, and confirmed their attribution to MHs. Finally, Zanolli et al. (2012) used the analysis of dental tissue proportions to support a preliminary classification to *Homo erectus* of two deciduous molars from the Pleistocene deposits of the Sangiran Dome (Java, Indonesia).

The paucity of methodologically advanced studies focused on deciduous dentition is most probably due to the rarity of these remains in the fossil records. Conversely, one can usually form larger samples when investigating permanent teeth, where the likelihood of including well-preserved, unworn, or only slightly worn crowns increases. An adequate sample size represents an essential requirement for many morphometric analyses, such as the quantification of 2D and 3D enamel thickness or landmark-based analyses.

We acknowledge the need to overcome the problem of sample size and, in any case, to be able to study heavily worn or damaged teeth for which it is no longer possible to recognize anatomical landmarks on the crown. It is crucial to apply methods that focus on the features still observable, which, hopefully, must still possess taxonomical resolution. For example, the crown of a specimen-like Cavallo A (dm_2; Fig. 1) cannot be used for current landmark-based techniques [such as those proposed, e.g., by Martinón-Torres et al. (2006) or Skinner et al. (2008)], because most of the anatomical features of the occlusal surface, including the dentine horn tips, are obliterated. As a consequence, this tooth and other dm_2s (like Couvin, Krapina d66, Scladina 4A-13) would simply be discarded from the analysis. Nonetheless, the crown outline and the cervix are also usually preserved in worn teeth. These features have been demonstrated to convey morphological information useful for distinguishing between Neanderthal and MH permanent first molars (Benazzi et al., 2011b) and deciduous upper molars (Benazzi et al., 2011a) and might also be useful for the dm_2 when other crown features (e.g., midtrigonid crest and anterior fovea) are lost.

In this contribution, we apply GM methods to analyze the crown and cervical outlines of dm_2s for the purpose of taxonomic discrimination between Neanderthals and MHs. We aim to assess the discriminant power of these variables with respect to these two human taxa with particular interest in the cervical outline, which might be one of the very few features identifiable in a very worn or damaged dental crown. As a corollary to the main core of this contribution, we show how the crown outline analysis can be successfully applied to published images of teeth in occlusal view. In particular, we used the image data of the deciduous molar Bondi 1 (from Bondi Cave, near the town of Chiatura, Western Georgia), published in a journal article by Tushabramishvili et al. (2012), because its taxonomic attribution is still controversial.

MATERIALS AND METHODS

Sample

Our sample consists of 54 dm_2s, including 14 Neanderthal (N) specimens, seven UPMH, and 31 recent modern humans (RMH). Provenance, taxonomy, laterality, and wear stage [based on Smith (1984)] are provided in Table 1.[1]

In addition, the sample includes two debated specimens. One of these is the Lagar Velho child, which is usually attributed to UPMH, but possesses mixed Neanderthal- and MH-like morphological features (Duarte et al., 1999; Bayle et al., 2010). The second specimen is the

[1]The dental remains from Grotta Paglicci, Apulia, Italy, are unpublished; therefore, we provide below additional archeological information. Paglicci 38 was unearthed by Palma di Cesnola from level 21d, an evolved phase of the Gravettian, chronologically dated 24.720 6 420 BP (F 55 14C uncal on charcoal; Palma di Cesnola, 1975). Paglicci 39–42 were found in a deposit that was severely disturbed by intruders at the beginning of the last century. They penetrated from a small aperture into the hall room of the cave with the intention of reaching an inner room, the so-called room 2. Before this violation, the cave had been sealed by a collapse dating back to the late Upper Paleolithic. The sieving of the disturbed deposit has supplied some human and faunal remains, artworks, and lithic tools representing the entire Epigravettian sequence of the cave (but neither Gravettian nor Aurignacian were documented in this deposit). A new 14C dating of a faunal specimen found in the disturbed deposit has been dated to the Tardiglacial (LABEL, University of Florence; data unpublished), confirming the attribution of Paglicci 39–42 to a late phase of the Upper Paleolithic.

TABLE 1. List of fossil and extant human dm_2s

Taxon	Specimen	Country	Side	Source	Wear stage[a]
N[c]	Abri Suard S14–5	France	R	NESPOS (µCT)[b]	2
	Abri Suard S37	France	R	NESPOS (µCT)[b]	1
	Abri Suard S42	France	R	NESPOS (µCT)[b]	1
	Cavallo A	Italy	L	Benazzi et al. (2011c) (µCT)	5
	Couvin	Belgium	R	Toussaint et al. (2010) (µCT)	3
	Engis 2	Belgium	R	Toussaint et al. (2010) (µCT)	3
	Krapina d62	Croatia	L	NESPOS (µCT)[b]	2
	Krapina d63	Croatia	L	NESPOS (µCT)[b]	3
	Krapina d64	Croatia	L	NESPOS (µCT)[b]	3
	Krapina d65	Croatia	L	NESPOS (µCT)[b]	1
	Krapina d66	Croatia	L	NESPOS (µCT)[b]	4
	Krapina d68	Croatia	R	NESPOS (µCT)[b]	1
	Roc de Marsal 1	France	L	NESPOS (µCT)[b]	1
	Scladina 4A-13	Belgium	L	NESPOS (µCT)[b]	6
UPMH[d]	Dolní Věstonice 36–6	Czech Republic	L	Toussaint et al. (2010) (µCT)	1
	La Madeleine 4	France	L	Original data (µCT)	1
	Paglicci 38	Italy	R	NESPOS (µCT)[b]	1
	Paglicci 39	Italy	L	Original data (surface scan of the cast)	3
	Paglicci 40	Italy	R	Original data (surface scan of the cast)	1
	Paglicci 41	Italy	L	Original data (surface scan of the cast)	3
	Paglicci 42	Italy	L	Original data (surface scan of the cast)	6
Unclassified	Bondi 1	Georgia	R	Original data (surface scan of the cast)	7
	Lagar Velho 1	Portugal	R	Tushabramishvili et al. (2012) (2D image)	2
RMH[e]	From Medieval and contemporary samples[f]	Austria 5 14	L 5 9; R 5 5	NESPOS (µCT)[b] Original data (µCT)	Wear stage 1 5 21
		France 5 7	L		Wear stage 2 5 6
		Italy 5 10	L	Bayle et al. (2010), NESPOS (µCT)[b]	Wear stage 3 5 4

[a] Based on Smith (1984).
[b] NESPOS Database/www.nespos.org.
[c] N, Neanderthals.
[d] UPMH, Upper Paleolithic modern humans.
[e] RMH, recent modern humans.
[f] Hosted at the Department of Anthropology (University of Vienna, Austria), the University of Bordeaux, the Institut d'Anatomie of Strasbourg (France), and the Department of History and Method for the Conservation of Cultural Heritage, University of Bologna (Ravenna, Italy).

human tooth Bondi 1 [presumably a right dm_2 based on several morphological traits, i.e., rectangular shape, bulbous morphology, and the shape of the preserved parts of the roots; see Tushabramishvili et al. (2012)]. Bondi 1 represents the oldest human remain in an Upper Paleolithic context in Georgia (dated to between 25.7 and 29.5 ka Cal BP), for which Tushabramishvili et al. (2012) hypothesize an attribution to *Homo sapiens sp.* Nonetheless, these authors have pointed out that further hominin material from the site is needed to confirm whether Bondi 1 should be classified as Neanderthal or MH.

All molars are regarded as left molars, where actual right molars were mirror-imaged before any further computation. From this dental sample, 54 crown outlines and 51 cervical outlines were collected.

Scanning and 3D reconstruction of the specimens

Microcomputed tomography (µCT) scans of all the specimens, with the exception of the UPMH sample from Grotta Paglicci (see below), were undertaken by means of industrial and synchrotron-based µCT scanners at isotropic voxel length between 15 and 55 µm. Part of the µCT scans ("original data" in Table 1) was produced with a Viscom X8060 µCT scanner using the following scan parameters: 130 kV, 100 mA, and voxel size 5 25 μm^3. Details about the µCT scanning procedure for the other specimens can be found in Bayle et al. (2009a,b, 2010), Toussaint et al. (2010), Benazzi et al. (2011c), and the NESPOS (Neanderthal Studies Professional Online Service) Database 2011.

The µCT images were virtually segmented following the half-maximum height protocol (Spoor et al., 1993), and 3D digital models of the external surface were then reconstructed using the software package Amira 5.4 (Mercury Computer Systems, Chelmsford, MA). Conversely, the 3D digital surface models of the teeth from Grotta Paglicci were obtained as follows. The teeth were molded using Provil[1] Novo Light C.D.2 (Heraeus Kulzer GmbH) silicone, and the methyl methacrylate-based resin Technovit 3040 (Heraeus Kulzer GmbH) was used to obtain the positive replica. The digital models were generated using a white-light scanning system with a resolution of 50 µm (ScanProbe ST, ScanSystems s.r.l.). The postprocessing of the scan-data point clouds was carried out in RapidForm XOR2 (INUS Technology).

Morphometric analysis

The cervical line of each tooth was digitized with a "spline curve" in RapidForm XOR2 (Fig. 2a), and the best-fit plane of the cervical line (here, cervical plane) was computed (Fig. 2b). Each tooth was then aligned with the cervical plane parallel to the *xy*-plane of the Cartesian coordinate system and rotated around the *z*-axis in order to comply with the following criteria: the mesiodistal groove parallel to the *x*-axis; the lingual groove parallel to the *y*-axis; the *x*-axis parallel to the tangent to the geometrical minimum of the two lobes of the lingual side (Fig. 2c,d). In some cases (e.g., extremely

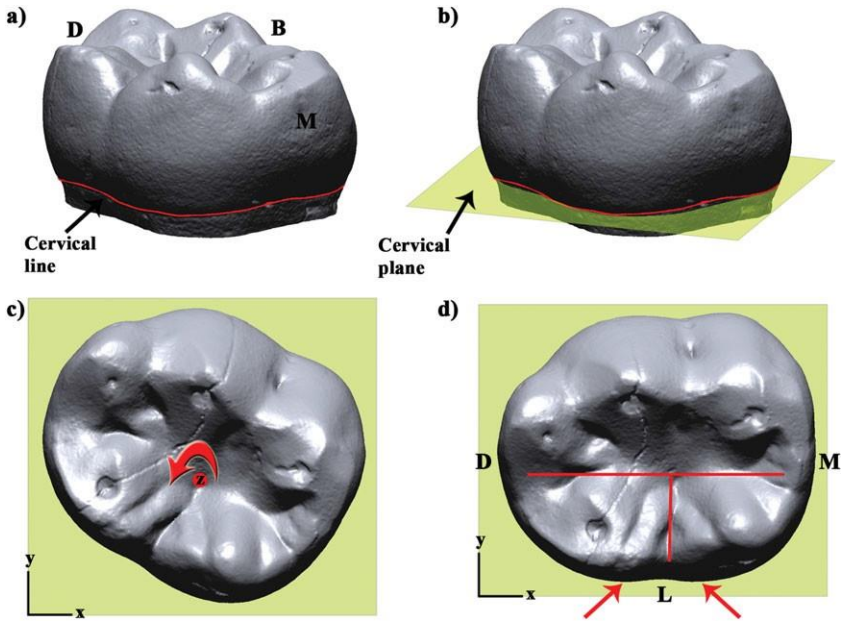

Fig. 2. 3D digital model of a modern human specimen. (a) A spline curve was digitized on the cervical line. (b) A best-fit plane of the curve was computed. (c) The tooth was realigned with the cervical plane parallel to the *xy*-plane of the Cartesian co-ordinate system and rotated along the *z*-axis to comply with the following criteria. (d) The mesiodistal groove is parallel to the *x*-axis, the lingual groove is parallel to the *y*-axis; the *x*-axis parallel to the tangent to the geometrical minimum of the two lobes of the lingual side. B, buccal; D, distal; L, lingual; M, mesial.

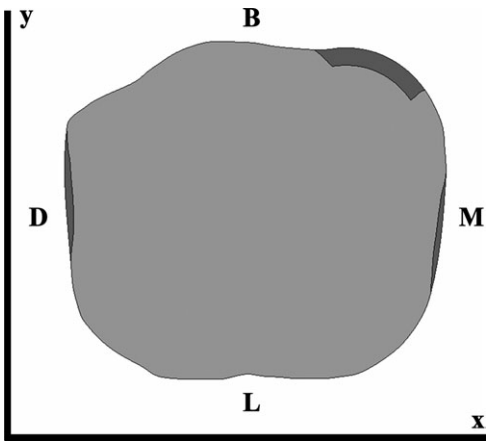

Fig. 3. 2D virtual reconstruction of Bondi 1 crown outline. The crown outline of the original tooth is in gray; the reconstructed portions are shown in dark gray. The specimen is oriented with the lingual side parallel to the *x*-axis (namely, the tangent to the geometrical minimum of the two lobes of the lingual side is parallel to the *x*-axis). B, buccal; D, distal; L, lingual; M, mesial.

worn teeth where grooves might be obliterated, lingual side forming one single concavity), only subsets of these criteria were used.

The contour of the section identified by the cervical plane represents the cervical outline (Benazzi et al., 2011a,b). The crown outline corresponds to the silhouette of the oriented crown as seen in occlusal view and projected onto the cervical plane. Where teeth showed interproximal wear, the crown outline of the original mesial or distal borders was corrected with reference to the buccolingual extent of the wear facet, the outline curvature following the crown margins in occlusal view [as performed by Wood and Engleman (1988), Bailey (2004), Benazzi et al. (2011b), among others].

A different approach was needed for Bondi 1, where only the crown outline could be sampled from the image of the tooth in occlusal view, published by Tushabramishvili et al. (2012; Fig. 4a, p. 183). The picture was imported in Rhino 4.0 Beta CAD environment (Robert McNeel & Associates, Seattle, WA). The image was aligned to the *xy*-plane of the Cartesian co-ordinate system and rotated around the *z*-axis with reference to the lingual side (namely, the tangent to the geometrical minimum of the two lobes of the lingual side is parallel to the *x*-axis). The crown outline was manually digitized and then mirrored to obtain a left dm_2 crown outline (Fig. 3). The missing region of the enamel outline on the mesiobuccal side was restored virtually through offset of the corresponding dentine outline by a length equal to the enamel thickness measured in the fracture (Fig. 3). The interproximal wear was virtually compensated as mentioned earlier. However, because Bondi 1 could obviously not be oriented following our protocol, the results it provide must be considered with caution.

In Rhino 4.0, both crown outlines and cervical outlines were centered superimposing the centroids of their area. All the outlines were represented by 16 pseudolandmarks obtained by equiangularly spaced radial vectors out of the centroid. The first radius is directed buccally and parallel to the *y*-axis of the Cartesian coordinate system (Fig. 4a,b; Benazzi et al., 2011b). Finally, we removed size information from the oriented and centered outlines with a uniform scaling of the pseudo-landmark configurations to unit Centroid Size. It is important to emphasize that the procedure followed differs from a proper generalize procrustes analysis, wherein rotation, translation, and scaling are driven by the landmark configurations. In our GM approach, that still provides

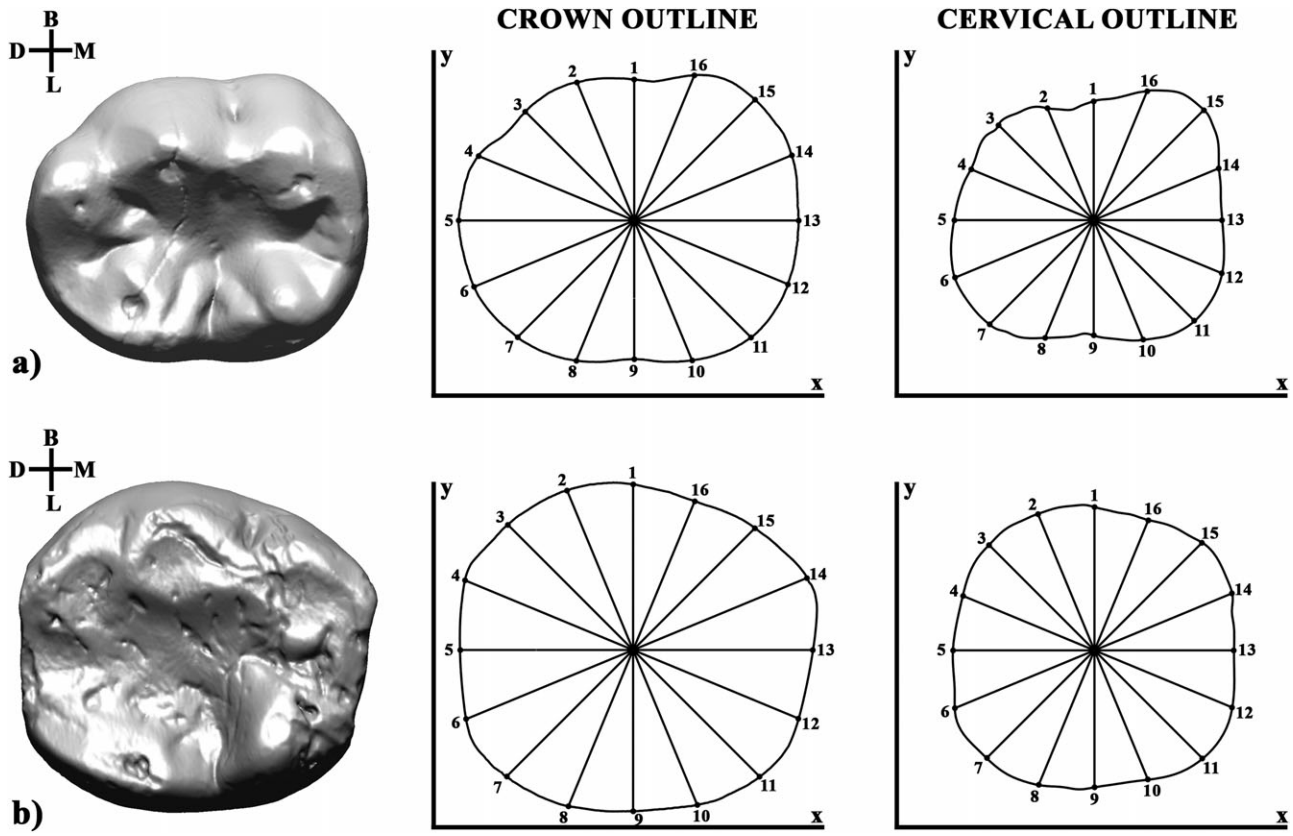

Fig. 4. (a) 3D digital model of a modern human specimen (left); crown outline (middle) and cervical outline (right) area subdivided into 16 equiangular radii out of the centroid; (b) 3D digital model of the Neanderthal specimen Cavallo A (left); crown outline (middle) and cervical outline (right) area subdivided into 16 equiangular radii out of the centroid. In both cases, the first radius is buccally directed and parallel to the *y*-axis of the Cartesian coordinate system. B, buccal; D, distal; L lingual; M mesial.

shape coordinates, we tackled the problem related to rotation and translation by constraining the orientation of the teeth based on anatomical considerations (see above). For the same reason, we did not slide the pseudo landmarks, both because caution has been suggested in using sliding semilandmark techniques (i.e., minimization of Procrustes distance and minimization of bending energy) to analyze individual curves (De Groote et al., 2010), and because our interpretation of the biological nature of the anatomical variation might be influenced in different ways by each of these techniques (Bruner and Bastir, 2009).

A principal component analysis (PCA) of the matrix of shape co-ordinates was carried out separately for the dm_2 crown and cervical outlines. Neanderthals were compared both to the complete MH sample (MH 5 RMH 1 UPMH) and separately with the UPMH sample alone. Because the specimens Lagar Velho 1 and Bondi 1 were considered to be taxonomically undetermined, the shape variables of their crown outlines as well as the cervical outline of Lagar Velho 1 were projected into the space built from the comparative sample only to assess their dental outline shapes with respect to the MH and the Neanderthal outline shape variation.

We used leave-one-out cross-validation quadratic discriminant analysis (QDA) of a subset of PCs to classify the specimens. To evaluate the number of PCs needed for QDA, we applied Anderson's formula to test the deviation from joint equality of any sequence of consecutive eigenvalues (Anderson, 1963). We built up QDA models leaving out the data of Lagar Velho 1 and Bondi 1. The computation of the posterior probabilities (P_{post}) was made with an equal prior probability (P_{prior}) of 0.5 for Neanderthal and MH groups. We used a cross-validation approach (leave-one-out method) to assign each of the specimens to the group with the higher posterior probability. The Lagar Velho 1 and Bondi 1 specimens have been tested through all the iterations of leave-one-out cross-validation QDAs.

The data was processed and analyzed through software routines written in R (R Development Core Team, 2010).

Intraobserver and interobserver error

It has already been proved that lCT scan and the white-light scanning system provide very reliable digital models (i.e., Olejniczak et al., 2007; Fiorenza et al., 2009) and that molars can be consistently oriented using the cervical line (Benazzi et al., 2009, 2011a,b,c). Similarly, the identification of the cervical plane, the projection of the crown outline onto this plane, and all the procedures to collect the 16 pseudolandmarks on the centered outlines are semiautomatic processes that require minimal or even no subjective intervention. On the contrary, the rotation of the tooth around the *z*-axis requires a manual intervention and is thus subjective. To evaluate the intra- and interobserver error associated

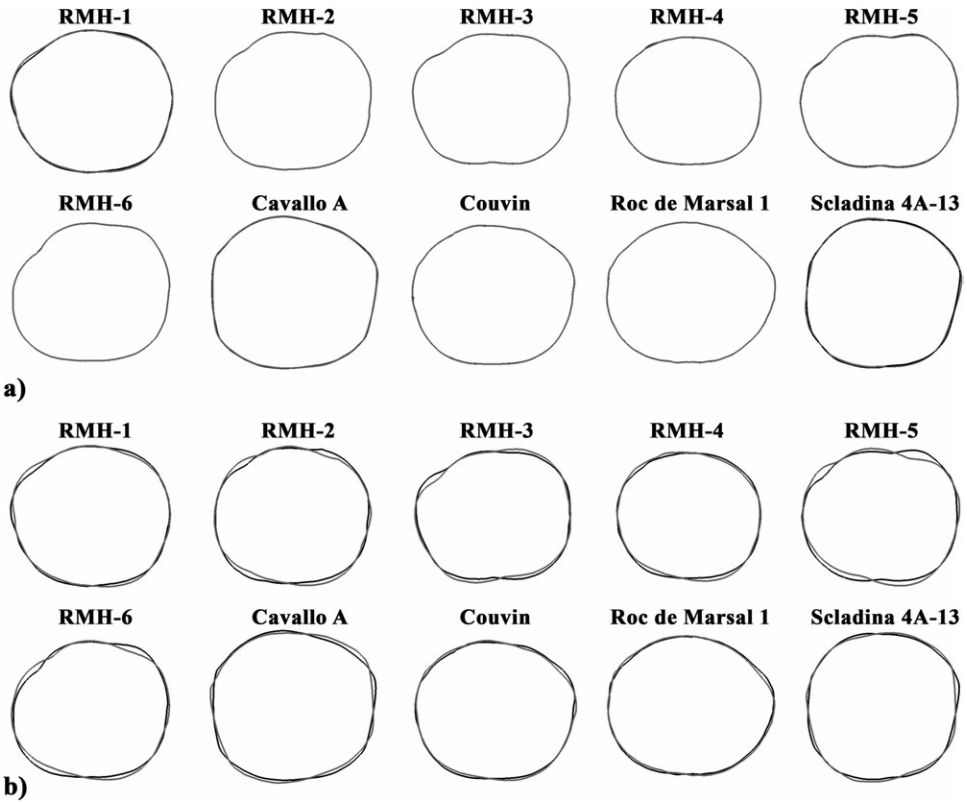

Fig. 5. (a) Ten outlines reoriented by SB and CF, superimposed on the centroid of their area; (b) Ten specimens intentionally reoriented in a slightly wrong position superimposed onto 10 specimens oriented following the method explained in the text.

with this manual rotation, a subsample of 10 specimens was randomly sampled using R software ($N = 4$; MH = 6), and two of us (SB and CF) reoriented them two times each in a time span of about 10 months (Fig. 5a). For each specimen, the Euclidian distance to the mean of the same form was measured, and the analysis of variance (ANOVA) was used to compare the means of the groups (observations). No statistical differences were observed for both the intraobserver (SB: F value = 0.253, $P = 0.778$; CF: F value = 0.234, $P = 0.634$) and interobserver error (F value = 0.758, $P = 0.388$). To further check for the reliability of the orientation, we perturbed the system by including one additional group, wherein the 10 specimens were intentionally reoriented in a wrong position (range of rotation angle between 78 and 168; Fig. 5b). Afterward, we carried out an ANOVA with Tukey's post hoc tests to determine differences between groups. Although the pairwise comparisons between the first four group means were not significant ($P > 0.752$), the new group showed significant differences from all the others ($P < 0.001$). This result further confirms that the approach we used to orient the dm_2s is very precise.

RESULTS

Figure 6a,b shows the results of the PCAs of Neanderthal and of MH (RMH + UPMH) dm_2 crown outlines (Fig. 6a) and cervical outlines (Fig. 6b). For the crown outlines, the first three PCs account for about 80% of the total variance. Neanderthals and MHs separate along PC2 (31.3%), which expresses size-dependent shape variation (static allometry, $r = 20.588$; $P < 0.001$), while there is no such trend for PC1 and PC3 (the latter is not shown). Neanderthals show a buccodistal outline expansion and a convex lingual outline shape (PC2 high scores), while RMH and UPMH specimens are associated with a buccodistal reduction of the outline and a straighter lingual side (PC2 low scores). Along PC1 (41.5%), which characterizes size-independent shape variation ($r = 0.025$; $P = 0.859$), higher scores are associated with a wide mesiodistal outline (subrectangular shape), while lower scores show a subcircular shape. Along PC1, the UPMH sample shows a much wider variability compared to RMH. Bondi 1 plots well within the range of variability of the MH sample, while Lagar Velho 1 falls between the two groups.

The result of the cross-validation QDA of the first three PCs (applied to the sample of 52 crown outlines, without Lagar Velho 1 and Bondi 1) shows that about 92% of the Neanderthals and MHs is correctly classified (Table 2). Among the misclassified MH, one belongs to the UPMH group (Paglicci 39). Based on the prediction model, both Lagar Velho 1 and Bondi 1 are classified as MH with a P_{post} of 0.58 and 0.99, respectively.

In the analysis of the dm_2 cervical outlines (Fig. 6b), the first three PCs account for about 74.7% of the total variance. Neanderthals and MHs separate along PC1 (35.5%), which expresses size-dependent shape variation (static allometry, $r = 0.59$; $P < 0.001$), but they overlap along PC2 and PC3 (the latter not shown). Neanderthal dm_2s are characterized by a subcircular cervical outline, with a buccodistal expansion and convex lingual outline shape (high-score PC1), while MH (RMH + UPMH) specimens have subsquare outlines with a strong buccodistal reduction and straighter lingual side (low-score PC1). PC2 (24.7%) shows shape changes not related with

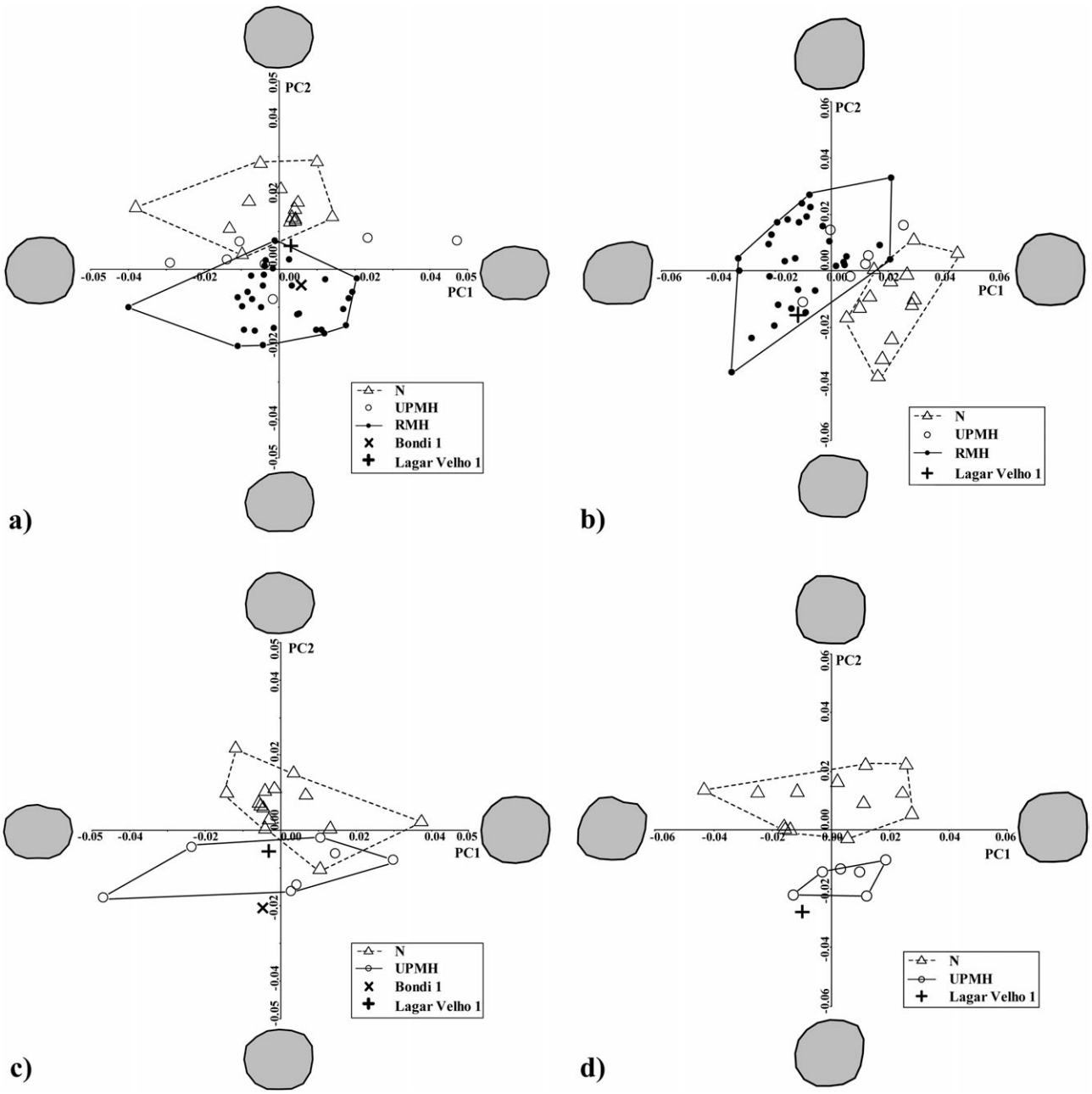

Fig. 6. Shape-space PCA plots of Neanderthals and MH (RMH 1 UPMH) dm_2 crown outlines (a) and cervical outlines (b). Shape-space PCA plots of Neanderthals and UPMH dm_2 crown outlines (c) and cervical outlines (d). The deformed mean outlines in the four directions of the PCs are drawn at the extremity of each axis. N, Neanderthal; UPMH, Upper Paleolithic modern human; RMH, recent modern human.

size (r 5 20.22; P 5 0.116). Low scores account for subsquare outlines and slight buccodistal outline expansion, while high scores are related to subsquare shapes with buccodistal reduction. Lagar Velho 1 plots within the MH range.

The cross-validation QDA of the first three PCs (applied to the whole sample of 50 cervical outlines, without Lagar Velho 1) leads to a correct classification of 96% of the specimens and attributes Lagar Velho 1 to MHs with a P_{post} [0.98.

Results do not change when Neanderthals are compared to the UPMH sample alone (Fig. 6c,d; Table 2). Even though we acknowledge the small UPMH sample size, both for crown outline (PC1 5 55.5%; PC2 5 19.9%; Fig. 6c) and, to a greater extent, for cervical outline (PC1 5 41.7%; PC2 5 23.9%; Fig. 6d), UPMH and Neanderthals separate along PC2, based on the same morphological features previously described. It is worth noting, however, that in both cases, PC2 is not correlated with size (for crown outline, r 5 0.313; P 5 0.167; for cervical outline, r 5 0.396; P 5 0.08), so that the morphological differences observed between the two groups should not be interpreted in terms of allometry. As observed previously, two Neanderthals and Paglicci 39 are misclassified

TABLE 2. Results of the cross-validation QDA for the dm_2 crown and cervical outline

Parameter	n	Misclassified		Total misclassified	Correctly classified (%)	n	Misclassified		Total misclassified	Correctly classified (%)
		MH[a]	N[b]				UPMH	N		
Crown outline	52[c]	2	2	4	92.3	21[e]	1	2	3	85.7
Cervical outline	50[d]	1	1	2	96.0	19[f]	0	0	0	100

[a] Recent modern humans (RMH) and Upper Paleolithic modern humans (UPMH).
[b] Neanderthals.
[c] Without Lagar Velho 1 and Bondi 1.
[d] Without Lagar Velho 1.
[e] UPMH and Neanderthals, without Lagar Velho 1 and Bondi 1.
[f] UPMH and Neanderthals, without Bondi 1.

based on the crown outline, but all the specimens are correctly classified using the cervical outline (Table 2). Once again, in both cases, Bondi 1 and Lagar Velho 1 are attributed to UPMH, the latter with a $P_{post} = 0.78$ and $P_{post} > 0.99$ for the crown outline and the cervical outline, respectively.

DISCUSSION AND CONCLUSIONS

Teeth are the most abundant hominin remains found in the fossil assemblages, hence numerous morphological and morphometric approaches have been developed for their description and analysis. In the scientific literature, the studies of permanent dentition predominate over those focused on deciduous teeth (i.e., Bayle et al., 2009a,b, 2010; Toussaint et al., 2010; Benazzi et al., 2011a,c; Zanolli et al., 2012). Moreover, most of the computer-based methods currently in use in dental biology are conceived for unworn or slightly worn teeth and few deal with the issue of wear (i.e., Hillson et al., 2005; Benazzi et al., 2011a,b,c). The morphometric methods focused on cusp morphology cannot be applied on worn teeth (e.g., Martinón-Torres et al., 2006; Gómez-Robles et al., 2007). To overcome the problem of wear in landmark-based studies of the dental cusps, some researchers have suggested carrying out an approximation of the position of the original cusp's apex, either in the center of the exposed dentine (Bailey, 2004) or in the center of the wear facet (Martinón-Torres et al., 2006), but the accuracy of such approximations has never been tested. Indeed, the position, shape, and size of wear facets and dentine basins are extremely variable, depending on crown morphology, antagonistic relation, occlusal movements, food properties, environmental, and behavioral factors (e.g., Lussi, 2006; Fiorenza et al., 2011b; Kullmer et al., 2012). A similar problem occurs when investigating the enamel dentine junction—EDJ [like in Skinner et al. (2008)] if wear has already affected the dentine. The analyses of the enamel thickness and dental tissue proportions (Olejniczak et al., 2008) also require unworn teeth or, at least, a uniform degree of wear across the sample (Benazzi et al., 2011a).

Therefore, there is no doubt that heavily worn teeth, on which no anatomical landmarks are preserved, represent a great challenge for morphometric analysis, and we cannot presume to develop methods that entirely overcome the lack of data. In this study, we use crown and cervical outlines for the taxonomic discrimination of worn Neanderthal and MH lower second deciduous molars (dm_2s), because these are variables still present in worn teeth and, at the same time, have been demonstrated to discriminate between Neanderthals and MHs for other dental types (Benazzi et al., 2011a,b). Our protocol for the orientation of the dental images is highly reproducible, and even the most subjective of its phases, namely the rotation of the oriented crown along the z-axis, is not associated with significant intra- and inter-observer error. Among the advantages of our method, we emphasize in the first place the possibility of considering dental specimens affected by a high degree of occlusal wear (even though this approach could be effectively applied to the study of heterogeneously worn dental samples or even unworn teeth). This is a way to overcome the problem of the small sample size, which is recurrent in anthropology and paleoanthropology.

The results of this analysis indicate that both outlines successfully separate Neanderthals and MH, with more than 96% of the specimens correctly classified. The same outcome is obtained when Neanderthals are compared to the UPMH sample only. In both analyses (with and without RMH), the morphological differences observed for Neanderthals (buccodistal expansion and convex lingual outline shape) and for MHs (buccodistal reduction and straight lingual outline shape) crown outlines are also reflected in the cervical outline. Nonetheless, whereas in the first case (RMH included), the separation between the two groups is accounted for by allometric components of variation (size-dependent shape variation), in the second case, (RMH excluded), the same morphological features, which distinguish Neanderthals and UPMHs, are uncorrelated with size. To some extent, this result suggests that RMH dm_2s have generally maintained the UPMH dm_2 morphology, but with a size reduction.

Some further considerations are needed for the UPMH sample and in particular for Lagar Velho 1 and Bondi 1. Despite the fact that the UPMHs tend to separate from the Neanderthal group, the UPMH crown outlines are not only more variable than the RMH crown outlines (with some specimens close to the Neanderthal range of variability), but they are even more variable than the cervical outlines of the same group. This might explain the attribution of Lagar Velho 1 to UPMH with a low P_{post} based on the crown outline. This ambiguous result is remarkably consistent with the former characterization of this tooth as a mixed Neanderthal-MH-like morphology (Duarte et al., 1999; Bayle et al., 2010). This specimen has been used to argue in favor of a Neanderthal/MH admixture in the Iberian Peninsula (Zilhão et al., 2010). Nonetheless, we should also point out that another UPMH specimen, Paglicci 39, was incorrectly classified as Neanderthal based on the crown outline, but correctly attributed to MHs on the basis of the cervi-

cal outline. Based on our sample, these results suggest that the UPMH dm_2s shows a morphological variability higher than that of RMH and Neanderthals. However, we also emphasize that a larger UPMH dm_2 sample and a RMH dm_2 sample including geographically distinct populations are needed in order to obtain more comprehensive information on the morphological differences both between RMHs and UPMHs and between Neanderthals and UPMHs. If future research confirms our assumption that UPMH shows a larger morphological variability than RMH, then caution is needed when Neanderthals are compared to MH samples mainly represented by RMH specimens. In fact, it would be reasonable to think that the latter might not represent the variability of early MHs.

Tushabramishvili et al. (2012) hypothesized that Bondi 1 dm_2 belongs to MHs, but they could not assess with certainty the taxonomic attribution on the basis of the morphological features due to the heavy wear of this tooth. Our results also suggest that Bondi 1 belongs to MHs. Even though the picture of the tooth we used for the analysis was not oriented consistently with the rest of the sample, we believe that these results should be taken into account. Accordingly, we suggest that a standard approach for the orientation of teeth should be used before the acquisition of photos in occlusal view [as such, e.g., proposed by Benazzi et al. (2009) and based on the identification of three points at the cervical line of upper and lower M1s]. This would give easy access to the published data for rigorous analyses.

To conclude, the cervical outline represents a reliable parameter for distinguishing between Neanderthal and MH dm_2s and can be used when the dm_2 crowns are too worn or damaged. Interestingly, similar but less clear results were obtained for the permanent lower first molars, M_1s (Benazzi et al., 2011b). The M_1 crown outline was proved to be a more effective taxonomic indicator than the cervical outline. Nonetheless, the authors recognized the same morphology of the M_1 crown outline (for the most part) and the cervical outline in the dm_2s (namely, buccodistal expansion/reduction, and convex/straight lingual outline shape). These results confirm the general notion that dm2s have a marked resemblance to M1s (i.e., Hillson, 1996). Moreover, the shape differences in the distobuccal side between Neanderthal and MH dm_2s have been observed in the distolingual side of the maxillary counterparts too (Benazzi et al., 2011a), but the degree of correlation between upper and lower deciduous molar morphology is yet to be ascertained.

ACKNOWLEDGMENTS

The authors thank Priscilla Bayle and Jiří Svoboda for providing fossil and modern human specimens used in this work. We are grateful to the Portuguese Ministério da Cultura, the French Musée National de Préhistoire, and the UMR 5199 Université Bordeaux 1. Access to the fossil specimens was made possible by the NESPOS (Neanderthal Studies Professional Online Service) Database 2011 (https://www.nespos.org/display/openspace/Home). We thank the Soprintendenza per i Beni Archeologici della Puglia, which facilitated the excavation of Grotta Paglicci and Grotta del Cavallo over the years and encouraged the collaboration with the University of Siena for the study of the archaeological remains. We also thank Caterina Minghetti for the surface scan of Paglicci dental sample. We acknowledge the Laboratory of Anthropology of the Department of History and Methods for the Conservation of Cultural Heritage (University of Bologna, Italy) for providing the white-light scanning system ScanProbe ST.

LITERATURE CITED

Anderson TW. 1963. Asymptotic theory for principal component analysis. Ann Math Stat 34:122–148.

Bailey SE. 2004. A morphometric analysis of maxillary molar crowns of Middle-Late Pleistocene hominins. J Hum Evol 47:183–198.

Bayle P, Braga J, Mazurier A, Macchiarelli R. 2009a. Dental developmental pattern of the Neanderthal child from Roc de Marsal: a high-resolution 3D analysis. J Hum Evol 56:66–75.

Bayle P, Braga J, Mazurier A, Macchiarelli R. 2009b. Brief communication: high-resolution assessment of the dental developmental pattern and characterization of tooth tissue proportions in the late Upper Paleolithic child from La Madeleine, France. Am J Phys Anthropol 138:493–498.

Bayle P, Macchiarelli R, Trinkaus E, Duarte C, Mazurier A, Zilhão J. 2010. Dental maturational sequence and dental tissue proportions in the early Upper Paleolithic child from Abrigo do Lagar Velho, Portugal. Proc Natl Acad Sci 107:1338–1342.

Benazzi S, Fantini M, De Crescenzio F, Persiani F, Gruppioni G. 2009. Improving the spatial orientation of human teeth using a virtual 3D approach. J Hum Evol 56:286–293.

Benazzi S, Douka K, Fornai C, Bauer CC, Kullmer O, Svoboda J, Pap I, Mallegni F, Bayle P, Coquerelle M, Condemi S, Ronchitelli A, Harvati K, Weber GW. 2011a. Early dispersal of modern humans in Europe and implications for Neanderthal behaviour. Nature 479:525–528.

Benazzi S, Coquerelle M, Fiorenza L, Bookstein F, Katina S, Kullmer O. 2011b. Comparison of dental measurement systems for taxonomic assignment of first molars. Am J Phys Anthropol 144:342–354.

Benazzi S, Fornai C, Bayle P, Coquerelle M, Kullmer O, Mallegni F, Weber GW. 2011c. Comparison of dental measurement systems for taxonomic assignment of Neanderthal and modern human lower second deciduous molars. J Hum Evol 61:320–326.

Benazzi S, Viola B, Kullmer O, Fiorenza L, Harvati K, Paul T, Gruppioni G, Weber GW, Mallegni F. 2011d. A reassessment of the Neanderthal teeth from Taddeo Cave (southern Italy). J Hum Evol 61:377–387.

Bruner E, Bastir M. 2009. Landmarks could slide, brains cannot: interpreting models of shape variation. Paleontol I Evol 3:33.

De Groote I, Lockwood CA, Aiello LC. 2010. Technical note: a new method for measuring long bone curvature using 3D landmarks and semi-landmarks. Am J Phys Anthropol 141:658–64.

Duarte C, Maurício J, Pettitt PB, Souto P, Trinkaus E, van der Plicht H, Zilhão J. 1999. The early Upper Paleolithic human skeleton from the Abrigo do Lagar Velho (Portugal) and modern human emergence in Iberia. Proc Natl Acad Sci 96:7604–7609.

Emonet EG, Tafforeau P, Chaimanee Y, Guy F, de Bonis L, Koufos G, Jaeger JJ. 2012. Three-dimensional analysis of mandibular dental root morphology in hominoids. J Hum Evol 62:146–154.

Fiorenza L, Benazzi S, Kullmer O. 2009. Morphology, wear and 3D digital surface models: materials and techniques to create high-resolution replicas of teeth. J Anthropol Sci 87:211–218.

Fiorenza L, Benazzi S, Viola B, Kullmer O, Schrenk F. 2011a. Relationship between cusp size and occlusal wear pattern in Neanderthal and *Homo sapiens* first maxillary molars. Anat Rec 294:453–461.

Fiorenza L, Benazzi S, Tausch J, Kullmer O, Bormage TG, Schrenk F. 2011b. Molar macrowear reveals Neanderthal eco-geographic dietary variation. PLoS ONE 6:e14769.

Gómez-Robles A, Martinón-Torres M, Bermúdez de Castro JM. 2007. A geometric morphometric analysis of hominin upper first molar shape. J Hum Evol 53:272–285.

Hillson S. 1996. Dental anthropology. Cambridge: Cambridge University Press.

Hillson S, Fitzgerald C, Flinn H. 2005. Alternative dental measurements: proposals and relationships with other measurements. Am J Phys Anthropol 126:413–426.

Kondo S, Townsend GC. 2006. Associations between Carabelli trait and cusp areas in human permanent maxillary first molars. Am J Phys Anthropol 129:196–203.

Kullmer O, Schulz D, Benazzi S. 2012. An experimental approach to evaluate the correspondence between wear facet position and occlusal movements. Anat Rec 295:846–852.

Kupczik K, Hublin J-J. 2010. Mandibular molar root morphology in Neanderthals and Late Pleistocene and recent *Homo sapiens*. J Hum Evol 59:525–541.

Lussi A. 2006. Dental erosion—from diagnosis to therapy. In: Whitford GM, editor. Monographs in oral science, Vol. 20. Basel: Karger.

Martinón-Torres M, Bastir M, Bermúdez de Castro JM, Gómez-Robles A, Sarmiento S, Muela A, Arsuaga JL. 2006. Hominin lower second premolar morphology: evolutionary inferences through geometric morphometric analysis. J Hum Evol 50:523–533.

Olejniczak AJ, Tafforeau P, Smith TM, Temming H, Hublin J-J. 2007. Technical note: compatibility of microtomographic imaging systems for dental measurements. Am J Phys Anthropol 134:130–134.

Olejniczak AJ, Smith TM, Feeney RNM, Macchiarelli R, Mazurier A, Bondioli L, Rosas A, Fortea J, de la Rasilla M, Garcia-Tabernero A, Radovcîc' J, Skinner MM, Toussaint M, Hublin J-J. 2008. Molar tissue proportions and enamel thickness distinguish Neanderthals from modern humans. J Hum Evol 55:12–23.

Palma di Cesnola A. 1975. Il Gravettiano della Grotta Paglicci nel Gargano. I. L'industria litica e la cronologia assoluta. Rivis Sci Preistoriche XXX:3–178.

Peretz B, Nevis N, Smith P. 1998. Morphometric analysis of developing crowns of maxillary primary second molars and permanent first molars in humans. Arch Oral Biol 43:525–533.

R Development Core Team. 2010. R: a language and environment for statistical computing. Vienna, Austria: R Foundation for Statistical Computing.http://www.r-project.org.

Skinner MM, Gunz P, Wood BA, Hublin J-J. 2008. Enamel-dentine junction (EDJ) morphology distinguishes the lower molars of *Australopithecus africanus* and *Paranthropus robustus*. J Hum Evol 55:979–988.

Smith BH, 1984. Patterns of molar wear in hunter-gatherers and agriculturists. Am J Phys Anthropol 63:39–56.

Smith TM, Tafforeau P, Reid DJ, Pouech J, Lazzari V, Zermeno JP, Guatelli-Steinberg D, Olejniczak AJ, Hoffman A, Radovcic J, Makaremi M, Toussaint M, Stringer C, Hublin J-J. 2010. Dental evidence for ontogenetic differences between modern humans and Neanderthals. Proc Natl Acad Sci 107:20923–20928.

Smith TM, Toussaint M, Reid DJ, Olejniczak AJ, Hublin J-J. 2007. Rapid dental development in a Middle Paleolithic Belgian Neanderthal. Proc Natl Acad Sci 104:20220–20225.

Spoor CF, Zonneveld FW, Macho GA. 1993. Linear measurements of cortical bone and dental enamel by computed tomography: applications and problems. Am J Phys Anthropol 91:469–484.

Toussaint M, Olejniczak AJ, El Zaatari S, Cattelain P, Flas D, Letourneux C, Pirson S. 2010. The Neanderthal lower right deciduous second molar from Trou de l'Abîme at Couvin, Belgium. J Hum Evol 58:56–67.

Tushabramishvili N, Pleurdeau D, Moncel MH, Agapishvili T, Vekua A, Bukhsianidze M, Maureille B, Muskhelishvili A, Mshvildadze M, Kapanadze N, Lordkipanidze D. 2012. Human remains from a new Upper Pleistocene sequence in Bondi Cave (Western Georgia). J Hum Evol 62:179–185.

Wood BA, Abbott SA, Graham SH. 1983. Analysis of the dental morphology of Plio-Pleistocene hominids. II. Mandibular molars-study of cusp areas, fissure pattern and cross sectional shape of the crown. J Anat 137:287–314.

Zanolli C, Bondioli L, Mancini L, Mazurier A, Widianto H, Macchiarelli R. 2012. Brief communication: two human fossil deciduous molars from the Sangiran Dome (Java, Indonesia): outer and inner morphology. Am J Phys Anthropol 147:472–481.

Zilhão J, Davis SJ, Duarte C, Soares AM, Steier P, Wild E. 2010. Pego do Diabo (Loures, Portugal): dating the emergence of anatomical modernity in westernmost Eurasia. PLoS One 5:e8880.

2.4. Technical Note: Guidelines for the digital computation of 2D and 3D enamel thickness in hominoid teeth.

Benazzi, S., Panetta, D., Fornai, C., Toussaint, M., Gruppioni, G., Hublin, J.-J.

American Journal of Physical Anthropology 2014; 153, 305-313.

Synopsis

With the advent of CT-based imaging techniques, new approaches for the investigation of the enamel thickness have proliferated. This chapter represents a contribution to the literature focused on the analysis of the enamel thickness and dental tissue proportions in hominoid teeth. It reviews in a comparative and quantitative way various methods proposed by different authors and suggests a standardization of the methods through accurate, automated, and highly reproducible protocols for the evaluation of both 2D and 3D enamel thickness of the different dental types in hominoids.

Contribution

Minor participation in the data collection, discussion of the protocols, and editing of the manuscript.

Technical Note: Guidelines for the Digital Computation of 2D and 3D Enamel Thickness in Hominoid Teeth

Stefano Benazzi,[1]* Daniele Panetta,[2] Cinzia Fornai,[3] Michel Toussaint,[4] Giorgio Gruppioni,[5] and Jean-Jacques Hublin[1]

[1]*Department of Human Evolution, Max Planck Institute for Evolutionary Anthropology, Deutscher Platz 6, Leipzig 04103, Germany*
[2]*CNR Institute of Clinical Physiology, National Research Council, Via G. Moruzzi 1, Pisa 56124, Italy*
[3]*Department of Anthropology, University of Vienna, Althanstrasse 14, Vienna 1090, Austria*
[4]*Direction de l'Archeologie, Service Public de Wallonie, 1 rue des Brigades d'Irlande, Namur B-5100, Belgium*
[5]*Department of Cultural Heritage, University of Bologna, Via degli Ariani 1, Ravenna 48121, Italy*

KEY WORDS enamel thickness; digital methods; micro-computed tomography; hominoid teeth

ABSTRACT The study of enamel thickness has received considerable attention in regard to the taxonomic, phylogenetic and dietary assessment of human and non-human primates. Recent developments based on two-dimensional (2D) and three-dimensional (3D) digital techniques have facilitated accurate analyses, preserving the original object from invasive procedures. Various digital protocols have been proposed. These include several procedures based on manual handling of the virtual models and technical shortcomings, which prevent other scholars from confidently reproducing the entire digital protocol. There is a compelling need for standard, reproducible, and well-tailored protocols for the digital analysis of 2D and 3D dental enamel thickness. In this contribution we provide essential guidelines for the digital computation of 2D and 3D enamel thickness in hominoid molars, premolars, canines and incisors. We modify previous techniques suggested for 2D analysis and we develop a new approach for 3D analysis that can also be applied to premolars and anterior teeth. For each tooth class, the cervical line should be considered as the fundamental morphological feature both to isolate the crown from the root (for 3D analysis) and to define the direction of the cross-sections (for 2D analysis). Am J Phys Anthropol 153:305–313, 2014. v 2013 Wiley Periodicals, Inc.

Enamel thickness analysis plays an important role in the taxonomic, phylogenetic, and dietary assessment of extant and fossil primates (Schwartz, 2000; Martin et al., 2003; Grine et al., 2005; Olejniczak et al., 2007; Smith et al., 2012). Following Martin's method for measuring enamel thickness using a single physical cross-section on primate teeth (1985), non-destructive methods based on both synchrotron and standard micro-computed tomography (micro-CT) have been suggested to refine the two-dimensional (2D) enamel thickness analysis and to study the thickness of dental enamel in its full three-dimensional (3D) form (Kono, 2004; Tafforeau, 2004; Olejniczak, 2006; Olejniczak et al., 2008). Indeed, physical cross-sections of the teeth passing through dentine horn tips do not only fail to convey the information carried by the enamel cap morphology, but they are also prone to introduce errors due to slightly oblique planar sections (Suwa and Kono, 2005). To overcome this limitation, 3D digital models must be oriented based on a reference plane, which allows for both the creation of ideal planes of section (for 2D analysis) and for separating the crown from the root(s) (for 3D analysis).

Several studies have focused on the investigation of enamel thickness in permanent and deciduous molars (Schwartz, 2000; Martin et al., 2003; Grine et al., 2005; Olejniczak et al., 2008; Benazzi et al., 2011a–c, 2013). With regards to permanent molars, Kono (2004; but see also Suwa and Kono, 2005) identified the reference plane by iterative oscillation of the model to view the maximum occlusal surface. Tafforeau (2004) suggested two ways to create the reference plane: the first method aims to define a plane that approximates the cervical line, while the second method envisages a system of animation that orients the digital model based on the best-fit plane containing the major dentine horn tips. Olejniczak (2006) cautioned about Kono's approach, because not entirely independent of the enamel thickness to be measured. Furthermore, he considered Tafforeau's first method less effective than the method based on the dentine horn tips due to the difficulty in fitting a plane into the cervical line. Therefore, for 2D enamel thickness analysis Olejniczak (2006) simplified Tafforeau's second method, reorienting the micro-CT image volume of each tooth according to the plane intersecting the dentine

Additional Supporting Information may be found in the online version of this article.

Abbreviations: AET, Average enamel thickness; ANOVA, Analysis of variance; EDJ, Enamel-dentine junction; micro-CT, Micro-computed tomography; RET, Relative enamel thickness

Grant sponsor: Max Planck Society, A.E.R.S. Dental Medicine Organisations GmbH, Vienna, Austria.

*Correspondence to: Dr. Stefano Benazzi, Deutscher Platz 6, Leipzig 04103, Germany. E-mail: stefano_benazzi@eva.mpg.de

Received 14 June 2013; accepted 22 October 2013

DOI: 10.1002/ajpa.22421
Published online 18 November 2013 in Wiley Online Library (wileyonlinelibrary.com).

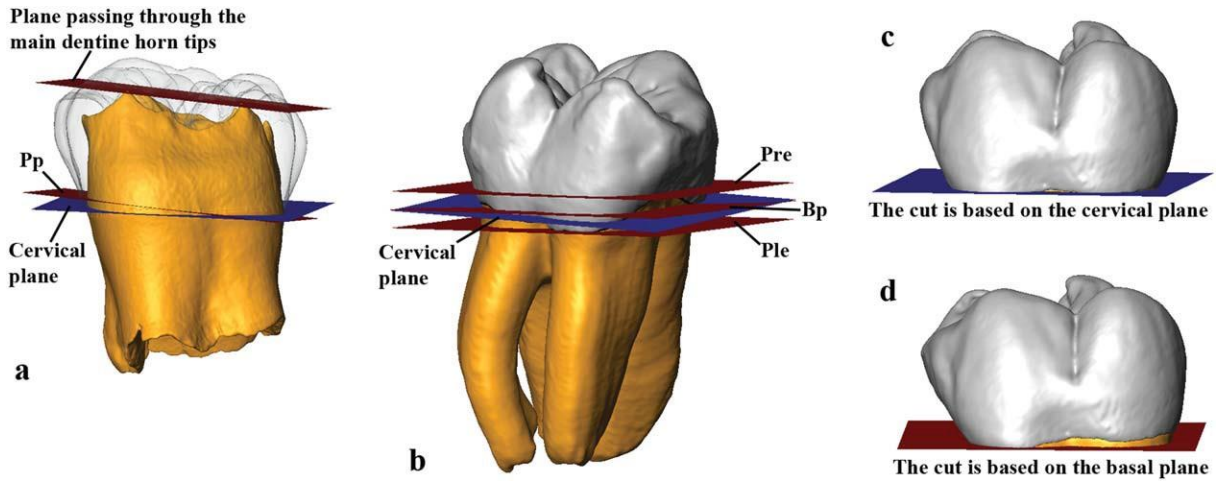

Fig. 1. (a) The three-dimensional (3D) digital model of the Neandertal upper right second molar (RM^2) SCLA_4A_3 (buccal view); the enamel is transparent to better show the plane intersecting the three main dentine horn tips and a plane parallel to the latter (Pp) placed at the level of the cervical line to compare its orientation with the cervical plane (the best-fit plane of the cervical line). (b) Mesiobuccal view of the 3D digital model of the gorilla specimen 31,435 (LM^2); plane Bp (basal plane) is the average plane between the most apical plane of section containing a continuous ring of enamel at the cervix (Pre) and the most apical plane that is both parallel to the continuous ring of enamel and which contains the most apical extension of enamel (Ple). On the right, lingual view of the LM^2 crown of the gorilla specimen 31,435 separated from the root based on the cervical plane (c) and the basal plane (d).

horn tips of the three principal cusps. A virtual section, perpendicular to the above-mentioned plane and passing through the two mesial dentine horn tips, provides the essential information for 2D mesial enamel thickness analysis. For 3D enamel thickness analysis, Olejniczak suggested to isolate the crown from the root based on an average plane ("basal plane") computed between "The most apical plane of section containing a continuous ring of enamel at the cervix (which represents the plane of section suggested by Kono to separate the crown cap)…" and "…the most apical plane that is both parallel to the continuous ring of enamel and which contains the most apical extension of enamel…" (Olejniczak, 2006: 127).

However, shortcomings in both 2D and 3D methods proposed by Olejniczak might affect the reliability of the final outcome and limit their use by other scholars. With regard to 2D enamel thickness analyses, it is evident from Figure 1a that the plane passing through the main dentine horn tips might be oblique with respect to the cervical margin of the tooth. With regard to 3D enamel thickness analysis, the orientation of the image stack was manually adjusted (by rotation and translation) to acquire the most apical continuous ring of enamel (Fig. 1b), as suggested by Kono (2004). Therefore, the identification of the basal plane would be operator-dependent and hence prone to error. The final position of the basal plane, and consequently the dental tissue proportion values, also depends on the most apical extension of the cervical enamel. If a tooth presents a localized and pronounced apical enamel extension (as can happen in hominoid molars), then the basal plane will be more apically placed. This would result in an increase of dentine volume with minimum effect on the enamel volume (Fig. 1b–d). Finally, Olejniczak's (2006), Kono's (2004) and Tafforeau's (2004) 3D methods, are all conceived for molar teeth, but cannot be applied to premolars and anterior teeth.

There is a lack in the literature of methods for the analysis of enamel thickness in premolars, canines and incisors, where the data available is mostly derived from physical cross-sections of the teeth (Schwartz and Dean, 2005; Saunders et al., 2007; Smith et al., 2008, 2012). Feeney et al. (2010) addressed this issue, but the digital approach they developed presents several limitations. First of all, it has been developed for modern human canines and premolars, but it does not apply to other hominoid teeth with more complex morphology; second, it is still limited to a plane of section (2D analysis); third, it implies a manual (and therefore subjective) handling (or translation and rotation) of the micro-CT image stack both to orient the tooth and to identify a ring of enamel with uniform width near the cervical margin. Moreover, measurements are not obtained directly from the software used to create the section (3D modeling or Computer-Aided Design, CAD, software), but several intermediate steps are needed: once virtual sections are created "… a scale bar was inserted and the image was exported into Adobe Photoshop CS3 (v. 10.0) and subsequently saved as a TIFF image before measurement with ImageJ" (Feeney et al., 2010: 193).

There is a compelling need for standard, reproducible, and well-tailored protocols for the digital analysis of 2D and 3D enamel thickness of hominoid teeth to facilitate researchers in using them, and to produce comparable results. In this contribution, we provide guidelines to compute the 2D and 3D enamel thickness for complete hominoid crowns from molars, premolars, canines, and incisors. For molars, we suggest two alternative methods for the computation of the 3D enamel thickness. For premolars, canines and incisors we have developed an entirely new protocol for 3D enamel thickness analysis and we have refined Feeney and colleagues (2010) approach to compute the values of the components of 2D enamel thickness in hominoid teeth. In addition, we carried out the 2D and 3D analysis of enamel thickness for a small sample of molars in order to compare the results of our approach to that of Olejniczak (2006), who carefully reviewed the methods previously published by

TABLE 1. Abbreviations of the methods compared to separate the coronal dentine from the root dentine (for 3D), and to identify the ideal planes of section (for 2D)

	Method	Description	Source
For 3D	3D-a	Separation based on the best-fit plane of the cervical line	Standardization and automation of Tafforeau's first method (2004)
	3D-b	Separation based on the cervical line itself	Original method
	3D-c	Separation based on the average (basal) plane between the most apical plane of section containing a continuous ring of enamel at the cervix and the most apical plane that is both parallel to the continuous ring of enamel and which contains the most apical extension of enamel	Olejniczak (2006)
For 2D	2D-a	Section perpendicular to the best-fit plane of the cervical line	Standardization and automation of Tafforeau's first method (2004)
	2D-b	Section passing through two points digitized on the widest labiolingual bi-cervical diameter and the dentine horn tip (or central mamelon in incisors)	Refinement of Feeney and colleagues' (2010) approach
	2D-c	Section perpendicular to the plane intersecting the three main dentine horn tips	Olejniczak (2006)

TABLE 2. List of teeth used for enamel thickness analysis

Taxon	Specimen ID	Tooth class
Homo sapiens[a]	09–162	Upper left second incisor—LI^2
	08–298	Upper right canine—RC^1
	M35	Lower right third premolar—RP_3
	M125	Upper left second molar—LM^2
Homo neanderthalensis[b]	SCLA_4A_12	Lower right canine—RC_1
	SCLA_4A_6	Lower right third premolar—RP_3
	SCLA_4A_3	Upper right second molar—RM^2
Pan troglodytes verus[c]	11800	Lower right canine—RC_1
	15012	Lower left third premolar—LP_3
	14999	Upper left second molar—LM^2
Gorilla gorilla[d]	31435	Lower right second incisor—RI_2
	31435	Upper left third premolar—LP^3
	31435	Upper left second molar—LM^2

[a] Housed at the Max Planck Institute for Evolutionary Anthropology, Leipzig, Germany.
[b] Specimens from Scladina, Belgium.
[c] Specimens from the Taï Chimpanzee Skeletal Collection, housed at the Max Planck Institute for Evolutionary Anthropology, Leipzig, Germany.
[d] Female skull stored at the Museum für Naturkunde, Humboldt Universität, Berlin, Germany.

Kono (2004) and Tafforeau (2004). The methods used in this contribution and their abbreviations are listed in Table 1 and are described in more detail below.

MATERIALS AND METHODS

The dental sample included in this study comprises 13 teeth (Table 2): four recent *Homo sapiens* (LI^2, RC^1, RP_3, LM^2), three *Homo neanderthalensis* (RC_1, RP_3, RM^2), three *Pan troglodytes verus* (RC_1, LP_3, LM^2), and three *Gorilla gorilla* (RI_2, LP^3, LM^2). All the teeth are unworn, except for the *Pan* canine and the *Gorilla* incisor, which are slightly worn.

The *Homo sapiens*, Neandertal and *Pan* specimens were scanned with a Skyscan 1172 micro-CT (Max Planck Institute for Evolutionary Anthropology, Leipzig, Germany) using the following scan parameters: 100 kV, 100 μA, with an aluminum/copper filter (0.5 mm/0.04 mm thickness). Volume data were reconstructed using isometric voxels ranging between 13.39 and 28.07 μm. The gorilla's skull was micro-CT scanned at the Bundesanstalt für Materialforschung und –prüfung, Berlin, Germany (scan parameters: 160 kV, 150 μA, 1.0 mm copper filter). Volume data were reconstructed using isometric voxels of 61 μm. The image stack was segmented using a semiautomatic threshold-based approach in Avizo 7 (Visualization Sciences Group) to separate the enamel and the dentine and to reconstruct a 3D digital model of the tooth (Figs. 1–4).

The digital models were then imported in Rapidform XOR2 (INUS Technology, Seoul, Korea), which allows digitizing curves and points on the teeth, creating planes of section passing through specific points and perpendicular to previously defined planes, as well as computing volume, surface and length of digital entities (but other software packages for 3D image processing and CAD, such as PolyWorks, 3D Studio Max, Rhinoceros can be used for the same purposes).

Molars

3D enamel thickness. Hominin molars have a nearly planar cervical line, while in great apes such as *Gorilla* and *Pan* it is more sinuous. We propose two methods for

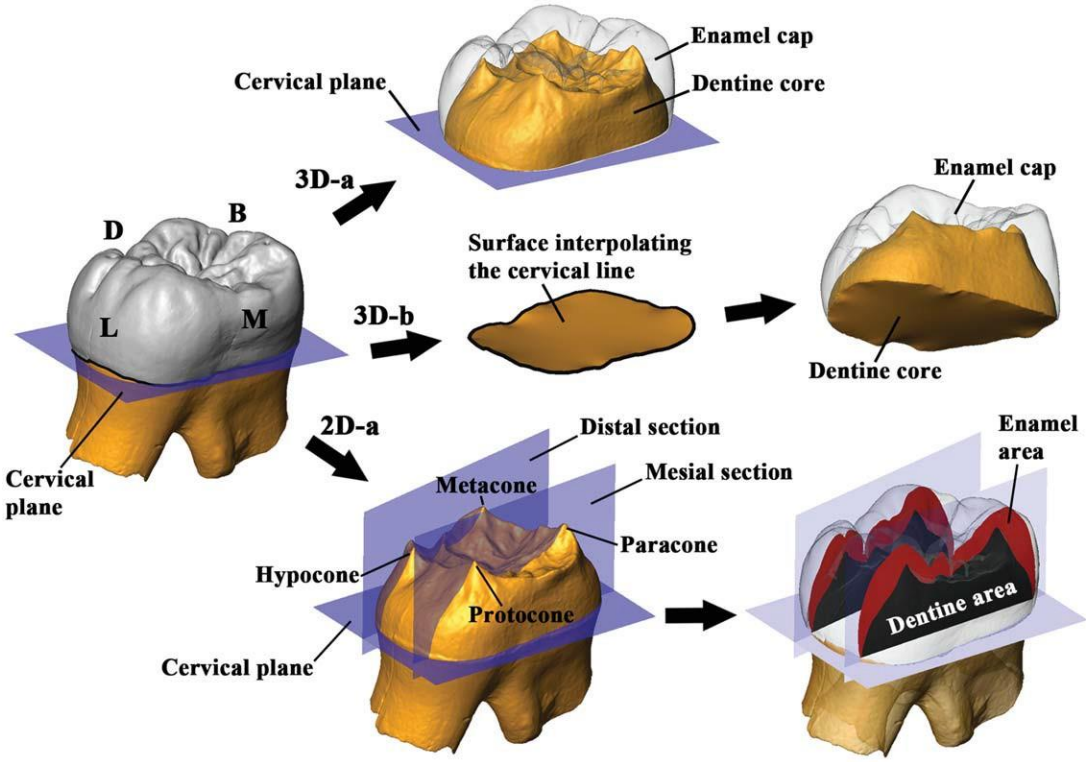

Fig. 2. On the left, a spline curve (black) was digitized on the cervical line of SCLA_4A_3 upper right second molar (RM^2), and the best-fit plane of the curve (cervical plane) was computed. For 2D enamel thickness, the mesial and distal sections are perpendicular to the cervical plane, and pass through the mesial (paracone and protocone) and distal (metacone and hypocone) dentine horn tips, respectively (method 2D-a). For 3D enamel thickness, two methods are visualized: 3D-a, where the crown was separated from the root based on the cervical plane; 3D-b, where the coronal dentine was separated from the root dentine based on the cervical line, which was then interpolated by a smooth surface to seal the bottom of the coronal dentine. B 5 buccal; D 5 distal; L 5 lingual; M 5 mesial.

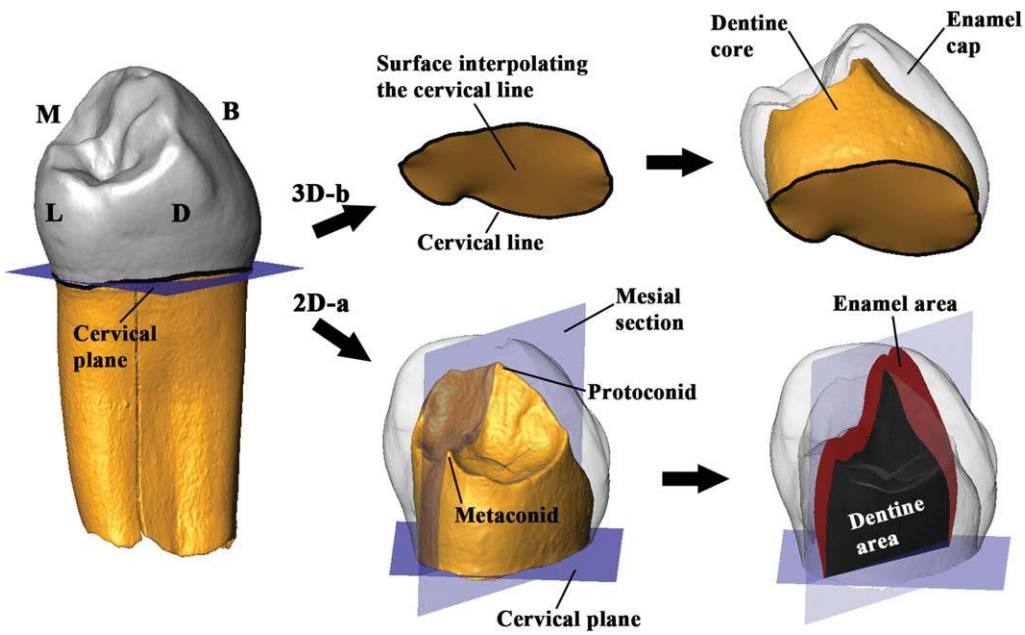

Fig. 3. On the left, a spline curve (black) was digitized on the cervical line of SCLA_4A_6 lower right third premolar (RP_3). For 2D enamel thickness, the best-fit plane of the curve was computed (cervical plane), and a mesial section perpendicular to this plane and passing through the mesial (protoconid and metaconid) dentine horn tips was created (method 2D-a). For 3D enamel thickness, the coronal dentine was separated from the root dentine based on the cervical line, which was then interpolated by a smooth surface to seal the bottom of the dentine core (method 3D-b). B 5 buccal; D 5 distal; L 5 lingual; M 5 mesial.

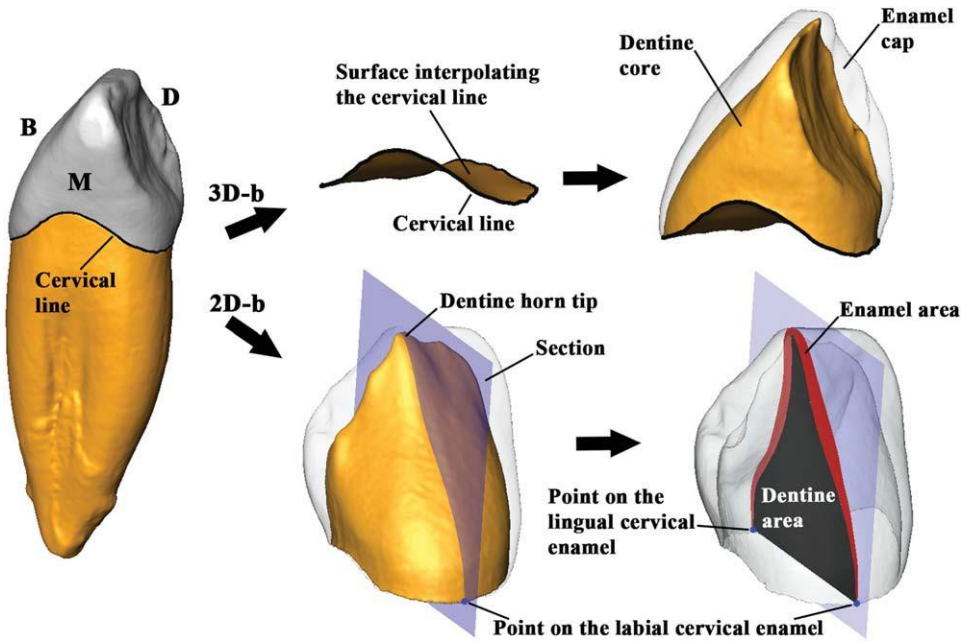

Fig. 4. On the left, a spline curve (black) was digitized on the cervical line of SCLA_4A_12 lower right canine (RC_4). For 3D enamel thickness, the coronal dentine was separated from the root dentine based on the cervical line, which was then interpolated by a smooth surface to seal the bottom of the dentine core (method 3D-b). For 2D enamel thickness, the cross-section passes through two points digitized on the widest labiolingual bi-cervical diameter and one point digitized on the dentine horn tip (method 2D-b). B = buccal; D = distal; M = mesial.

3D enamel thickness analysis of molars, the first of which is suitable in the case the cervical line is almost planar. In both cases, the cervical line was sampled using a spline curve (namely, a curve which requires being continuous and smooth, and is generated by placing numerous points along the cervical line itself). In the first method (hereafter called 3D-a; see Table 1), a best-fit plane through the points of the curve was computed (cervical plane) to separate the crown from the roots (Fig. 2) and most probably from a small portion of cervical enamel. This approach represents a standardization and automation of Tafforeau's first method (2004; see above). In our second method (hereafter called 3D-b) the entire enamel cap was considered, and the coronal dentine was separated from the root dentine using the curve digitized along the cervical line itself, instead of its best-fit plane. Finally, this curve was interpolated with a smooth surface to seal the bottom of the dentine core (Fig. 2). It stands to reason that if the cervical line was perfectly planar, then both methods would provide the same results, because the interpolating surface would correspond to the best-fit plane.

2D enamel thickness. Digital cross-sections perpendicular to the cervical plane and passing through the two mesial (for the mesial section) dentine horn tips (paracone and protocone in upper molars; protoconid and metaconid in lower molars) or distal (for the distal section) dentine horn tips (metacone and hypocone in upper molars; hypoconid and entoconid in lower molars) were created (method 2D-a; see Table 1). Even though the 2D enamel thickness analysis is traditionally measured on mesial sections, we believe that distal sections might be useful when the mesial cusps are damaged, as other scholars shown (Smith et al., 2005). To seal the section at its base, a line was digitized to join the most buccal to the most lingual apical extension of the enamel (Fig. 2; the same approach is used for premolars and anterior teeth; see below). Note that here the best-fit plane is used as a reference to identify sections perpendicular to it, but is not used as a base for the section.

Premolars

3D enamel thickness. In premolars the trend of the cervical line is halfway between the nearly straight line of molars and the wavy appearance of the anterior teeth. Therefore, for 3D enamel thickness it is more rigorous to use our method 3D-b, which takes into account the sinuous trend of the cervical line (Fig. 3).

2D enamel thickness. We suggest to apply the same approach described for molars (method 2D-a), which implies the use of a virtual section of the tooth perpendicular to the best-fit plane of the cervical line and passing through the main dentine horn tips (protoconid and metaconid in lower premolars; paracone and protocone in upper premolars) (Fig. 3). However, when a lingual cusp is not present (as in some hominoid P3s), we suggest to digitize a point on the labial cervical enamel in correspondence with the widest labiolingual bi-cervical diameter.

Canines and incisors

3D enamel thickness. The wavy course of the cervical line in the anterior teeth does not allow us to compute a reliable cervical plane to separate the crown from the root. Owing to its buccal and lingual apical convexity, as well as its strong mesial and distal apical concavity, the cervical plane would both remove portions of the buccal

and lingual enamel and include large portions of dentine from the mesial and distal sides of the root. Only method 3D-b is suggested for 3D enamel thickness analysis of the anterior teeth. Therefore, a spline curve was digitized on the cervical line of the canines and incisors to isolate the coronal dentine, which was then closed by interpolating the curve with a smooth surface (Fig. 4).

2D enamel thickness. We slightly modified Feeney et al. (2010) approach (method 2D-b; see Table 1). The virtual section passes through two points digitized on the widest labiolingual bi-cervical diameter and the dentine horn tip (or central mamelon in incisors) (Fig. 4). If a central mamelon cannot be clearly defined, a curve is digitized on the dentine occlusal edge, and the mid-point of this curve should be used.

It is worth noting that despite what software and technical procedures are used, what matters is to achieve the isolation of the crown from the roots and the orientation of the sections as suggested above. Software for image manipulation and CAD can be flexible and versatile: for example, all the steps mentioned above to create virtual sections in molars, premolars and anterior teeth (e.g., tooth orientation based on the best-fit plane of the cervical line, digitization of the two points at the widest labiolingual bi-cervical diameter) can be also performed prior to segmentation using an isosurface of the tooth (e.g., in Avizo). The virtual section only would be segmented and exported in Rapidform to record measurements for the analysis of 2D enamel thickness.

Data collection

3D analysis. For all tooth classes, the following measurements were obtained from the crown (Olejniczak et al., 2008): the volume of the enamel cap (mm^3); the volume of the dentine core (which includes the volume of the coronal pulp—mm^3); the enamel-dentine junction (EDJ) surface (the interface between the enamel cap and the dentine core—mm^2) (Figs. 2–4). These measurements, which were rendered by the software, were used for the computation of both the 3D average enamel thickness index (3D AET 5 volume of enamel divided by the EDJ surface; index in millimeters) and the 3D relative enamel thickness index (3D RET 5 3D AET divided by the cubic root of dentine volume; scale-free index).

2D analysis. The following measurements were recorded from the sections (Martin, 1985): the area of the enamel cap (mm^2); the area of the coronal dentine, which includes the coronal pulp (mm^2); the length of the EDJ (the linear interface between the enamel area and the dentine area—mm) (Figs. 2–4). These were used for the computation of the 2D average enamel thickness index (2D AET 5 the area of the enamel cap divided by the length of the EDJ; index in millimeters) and the 2D relative enamel thickness index (2D RET 5 2D AET divided by the square root of the coronal dentine area; scale-free index).

Intra- and inter-observer error

To assess the intra- and inter-observer error SB and CF independently digitized three times the cervical margin of four specimens, each of them representing a different tooth class (incisor, canine, premolar, and molar), allowing for some days between the samplings (Supporting Information Table S1). For both intra- and inter-observer error there were no statistically significant differences between group means (in any comparison $P > 0.97$) as determined by ANOVA (the analysis of variance was carried out in in R v. 2.15.1; R Development Core Team, 2012).

Metric comparison on molars

Results for the 2D and 3D enamel thickness computed for the molar sample were compared to those obtained using Olejniczak's (2006) protocol (for 2D analysis hereafter called 2D-c, and for 3D analysis hereafter called 3D-c; see Table 1), but due to the small sample size tests for statistical significance were not used.

RESULTS

The results of the 2D and 3D enamel thickness analyses for the teeth considered in this work are shown in Tables 3 and 4, respectively. As already emphasized by Olejniczak et al. (2008), discrepancies between the results for 2D and 3D analyses are due to the loss of one dimension in 2D. Except for the molars, 2D indices computed for the P3s, Cs, and I2s are generally lower than those obtained using volumetric measurements. This is not surprising, also because the 2D sections (sealed by a straight line connecting the most apical enamel points) include proportionally more dentine than the 3D crown (sealed by a cervical plane, a basal plane or a curved surface). However, despite the small sample size, both 2D (mesial and distal sections) and 3D enamel thickness of the molars are consistent in showing larger RET values for *H. sapiens*, followed by *H. neanderthalensis*, and *Pan*, with *Gorilla* having the lowest indices. The RET index measured for the mesial section perpendicular to the cervical plane (method 2D-a) is generally more similar to the value generated through the 3D approaches than the index obtained from the other sections (Tables 3 and 4). This result justifies the preference traditionally granted to mesial cross-sections for 2D enamel thickness analysis (Martin, 1985, 2003; Schwartz, 2000; Grine, 2005; Smith et al., 2008, 2012).

The three 3D methods compared for the molar sample (3D-a, 3D-b, and 3D-c) provide similar results. We consider method 3D-b the most rigorous and technically sound as it exploits the entire enamel volume and the portion of coronal dentine that this encompasses. The differences in the 3D RET indices between method 3D-a/3D-b are <2.3%, and between method 3D-c/3D-b are <3.6% (Table 4). The comparison 3D-a/3D-c shows that results differ more in molars with sinuous cervical margin (such as in *Pan* and *Gorilla*) than in molars with almost planar cervix (such as in *H. sapiens* and Neandertal), even though this trend is less clear for the 2D RET indices (Table 3).

DISCUSSION AND CONCLUSIONS

Several methods have been proposed for the digital computation of 2D and 3D enamel thickness (Kono, 2004; Tafforeau, 2004; Olejniczak, 2006; Olejniczak et al., 2008; Feeney et al., 2010). All these methods include either operator-dependent procedures or other technical shortcomings that might bias the final outcome and constrain the analysis to specific tooth classes.

TABLE 3. Values of the components of two-dimensional (2D) enamel thickness

Tooth class	Taxon (specimen ID)	Method (Section)	Enamel surface (mm^2)	Coronal dentine 1 pulp surface (mm^2)	EDJ length (mm)	2D AET (mm)	2D RET (scale-free)
I2	HS (09_162)	2D-b	10.63	24.03	18.18	0.58	11.93
	Gorilla (31435)	2D-b	13.02	56.05	25.43	0.51	6.84
C	HS (08_298)	2D-b	19.16	40.47	20.61	0.93	14.61
	N (Scla_4A_12)	2D-b	12.53	38.38	20.35	0.62	9.94
	Pan (11800)	2D-b	14.54	82.49	28.87	0.50	5.55
P3	HS (M35)	2D-a (M)	17.71	31.15	17.36	1.02	18.28
	N (Scla_4A_6)	2D-a (M)	16.14	33.81	17.59	0.92	15.78
	Pan (15012)	2D-a (M)	10.84	47.89	20.40	0.53	7.68
	Gorilla (31435)	2D-a (M)	25.11	83.58	29.56	0.85	9.29
M2	HS (M125)	2D-a (M)	26.13	30.84	17.32	1.51	27.17
		2D-c (M)	25.97	29.30	16.99	1.53	28.24
		2D-a (D)	20.48	17.82	12.32	1.66	39.38
		2D-c (D)	20.17	21.47	13.57	1.49	32.08
	N (Scla_4A_3)	2D-a (M)	22.14	38.11	19.33	1.15	18.55
		2D-c (M)	23.09	37.06	19.37	1.19	19.58
		2D-a (D)	19.61	30.31	16.91	1.16	21.06
		2D-c (D)	20.07	30.91	17.25	1.16	20.93
	Pan (14999)	2D-a (M)	16.26	34.03	18.95	0.86	14.71
		2D-c (M)	15.87	34.28	18.92	0.84	14.33
		2D-a (D)	16.85	31.26	17.79	0.95	16.94
		2D-c (D)	17.00	31.38	17.77	0.96	17.08
	Gorilla (31435)	2D-a (M)	35.32	77.72	28.41	1.24	14.10
		2D-c (M)	34.75	81.36	28.40	1.22	13.57
		2D-a (D)	36.79	75.29	27.66	1.33	15.33
		2D-c (D)	36.49	74.26	27.51	1.33	15.39

Recent Homo sapiens (HS); Neandertal (N); Method 2D-a 5 the section is perpendicular to the cervical plane; Method 2D-b 5 refinement of Feeney and colleagues' (2010) approach; Method 2D-c 5 Olejniczak's (2006) protocol (see Table 1 for more information); Mesial section (M); Distal section (D); AET 5 average enamel thickness; RET 5 relative enamel thickness

TABLE 4. Values of the components of three-dimensional (3D) enamel thickness

Tooth class	Taxon (specimen ID)	Method	Enamel volume (mm^3)	Coronal dentine 1 pulp volume (mm^3)	EDJ surface (mm^2)	3D AET (mm)	3D RET (scale-free)
I2	HS (09_162)	3D-b	57.61	70.30	91.70	0.63	15.22
	Gorilla (31435)	3D-b	112.91	190.3	183.41	0.62	10.70
C	HS (08_298)	3D-b	128.33	147.04	129.34	0.99	18.80
	N (Scla_4A_12)	3D-b	99.56	160.67	144.11	0.69	12.71
	Pan (11800)	3D-b	122.16	367.41	245.11	0.50	6.96
P3	HS (M35)	3D-b	112.57	100.37	106.37	1.06	22.77
	N (Scla_4A_6)	3D-b	120.58	144.40	131.68	0.92	17.45
	Pan (15012)	3D-b	103.55	218.89	162.52	0.64	10.57
	Gorilla (31435)	3D-b	227.39	430.84	273.91	0.83	10.99
M2	HS (M125)	3D-a	185.86	146.63	127.52	1.46	27.64
		3D-b	186.13	147.58	127.34	1.46	27.66
		3D-c	185.71	147.33	127.9	1.45	27.49
	N (Scla_4A_3)	3D-a	228.29	264.81	194.67	1.17	18.26
		3D-b	228.67	276.72	195.61	1.17	17.94
		3D-c	228.14	265.35	194.98	1.17	18.21
	Pan (14999)	3D-a	187.70	239.38	188.67	0.99	16.02
		3D-b	188.06	247.32	189.00	1.00	15.85
		3D-c	187.36	235.18	186.57	1.00	16.27
	Gorilla (31435)	3D-a	503.84	728.03	391.40	1.29	14.31
		3D-b	506.21	703.32	388.68	1.30	14.64
		3D-c	502.51	736.35	393.97	1.28	14.12

Recent *Homo sapiens* (HS); Neandertal (N); Method 3D-a 5 the crown was separated from the root based on the cervical plane; Method 3D-b 5 the coronal dentine was separated from the root dentine based on the cervical line; Method 3D-c 5 Olejniczak's (2006) protocol (see Table 1 for more information); AET 5 average enamel thickness; RET 5 relative enamel thickness.

Therefore, for 2D enamel thickness, we have modified previous methods suggested by Feeney et al. (2010) for modern human premolars and canines both to include hominoid teeth in the analysis and to remove manual (subjective) interactions with the micro-CT image stack (method 2D-b). With regard to the molars, our results suggest using planes of section perpendicular to the cervical plane (method 2D-a, which follows Martin's (1985)

recommendation) instead of planes of section perpendicular to the reference plane passing through the main horn tips (method 2D-c; see also Fig. 1a).

For 3D enamel thickness analysis, we suggest the use of our approach 3D-b, which considers the entire dental crown. This approach is the only one that suits the morphology of the anterior teeth and premolars, owing to their wavy cervical line. However, for molars where the cervical line is nearly planar our method 3D-a, which uses the best-fit plane of the cervical line to separate the crown from the root, is also suitable. The two methods provide very similar results (Table 4), with differences in RET index of small magnitude. The method based on the best-fit plane, however, is technically more straightforward and less time consuming than the method based on the interpolating surface, as software handling digital objects are often suitable to create user-defined planes to cut the models (e.g., Avizo, Geomagic), but only software with implemented CAD options can compute interpolating surfaces. The best-fit plane was previously used with success in digital analysis of teeth (Benazzi et al., 2009; 2011a-d; 2012; 2013; Kupczik and Hublin, 2010; Fiorenza et al., 2011), because it is less dependent on local irregularity of the cervical line with respect to the method suggested by Olejniczak (2006). Even though for Neandertal and *H. sapiens* the results of our methods 3D-a and 3D-b are very similar to the values obtained following Olejniczak's (2006) protocol (3D-c), Olejniczak's basal (average) plane might return an incongruent representation of the tooth crown if the cervical margin is rather sinuous (Fig. 1b–d). Moreover, the identification of the basal plane requires an operator-dependent interaction with the image stack; therefore, it lacks both accuracy and precision, so that the discrepancy might increase as a consequence of operator's inexperience. Even though the differences observed here might not undermine an analysis aimed at discriminating among different genera (such as *Gorilla*, *Pan*, and *Homo*), small biases in the RET index such as those generated by the use of method 3D-c could have important drawbacks masking the potential differences existing between closely related species (for example, when assessing the enamel thickness variation within the genus *Homo*; see Smith et al., 2012).

In conclusion, we believe that both methods 3D-a and 3D-b can be applied alternatively with success to complete molar crowns, but method 3D-b should be preferred for molars with wavy cervical line.

When small portions of the cervix are missing, a best-fit plane can still be calculated, therefore method 3D-a might still be used, while method 3D-b requires a well preserved cervical margin. In case larger parts of the cervical margin are lost, the dental crown might not be suitable for the 3D analysis, but it might still be possible to perform the 2D analysis where the best-fit plane is calculated based on the portions of cervical margin still preserved. A tooth which lacks all or most of its cervical margin cannot be used to attempt a precise measure of AET and RET. Olejniczak's (2006) protocol cannot be considered an alternative solution. This method (as well as those proposed by, e.g., Kono, 2004; Feeney et al., 2010) still requires a well preserved basal portion of the crown to identify a ring of enamel with uniform width near the cervical margin. As teeth from fossil and archaeological sites are often damaged and worn, further methods are required to confidently compute AET and RET indexes for these specimens.

We believe the protocols described above will enable researchers to better comply with an accurate and reproducible digital computation of 2D and 3D enamel thickness, and we hope it will promote the comparison of the results. The methods we have described are highly reproducible, free of operator-dependent choices, and can be applied to all hominoid tooth classes.

ACKNOWLEDGMENTS

The authors thank Christophe Boesch, the Ministry of Environment and Eaux et Fôrets, the Ministry of Scientific Research, and the Direction of the Taï National Park as well as the Swiss Centre of Scientific Research for access to specimens. They also thank M. Skinner, R. Feeney, and K. Kupczik for scanning assistance. They are grateful to A. Reid for proof-reading this manuscript. They also thank the Editor (Dr. C. Ruff), the Associate Editor and two anonymous reviewers for their important comments, which tremendously improved the manuscript.

LITERATURE CITED

Benazzi S, Fantini M, De Crescenzio F, Persiani F, Gruppioni G. 2009. Improving the spatial orientation of human teeth using a virtual 3D approach. J Hum Evol 56:286–293.

Benazzi S, Viola B, Kullmer O, Fiorenza L, Harvati K, Paul T, Gruppioni G, Weber GW, Mallegni F. 2011a. A reassessment of the Neanderthal teeth from Taddeo Cave (southern Italy). J Hum Evol 61:377–387.

Benazzi S, Douka K, Fornai C, Bauer CC, Kullmer O, Svoboda J, Pap I, Mallegni F, Bayle P, Coquerelle M, Condemi S, Ronchitelli A, Harvati K, Weber GW. 2011b. Early dispersal of modern humans in Europe and implications for Neanderthal behaviour. Nature 479:525–528.

Benazzi S, Fornai C, Bayle P, Coquerelle M, Kullmer O, Mallegni F, Weber GW. 2011c. Comparison of dental measurement systems for taxonomic assignment of Neanderthal and modern human lower second deciduous molars. J Hum Evol 61:320–326.

Benazzi S, Coquerelle M, Fiorenza L, Bookstein F, Katina S, Kullmer O. 2011d. Comparison of dental measurement systems for taxonomic assignment of first molars. Am J Phys Anthropol 144:342–354.

Benazzi S, Fornai C, Buti L, Toussaint M, Mallegni F, Ricci S, Gruppioni G, Weber G, Condemi S, Ronchitelli A. 2012. Cervical and crown outline analysis of worn Neanderthal and modern human lower second deciduous molars. Am J Phys Anthropol 149:537–546.

Benazzi S, Bailey SE, Mallegni F. 2013. A morphometric analysis of the Neandertal upper second molar Leuca I. Am J Phys Anthropol 152:300–305.

Feeney RNM, Zermeno JP, Reid DJ, Nakashima S, Sano H, Bahar A, Hublin J-J, Smith TM. 2010. Enamel thickness in Asian human canines and premolars. Anthropol Sci 118:191–198.

Fiorenza L, Benazzi S, Tausch J, Kullmer O, Bromage TG, Schrenk F. 2011. Molar macrowear reveals Neanderthal eco-geographic dietary variation. PLoS One 6:e14769.

Grine FE. 2005. Enamel thickness of deciduous and permanent molars in modern Homo sapiens. Am J Phys Anthropol 126: 14–31.

Grine FE, Spencer MA, Demes B, Smith HF, Strait DS, Constant DA. 2005. Molar enamel thickness in the chacma baboon, Papio ursinus (Kerr 1792). Am J Phys Anthropol 128: 812–822.

Kono R. 2004. Molar enamel thickness and distribution patterns in extant great apes and humans: new insights based on a three-dimensional whole crown perspective. Anthropol Sci 112:121–146.

Kupczik K, Hublin J-J. 2010. Mandibular molar root morphology in Neanderthals and Late Pleistocene and recent Homo sapiens. J Hum Evol 59:525–541.

Martin LB. 1985. Significance of enamel thickness in hominoid evolution. Nature 314:260–263.

Martin LB, Olejniczak AJ, Maas MC. 2003. Enamel thickness and microstructure in pitheciin primates, with comments on dietary adaptations of the Middle Miocene hominoid Kenyapithecus. J Hum Evol 45:351–367.

Olejniczak AJ. 2006. Micro-computed tomography of primate molars. Ph.D. Thesis. Stony Brook, NY: Stony Brook University.

Olejniczak AJ, Gilbert CC, Martin LB, Smith TM, Ulhaas L, Grine FE. 2007. Morphology of the enamel-dentine junction in sections of anthropoid primate maxillary molars. J Hum Evol 53:292–301.

Olejniczak AJ, Smith TM, Feeney RNM, Macchiarelli R, Mazurier A, Bondioli L, Rosas A, Fortea J, de la Rasilla M, Garcia-Tabernero A, Radovčić J, Skinner MM, Toussaint M, Hublin J-J. 2008. Dental tissue proportions and enamel thickness in Neandertal and modern human molars. J Hum Evol 55:12–23.

R Development Core Team, 2012. R: a language and environment for statistical computing, R v. 2.15.1. Vienna, Austria: R Foundation for Statistical Computing. Available at: http://www.r-project.org

Saunders SR, Chan AHW, Kahlon B, Kluge HF, FitzGerald CM. 2007. Sexual dimorphism of the dental tissues in human permanent mandibular canines and third premolars. Am J Phys Anthropol 133:735–740.

Schwartz GT. 2000. Taxonomic and functional aspects of the patterning of enamel thickness distribution in extant large-bodied hominoids. Am J Phys Anthropol 111:221–244.

Schwartz GT, Dean MC. 2005. Sexual dimorphism in modern human permanent teeth. Am J Phys Anthropol 128:312–317.

Smith TM, Olejniczak AJ, Martin LB, Reid DJ. 2005. Variation in hominoid molar enamel thickness. J Hum Evol 48:575–592.

Smith TM, Olejniczak AJ, Reh S, Reid DJ, Hublin J-J. 2008. Brief communication: enamel thickness trends in the dental arcade of humans and chimpanzees. Am J Phys Anthropol 136:237–241.

Smith TM, Olejniczak AJ, Zermeno JP, Tafforeau P, Skinner MM, Hoffmann A, Radovčić J, Toussaint M, Kruszynski R, Menter C, Moggi-Cecchi J, Glasmacher UA, Kullmer O, Schrenk F, Stringer C, Hublin J-J. 2012. Variation in enamel thickness within the genus Homo. J Hum Evol 62:395–411.

Suwa G, Kono RT. 2005. A micro-CT based study of linear enamel thickness in the mesial cusp section of human molars: reevaluation of methodology and assessment of within-tooth, serial, and individual variation. Anthropol Sci 113:273–289.

Tafforeau P. 2004. Phylogenetic and functional aspects of tooth enamel microstructure and three-dimensional structure of modern and fossil primate molars. Ph.D. Dissertation, Universitè de Montpellier II.

TABLE S1. Intra- and inter-observer error in digitizing the cervical line to compute the values of the components of 2D and 3D enamel thickness

Specimen	3D measurements	Enamel volume (mm^3)	Coronal dentine + pulp volume (mm^3)	EDJ surface (mm^2)	3D AET (mm)	3D RET (scale-free)
Gorilla (31435, RI_2)[a]	SB-1[e]	112.91	190.3	183.41	0.62	10.70
	SB-2	112.91	189.99	183.48	0.62	10.70
	SB-3	112.91	190.85	183.42	0.62	10.69
	CF-1	112.91	192.31	184.1	0.61	10.63
	CF-2	112.91	192.85	184.11	0.61	10.61
	CF-3	112.91	191.78	184.13	0.61	10.63
HS (08-298, RC_1)[a]	SB-1[e]	128.33	147.04	129.34	0.99	18.80
	SB-2	128.33	146.61	129.25	0.99	18.83
	SB-3	128.33	146.07	129.21	0.99	18.86
	CF-1	128.33	146.63	129.36	0.99	18.81
	CF-2	128.33	146.71	129.57	0.99	18.78
	CF-3	128.33	146.79	129.4	0.99	18.80
Gorilla (31435, LP^3)[a]	SB-1[e]	227.39	430.84	273.91	0.83	10.99
	SB-2	227.39	429.22	273.72	0.83	11.01
	SB-3	227.39	424.93	273.6	0.83	11.05
	CF-1	227.39	431.49	275.09	0.83	10.94
	CF-2	227.39	431.32	274.45	0.83	10.97
	CF-3	227.39	434.65	274.51	0.83	10.94
N (SCLA_4A_3, RM^2)[b]	SB-1[e]	228.29	264.81	194.67	1.17	18.26
	SB-2	228.29	265.34	194.93	1.17	18.23
	SB-3	228.34	267.00	195.59	1.17	18.13
	CF-1	228.33	266.76	195.50	1.17	18.14
	CF-2	228.34	266.87	195.54	1.17	18.14
	CF-3	228.41	269.82	196.73	1.16	17.97

Specimen	2D measurements	Enamel surface (mm^2)	Coronal dentine + pulp surface (mm^2)	EDJ length (mm)	2D AET (mm)	2D RET (scale-free)
Gorilla (31435, RI_2)[c]	SB-1[e]	13.02	56.05	25.43	0.51	6.84
	SB-2	12.87	56.10	25.68	0.50	6.69
	SB-3	12.85	56.14	25.53	0.50	6.72
	CF-1	12.98	55.97	25.53	0.51	6.80
	CF-2	13.00	56.04	25.61	0.51	6.78
	CF-3	12.86	56.32	25.40	0.51	6.75
HS (08-298, RC_1)[c]	SB-1[e]	19.16	40.47	20.61	0.93	14.61
	SB-2	18.99	40.91	20.61	0.92	14.41
	SB-3	19.06	40.69	20.62	0.92	14.49
	CF-1	18.93	41.03	20.62	0.92	14.33
	CF-2	18.92	40.91	20.57	0.92	14.38
	CF-3	18.98	40.80	20.63	0.92	14.40
Gorilla (31435, LP^3)[d]	SB-1[e]	25.11	83.58	29.56	0.85	9.29
	SB-2	25.24	82.91	29.58	0.85	9.37
	SB-3	25.23	82.23	29.54	0.85	9.42
	CF-1	25.22	82.62	29.47	0.86	9.42
	CF-2	25.36	82.67	29.55	0.86	9.44
	CF-3	25.23	82.23	29.54	0.85	9.42
N (SCLA_4A_3, RM2)[d]	SB-1[e]	22.14	38.11	19.33	1.15	18.55
	SB-2	22.01	38.14	19.34	1.14	18.43
	SB-3	22.01	38.10	19.34	1.14	18.44

	CF-1	21.99	38.07	19.34	1.14	18.43
	CF-2	22.12	38.09	19.33	1.14	18.54
	CF-3	22.00	38.05	19.35	1.14	18.43

[a]Based on method 3D-b; [b]Based on method 3D-a; [c]Based on method 2D-b;[d]Based on method 2D-a; [e]SB-1 corresponds to the values provided in the main text; SB=Stefano Benazzi; CF=Cinzia Fornai

2.5. Enamel thickness variation of deciduous first and second upper molars in modern humans and Neanderthals.

Fornai C., Benazzi S., Svoboda J., Pap I., Harvati K., Weber G. W.

Journal of Human Evolution 2014; 76, 83-91.

Synopsis

In this chapter, we explored the variability of enamel thickness in deciduous first and second upper molars from both Neanderthals and modern humans. The 2D relative enamel thickness and the dental proportions, features considered diagnostic between Neanderthals and modern humans, were evaluated using the protocols defined in chapter 2.4 for unworn molars. These were also adapted for teeth presenting enamel-dentin junction (lightly) altered by wear. Using virtual techniques for handling and manipulating images from μCT scans, we further demonstrated how classic topics on dental anthropology can be investigated using new methods. For example, the buccal section could be considered in addition to the mesial one, whereas physical sections through the buccal cusps of the teeth are not easy to obtain. Moreover, this paper contributed raw data to be exploited for further studies.

Contribution

Study design, data collection, interpretation of the data, drafting and editing of the manuscript.

Journal of Human Evolution 76 (2014) 83e91

Contents lists available at ScienceDirect

Journal of Human Evolution

journal homepage: www.elsevier.com/locate/jhevol

Enamel thickness variation of deciduous first and second upper molars in modern humans and Neanderthals

Cinzia Fornai [a, *], Stefano Benazzi [b, c], Ji Svoboda [d, e], Ildikó Pap [f], Katerina Harvati [g], Gerhard W. Weber [a]

[a] Department of Anthropology, University of Vienna, Althanstrasse 14, 1090 Vienna, Austria
[b] Department of Cultural Heritage, University of Bologna, Via degli Ariani 1, 48121 Ravenna, Italy
[c] Department of Human Evolution, Max Planck Institute for Evolutionary Anthropology, Deutscher Platz 6, 04103 Leipzig, Germany
[d] Institute of Archaeology, Academy of Sciences of the Czech Republic, Královopolská 147, 612 00 Brno, Czech Republic
[e] Department of Anthropology, Faculty of Science, Masaryk University, Vinařská 5, 603 00 Brno, Czech Republic
[f] Department of Anthropology, Hungarian Natural History Museum, Ludovika tér 2-6, 1083 Budapest, Hungary
[g] Paleoanthropology, Senckenberg Center for Human Evolution and Paleoenvironments, Eberhard Karls Universität Tübingen, Rümelnstrasse 23, Tübingen 72070, Germany

a r t i c l e i n f o

Article history:
Received 17 April 2013
Accepted 8 May 2014
Available online 3 October 2014

Keywords:
Dental tissue proportions
Tooth wear
Deciduous dentition
Homo neanderthalensis
Homo sapiens
Pleistocene

a b s t r a c t

Enamel thickness and dental tissue proportions have been recognized as effective taxonomic discriminators between Neanderthal and modern humans teeth. However, most of the research on this topic focused on permanent teeth, and little information is available for the deciduous dentition. Moreover, although worn teeth are more frequently found than unworn teeth, published data for worn teeth are scarce and methods for the assessment of their enamel thickness need to be developed. Here, we addressed this issue by studying the 2D average enamel thickness (AET) and 2D relative enamel thickness (RET) of Neanderthal and modern humans unworn to moderately worn upper first deciduous molars (dm^1s) and upper second deciduous molars (dm^2s). In particular, we used 3D μCT data to investigate the mesial section for dm^1s and both mesial and buccal sections for dm^2s. Our results confirmed previous findings of an Neanderthal derived condition of thin enamel, and thinner enamel in dm^1s than dm^2s in both Neanderthal and modern humans. We demonstrated that the Neanderthal 2D RET indices are significantly lower than those of modern humans at similar wear stages in both dm^1s and dm^2s ($p < 0.05$). The discriminant analysis showed that using 2D RET from dm^1 and dm^2 sections at different wear stages up to 93% of the individuals are correctly classified. Moreover, we showed that the dm^2 buccal sections, although non-conventionally used, might have an advantage on mesial sections since they distinguish as well as mesial sections but tend to be less worn. Therefore, the 2D analysis of enamel thickness is suggested as a means for taxonomic discrimination between modern humans and Neanderthal unworn to moderately worn upper deciduous molars.

Introduction

Tooth enamel thickness and enamel distribution in primate teeth have been extensively analyzed for their functional implications and for life history assessment (e.g., Martin, 1985; Gantt and Rafter, 1998; Schwartz, 2000; Shimizu et al., 2005; Macchiarelli et al., 2006; Mahoney, 2013; Strait et al., 2013). Various aspects of enamel thickness have been the focus of anthropological research for their taxonomic and phylogenetic relevance (e.g., Grine and Martin, 1988; Macho and Thackeray, 1992; Martin et al., 2003; Hlusko et al., 2004). Analyses of enamel thickness and dental tissue proportions have been carried out to investigate dental morphological variation among hominoids (Kono, 2004; Suwa and Kono, 2005; Smith et al., 2005, 2012a; Alba et al., 2010) and within the genus *Homo* (Kono et al., 2002; Smith et al., 2012b). In particular, it has been recognized that enamel thickness distinguishes between modern human and Neanderthal permanent and deciduous teeth (Zilberman et al., 1992; Olejniczak et al., 2008a; Smith et al., 2009, 2010; Bayle et al., 2009a,b, 2010; Crevecoeur et al., 2010; Toussaint et al., 2010; Benazzi et al., 2011a), as Neanderthal teeth showed a derived condition of thinner enamel respect to modern humans, as recognized previously by some scholars

* Corresponding author.
E-mail address: cinzia.fornai@univie.ac.at (C. Fornai).

http://dx.doi.org/10.1016/j.jhevol.2014.05.013
0047-2484/

(Zilberman et al., 1992; Zilberman and Smith, 1992; Molnar et al., 1993; Rozzi, 1996). This matter was thoroughly investigated by Olejniczak et al. (2008a) who explained the differences between the two taxa showing that Neanderthals possessed a comparable absolute enamel volume to modern humans, but distributed on a larger coronal dentine area (in accordance with Grine, 2002, 2005; Macchiarelli et al., 2006). Previous investigation on deciduous teeth (Macchiarelli et al., 2006; Bayle et al., 2009a,b, 2010; Toussaint et al., 2010; Zanolli et al., 2010; Benazzi et al., 2011a,b) confirmed this trend of derived thinner enamel in Neanderthals. However our knowledge on dental tissues variability in Neanderthal and modern human deciduous teeth is still very limited (Macchiarelli et al., 2006). Furthermore, most scholars have focused on unworn or slightly worn teeth (Grine, 2002, 2005; Smith et al., 2005; Olejniczak et al., 2008a; among the others), because dental wear causes an alteration on the proportions of dental tissues (see discussion in Benazzi et al., 2011a; and our illustration in Fig. S1 in Supplementary Online Material [SOM]). Since wear most often affects fossil teeth to various degrees, investigating dental tissues variability in worn teeth is crucial for evaluating enamel thickness as a means of taxonomic discrimination.

Imaging techniques based on microcomputed tomography (mCT) have made it possible to investigate the dental surfaces and inner tooth structures, avoiding destructive interventions and allowing for digital procedures for the analysis of enamel thickness. These virtual techniques build upon protocols developed for physical sections by Martin (1985) and later adapted to suit the purposes of dental analyses on virtual images. While enamel thickness has been traditionally measured on mesial sections (Martin, 1983, 1985), imaging techniques allow consideration of other sections or multiple sections (2D enamel thickness: Smith et al., 2006; Olejniczak et al., 2008a,b,c,d; Bayle et al., 2009a,b, 2010; Crevecoeur et al., 2010; Zanolli et al., 2010; Benazzi et al., 2011a; Fornai et al., 2012), as well as the whole crown (3D enamel thickness: Martin et al., 2003; Olejniczak et al., 2008b,c,d; Bayle et al., 2009a,b, 2010; Crevecoeur et al., 2010; Zanolli et al., 2010; Benazzi et al., 2011c, 2013). The various digital protocols used so far for the orientation and isolation of the dental crown (for both 2D and 3D enamel thickness), and identification of the coronal sections have been comparatively reviewed by Benazzi et al. (2014b) who, based on preexisting methods (Martin, 1985; Olejniczak et al., 2008a), proposed also accurate and standardized methods for molar enamel thickness analysis. The guidelines by Benazzi et al. (2014b) provide instructions only for the image processing of teeth in which the dentine is not yet exposed. Therefore, a reliable approach for the quantification of tissue proportions in moderately worn teeth is still needed.

Here, we carried out the analysis of 2D enamel thickness in mesial and buccal sections of Neanderthal and modern human upper first deciduous molars (dm^1s) and upper second deciduous molars (dm^2s) at different wear stages (1e3 according to Molnar, 1971). For the identification of the 2D sections we referred to the guidelines by Benazzi et al. (2014b), but we established new methods for the identification of 2D mesial and buccal sections in (deciduous) molars presenting exposed patches of dentine. In the current work, we analyzed the sample systematically on the basis of its degree of wear to investigate the range of variability of enamel thickness in modern human and Neanderthal dm^1s and dm^2s. Furthermore, we aimed to assess whether enamel thickness is suitable for the taxonomic discrimination of moderately worn modern human and Neanderthal dm^1s and dm^2s. In this contribution, we provided also the raw data for the values of the enamel tissue components for the entire sample, which may serve future studies on the subject. We evaluated the enamel thickness and dental tissue proportions from the mesial sections (for both dm^1s and dm^2s) and buccal section (for dm^2s) as taxonomic discriminators between *Homo sapiens* and Neanderthals and compared the outcome for dm^2 buccal sections with that of the most traditionally used mesial sections.

Materials and methods

Our sample comprised both dm^1s and dm^2s from European specimens of recent modern humans (RHS; dm^1 ¼ 23; dm^2 ¼ 32), Upper Paleolithic modern humans (UPHS; dm^1 ¼ 2; dm^2 ¼ 2), and Neanderthals (dm^1 ¼ 4; dm^2 ¼ 9), as listed in Table 1. We included only teeth with a wear stage not exceeding 3 according to Molnar's classification (1971). Teeth showing severe damage in the areas of interest (e.g., cracks, decay) were excluded, as well as teeth showing signs of enamel hypoplasia, while minor damage on the

Table 1
List of dm^1s and dm^2s considered for the investigation of the enamel thickness and dental tissue proportions.

Taxon	dm^1				dm^2				
	Individual	Provenience	Source for CT	Wear at mesial section	Individual	Provenience	Source for CT	Wear at mesial section	Wear at buccal section
RHS	Medieval and contemporary (*n* ¼ 23*)	Central Europe	C. d. M[a]	Stage 1 ¼ 4	Medieval and contemporary (*n* ¼ 32*)	Central Europe	C. d. M.[a]	Stage 1 ¼ 14	Stage 1 ¼ 14
			P.H.R.C.T. Lab[b]	Stage 2 ¼ 4			P.H.R.C.T. Lab[b]	Stage 2 ¼ 9	Stage 2 ¼ 18
			Vienna CT Lab[c]	Stage 3 ¼ 16			Vienna CT Lab[c]	Stage 3 ¼ 11	Stage 3 ¼ 6
UPHS	Dolní V□stonice 36-2	Czech Republic	Vienna CT Lab[c]	Stage 1	Dolní V□stonice 36-3	Czech Republic	Vienna CT Lab[c]	Stage 1	Stage 1
	La Rochette	France	P.H.R.C.T. Lab[b]	Stage 3	La Rochette	France	P.H.R.C.T. Lab[b]	Stage 1	Stage 2
N	Krapina d181	Croatia	NESPOS[d]	Stage 3	Krapina d185	Croatia	NESPOS[d]	Stage 1	Stage 1
	Krapina d183	Croatia	NESPOS[d]	Stage 3	Krapina d186	Croatia	NESPOS[d]	Stage 2	Stage 1
	Roc de Marsal 1 L	France	NESPOS[d]	Stage 3	Krapina d187	Croatia	NESPOS[d]	Stage 3	Stage 3
	Pech-de-l'Azè I L	France	NESPOS[d]	Stage 3	Krapina d188	Croatia	NESPOS[d]	Stage 2	Stage 1
					Krapina d189	Croatia	NESPOS[d]	Stage 3	Stage 3
					Krapina d190	Croatia	NESPOS[d]	Stage 3	Stage 3
					Pech-de-l'Azè I L	France	NESPOS[d]	Stage 3	Stage 1
					Roc de Marsal 1 L	France	NESPOS[d]	Stage 2	Stage 1
					Subalyuk-2 L	Hungary	Vienna CT Lab[c]	Stage 3	Stage 3

We report the provenience, source of the CT data, and wear stage (according to Molnar, 1971) at the sections of interest.
*The number of sections do not sum up to the number of individuals because we used both antimeres from the same individual when they showed different wear stages.
L ¼ left; RHS ¼ recent modern humans; UPHS ¼ Upper Paleolithic modern humans; N ¼ Neanderthals.
[a] Centre de Microtomographie, Université de Poitiers;
[b] Paleoanthropology High Resolution Computing Tomography Laboratory, Eberhard Karls Universität Tübingen;
[c] Vienna CT Lab, University of Vienna;
[d] NESPOS Database/www.nespos.org;

sections were corrected virtually. None of the included teeth presented extensive damage along the cervical margin. When both antimeres were available from one individual, only the left tooth was considered. Both antimeres were included only when they showed diverse wear stages (namely, 1e2 against 3). The UPHS and RHS specimens were combined for the statistical analysis (together referred to as modern humans) to avoid the use of excessively small samples, but the individual data are provided in SOM Table S1.

mCT scans were undertaken by means of industrial and synchrotron-based mCT scanners at various facilities as detailed in Table 1. The isotropic voxel size ranged between 15 and 55 mm. Further details about the mCT scanning procedure can be found in Bayle et al. (2009a,b, 2010) and Benazzi et al. (2011a,b). The Krapina teeth were downloaded from the Neanderthal Studies Professional Online Service e NESPOS Database 2011 (www.nespos.org).

To compute the enamel thickness and dental tissue proportions, the following steps were required. The mCT scans were segmented using Amira 5.4 (Mercury Computer Systems, Chelmsford, MA) to virtually separate the enamel from the dentine (Spoor et al., 1993) and 3D surface models were generated. To orient the image stack, we followed method '3D-a' described in Benazzi et al. (2014b), i.e., locating the best-fit plane by interpolating the cervical margin (cervical plane). Then, the image stack was realigned so that the cervical plane was parallel to the x, y plane (Fig. 1).

We examined the dm^1 and dm^2 mesial sections crossing the mesial dentine horn tips. In addition to this, we considered the dm^2 buccal sections since the leading cusps (paracone and metacone) are more likely to be less worn than the trailing cusps (protocone and hypocone). Instead, we did not consider the dm^1s buccal section since the bucco-distal cusp (metacone) is often reduced or absent in human dm^1s. For teeth in which the horn tips were not affected by wear (wear stages 1e2), we followed the guidelines put forth by Benazzi et al. (2014b): a plane perpendicular to the cervical plane and passing through the highest point of two dentine horns was used to identify the section of the dental crown to analyze. To facilitate the process of orientation of the

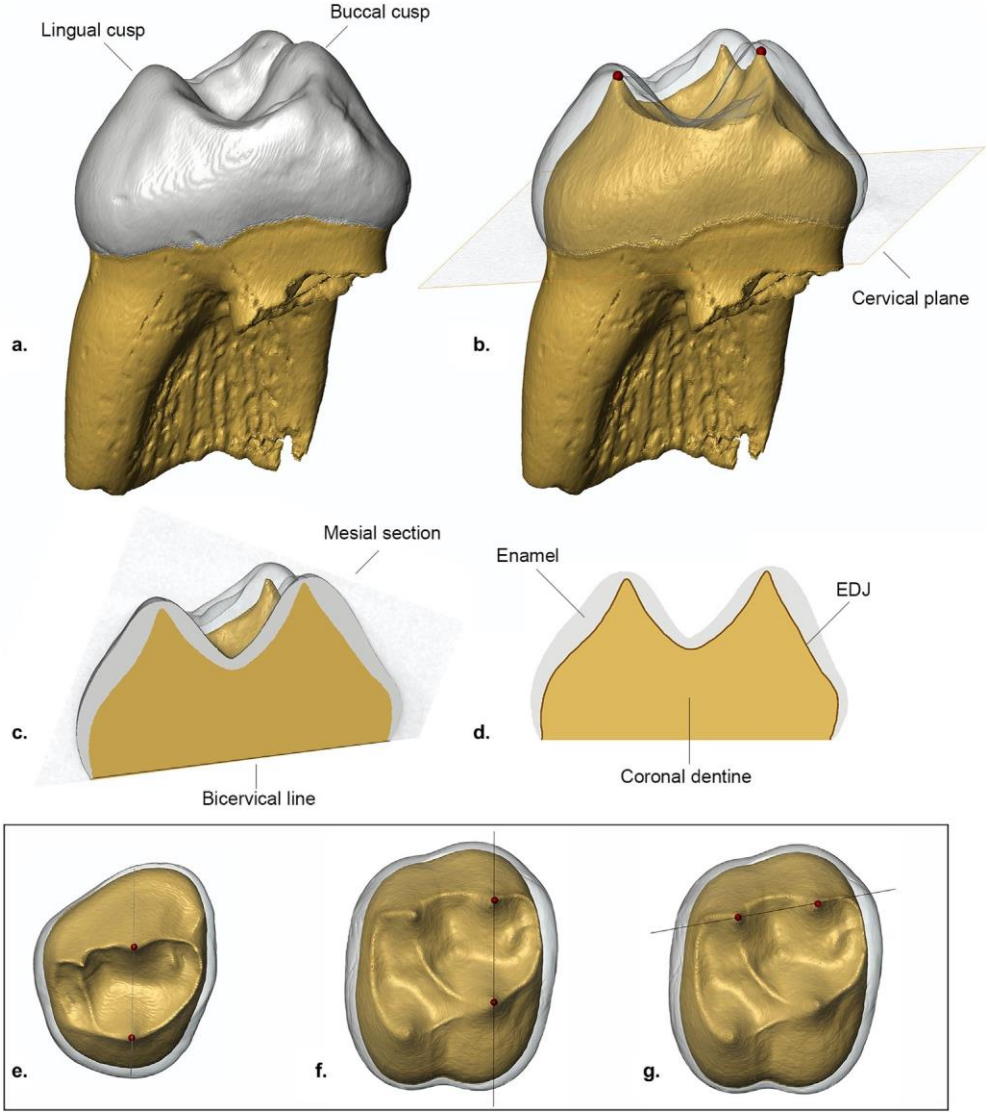

Figure 1. Procedure for the identification of 2D sections from 3D image data. a. Recent modern human upper first deciduous molar (dm^1). b. The best-fit plane of the cervical line (cervical plane) is identified to orient the image stack. Two landmarks (red dots) are located on the dentine horn tips of the mesial cusps. c. A plane perpendicular to the cervical plane and passing through the two landmarks identifies the section to analyze. d. From each section the enamel area (mm^2), the coronal dentine area (mm^2) and the length of the enamel-dentine junction (EDJ; mm) are collected. For the dm^2s the same procedure is followed, but both the mesial and buccal sections are considered. In the box at the bottom the occlusal views of a recent modern human dm^1 (e.) and dm^2 (f., g.) are shown. The mesial (e. and f.) and buccal (g.) sections are visible through the enamel cap set as transparent.

section, the dentine horn tips were marked with a landmark point on the segmented enamel-dentine junction (EDJ). Since the Benazzi et al. (2014b) guidelines were conceived for unworn teeth (or at least for teeth in which the dentine horn tips are not affected by wear), we had to establish a protocol for wear stage 3 deciduous upper molars for the identification of alternative points to horn tips through which the section should pass (Fig. 2). In particular, we used a spline curve (a continuous and smooth curve) to prolong virtually the occlusal ridges on the exposed dentine patches, as follows: For dm^1 and dm^2 mesial sections, a spline curve was traced along the EDJ occlusal edge in proximity to the mesio-buccal (Fig. 2a. and a^1.) and mesio-lingual (Fig. 2a. and a^2.) dentine horn. The mid-point of the segment of the spline curve along the edge of the exposed dentine patch is identified on both mesial cusps. These points (together with the cervical plane) identify the cutting plane for the mesial section. For the buccal section: A spline curve is traced along the EDJ occlusal edge in proximity to the mesio-buccal dentine horn (Fig. 2b. and b^1.) and disto-buccal cusp (Fig. 2b. and b^2.). Differently from the mesial section, for buccal sections the spline curve did not follow the buccal edge of the exposed dentine patches, since the bucco-lingual position of the cutting points is crucial for the identification of the buccal section itself. The spline curve instead crossed the dentine patches joining the highest points of the EDJ buccal edge still visible. The mid-point of the segment of the spline curve along the exposed dentine patch was identified on both buccal dentine horns. Note that the procedure used for buccal cusps in which the spline curve crosses the exposed dentine patch could be used to identify the mesial section, too. However, since in the latter case only the mesio-distal position of the cutting points matters, it is more convenient to place the landmark on the margin of the dentine patch rather than on its occlusal surface, which is often concave.

In all cases, the sections were sealed at the bottom using the bi-cervical line, which connected the most apical points of the enamel cap (as in Benazzi et al., 2014b).

The following measurements were recorded for each section in Rapidform XOR2 (INUS Technology, Inc., Seoul, Korea): the area of the enamel cap (mm^2), the area of the coronal dentine (including the coronal pulp; mm^2) and the length of the EDJ (mm). These values were used to calculate the 2D AET index (the area of the enamel cap divided by the length of the EDJ; index in mm) and the 2D RET index (the average enamel thickness divided by the square root of the coronal dentine area; scale free index) (Martin, 1985). In the EDJ length for wear stage 3 sections we included the length of the EDJ where the enamel was still present and excluded the length of the exposed dentine (see SOM Fig. S2). The segmentation process and the parameter measurements were carried out by C. F. and S. B. A subsample of three fossil teeth was entirely re-processed by both authors to evaluate the inter-observer error, which was lower than 3% in all cases.

The differences between the enamel thickness components (enamel area, dentine area, EDJ length, 2D AET and 2D RET) indices of Neanderthals and modern humans were tested via a permutation test (n ¼ 1000) on group mean and variance for the subsamples distinguished on the bases of the tooth class, section orientation, and dental wear stage (Table 1).

We used leave-one-out cross-validation quadratic discriminant analysis (QDA) for the taxonomic discrimination of the modern human and Neanderthal samples based on the 2D RET indices (in

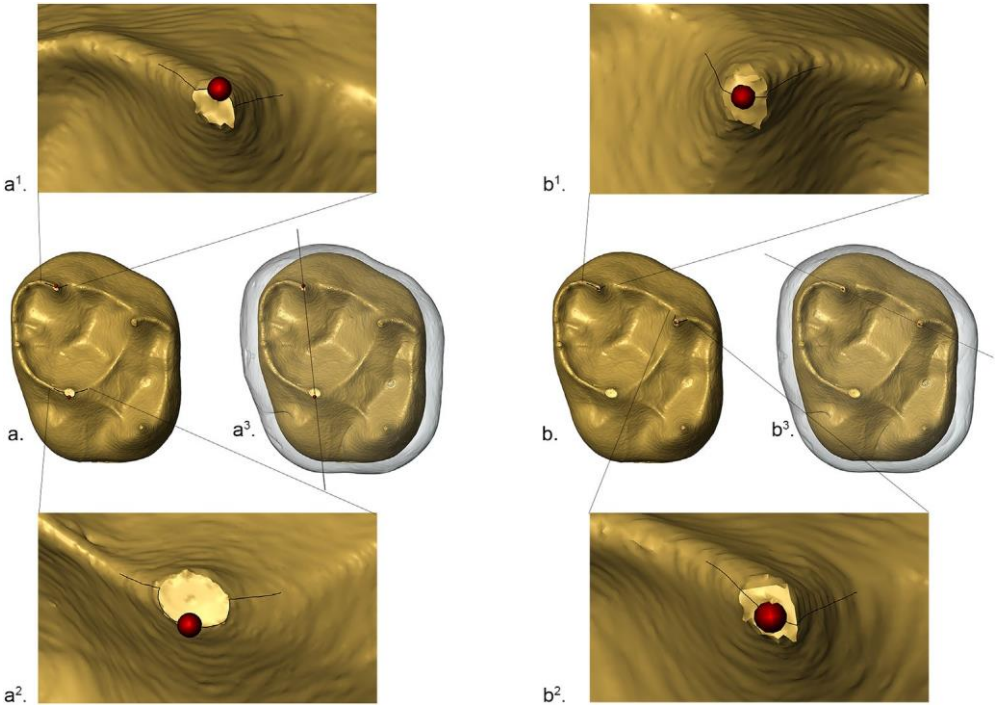

Figure 2. Procedure for the identification of 2D sections from upper deciduous molars at wear stage 3 (Molnar, 1971). a. Mesial section (the image shows a dm^2, but the same procedure is used for dm^1s). A spline curve is traced along the buccal edge of the EDJ in proximity to the mesio-buccal dentine horn (a. and close-up in a^1.) and along the lingual edge of the EDJ in proximity of the mesio-lingual dentine horn (a. and a^2.). The mid-point of the segment of the spline curve marking the exposed dentine patch is identified on both mesial dentine horns (red dots, which represent the cutting points for the mesial section (a^3.)). b. Buccal section: A spline curve is traced along the buccal edge of the EDJ in proximity to the mesio-buccal dentine horn (b. and close-up in b^1.) and along the buccal edge of the EDJ in proximity to the disto-buccal dentine horn (b. and b^2.). The spline curve crosses the dentine patches joining the highest points of the EDJ buccal edge still visible. The mid-point of the segment of the spline curve along the exposed dentine patch is identified on both buccal dentine horns (red dots, which represent the cutting points for the buccal section (b^3.)). (For interpretation of the references to colour in this figure legend, the reader is referred to the web version of this article.)

QDA there is no assumption that the covariance of each of the classes is identical, as it is the case for linear discriminant analysis). The computation of the posterior probabilities (Ppost) was made with an equal prior probability (Pprior) of 0.5 for Neanderthals and modern humans.

The dental tissues proportions were calculated for all sections available, included modern human dm^1 mesial sections at wear stage 1 and 2, for which any Neanderthal comparative samples was available to us for inter-specific comparison.

The data were processed and analyzed through software routines written in R.

Results

The values for enamel thickness components (mean, standard deviation and range) from Neanderthal and modern human dm^1 mesial sections (n ¼ 9, wear stage 1e2; n ¼ 21, wear stage 3), and dm^2 mesial (n ¼ 29, wear stage 1e2; n ¼ 16, wear stage 3) and buccal sections (n ¼ 34, wear stage 1e2; n ¼ 10, wear stage 3; n ¼ 1) are reported in Table 2. The raw values for each of the individuals considered can be found in SOM Table S1. Within a sample of 16 dm^2s showing a wear stage 3 in the mesial section, six specimens (HS ¼ 5; N ¼ 1) showed a lesser degree of wear on the buccal section, and therefore increased the wear stage 1e2 sample size (note that one of them had to be discharged because its antimere was already present in that sample).

The results for the comparative analyses between Neanderthals and modern humans showed that the 2D RET indices for the Neanderthal deciduous upper molars were significantly lower than those of modern humans at similar wear stages ($p < 0.05$; see Fig. 3 and Table 3), where only the 2D RET from dm^2 buccal sections at wear stage 3 is close to non-significance. The UPHS showed 2D RET values among the highest. The p-values for the 2D AET indices are significant for the mesial and buccal dm^2 sections. The dentine area is significantly different in all cases, with the exception of the dm^2 mesial sections at wear stage 3. The EDJ length discriminates significantly between modern humans and Neanderthals only in the case of the dm^2 buccal sections. In all cases, the absolute enamel area showed non-significant p-values.

The results of the cross-validation QDA based on 2D RET indices (Table 4), showed that this index discriminates successfully between Neanderthal and modern human dm^1s mesial sections (wear stage 3) in 89% of the cases. The 2D RET index calculated for the dm^2s wear stage 1e2 for the mesial sections classified correctly 93% of the individuals. The 2D RET index calculated for the dm^2s wear stage 1e2 buccal sections is nearly as successful as in mesial sections and classifies correctly in 91% of the cases. For the mesial and buccal dm^2s sections at wear stage 3 our samples have small sizes (n ¼ 16 and 10, respectively). Nonetheless, the 2D RET indices are significantly different for the mesial section, but close to non-significance for the buccal section. The results of the cross-validation QDA showed that the RET index discriminates well between modern human and Neanderthal mesial section in 81% of the cases, while it classified correctly 80% of the buccal sections. However, larger samples are needed to provide more robust results.

The dental tissue proportions for the entire sample are shown in Fig. 4 by means of pie charts (produced in Excel, Microsoft Office). The picture presented here is in accord with the findings of previous research on Neanderthal and modern human permanent molars (Olejniczak et al., 2008a), in that the modern humans enamel area is greater than in Neanderthals for all groups. Obviously, the wear stage 3 sections from both modern humans and Neanderthals showed a smaller enamel area than the sections from the same tooth types at wear stage 1e2. Moreover, we noted

Table 2
Mean, standard deviation (SD; in brackets) and range of variation for the different components of enamel thickness from modern human (HS) and Neanderthal (N) dm^1s and dm^2s.

Tooth class	Taxon	Wear stage[a]	Number	Enamel area (mm^2)		Dentine area (mm^2)		Length of the enamel-dentine junction (mm)		Average enamel thickness (mm)		Relative enamel thickness (scale free)	
				Mean (SD)	Range	Mean (SD)	Range	Mean (SD)	Range	Mean (SD)	Range	Mean (SD)	Range
dm^1 (mesial section)	HS	1e2	9	8.43 (1.35)	6.55e10.12	27.76 (3.07)	23.91e33.87	16.71 (1.24)	14.70e18.04	0.50 (0.06)	0.41e0.59	9.57 (1.08)	8.33e10.79
	HS	3	17	7.35 (1.02)	6.00e10.11	29.15 (2.71)	24.54e35.39	16.42 (1.43)	14.80e21.30	0.45 (0.06)	0.32e0.60	8.31 (0.95)	6.08e10.15
	N	3	4	6.88 (0.99)	5.74e7.74	33.16 (2.97)	29.34e36.57	17.49 (0.57)	16.77e18.08	0.45 (0.06)	0.34e0.44	6.82 (0.71)	5.90e7.45
dm^2 (mesial section)	HS	1e2	25	13.33 (2.17)	9.82e19.41	31.54 (2.87)	26.74e38.03	18.33 (0.98)	16.92e20.17	0.72 (0.09)	0.53e0.96	12.90 (1.29)	9.32e15.60
	N	1e2	4	12.03 (1.41)	10.42e13.37	36.58 (3.14)	32.79e39.80	19.33 (0.71)	18.47e19.93	0.62 (0.08)	0.52e0.70	10.29 (0.89)	9.15e11.33
	HS	3	11	12.05 (1.94)	9.60e16.67	33.96 (2.20)	30.31e36.64	18.44 (0.87)	16.49e19.33	0.65 (0.09)	0.52e0.86	11.20 (1.46)	9.16e14.25
	N	3	5	10.87 (2.36)	8.33e14.42	36.86 (7.01)	29.64e44.64	18.62 (1.85)	16.49e21.36	0.58 (0.07)	0.48e0.68	9.57 (0.69)	8.74e10.23
dm^2 (buccal section)	HS	1e2	29	12.79 (2.21)	9.08e18.90	26.71 (2.34)	23.24e30.03	16.92 (1.07)	14.47e19.00	0.75 (0.11)	0.53e1.06	14.59 (1.82)	9.99e19.00
	N	1e2	5	12.36 (1.10)	10.96e13.82	33.12 (3.58)	29.43e37.57	19.06 (1.06)	18.00e20.20	0.65 (0.05)	0.60e0.70	11.29 (0.57)	10.78e12.11
	HS	3	6	11.60 (1.18)	9.35e12.56	28.27 (2.43)	24.67e30.78	17.12 (0.99)	15.79e18.53	0.68 (0.08)	0.55e0.77	12.84 (1.86)	10.14e15.47
	N	3	4	11.48 (1.71)	9.91e13.59	35.45 (6.43)	29.02e30.78	18.33 (1.89)	16.68e20.88	0.62 (0.03)	0.58e0.65	10.55 (0.47)	10.06e11.11

[a] Based on Molnar (1971).

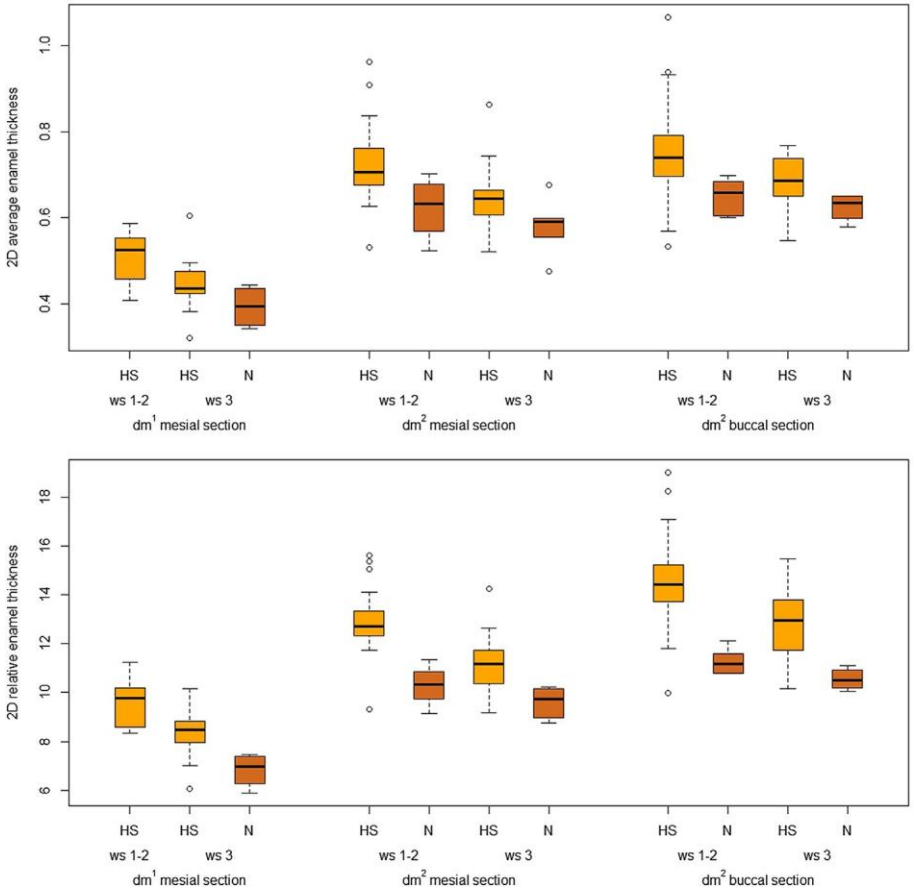

Figure 3. Boxplots for the 2D AET and 2D RET indices of modern human (HS) and Neanderthals (N) dm^1 and dm^2 sections at different wear stages (ws; 1e2 and 3 according to Molnar, 1971).

a different percentage of tissue loss on sections with respect to our explicative 3D example in SOM Fig. S2, most probably owed to the loss of one dimension. The enamel loss from wear stage 1e2 to 3 is greater in modern humans than in Neanderthals, as previously pointed out by some scholars investigating permanent teeth (Smith et al., 2012b): dm^2 mesial sections: 4% versus 2%; dm^2 buccal sections: 3% versus 2% (modern human dm^1 mesial sections: 3%).

In both Neanderthals and modern humans the dm^1 possessed absolutely and relatively thinner average enamel than the dm^2, as found by Mahoney (2013) for modern human deciduous molars (Table 5). The within-species differences in 2D AET between dm^2 buccal and mesial sections are not significant.

Discussion

Some features of the dentition such as the enamel thickness and the dental tissue proportions can be species-specific even in closely related hominins (Martin, 1985; Beynon et al., 1991; Smith et al., 2012a,b), and can therefore be used to discriminate among taxa. Researchers have put more effort in studying unworn teeth, even though the human fossil record is mainly composed of worn teeth. Similarly, in contrast to the more abundant permanent teeth, deciduous dentition has gained attention only more recently in the paleoanthropological literature (Zilberman et al., 1992; Grine, 2005; Macchiarelli et al., 2006; Bayle et al., 2009a,b, 2010; Crevecoeur et al., 2010; Smith et al., 2010; Toussaint et al., 2010; Zanolli et al., 2010; Benazzi et al., 2011a, 2014a; Mahoney, 2013).

Table 3
Permutation test for differences in the components of enamel thickness between modern human and Neanderthal dm^1s and dm^2s.

Tooth class	Wear stage[a]	Number	Enamel area	Dentine area	EDJ length	AET	RET
			p	*p*	*p*	*p*	*p*
dm^1 (mesial section)	3	21	0.422	0.017	0.179	0.109	0.007
dm^2 (mesial section)	1e2	29	0.252	0.003	0.061	0.046	0.001
	3	11	0.287	0.219	0.795	0.152	0.032
dm^2 (buccal section)	1e2	34	0.695	0.001	0.001	0.038	0.004
	3	10	0.855	0.018	0.243	0.156	0.050

Significant *p*-values are in bold.
[a] Based on Molnar (1971).

Table 4
Percentage of modern human and Neanderthal individuals correctly classified through dm^1s and dm^2s mesial and buccal sections.

Tooth class	Wear stage[a]	Number	Percentage of individuals correctly classified (%)	
			AET	RET
dm^1 (mesial section)	3	21	67	89
dm^2 (mesial section)	1e2	29	66	93
	3	16	63	81
dm^2 (buccal section)	1e2	34	65	91
	3	10	70	80

[a] Based on Molnar (1971).

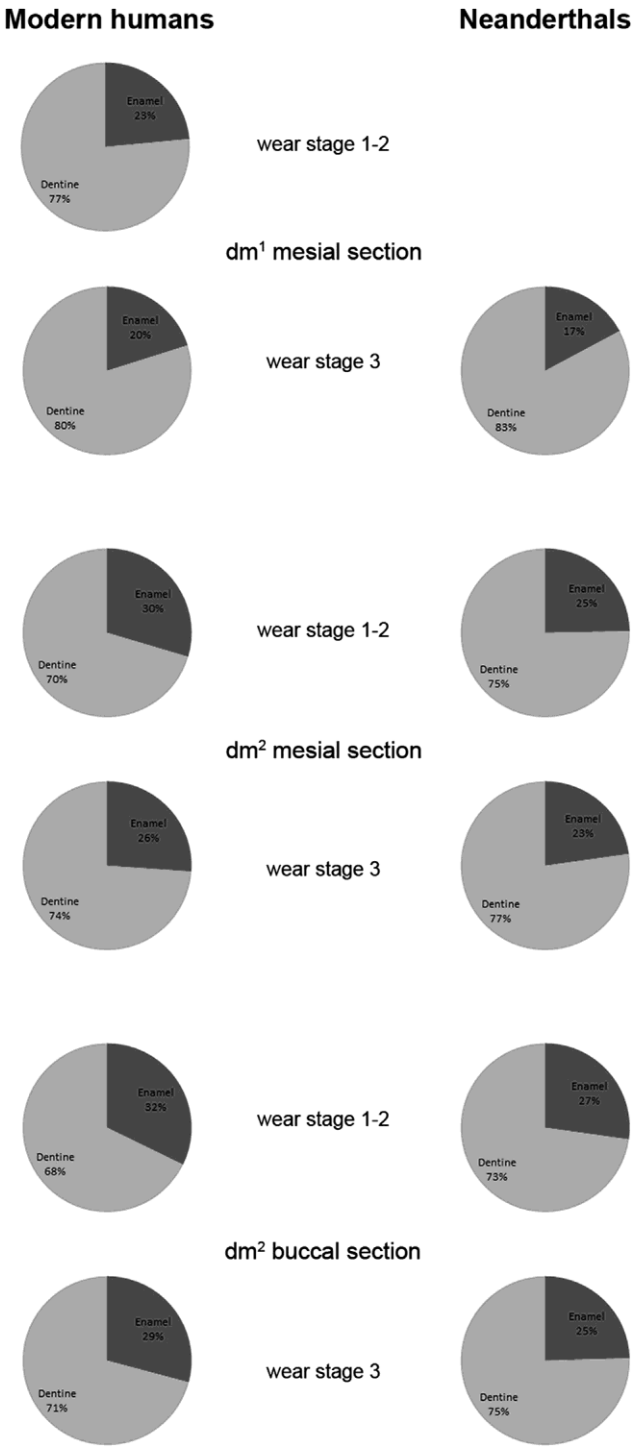

Figure 4. Pie charts showing the 2D dental tissue proportions in modern human (HS) and Neanderthal (N) dm^1 and dm^2calculated from mesial and buccal sections at wear stages 1e2 and 3 (according to Molnar (1971)).

There is a cogent need to establish methods for the taxonomic discrimination based on dental material, which is coupled with the need to build comparative databases.

Deciduous upper molars showed the same pattern as permanent upper molars in terms of 2D RET, in that Neanderthals present relatively thinner enamel than modern humans (Zilberman et al., 1992; Zilberman and Smith, 1992; Molnar et al., 1993; Rozzi, 1996; Olejniczak et al., 2008a). All types of sections considered

Table 5
Permutation test for the within species difference between dm^1 and dm^2 2D AET, measured on mesial sections.

Taxon	Section	Wear stage[a]	AET
			p
HS	mesial section	1e2	0.0010
HS	mesial section	3	0.0010
N	mesial section	3	0.0170

Significant *p*-values are in bold.

[a] Based on Molnar (1971); HS ¼ modern humans; N ¼ Neanderthals.

distinguished well between Neanderthal and modern human deciduous upper molars, but at similar wear stage dm^1 sections are more effective. The diminished discriminant power in worn dm^2 mesial and especially buccal sections might be due either to the loss of dental materials or to the smaller sample sizes used, or both. Coupling our results to those previously published by Benazzi et al. (2011b) on 3D lateral enamel thickness for lower deciduous second molars (dm_2s), we believe that a loss of dental tissues negatively affects the discriminant power of the enamel thickness components. Benazzi et al. (2011b) simulated virtually a wear stage of 5e6 (Molnar, 1971) and reported a successful classification of Neanderthal and modern human dm_2s in about 70% of the cases, against our ca. 80% for (natural) wear stage 3 dm^2s and over 90% for wear stage 1e2 dm^2s. However, we found that among the sections at wear stage 3, the dm^1 mesial section seems to be more effective in discriminating between Neanderthals and modern humans than both dm^2 sections, but again, differences in sample size should be considered. We have shown that the buccal sections from dm^2s can be used alternatively to mesial sections since they are equally successful at distinguishing between Neanderthals and modern humans. Physical sections through the mesial cusps of molar teeth have been traditionally considered for enamel thickness analysis since they are relatively easier to obtain in comparison to the distal ones (Martin, 1983). Following the tradition of the classical approach, virtual image studies have mostly considered mesial sections, together with distal sections for the functional significance of enamel thickness along the dental row (Smith et al., 2005; Mahoney, 2010). However, imaging techniques make it possible to use sections other than the mesial, or even multiple sections, which represents an advantage in the case of worn teeth, or when the lingual cusps are unusable. Moreover, a 2D analysis focused on specific sections generally allows for a larger sample with respect to a 3D analysis. Increasing the sample size might provide clearer evidence of the (negative) contributions of wear and sample size to the classification power of 2D AET and RET. Interestingly, the UPHS sections showed the highest values for the enamel thickness components and 2D AET and 2D RET indices. This suggests that further studies are needed for the assessment of the variability of enamel thickness in deciduous molars within the genus *Homo*, which might mirror that observed by Smith et al. (2012b) for permanent teeth. The UPHS specimens considered here have similar values to those published in Benazzi et al. (2011a) for the early Upper Paleolithic specimens Cavallo B dm^1 and Cavallo C dm^2. In particular, Cavallo B (wear stage 1) presents a 2D RET index higher than Dolní Vstonice 36 2 dm^1 (also unworn), and Cavallo C (wear stage 4 at the buccal section) gives a higher 2D RET index than both Dolní Vstonice 36 3 and La Rochette dm^2s in spite of its heavier degree of wear.

The analysis of the dental tissues proportions are broadly consistent with what has been generally acknowledged for Neanderthals and modern humans on the basis of both deciduous teeth (Macchiarelli et al., 2006) and permanent teeth (Olejniczak et al., 2008a; Benazzi et al., 2011a), namely, that Neanderthal dm^1s and dm^2s feature relatively thinner enamel than modern humans. In

particular, we have found non-significant differences in the absolute quantity of enamel, which is however distributed over a significantly greater dentine area in Neanderthals. In upper deciduous molars, we observed the phenomenon described by Smith et al. (2012b) for permanent teeth, namely that at similar wear stages the Neanderthal molars lose comparatively less enamel than modern human molars. In particular, we found that Neanderthals lost 1e2% less enamel area than modern humans, as assessed from 2D sections (Fig. 4). While this difference may be relevant for dental attrition and paleodemographic studies, it should not impair the use of 2D sections for taxonomic purposes, where the assessment of dental wear in Neanderthal teeth is carried out using criteria established for modern human teeth.

Furthermore, our study confirms the findings of Mahoney (2013) with regards to the average enamel thickness of modern human dm^1s compared with dm^2s, the latter having thicker enamel, which he interpreted as a functional and developmental condition. We found the same relation for Neanderthal dm^1 and dm^2, even though, given the taxonomic nature of our study, we did not investigate further on the functional significance of this condition. The comparison between our results for the mesial and buccal sections showed that the 2D AET does not differ significantly. However, from a visual comparison of the virtual sections (as shown in SOM Fig. S3), it seems that the lateral enamel contributes mostly to the total enamel area on the buccal section.

Finally, in addition to our contribution on the understanding of the variability of enamel thickness and dental tissue proportions in Neanderthal and modern human dm^1s and dm^2s, our work has provided a comparative database for 2D enamel thickness components, which will serve the purposes of further studies on enamel thickness and dental tissue proportions.

Conclusions

Our contribution has confirmed that 2D enamel thickness can be effectively used to discriminate between modern human and Neanderthal upper deciduous molars at different wear stages. In accordance with previous investigations (Macchiarelli et al., 2006; Olejniczak et al., 2008a; Bayle et al., 2009a,b, 2010; Benazzi et al., 2011a; Smith et al., 2012b), we found that Neanderthal and modern human deciduous upper molars present a similar pattern to permanent teeth with regard to the enamel thickness components, with modern humans possessing relatively thicker enamel. This condition results in statistically different 2D RET indices for dm^1 mesial sections and dm^2 mesial sections, while for the buccal sections the difference is close to non-significance probably owing to our small sample size. Consequently, at the same wear stage, Neanderthal deciduous upper molars have lost on sections about 1e2% less enamel than modern humans. We demonstrated that buccal sections from dm^2s can be used as well as mesial sections for the calculation of enamel thickness components for taxonomical purposes. The highest 2D AET and RET values within our sample are given by the UPHS and are similar to those found in the early Upper Paleolithic deciduous molars from Grotta del Cavallo, Italy (Benazzi et al., 2011a). We found that both modern human and Neanderthal dm^1s have absolute and relative thinner enamel than Neanderthal dm^2s, as already reported for modern human deciduous molars (Mahoney, 2013). The raw data we provided here might serve the purposes of further studies investigating enamel thickness and dental tissue proportions.

Acknowledgments

The authors would like to thank Priscilla Bayle for providing the CT data for part of the modern human sample, as well as those for Pech-de-l'Azé I, and Roc de Marsal 1. Access to the fossil specimens was made possible by the Croatian National History Museum, the French Musée National de Préhistoire, the French Muséum National d'Histoire Naturelle, Paleoanthropology, Eberhard Karls Universität Tübingen and the NESPOS Database 2011 (https://www.nespos.org/display/openspace/Home). We acknowledge the Centre de Microtomographie (Université de Poitiers), the Vienna micro-CT Laboratory (University of Vienna), VISCOM AG Hannover, the Paleoanthropology High Resolution Computing Tomography Laboratory (Eberhard Karls Universität Tübingen), the European Synchrotron Radiation Facility beamline ID17, and the AST-RX platform (French Muséum National d'Histoire Naturelle).

This research was financially supported by A.E.R.S. Dental Medicine Organisations GmbH (FA547013), Vienna, Austria and by

Appendix A. Supplementary data

Supplementary data related to this article can be found at http://dx.doi.org/10.1016/j.jhevol.2014.05.013

References

Alba, D.M., Fortuny, J., Moyà-Solà, S., 2010. Enamel thickness in the Middle Miocene great apes *Anoiapithecus, Pierolapithecus* and *Dryopithecus*. P. R. Soc. B 277, 2237e2245.

Bayle, P., Braga, J., Mazurier, A., Macchiarelli, R., 2009a. Brief communication: High-resolution assessment of the dental developmental pattern and characterization of tooth tissue proportions in the late Upper Paleolithic child from La Madeleine, France. Am. J. Phys. Anthropol. 138, 493e498.

Bayle, P., Braga, J., Mazurier, A., Macchiarelli, R., 2009b. Dental developmental pattern of the Neanderthal child from Roc de Marsal: a high-resolution 3D analysis. J. Hum. Evol. 56, 66e75.

Bayle, P., Macchiarelli, R., Trinkaus, E., Duarte, C., Mazurier, A., Zilhão, J., 2010. Dental maturational sequence and dental tissue proportions in the early Upper Paleolithic child from Abrigo do Lagar Velho, Portugal. Proc. Natl. Acad. Sci. 107, 1338e1342.

Benazzi, S., Douka, K., Fornai, C., Bauer, C.C., Kullmer, O., Svoboda, J., Pap, I., Mallegni, F., Bayle, P., Coquerelle, M., Condemi, S., Ronchitelli, A., Harvati, K., Weber, G.W., 2011a. Early dispersal of modern humans in Europe and implications for Neanderthal behaviour. Nature 479, 525e528.

Benazzi, S., Fornai, C., Bayle, P., Coquerelle, M., Kullmer, O., Mallegni, F., Weber, G.W., 2011b. Comparison of dental measurement systems for taxonomic assignment of Neanderthal and modern human lower second deciduous molars. J. Hum. Evol. 61, 320e326.

Benazzi, S., Viola, B., Kullmer, O., Fiorenza, L., Harvati, K., Paul, T., Gruppioni, G., Weber, G.W., Mallegni, F., 2011c. A reassessment of the Neanderthal teeth from Taddeo cave (southern Italy). J. Hum. Evol. 61, 377e387.

Benazzi, S., Bailey, S.E., Mallegni, F., 2013. Brief communication: A morphometric analysis of the Neandertal upper second molar Leuca I. Am. J. Phys. Anthropol. 152, 300e305.

Benazzi, S., Bailey, S.E., Peresani, M., Mannino, M.A., Romandini, M., Richards, M.P., Hublin, J.-J., 2014a. Middle Paleolithic and Uluzzian human remains from Fumane Cave, Italy. J. Hum. Evol. 70, 61e68.

Benazzi, S., Panetta, D., Fornai, C., Toussaint, M., Gruppioni, G., Hublin, J.-J., 2014b. Technical note: Guidelines for the digital computation of 2D and 3D enamel thickness in hominoid teeth. Am. J. Phys. Anthropol. 153, 305e313.

Beynon, A.D., Dean, M.C., Reid, D.J., 1991. On thick and thin enamel in hominoids. Am. J. Phys. Anthropol. 86, 295e309.

Crevecoeur, I., Bayle, P., Rougier, H., Maureille, B., Higham, T., van der Plicht, J., De Clerck, N., Semal, P., 2010. The Spy VI child: A newly discovered Neandertal infant. J. Hum. Evol. 59, 641e656.

Fornai, C., Benazzi, S., Bayle, P., Pap, I., Svoboda, J., Harvati, K., Weber, G.W., 2012. Enamel thickness and dental tissue proportions in Neanderthal and modern human upper deciduous molars. Am. J. Phys. Anthropol. 147, 145.

Gantt, D.G., Rafter, J.A., 1998. Evolutionary and functional significance of hominoid tooth enamel. Connect. Tissue Res. 39, 195e206, 221.

Grine, F.E., 2002. Scaling of tooth enamel thickness, and molar crown size reduction in modern humans: research letter. S. Afr. J. Sci. 98, 503e509.

Grine, F.E., 2005. Enamel thickness of deciduous and permanent molars in modern *Homo sapiens*. Am. J. Phys. Anthropol. 126, 14e31.

Grine, F.E., Martin, L.B., 1988. Enamel thickness and development in *Australopithecus* and *Paranthropus*. In: Grine, F.E. (Ed.), Evolutionary History of the 'Robust' Australopithecines. Aldine de Gruyter, New York, pp. 3e42.

Hlusko, L.J., Suwa, G., Kono, R.T., Mahaney, M.C., 2004. Genetics and the evolution of primate enamel thickness: A baboon model. Am. J. Phys. Anthropol. 124, 223e233.

Kono, R.T., 2004. Molar enamel thickness and distribution patterns in extant great apes and humans: new insights based on a 3-dimensional whole crown perspective. Anthropol. Sci. 112, 121e146.

Kono, R.T., Suwa, G., Tanijiri, T., 2002. A three-dimensional analysis of enamel distribution patterns in human permanent first molars. Arch. Oral. Biol. 47, 867e875.

Macchiarelli, R., Bondioli, L., Debenath, A., Mazurier, A., Tournepiche, J.-F., Birch, W., Dean, M.C., 2006. How Neanderthal molar teeth grew. Nature 444, 748e751.

Macho, G.A., Thackeray, J.F., 1992. Computed tomography and enamel thickness of maxillary molars of Plio-Pleistocene hominids from Sterkfontein, Swartkrans, and Kromdraai (South Africa): An exploratory study. Am. J. Phys. Anthropol. 89, 133e143.

Mahoney, P., 2010. Two-dimensional patterns of human enamel thickness on deciduous (dm1, dm2) and permanent first (M1) mandibular molars. Arch. Oral. Biol. 55, 115e126.

Mahoney, P., 2013. Testing functional and morphological interpretations of enamel thickness along the deciduous tooth row in human children. Am. J. Phys. Anthropol. 151, 518e525.

Martin, L.B., 1983. Relationships of the later Miocene Hominoidea. Ph.D. Dissertation, University College London.

Martin, L.B., 1985. Significance of enamel thickness in hominoid evolution. Nature 314, 260e263.

Martin, L.B., Olejniczak, A.J., Maas, M.C., 2003. Enamel thickness and microstructure in pitheciin primates, with comments on dietary adaptations of the middle Miocene hominoid *Kenyapithecus*. J. Hum. Evol. 45, 351e367.

Molnar, S., 1971. Human tooth wear, tooth function and cultural variability. Am. J. Phys. Anthropol. 34, 175e189.

Molnar, S., Hildebolt, C., Molnar, I.M., Radov[illegible]ć, J., Gravier, M., 1993. Hominid enamel thickness: I. The Krapina Neandertals. Am. J. Phys. Anthropol. 92, 131e138.

Olejniczak, A.J., Smith, T.M., Feeney, R.N.M., Macchiarelli, R., Mazurier, A., Bondioli, L., Rosas, A., Fortea, J., de la Rasilla, M., Garcia-Tabernero, A., Radov[illegible]ć, J., Skinner, M.M., Toussaint, M., Hublin, J.-J., 2008a. Dental tissue proportions and enamel thickness in Neandertal and modern human molars. J. Hum. Evol. 55, 12e23.

Olejniczak, A.J., Smith, T.M., Skinner, M.M., Grine, F.E., Feeney, R.N.M., Thackeray, J.F., Hublin, J.-J., 2008b. Three-dimensional molar enamel distribution and thickness in *Australopithecus* and *Paranthropus*. Biol. Lett. 4, 406e410.

Olejniczak, A.J., Smith, T.M., Wang, W., Potts, R., Ciochon, R., Kullmer, O., Schrenk, F., Hublin, J.-J., 2008c. Molar enamel thickness and dentine horn height in *Gigantopithecus blacki*. Am. J. Phys. Anthropol. 135, 85e91.

Olejniczak, A.J., Tafforeau, P., Feeney, R.N.M., Martin, L.B., 2008d. Three-dimensional primate molar enamel thickness. J. Hum. Evol. 54, 187e195.

Rozzi, F.R., 1996. Comment on the causes of thin enamel in Neanderthals. Am. J. Phys. Anthropol. 99, 625e626.

Schwartz, G.T., 2000. Taxonomic and functional aspects of the patterning of enamel thickness distribution in extant large-bodied hominoids. Am. J. Phys. Anthropol. 111, 221e244.

Shimizu, D., Macho, G.A., Spears, I.R., 2005. Effect of prism orientation and loading direction on contact stresses in prismatic enamel of primates: Implications for interpreting wear patterns. Am. J. Phys. Anthropol. 126, 427e434.

Smith, T.M., Olejniczak, A.J., Martin, L.B., Reid, D.J., 2005. Variation in hominoid molar enamel thickness. J. Hum. Evol. 48, 575e592.

Smith, T.M., Olejniczak, A.J., Reid, D.J., Ferrell, R.J., Hublin, J.J., 2006. Modern human molar enamel thickness and enamel-dentine junction shape. Arch. Oral. Biol. 51, 974e995.

Smith, T.M., Harvati, K., Olejniczak, A.J., Reid, D.J., Hublin, J.-J., Panagopoulou, E., 2009. Brief communication: Dental development and enamel thickness in the Lakonis Neanderthal molar. Am. J. Phys. Anthropol. 138, 112e118.

Smith, T.M., Tafforeau, P., Reid, D.J., Pouech, J., Lazzari, V., Zermeno, J.P., Guatelli-Steinberg, D., Olejniczak, A.J., Hoffman, A., Radov[illegible]ić, J., Makaremi, M.,
Toussaint, M., Stringer, C., Hublin, J.-J., 2010. Dental evidence for ontogenetic differences between modern humans and Neanderthals. Proc. Natl. Acad. Sci. 107, 20923e20928.

Smith, T.M., Kupczik, K., Machanda, Z., Skinner, M.M., Zermeno, J.P., 2012a. Enamel thickness in Bornean and Sumatran orangutan dentitions. Am. J. Phys. Anthropol. 147, 417e426.

Smith, T.M., Olejniczak, A.J., Zermeno, J.P., Tafforeau, P., Skinner, M.M., Hoffmann, A., Radov[illegible]ić, J., Toussaint, M., Kruszynski, R., Menter, C., Moggi-Cecchi, J., Glasmacher, U.A., Kullmer, O., Schrenk, F., Stringer, C., Hublin, J.-J., 2012b. Variation in enamel thickness within the genus *Homo*. J. Hum. Evol. 62, 395e411.

Spoor, C.F., Zonneveld, F.W., Macho, G.A., 1993. Linear measurements of cortical bone and dental enamel by computed tomography: Applications and problems. Am. J. Phys. Anthropol. 91, 469e484.

Strait, D.S., Constantino, P., Lucas, P.W., Richmond, B.G., Spencer, M.A., Dechow, P.C., Ross, C.F., Grosse, I.R., Wright, B.W., Wood, B.A., Weber, G.W., Wang, Q., Byron, C., Slice, D.E., Chalk, J., Smith, A.L., Smith, L.C., Wood, S., Berthaume, M., Benazzi, S., Dzialo, C., Tamvada, K., Ledogar, J.A., 2013. Viewpoints: Diet and dietary adaptations in early hominins: The hard food perspective. Am. J. Phys. Anthropol. 151, 339e355.

Suwa, G., Kono, R.T., 2005. A micro-CT based study of linear enamel thickness in the mesial cusp section of human molars: reevaluation of methodology and assessment of within-tooth, serial, and individual variation. Anthropol. Sci. 113, 273e289.

Toussaint, M., Olejniczak, A.J., El Zaatari, S., Cattelain, P., Flas, D., Letourneux, C., Pirson, S., 2010. The Neandertal lower right deciduous second molar from Trou de l'Abîme at Couvin, Belgium. J. Hum. Evol. 58, 56e67.

Zanolli, C., Bayle, P., Macchiarelli, R., 2010. Tissue proportions and enamel thickness distribution in the early Middle Pleistocene human deciduous molars from Tighenif, Algeria. C.R. Palevol 9, 341e348.

Zilberman, U., Smith, P., 1992. A comparison of tooth structure in Neanderthals and early *Homo sapiens sapiens*: a radiographic study. J. Anat. 180, 387e393.

Zilberman, U., Skinner, M., Smith, P., 1992. Tooth components of mandibular deciduous molars of *Homo sapiens sapiens* and *Homo sapiens neanderthalensis*: A radiographic study. Am. J. Phys. Anthropol. 87, 355e363.

Table S1

Raw data for the enamel thickness components from dm^1 mesial sections and dm^2 mesial and buccal sections. **RHS = recent modern humans; UPHS = Upper Paleolithic modern humans; N = Neanderthals.**

Tooth class	Section	Taxon	Individual	Enamel area	Dentine area	EDJ length	AET	RET	Wear stage (Molnar, 1971)
dm^1	mesial	RHS	Med1_1	6.55	23.91	16.03	0.40860886	8.35637632	1
			CA_T19	9.70	29.70	17.94	0.54069119	9.92135686	2
			CA_T17	7.90	27.61	16.84	0.46912114	8.92795106	1
			EH_U21	6.68	25.31	15.50	0.43096774	8.56640675	2
			EH_U56	9.30	27.20	15.85	0.58675079	11.25043280	1
			EH_U57	7.73	23.73	14.70	0.52585034	10.79476743	1
			322L	8.10	30.06	17.74	0.45659526	8.32792711	2
			sa27_54+64	9.83	29.45	17.79	0.55255762	10.18204285	2
			Guid_T49	7.38	28.17	15.74	0.46886912	8.83401659	3
			Tb59a	6.00	29.71	15.74	0.38119441	6.99350994	3
			Casf_Tb36	7.76	28.45	16.33	0.47519902	8.90911164	3
			SMBT_Tb37	8.15	27.18	17.33	0.47028275	9.02057704	3
			Casf_Tb44R	6.90	29.36	15.95	0.43260188	7.98381340	3
			SMBT_Tb92	7.08	30.49	16.24	0.43596059	7.89529789	3
			CASF_Tb49	7.16	28.94	16.59	0.43158529	8.02264126	3
			322	6.61	31.63	15.61	0.42344651	7.52920220	3
			549	7.77	25.92	15.98	0.48623279	9.55051399	3
			Nuspligen_1165_L	7.84	31.13	16.58	0.47285887	8.47504428	3
			Csok_13	10.11	35.39	16.74	0.60394265	10.15208910	3
			Csok_288	6.67	28.96	15.44	0.43199482	8.02748050	3
			Csok_444	6.01	25.41	15.02	0.40013316	7.93783755	3
			Csok_471	6.26	24.54	14.80	0.42297297	8.53837724	3
			Nr75	8.13	29.43	17.12	0.47488318	8.75369991	3
			Nr396	6.84	27.93	21.30	0.32112676	6.07632550	3

		UPHS	Dolní Věstonice 36_2	10.12	32.87	18.04	0.56097561	9.78462368	1
			La Rochette	8.25	32.90	16.65	0.49549550	8.63856811	3
		N	Krapina d181	5.74	33.67	16.77	0.34227788	5.89871307	3
			Krapina d183	7.67	36.57	17.33	0.44258511	7.31870633	3
			Roc de Marsal L	6.38	29.34	17.77	0.35903208	6.62831587	3
			Pech de l'Azé L	7.74	33.03	18.08	0.42809735	7.44883317	3
dm^2	mesial	RHS	Med1_1	10.75	27.76	17.15	0.62682216	11.89692186	1
			CA-T19	14.28	32.72	18.77	0.76078849	13.30017292	1
			Guid_T52	11.27	26.74	17.13	0.65791010	12.72289232	1
			Tb59a	9.82	32.44	18.50	0.53081081	9.31964429	2
			PM	12.04	29.21	17.96	0.67037862	12.40378918	2
			Tb37	12.90	33.22	19.10	0.67539267	11.71808190	2
			Tb44R	13.41	33.24	19.13	0.70099320	12.15859242	2
			T49	14.04	33.92	19.23	0.73010920	12.53602651	1
			Guid_T49	13.80	33.46	19.32	0.71428571	12.34835186	2
			EH-U21	11.14	28.33	16.97	0.65645256	12.33332174	1
			EH-U56	11.97	31.07	16.94	0.70661157	12.67681399	1
			EH-U57	11.97	29.29	17.07	0.70123023	12.95689512	1
			Cs444	11.31	28.26	17.30	0.65375723	12.29788487	1
			Nr115	12.09	27.87	17.87	0.67655288	12.81543240	1
			Nr116	14.77	31.14	18.77	0.78689398	14.10122748	2
			Nr75	12.53	31.71	17.99	0.69649805	12.36863537	1
			322_L	13.05	32.05	18.12	0.72019868	12.72149939	1
			549_L	14.91	29.64	17.83	0.83623107	15.35985800	1
			sa27_55_R	16.10	34.05	19.55	0.82352941	14.11303947	1
			sa27_65_L	15.08	34.14	19.25	0.78337662	13.40722350	1
			Nuspligen_1165_R	13.29	33.69	19.30	0.68860104	11.86361833	2
			319	13.98	31.94	18.76	0.74520256	13.18581206	2
			513	11.99	28.24	16.92	0.70862884	13.33479914	2
			Guid_Tb20	9.60	32.29	18.44	0.52060738	9.16170479	3

			Tb36	11.70	33.10	18.38	0.63656148	11.06436153	3
			Tb44L	11.19	36.14	19.23	0.58190328	9.67958478	3
			Tb92	10.86	36.17	18.96	0.57278481	9.52395288	3
			Cs288	10.93	31.88	17.35	0.62997118	11.15736206	3
			Cs13	16.67	36.64	19.33	0.86239007	14.24708493	3
			Cs290	12.03	31.57	18.66	0.64469453	11.47404891	3
			Nr396	11.97	30.31	18.18	0.65841584	11.95934249	3
			Cs305	14.35	34.48	19.32	0.74275362	12.64914440	3
			322_R	12.45	35.60	18.55	0.67115903	11.24865089	3
			1115	10.85	35.33	16.49	0.65797453	11.06973601	3
		UPHS	Dolní Věstonice 36_3	17.45	36.36	19.23	0.90743630	15.04888106	1
			La Rochette	19.41	38.03	20.17	0.96232028	15.60473775	1
		N	Krapina d185	13.37	38.39	19.04	0.70220588	11.33327448	1
			Krapina d186	11.30	35.33	18.47	0.61180292	10.29294683	2
			Krapina d188	13.04	39.80	19.93	0.65429002	10.37119397	2
			Roc de Marsal L	10.42	32.79	19.89	0.52388135	9.14875984	2
			Krapina d187	9.16	32.49	16.49	0.55548817	9.74540657	3
			Krapina d189	11.05	44.64	18.47	0.59826746	8.95433400	3
			Krapina d190	14.42	44.12	21.36	0.67509363	10.16356947	3
			Subalyuk 2 L	8.33	29.64	17.50	0.47600000	8.74314846	3
			Pech de l'Azé L	11.40	33.39	19.29	0.59097978	10.22738051	3
dm^2	buccal	RHS	Med1_1	9.08	23.24	15.98	0.56821026	11.78666694	2
			CA-T19	12.95	26.11	16.53	0.78342408	15.33181178	1
			Guid_T52	10.07	24.64	14.47	0.69592260	14.01976028	2
			Guid_T59	9.38	28.48	17.59	0.53325753	9.99233548	2
			PM	11.43	24.60	16.80	0.68035714	13.71732395	2
			Tb37	11.53	26.46	16.76	0.68794749	13.37397087	1
			Tb36	11.62	27.77	16.71	0.69539198	13.19598272	2
			Tb44R	11.58	26.77	16.78	0.69010727	13.33805234	2
			Guid_T49	12.79	26.88	17.31	0.73887926	14.25144314	2
			Tb49	12.79	26.75	17.31	0.73887926	14.28603084	2

	EH-U21	10.19	24.13	15.55	0.65530547	13.34028567	2
	EH-U56	12.12	29.17	17.12	0.70794393	13.10782531	1
	EH-U57	11.64	25.20	15.95	0.72978056	14.53757682	1
	322_L	12.37	28.60	16.03	0.77167810	14.42956240	1
	549_L	15.38	26.50	16.40	0.93780488	18.21753239	1
	sa27_55_R	14.25	29.87	19.00	0.75000000	13.72282901	1
	sa27_65_L	14.28	28.39	18.50	0.77189189	14.48684398	1
	Nuspligen_1165_L	14.46	30.03	18.29	0.79059595	14.42702955	2
	319	13.66	26.44	18.46	0.73997833	14.39091067	2
	513	11.01	24.46	15.81	0.69639469	14.08079652	2
	Cs444	11.47	24.67	15.69	0.73103888	14.71824065	1
	Nr115	11.30	23.61	16.09	0.70229956	14.45354590	2
	Nr116	14.56	29.45	17.99	0.80933852	14.91377415	1
	Cs13	17.39	29.71	18.67	0.93144081	17.08849982	2
	Nr75	13.66	25.72	15.99	0.85428393	16.84483470	1
	Nr396	12.54	21.68	17.18	0.72991851	15.67634231	2
	Cs305	13.89	27.91	17.27	0.80428489	15.22404258	2
	Guid_Tb20	9.35	29.02	17.11	0.54646406	10.14408541	3
	Tb44L	12.51	30.42	18.53	0.67512142	12.24058814	3
	Tb92	11.64	30.78	17.88	0.65100671	11.73413710	3
	1115_UR	11.65	28.66	15.79	0.73780874	13.78179236	3
	Cs288	12.56	24.67	16.35	0.76819572	15.46633126	3
	Cs290	11.90	26.06	17.04	0.69835681	13.68012814	3
UPHS	La Rochette	18.90	31.42	17.75	1.06478873	18.99592107	2
	Dolní Věstonice 36_3	14.62	25.94	16.84	0.86817102	17.04591426	2
N	Kr_d185	13.02	36.29	18.65	0.69812332	11.58880523	1
	Kr_d186	10.96	30.95	18.27	0.59989053	10.78305152	1
	Kr_d188	13.82	37.57	20.20	0.68415842	11.16184728	1
	Roc de Marsal L	12.19	31.35	20.20	0.60346535	10.77788545	1
	Pech de l'Azé L	11.83	29.43	18.00	0.65722222	12.11482398	1
	Kr_d187	10.29	30.82	16.68	0.61690647	11.11227579	3

Kr_d189	12.11	40.04	18.61	0.65072542	10.28373166	3
Kr_d190	13.59	41.87	20.88	0.65086207	10.05859870	3
Subalyuk 2 L	9.91	29.08	17.13	0.57851722	10.72800804	3

RHS: recent *Homo sapiens*; UPHS: Upper Paleolithic *H. sapiens*; N: *H. neanderthalensis*.

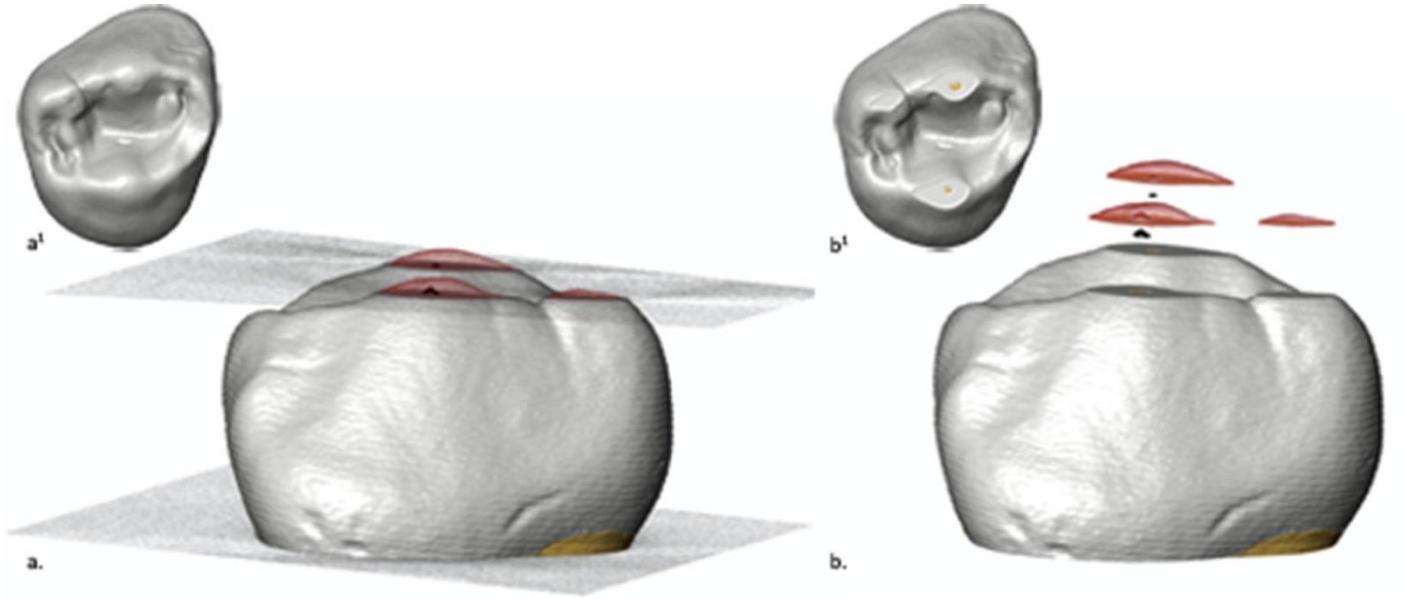

Fig. S1 – Example simulating the diverse effect of wear on a **recent modern human** dm^1 enamel cap and coronal dentine, using a cutting plane parallel to the cervical plane which simplifies a Molnar's wear stage 3 (1971). This example shows that the loss of enamel (red areas) is greater than the loss of dentine (black areas), namely, 1.21% of the total coronal enamel volume against virtually 0% of the coronal enamel volume are lost.

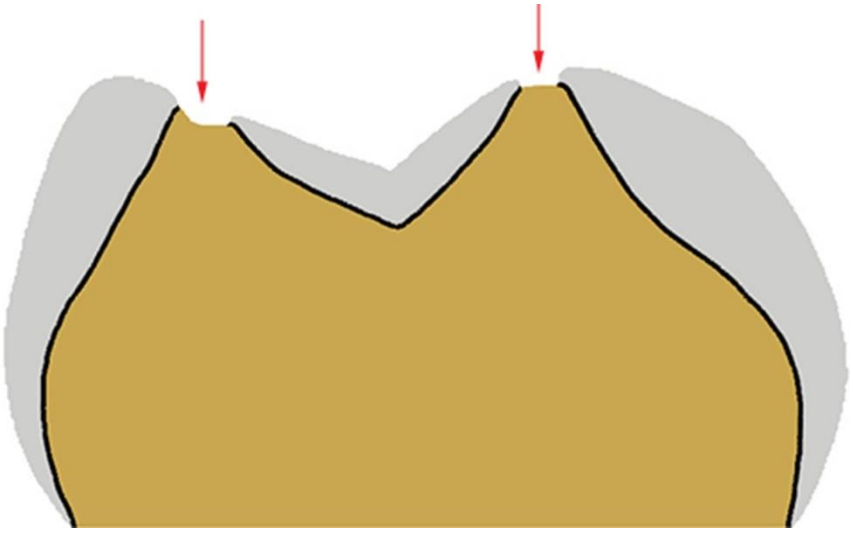

Fig. S2 – 2D section from a worn upper molar showing how the EDJ length is obtained. The lengths of the segments along which enamel and dentine are actually still in contact are summed up, while the length of the exposed dentine is not included.

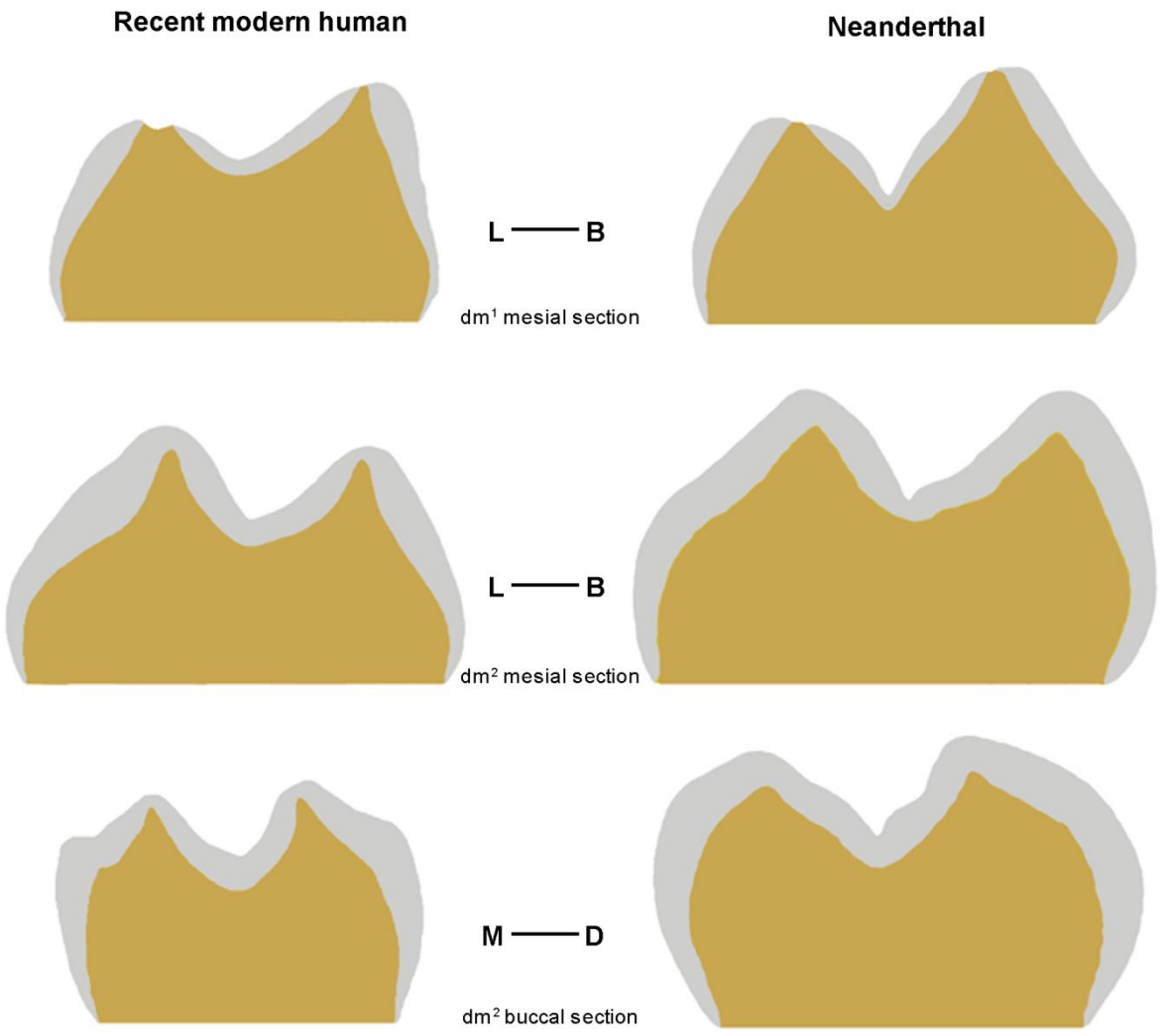

Fig. S3 – Comparison between recent modern human and Neanderthal dm1 mesial sections (wear stage 3) and dm2 mesial and buccal sections (wear stage 1-2). In modern human dm2s, the enamel is rather thick laterally with respect to Neanderthal (represented by Krapina d185 in this figure), especially on the buccal section. The mesial section for Neanderthal dm1 is taken from Pech-de-l'Azé. L = lingual; B = buccal; M = mesial; D = distal.

2.6. Variability of *Australopithecus* second maxillary molars from Sterkfontein Member 4.

Fornai, C., Bookstein, F.L., Weber, G.W.

Journal of Human Evolution 2015

Synopsis

In this chapter, we investigated the variability of upper second molars within an *Australopithecus africanus* sample, in comparison to *Paranthropus* and *Homo*. We used various geometric morphometric approaches in order to consider several aspects of the crown and test the hypothesis of the occurrence of a second *Australopithecus* species in Sterkfontein Member 4 and Makapansgat, as suggested by R. J. Clarke.
Our methods were able to distinguish between *Homo* and both *Australopithecus* and *Paranthropus*, but no separation occurred between *Australopithecus* and *Paranthropus*, and within *Australopithecus*. Instead we observed a gradient for these teeth, which was reminiscent of Clarke's interpretation of the Sterkfontein dental variability. We concluded that either the *Australopithecus* specimens used in our contribution represent one single species, or if two *Australopithecus* species existed at site, the upper second molar does not convey this information. The outcome of this work is also a warning to morphologists which aim to infer about paleotaxonomy or paleosystematic that a broader knowledge of human (dental) variability is necessary to understand how taxa should be delimited.

Contribution

Study design, data collection, interpretation of the data, drafting and editing of the manuscript.

Journal of Human Evolution xxx (2015) 1e12

Contents lists available at ScienceDirect

Journal of Human Evolution

journal homepage: www.elsevier.com/locate/jhevol

Variability of *Australopithecus* second maxillary molars from Sterkfontein Member 4

Cinzia Fornai [a, *], Fred L. Bookstein [a, b], Gerhard W. Weber [a]

[a] Department of Anthropology, University of Vienna, Austria
[b] Department of Statistics, University of Washington, USA

a r t i c l e i n f o

Article history:
Received 2 December 2014
Accepted 22 May 2015
Available online xxx

Keywords:
Paranthropus
South Africa
Dental morphology
Geometric morphometrics
Enameledentine junction

a b s t r a c t

The question of how many *Australopithecus* species lived at Sterkfontein Member 4 and Makapansgat continues to be controversial inasmuch as the fossils are poorly preserved, the stratigraphy is difficult to interpret, and the cranial, dental, and postcranial remains are mostly not associated. To proceed we applied the most intensive modern methods of 3D geometric morphometrics to dental form, specifically the shapes of the upper second molars (M^2s) in a sample combining 13 *Australopithecus*, 11 *Paranthropus*, and 23 *Homo*. We analyzed outer and inner crown surfaces, as well as crown and cervical outlines both separately and together, using a total of 16 landmarks, 51 curve semilandmarks, and 48 pseudolandmarks over the four structures. Outer and inner enamel surfaces are highly correlated in this dataset, while crown outline is the least informative of the four structures. *Homo* was easily distinguished from both *Australopithecus* and *Paranthropus* by these methods, likewise *Homo sapiens* from *Homo neanderthalensis*. There were, however, no stable classes within the *Australopithecus* sample or between *Australopithecus* and *Paranthropus*. Instead, there was a gradient along which *Australopithecus prometheus* and *Australopithecus africanus* lie toward the extremes, with *Paranthropus* overlapping both. If there are indeed different species at this site, then either their M^2 morphologies are uninformative or else the present sample is too small to make an accurate assessment. Our findings suggest that the variability of the *Australopithecus* specimens will be difficult to interpret authoritatively, independent of the method used.

1. Introduction

The taxonomy of the hominin fossils recovered from Sterkfontein Member 4, Makapansgat and Taung (recently reviewed in Grine, 2013) passed through an initial phase of splitting into different species and genera (Dart, 1925, 1948; Broom, 1936, 1938), then a successive lumping into the species *Australopithecus africanus* in the mid-1950s (Robinson, 1954, 1965; Le Gros Clark, 1955; Tobias, 1965), and lately another phase of splitting beginning in the 1980s, when several authors envisaged the presence of multiple species (Clarke, 1985a,b, 1988, 1994a, 2008, 2013; Kimbel and White, 1988; Kimbel and Rak, 1993; Calcagno et al., 1997; Lockwood and Moggi-Cecchi, 1998; Lockwood and Tobias, 1999, 2002; Schwartz and Tattersall, 2005; Moggi-Cecchi and Boccone, 2007). At the same time, other experts have considered these extinct hominins to belong to a single but variable taxon (Ahern, 1998; Lockwood and Tobias, 1999; Wood and Richmond, 2000; Grine, 2013). Several factors may account for this lack of taxonomic clarity, including the poor state of preservation of the fossils and the absence of association between cranial, dental, and postcranial remains (with few exceptions). Indeed there seems to be no expert consensus regarding the diagnostic features to be considered in any taxonomy (e.g., Rak, 1983; Clarke, 1988, 2008; Kimbel and White, 1988; Lockwood and Moggi-Cecchi, 1998; Lockwood and Tobias, 2002; Schwartz and Tattersall, 2005). Furthermore, the stratigraphy of the cave infills encasing the fossils is complicated (Clarke, 1994b; Partridge, 2000; Clarke and Partridge, 2002; Clarke et al., 2003; Clarke, 2006; Pickering and Kramers, 2010), providing further challenges to understanding the taxonomy of the hominins recovered from Sterkfontein. The Sterkfontein Formation has been divided into six Members by Partridge (1978), and since then two other infills, the StW 53 Infill and the Post-Member 6 Infill, have been recognized (Kuman and Clarke, 2000). Among all, Member 4 is the richest hominin-bearing infill and has mainly yielded *Australopithecus* remains, while Member 5 is known for the presence of *Homo* and *Paranthropus*.

* Corresponding author.
E-mail addresses: cinzia.fornai@univie.ac.at (C. Fornai), fred@brainmap.stat.washington.edu (F.L. Bookstein), gerhard.weber@univie.ac.at (G.W. Weber).

http://dx.doi.org/10.1016/j.jhevol.2015.05.013
0047-2484/

Taxonomic assessment of the hominin remains from Sterkfontein Member 4, Makapansgat, and Taung have focused mainly on craniofacial and dental characteristics, but there is also evidence for polymorphism within the hypodigm of *Au. africanus* in postcranial morphology (Clarke and Tobias, 1995; Partridge et al., 2003; Zipfel and Berger, 2009; DeSilva et al., 2012). This might reflect two different locomotor modes within both Member 2 and Member 4 at Sterkfontein. Lockwood and Tobias (2002), reviewing the morphological characteristics of the craniofacial remains for Sterkfontein Member 4 (integrated by Lockwood and Tobias, 1999 for the adult male StW 505), agreed with other authors about the presence of multiple species at Sterkfontein but confidently assigned only the juvenile maxilla StW 183 and the temporal bone StW 255, with associated 266a, to an unnamed group other than *Au. africanus*. Analyzing dental linear diameters of first and second upper molars along with qualitative features of the maxillary region, Kimbel and White (1988) explained the morphological variability of the best preserved specimens as evidence for two different hominin species at Sterkfontein Member 4, but they were vague about the alpha taxonomy of these individuals. Some authors have argued that Sterkfontein Member 4 might include a hominin form more derived towards the *Homo* condition (e.g., StW 151; Moggi-Cecchi et al., 1998).

The debate about the provenience and taxonomic attribution of the StW 53 cranial remains has further complicated the issue of the presence of multiple species at Sterkfontein. Initially allocated to *Homo habilis* (Hughes and Tobias, 1977; Howell, 1978; Tobias, 1978; Clarke, 1985a; Curnoe and Tobias, 2006), StW 53 was considered by Curnoe (2010) as belonging to a distinct early *Homo* species that he named *Homo gautengensis*, while others (Ferguson, 1989; Kuman and Clarke, 2000; Thackeray et al., 2000; Clarke, 2008, 2013) claimed it should belong to *Au. africanus*. The exact provenience of StW 53 is also a matter of disagreement. Tobias (1978) and Partridge (1978, 2000) considered StW 53 as coming from Member 5 or Extension site, while Kuman and Clarke (2000) described the StW 53 Infill as a Member 4 hanging remnant, chronologically intermediate between Member 4 and Member 5 breccias yielding artifacts. Herries et al. (2009) argued that there is considerable age difference between Member 4 and 5, and confidently placed StW 53 within Member 4 based on ESR dates for faunal teeth from the StW 53 sediments.

On the basis of several morphological features, most of which related to the masticatory apparatus, Clarke (1985a, 1988, 2008, 2013) concluded that the hominin fossils from Sterkfontein Member 4 and Makapansgat Limeworks represented two distinct *Australopithecus* species. Besides *Au. africanus*, typified by specimens such as Sts 5, Sts 52, StW 53, and TM 1511, he described a hominin with large teeth, characterized by more derived masticatory features, which he considered a precursor of *Paranthropus robustus*. Clarke assigned many individuals to this taxon, including StW 252, Sts 71, StW 183, StW 498, and StW 505, all of which are well preserved (Clarke, 2008, 2013). He considered the virtually complete skeleton StW 573 from Member 2 (Clarke, 1999) to ally with this second *Australopithecus* species (Clarke, 2008, 2013).

The hominin remains from Makapansgat have also been the object of taxonomic debate. The hominins from Member 2 and 3 were initially attributed to *Australopithecus prometheus* by Dart (1948) and then lumped into *Au. africanus* (Robinson, 1954). Aguirre (1970) considered the hominin remains from Makapansgat Member 2 as belonging to both *Australopithecus* and *Paranthropus*. Similarly to Sterkfontein Member 4, Schwartz and Tattersall (2005) sorted the hominins from Makapansgat into different morphs, some of which they claimed to have been present at Sterkfontein Member 4 as well. Clarke considered the second *Australopithecus* species he recognized in Sterkfontein Member 4 also to be represented in Makapansgat. In keeping with the principle of priority, he named this second species *Au. prometheus*, after Dart (1948).

Teeth are frequently studied elements in paleoanthropology since they are particularly durable. However, as Robinson (1956) noted, hominin teeth are built upon the same general plan that does not always allow us to resolve taxonomic issues unless clear synapomorphies accumulated (Corruccini, 1987). In extinct species the boundaries between inter- and intraspecific variation are difficult to determine, and methods that successfully distinguish some taxa might not work for others. For example, Skinner et al. (2008) found only subtle differences between South African *Australopithecus* and *Paranthropus* lower molars, but using a similar protocol Skinner et al. (2009) were able to discriminate between subspecies of *Pan* on the basis of M_2s.

Traditional two-dimensional approaches to dental anthropology, such as the analysis of dental diameters and the analysis of cusp pattern (Kimbel and White, 1988; Calcagno et al., 1997, 1999; Moggi-Cecchi, 2003; Boccone and Moggi-Cecchi, 2005; Moggi-Cecchi and Boccone, 2007; Grine et al., 2013), have generated a mass of results on the South African *Australopithecus* that, though far from definitive, indicate that teeth carry further biological information as yet unanalyzed. Kimbel and White (1988) found evidence for a second species when they analyzed the maxillary second molars, but not when they studied other tooth types. Calcagno et al. (1997, 1999) and Moggi-Cecchi (2003) found contrasting or inconclusive results using linear measurements. However, studying the occlusal cusp pattern on 2D images of the maxillary molars, Moggi-Cecchi and Boccone (2007) found that some of the teeth Clarke attributed to the second species showed a different occlusal pattern. Recently, Grine et al. (2013) analyzed the bucco-lingual and mesio-distal diameters from mandibular postcanine teeth from Sterkfontein Member 4 and Makapansgat, and from the Taung child. They found high variation within this sample that they considered not to exceed the intraspecific variability of a species (or of a chronospecies), and attributed it mostly to the highly variable expression of extra molar cuspulids and protostylids.

Clarke claimed *Au. prometheus* possessed *Paranthropus*-like molars with low and bulbous cusps, and cusp tips oriented towards the center of the crown, while *Au. africanus* had smaller molars with steeper side walls and outward-flaring cusp tips (Fig. 1). Interpreting Clarke's qualitative description of the molar teeth, Fornai et al. (2010) carried out a first attempt to overcome the limitations of 2D approaches for the analysis of the dental remains from Sterkfontein Member 4 via a 3D geometric morphometric

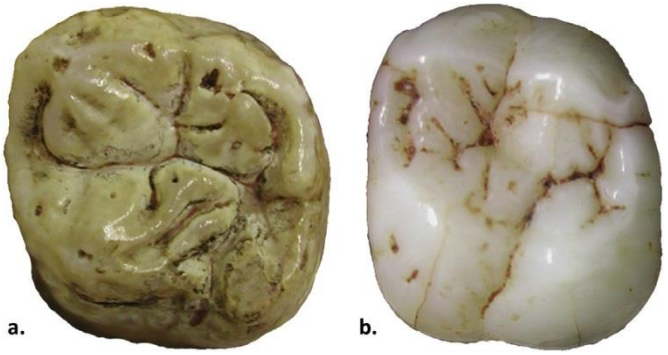

Figure 1. M^2 from a) Sts 56 *Au. africanus* and b) StW 183 *Au. prometheus* according to Clarke (2008). Sts 56 presents outward-flaring cusps and steeper sidewalls; in contrast, StW 183 shows blunt cusps with a bucco-lingually narrow occlusal basin. The teeth are scaled approximately to the same size (photos courtesy of S. Boccone, modified).

(GM) study of the occlusal aspect of the maxillary molars. Preliminary results seemed to suggest the presence of two distinct dental morphs at the site.

The present work builds upon that first GM analysis through a larger comparative sample and an improved set of variables (see Materials and methods). In order to assess the variability of the 3D morphology of the *Australopithecus* (M^2: upper second molars) sample, we used multiple GM resources, namely landmarks and curve semilandmarks from both the enameledentine junction (EDJ) and the outer enamel surface (OES) of unworn or slightly worn teeth. To enlarge the sample size, we also analyzed crown and cervical outlines gathered from virtual 3D surface models of the molar crowns, an approach that suits worn or slightly damaged teeth because it does not consider the occlusal aspect of the crown. (Wear per se is not the topic of our study.) We explore the extent to which the dental aspects considered are or are not concordant for the purposes of classification. We discuss the variability of the *Australopithecus* and *Paranthropus* dental specimens especially in the context of the hypothesis of the occurrence of a second *Australopithecus* species at Sterkfontein Member 4. We test whether the morphology of M^2s reflects the grouping of *Au. africanus* as suggested by Clarke (1988, 2008, pers. comm). (Our observations on *Australopithecus* dental variability at Makapansgat are limited to one individual only.)

2. Materials and methods

This study examined a total of 47 M^2s, of which 13 were *Australopithecus* specimens from the Plio-Pleistocene South African hominin sites of Sterkfontein Member 4 and Makapansgat (see details in Table 1). We labeled these individuals according to Clarke's classification as either *Au. africanus* or *Au. prometheus* (Clarke, 1988, 2008, pers. comm.). The comparative sample comprised 11 *Paranthropus* specimens from Swartkrans, Kromdraai, and Coopers Cave, along with SK 27 early *Homo* from Swartkrans (Clarke, 1977). We also included StW 151 from Sterkfontein Member 4, the morphology of which has been variously interpreted as showing more affinity either to *Australopithecus* or to early *Homo* (Spoor, 1993; Moggi-Cecchi et al., 1998; Grine et al., 2013). Curnoe (2010) considered both SK 27 and StW 151 as belonging to a distinct *Homo* species, *H. gautengensis*. In addition, the comparative sample included 15 *Homo sapiens* M^2s from Australia, Central Europe, Papua New Guinea, and Southern Africa, and 6 *Homo neanderthalensis* from Krapina, Croatia. M^2s were chosen because it is easier to find unworn or slightly worn M^2s than first molars (which participate in masticatory occlusion earlier), because M^2s in hominins show less intraspecific variability than third molars (e.g., Robinson, 1956; Wood and Engleman, 1988), and also because previous research based on 2D approaches (Kimbel and White,

Table 1
List of M^2 specimens indicating the taxon attribution, the provenience, the wear stage, and the dental features considered for each.[a]

Taxon	Specimen	Provenience	Wear stage[b]	OES	EDJ	Crown outline	Cervical outline
Australopithecus	MLD 6	Makapansgat	3			x	x
	Sts 8	Sterkfontein, M4	2	x	x	x	x
	Sts 22	Sterkfontein, M4	2	x	x	x	x
	Sts 28	Sterkfontein, M4	3		x	x	x
	Sts 52	Sterkfontein, M4	2	x	x	x	x
	Sts 56	Sterkfontein, M4	1	x			
	StW 183	Sterkfontein, M4	1	x	x	x	x
	StW 188	Sterkfontein, M4	2	x	x	x	x
	StW 204	Sterkfontein, M4	1	x	x		
	StW 252 K	Sterkfontein, M4	2	x	x	x	x
	StW 280[c]	Sterkfontein, M4	1	x		x	x
	StW 447	Sterkfontein, M4	1	x			
	StW 530	Sterkfontein, M4	3			x	x
Paranthropus robustus	CD 5774	Cooper's Cave	1	x	x	x	x
	SK 13/14	Swartkrans	1	x	x	x	x
	SK 16	Swartkrans	3		x	x	x
	SK 47	Swartkrans	1	x	x	x	x
	SK 48[c]	Swartkrans	3			x	x
	SK 49[c]	Swartkrans	3			x	x
	SK 98	Swartkrans	1	x	x	x	x
	SK 834	Swartkrans	3			x	x
	SKW 11	Swartkrans	3			x	x
	SKW 14	Swartkrans	1	x			
	TM 1517 A[c]	Kromdraai	3			x	x
Early *Homo*	SK 27	Swartkrans	1	x	x	x	x
Undetermined (tentatively early *Homo*[d])	StW 151	Sterkfontein, M4	2	x		x	x
Homo neanderthalensis	Kr 96	Krapina, Croatia	2	x	x	x	x
	Kr 98	Krapina, Croatia	1	x	x	x	x
	Kr 135	Krapina, Croatia	3		x	x	x
	Kr 165	Krapina, Croatia	2	x	x	x	x
	Kr 169	Krapina, Croatia	2	x	x	x	x
	Kr 177	Krapina, Croatia	2	x	x	x	x
Recent *Homo sapiens*	Southern Africans (n ¼ 7)	Southern Africa	1e2	n ¼ 6	n ¼ 7	n ¼ 6	n ¼ 6
	Papua New Guinea indigenous (n ¼ 4)	Papua New Guinea	1e2	n ¼ 4	n ¼ 4	n ¼ 4	n ¼ 4
	Europeans (n ¼ 3)	Central Europe	1e2	n ¼ 3	n ¼ 3	n ¼ 3	n ¼ 3
	Australian aborigines (n ¼ 1)	Australia	1e2	n ¼ 1	n ¼ 1	n ¼ 1	n ¼ 1

[a] OES: outer enamel surface; EDJ: enameledentine junction.
[b] Molnar (1971).
[c] A cast was used.
[d] Curnoe (2010).

1988; Calcagno et al., 1997) suggested that *Australopithecus* M^2s carried a taxonomic signal.

Our main criterion for inclusion in the present sample was the absence of major damage in the areas of interest. The occlusal area and/or the cervical margin had to be preserved. In case both antimeres were present, we examined the one that was better preserved. To evaluate occlusal wear we followed Molnar (1971). Since *Australopithecus* and *Paranthropus* possessed thicker enamel than *Homo*, we scored the wear stage as 3 when the molars showed "cusp pattern partially or completely obliterated" (Molnar, 1971: 178; Fig. 1), even if the dentine was not exposed. In this sense, Molnar's wear stage 3 corresponds to a medium wear stage according to Moggi-Cecchi et al. (2006). The wear stages for *H. sapiens* and *H. neanderthalensis* were scored again per Molnar (1971). The wear stage assessment is reported in Table 1.

2.1. Scanning, segmentation, and 3D surface reconstruction

We obtained high resolution CT data for all specimens (isometric voxel size: 20e65 mm). The South African material was scanned at NECSA (South African Nuclear Energy Corporation), Pelindaba, South Africa at the South African Neutron Radiography (SANRAD) facility (de Beer, 2005) using a CCD camera (Pentax lens FA 135 mm: F2.8, FOV ¼ 9 cm × 9 cm). Four hundred projections were taken around 360^0 with a time of exposure of 1 s per projection. Some of these datasets presented a low contrast that did not allow us to distinguish the enamel from the dentine. For these specimens the EDJ was not considered (as indicated in Table 1). The recent *H. sapiens* sample was scanned at the Vienna micro-CT Lab using a custom-built VISCOM X8060 (Germany) mCT scanner (130 kV, 100 mA, 0.75 mm copper filter). The *H. neanderthalensis* datasets were downloaded from NESPOS (Neanderthal Studies Professional Online Service; details can be found at www.nespos.org).

The image volume data were virtually segmented through semiautomatic procedures (thresholding according to the half maximum height protocol of Spoor et al. [1993] with some manual intervention) in order to produce 3D digital models of both OES and EDJ (we used Amira 5.6, FEI, http://www.vsg3d.com/). In some cases, only one of the surfaces could be used for a tooth (details in Table 1). Any right-side M^2 image data were flipped to obtain a homogeneous left-side sample.

2.2. Landmark-based analysis of the OES and EDJ

We used the OES of unworn or slightly worn teeth along with the unworn EDJs, since wear alters the original topography of the dental crown and a sample at different wear stages might bias the results of a landmark-based GM analysis. The OES dataset consisted of nine landmarks gathered from the occlusal region, along with 29 sliding semilandmarks on the occlusal ridge curve. The semilandmarks were slid along the whole curve, the landmarks acting as separators between curve segments. Similarly, the EDJ was represented by seven landmarks on the occlusal aspect and 22 semilandmarks along the occlusal ridge (Fig. 2, Table 2). Point landmarks and curves were collected in Amira. The OES occlusal aspect is naturally more blunt than the EDJ marginal ridge, which presents sharp edges. Nonetheless, we were able to sample the occlusal curve on the OES, tracing it along the highest path of the occlusal margin and in the midline of its edge. Some of the teeth presented a slight degree of wear affecting the enamel. We reduced the influence of wear in our OES analysis by excluding those teeth in which wear had already consistently altered the cusp configuration (i.e., score 3 and higher in Table 1). The semilandmarks were warped using the EVAN Toolbox (ET, http://evan-society.org) according to the criterion of minimum bending energy (Bookstein, 1989; Gunz et al., 2005; Gunz and Mitteroecker, 2013). Outer enamel surface and EDJ landmark configurations were kept separate throughout the analysis. Each sample of landmark configurations was registered using General Procrustes Analysis (GPA; Gower, 1975) and the resulting matrix of shape coordinates analyzed via a Principal Component Analysis (PCA) in order to assess its major dimensions of variability.

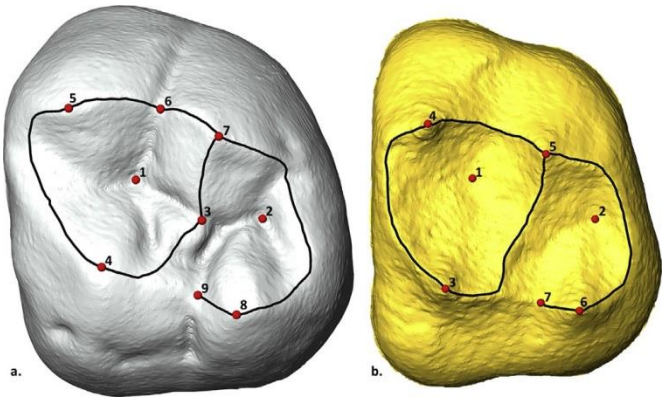

Figure 2. Occlusal aspects of a) outer enamel surface (OES) and b) enameledentine junction (EDJ). Nine landmarks (red points) were collected on the OES and seven on the EDJ. The black lines illustrate the curve on which the semilandmarks (29 for the OES and 22 for the EDJ) were slid. Refer to Table 2 for the description of the landmarks. (For interpretation of the references to color in this figure legend, the reader is referred to the web version of this article.)

2.3. Curve-based analyses of crown and cervical outlines

Preprocessing of the crown and cervical outline datasets was based on the instructions given in Benazzi et al. (2011a, b, 2012) with some modifications as follows. The 3D models of the crowns were cut at the best-fit plane of the cervical margin (i.e., "the cervical plane"). We oriented each crown in Rapidform XOR2 so as to make the cervical plane of each virtual crown parallel to the xy-plane of the Cartesian coordinate system, with the mesial margin of the cervical outline parallel to the y-axis (Supplementary Online Material [SOM] Fig. S1). Other aspects of the crown beside the mesial profile, such as the mesio-distal groove, the lingual groove, or the two lobes of the buccal side, proved too variable to be used as references for realignment. In this cervical alignment, the cervical outline was produced as the contour of the dental crown at the height of the cervical plane, while the crown outline was obtained by projecting onto the cervical plane the silhouette of the crown as seen from top view.

Any interproximal wear at the crown outline was corrected using a spline curve (meaning a continuous smooth curve, not a thin plate) at the mesial or distal border following the crown margins in occlusal view (see Wood and Engleman, 1988). Similarly, there was virtual restoration of the outlines in case of minor damage in any region of interest.

Crown and cervical outlines were separately imported into Rhino 4.0 (Robert McNeel and Associates, Seattle, WA) for further preparation. As outlines like these have no anatomical landmarks, we constructed 24 pseudolandmarks instead (Bookstein, 1997). The centroid of the area was calculated for each of the outlines and the outlines were translated so that their centroids coincided. Twenty-four equiangularly spaced radial vectors out of the centroid were produced, starting with one parallel to the y-axis specified above. Twenty-four pseudolandmarks were collected at the points of intersection between the radii and each of the outlines. After

Table 2
List of landmarks sampled from the outer enamel surface (OES) and enameledentine junction (EDJ).

OES		EDJ	
1	Deepest point of the central fovea	1	Deepest point of the central fovea
2	Deepest point of the distal fossa	2	Deepest point of the distal fossa
3	Point of intersection between the transversal crest and the distal ramus of the central fovea grooves	3	Protocone horn tip
4	Highest point of the protocone	4	Paracone horn tip
5	Highest point of the paracone	5	Metacone horn tip
6	Lowest point along the occlusal ridge between paracone and metacone	6	Hypocone horn tip
7	Highest point of the metacone	7	Lowest point along the marginal edge between protocone and hypocone horns
8	Highest point of the hypocone		
9	Lowest point along the occlusal ridge between protocone and hypocone		

re-centering the configurations of pseudolandmarks according to Bookstein and Ward (2013), these were scaled through a GPA, omitting the translation and rotation steps, and the resulting shape coordinates were sent through a PCA just as if they had arisen in the usual GPA registration.

Before interpreting the results of the PCAs, we applied Anderson's formula (Anderson, 1963; but see also Bookstein, 2014 on the topic) to consecutive pairs of eigenvalues (i.e., Procrustes variance explained by each PC) to test whether the PCs can be interpreted separately (Coquerelle et al., 2011). The *2N ln(a/g)* values represent an ordinary chi-square on two degrees of freedom, where N is the sample size, *a* the arithmetic mean, and *g* the geometric mean. The expected value is 2.0; therefore, if Anderson's value is smaller than 2.0 it means that their ordination is most probably reflecting only noise. A chi-square larger than 2.0 means that the PC with higher explained variance might be worth interpreting separately, since the variance explained by that pair of PCs is elliptical and thus, is more likely to reflect biological variability. We did not perform a discriminant analysis since it would assume what it is that we are trying to investigate (Bookstein, 2002), namely, whether Clarke's suggested classification has any objective basis in a stable dental morphospace.

2.4. Size

Because size is relevant to phylogenetic studies, PCA analyses were also carried out in form space (Mitteroecker et al., 2004a,b, 2005). The boxplots for the logarithm of Centroid Size (lnCS) for each of the analyses were produced using the R statistical package (R Core Team, 2013). To visualize the shape deformations of the OES and EDJ in the direction of the first PC(s) we used a thin-plate spline.

2.5. Two-block partial least square analysis (2B-PLS)

To assess the overlap of information content among the morphological features considered in this project, we carried out 2B-PLS (Rohlf and Corti, 2000) for each pair of the four landmark datasets collected from the OES surfaces, EDJ surfaces, crown outlines, and cervical outlines. There resulted six different analyses, each one performed using the EVAN toolbox.

3. Results

The results of the Anderson's test for the PCAs are reported in Table 3. We interpreted only the PCs for which the chi-square obtained in the comparison with its successor was bigger than 2.0. PCs that might reflect noise and for which the ordination might be random are neither described nor visualized.

3.1. Enameledentine junction

The PCA plot for the EDJ in shape space shows a clear picture (Fig. 3), in which *Homo* separates obviously from *Australopithecus* and *Paranthropus* along PC1 (30% of the variance explained) and *H. sapiens* and *H. neanderthalensis* form two separated groups along PC2 (18%). SK 27, an early *Homo*, plots at an extreme of the *Homo* distribution along PC2. *Australopithecus* and *Paranthropus* cluster rather closely, whereas *Paranthropus* does not separate from the other South African teeth. Of the three *Au. africanus* M^2s included in our sample, Sts 22 and StW 204 plot farther from the other *Australopithecus*. Sts 52 (an *Au. africanus* according to Clarke and others) plots within the *Au. prometheus* scatter. The warping along PC1 accounts for the relative bucco-lingual and mesio-distal proportions of the marginal ridge, along with the relative height of the dentine horns. In particular, *Australopithecus* and *Paranthropus* show a bucco-lingually narrow marginal edge with respect to *Homo* and lower cusps. *Au. prometheus* has the most extreme of these configurations, followed by *Paranthropus* and then *Au. africanus*. The relative mesio-distal expansion of the talon vis-à-vis the trigon accounts for PC2. This feature discriminates well between *H. neanderthalensis* (with expanded talon) and *H. sapiens* (with relatively smaller talon).

On the basis of the full Procrustes distances between the group means, we observed that the distances between *Paranthropus*, *Au. africanus*, and *Au. prometheus* are of similar magnitude (*Paranthropus*d*Au. africanus* ¼ 0.073, *Paranthropus*d*Au. prometheus* ¼ 0.078, *Au. africanus*d*Au. prometheus* ¼ 0.081), while the distance between *H. sapiens* and *H. neanderthalensis* is roughly one third larger (0.109).

3.2. Outer enamel surface

Again the OES separates *Homo* from both *Australopithecus* and *Paranthropus* along PC1 (25% of the shape variance; Fig. 4), but this separation is imperfect. Between *Australopithecus* and *Paranthropus* there is likewise no clear separation, but we observe the same trend

Table 3
Anderson's values[a] for the first three pairs of PCs for the analyses carried out in this study.[b]

	OES	EDJ	Crown outline	Cervical outline
PC1-2	4.332	2.154	3.354	13.463
PC2-3	0.416	2.254	2.085	1.579
PC3-4	0.112	0.104	2.715	1.032

[a] Anderson's formula (1963): 2N ln(a/g).

[b] *N* ¼ sample size; *a* ¼ arithmetic mean of the consecutive pairs of eigenvalues; *g* ¼ geometric mean for the same consecutive pairs of eigenvalues; OES ¼ outer enamel surface; EDJ ¼ enameledentine junction. Values in bold deviate from joint equality.

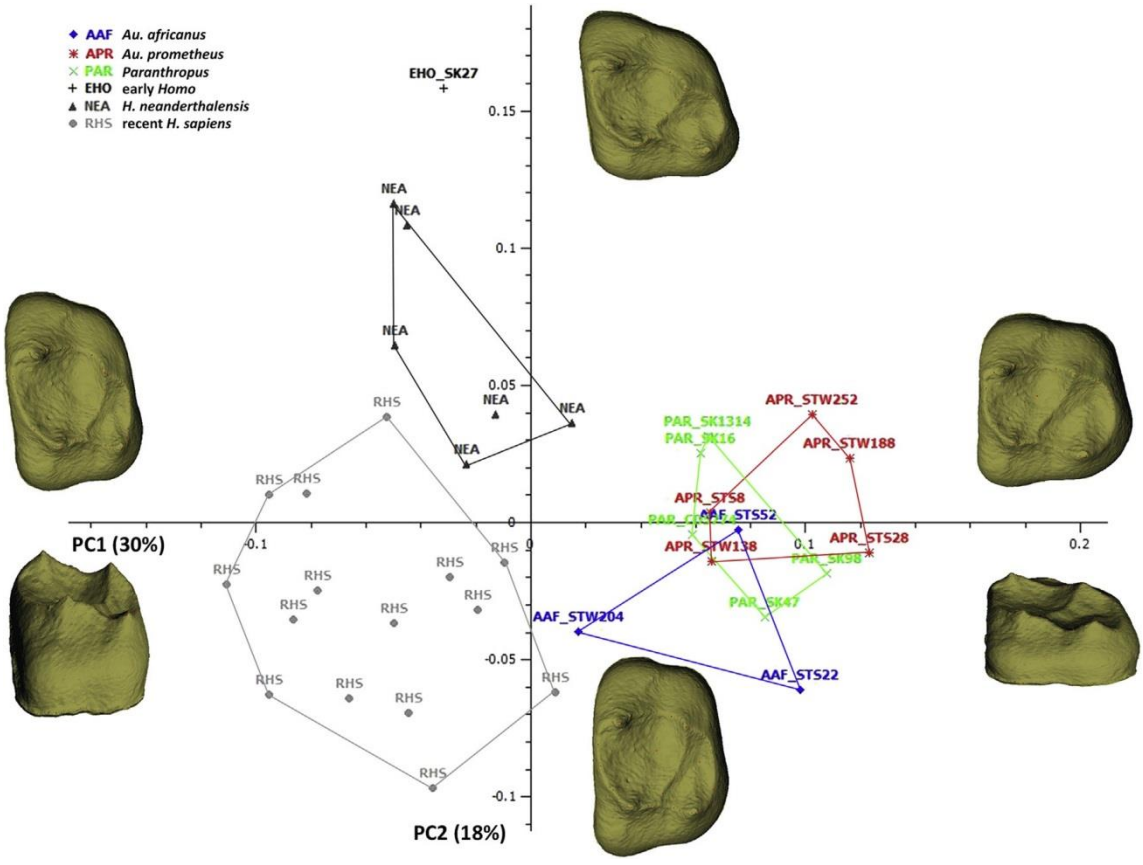

Figure 3. PCA plot for the EDJ in shape space. The separation between *Homo* and both *Australopithecus* and *Paranthropus* is neat. *Paranthropus* overlaps with *Australopithecus* and Sts 52 is indistinguishable from *Au. prometheus*. The shape changes along the first two axes are visualized through warps of the surface of Sts 8 at the end of the range of distribution.

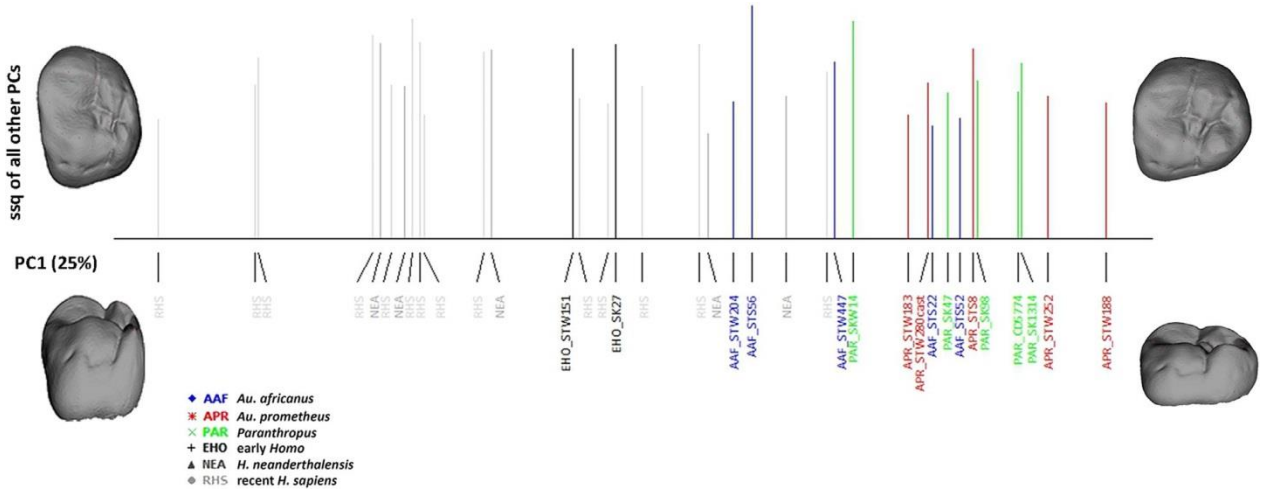

Figure 4. PCA plot for the OES in shape space. The horizontal axis represents PC1, and the vertical axis represents the squared root of the sum of squared PCs scores (PC2ePC36) for each of the individuals. PC1 distinguishes *Homo* from both *Australopithecus* and *Paranthropus* well. The shape changes along the first axis are visualized through warps of the surface of Sts 8 at the end of the range of distribution.

(with a similar but not identical scattering of the individuals) that we noted for the EDJ, again with *Au. prometheus* at one end of the distribution. According to the thin-plate spline, the main geometrical features of the occlusal aspect that account for this circumstance are the relative mesio-distal and bucco-lingual proportions of the occlusal ridge curve and the relative cusp heights. *Australopithecus* and *Paranthropus* possess a bucco-lingually narrow occlusal curve, while *Homo* presents a rather square shape. Also, *Australopithecus and Paranthropus* cusp height is relatively shorter than in *Homo*.

3.3. Crown outlines

The results for the crown outline in shape space (Fig. 5) show incomplete separation within *Homo* along PC1 (37%). An imperfect

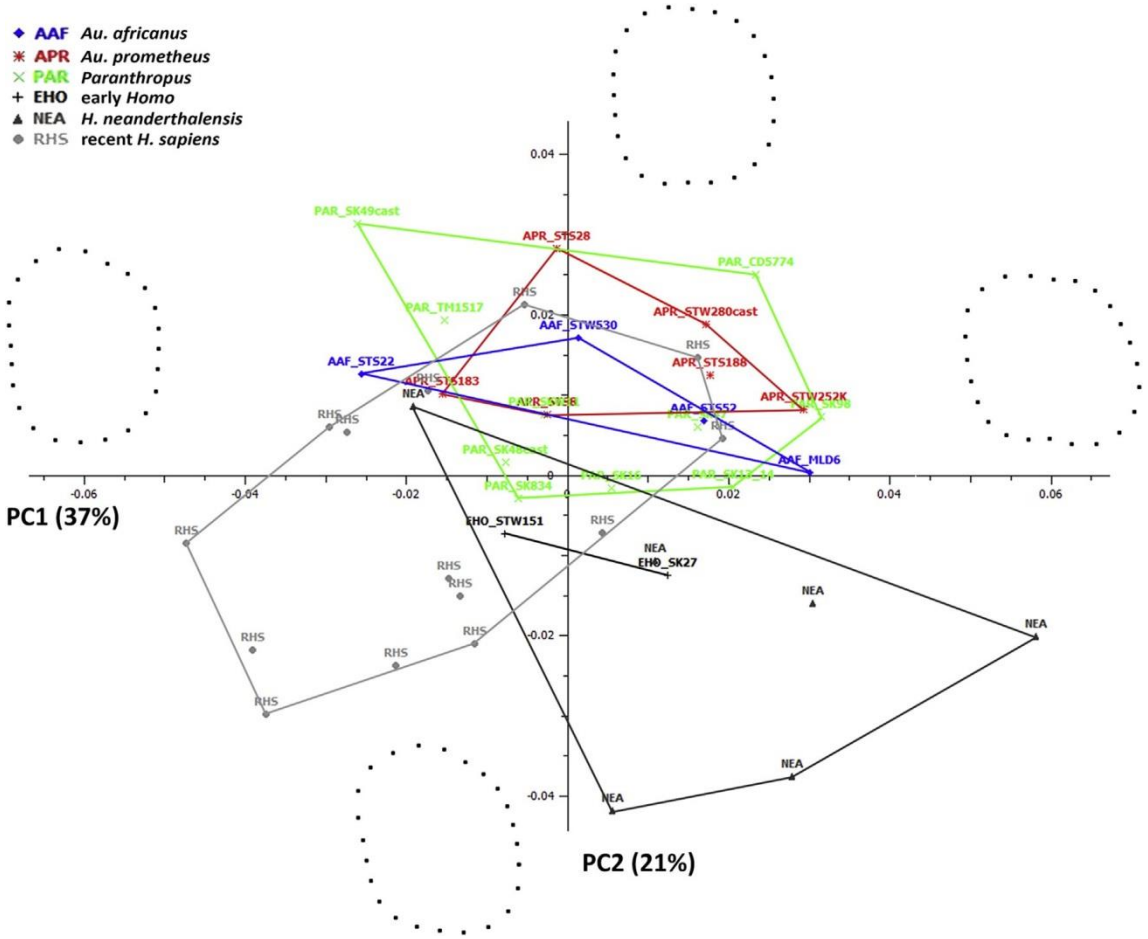

Figure 5. PCA plot for the crown outline in shape space. PC1 imperfectly separates *H. neanderthalensis* from *H. sapiens*, but no separation occurs from *Australopithecus* and *Paranthropus* and between the latter two taxa. PC2 distinguishes *Homo* (including SK 27) and StW 151 from *Australopithecus* and *Paranthropus*. The shape changes along the axes are visualized through estimated outlines at the end of the range of distribution.

separation between *Homo* and the *Australopithecus* and *Paranthropus* group occurs on PC2 (21%), and both SK 27 and StW 151 plot between them, yet within the *Homo* distribution. *Australopithecus* and *Paranthropus* overlap completely. Along the third component (13%), *Paranthropus* distribution more than encompasses the combination of *Au. africanus* and *Au. prometheus* together. Again, no separation between *Australopithecus* and *Paranthropus* is seen along PC3.

3.4. Cervical outlines

Consistently with the other analyses, *Homo* separates (imperfectly) from both *Australopithecus* and *Paranthropus* along PC1 (50%; Fig. 6). The same distribution pattern occurs between *Australopithecus* and *Paranthropus*, with *Au. prometheus* at the margin of the scatter, but once again, no separation is found within this sample of South African fossil teeth.

3.5. GM analyses in form space

We repeated all GM analyses in form space and found that in all of them the distribution stretches out when size is considered (SOM Fig. S2). As expected, *H. sapiens* is at one end of the distribution (the smallest lnCS) and *Australopithecus* and *Paranthropus* are at the other end (with the largest lnCS). Among the latter, *Au. prometheus* specimens are the largest followed by *Au. africanus*, with very little overlap for the crown and cervical outlines, but more overlap for the EDJ and especially OES. *Paranthropus* mostly plots among the *Australopithecus* specimens and its range of distribution never exceeds that of the *Australopithecus* specimens. The boxplots for the lnCS for all GM analyses are presented in Figure. 7. The pattern shown by the *Homo* sample is consistent in all plots and accords with our expectations, i.e., *H. sapiens* is smallest, Neanderthals are intermediate, and early *Homo* the largest. *Au. prometheus* is larger than *Au. africanus* and even *Paranthropus* in all features, except for the OES occlusal curve. The different size relationship between the crown outline and the OES occlusal curve in the two *Australopithecus* groups is reminiscent of the different proportions of the occlusal polygon with respect to the crown side walls observed by Clarke (1988, 2008), where *Au. prometheus* shows cusps shorter than *Au. africanus* with cusp tips oriented inward.

3.6. Two-block partial least squares

According to the 2B-PLS analyses, the morphometric features we considered are associated pairwise to different extents (Table 4). The highest correlation (r ¼ 0.95) is for OES with EDJ, followed by EDJ with cervical outline (r ¼ 0.90), and the lowest for EDJ and crown outline (r ¼ 0.76). In Figure. 8, we illustrate the results of the comparison of OES with EDJ. These singular warps reflect the combinations of shape changes seen along both PC1 and PC2 in the PCA analyses for OES and EDJ separately.

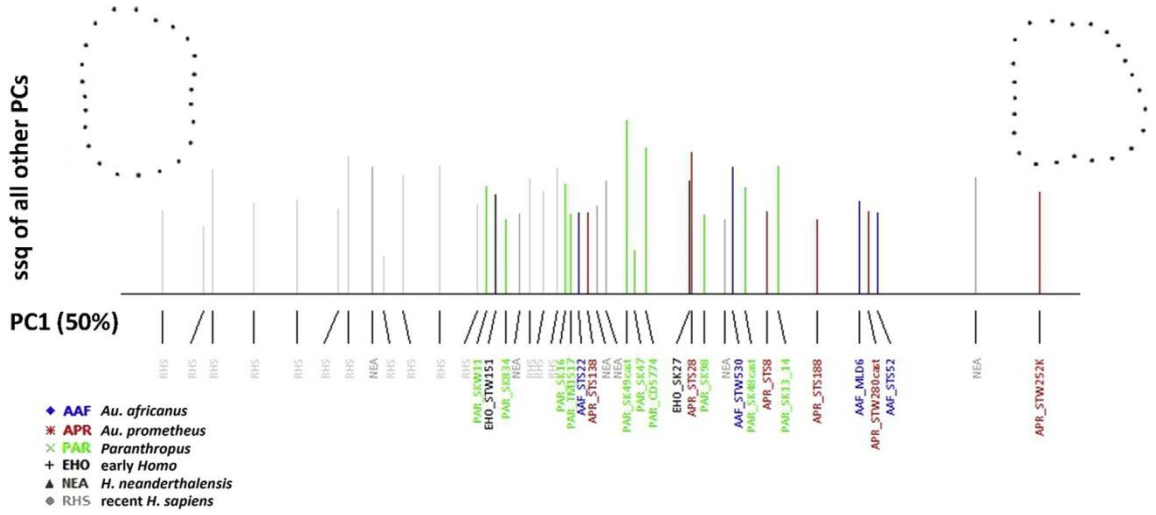

Figure 6. PCA plot for the cervical outline in shape space. The horizontal axis represents PC1, the vertical axis represents the squared root of the sum of squared PCs scores (PC2ePC42) for each of the individuals. PC1 distinguishes *Homo* from *Australopithecus* and *Paranthropus* well. The shape changes along the first axis are visualized through estimated outlines at the end of the range of distribution.

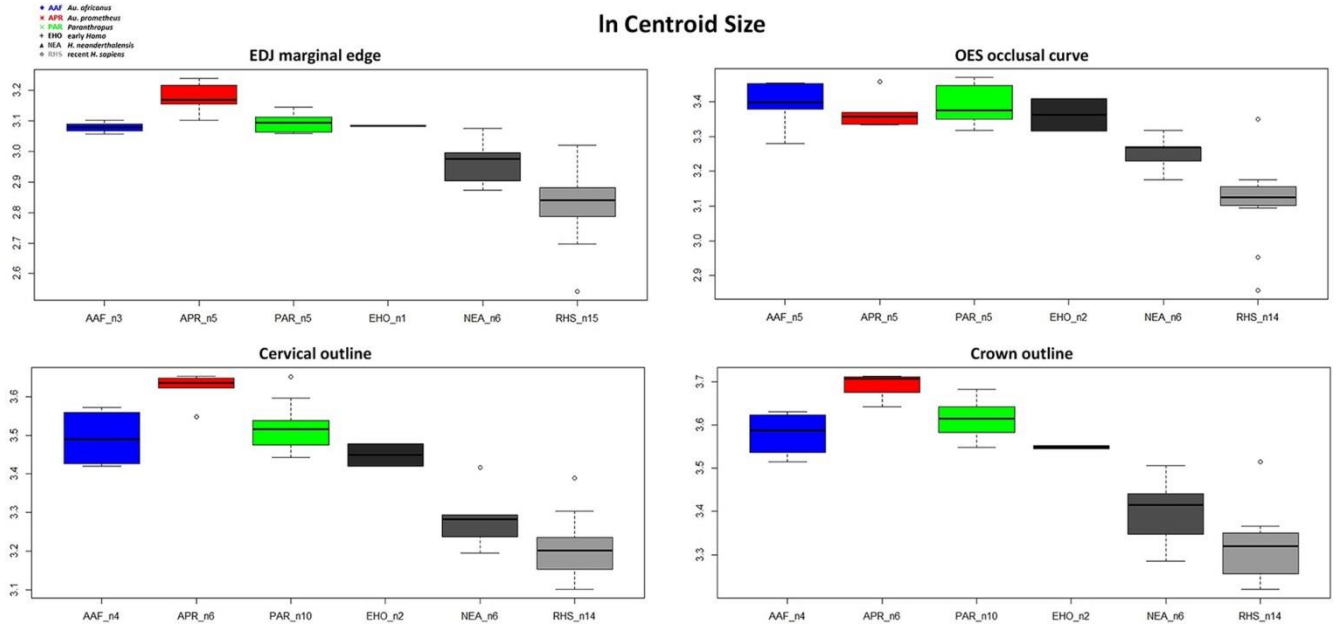

Figure 7. Boxplots for the log centroid sizes for the four GM analyses carried out (the sample count is indicated beside each of the group name abbreviations). The *Homo* samples show a consistent pattern in all plots. *Au. prometheus* tends to be larger than *Au. africanus* and *Paranthropus* in three analyses out of four, but is as large as the others for the OES occlusal curve. This condition accords with the differences stressed by Clarke (1988, 2008) between *Au. africanus* and *Au. prometheus*, where the occlusal polygon is bucco-lingually narrower and the cusps are shorter in *Au. prometheus*.

4. Discussion

Our study demonstrates that the various dental features we considered are correlated to different extents. The OES and EDJ co-vary strongly. This implies that the OES could be used as an alternative to the EDJ if the latter is inaccessible, although the OES is affected by wear much earlier in the lifespan than the EDJ. In addition, we found in our GM analyses that EDJ data provide clearer separation than OES data do. The least integrated feature is the crown outline, in agreement with previous observations (Dahlberg, 1971) regarding the enamel cap as more variable than the dentinal crown. Our analysis highlights that some regions of the enamel cap might be less variable than others. In particular, the occlusal OES seems to be less variable than lateral crown aspects (as detected by examination of the crown outline) where the cusp tips calcify in the early stages of tooth development. The cervical outline, where the enamel cap tapers away, is also less variable than the crown outline.

Table 4
Results of the 2B-PLS applied to the six possible combinations of the pair of landmark sets considered.

	EDJ	Crown outline	Cervical outline
OES	0.95	0.83	0.87
EDJ	e	0.76	0.90
Crown outline		e	0.88

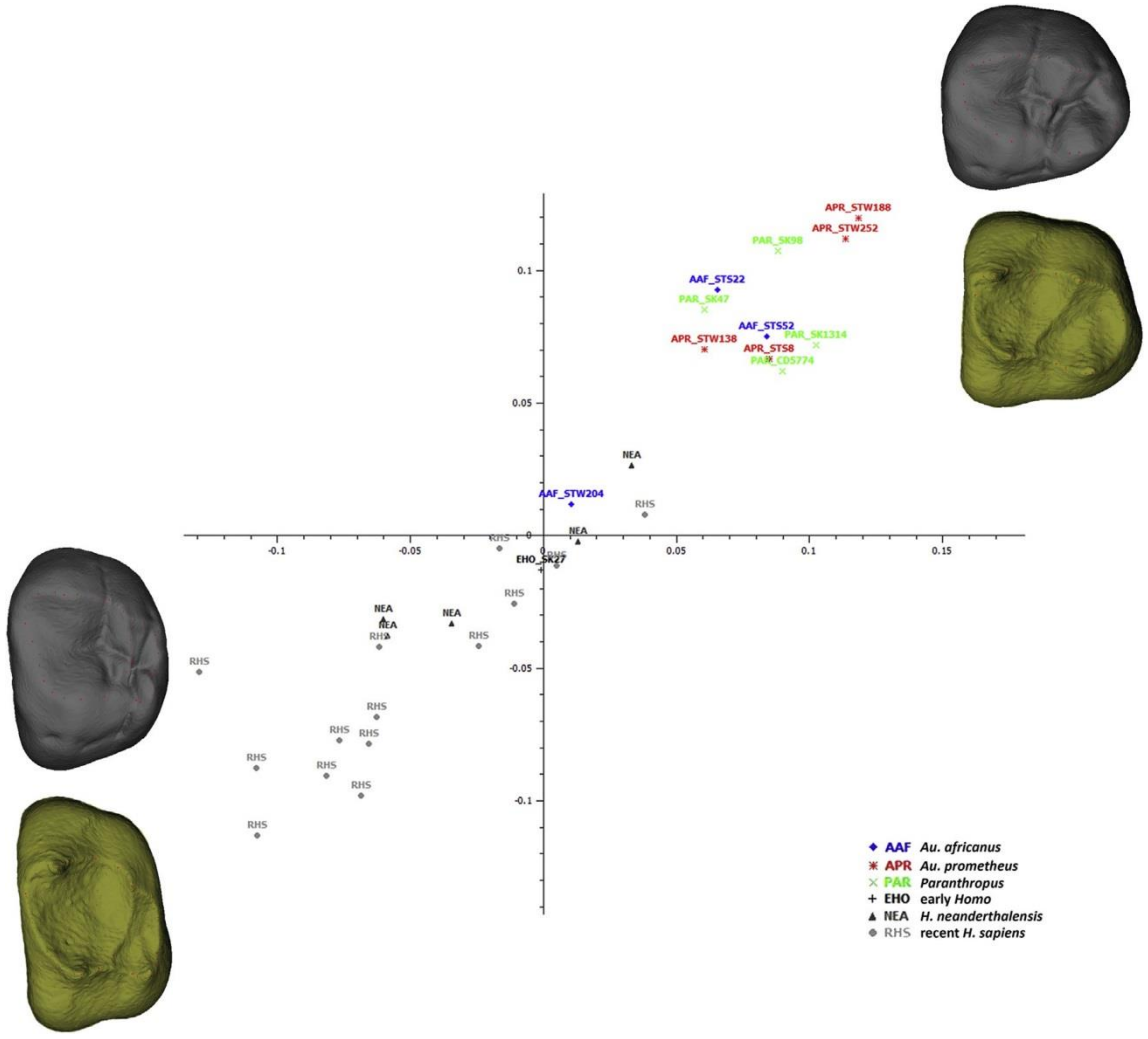

Figure 8. Plot and warped surfaces showing the results of the 2B-PLS for OES and EDJ. The first warp for OES and EDJ show the sum of the shape changes observed along PC1 and PC2 of the GM analysis for OES and EDJ.

The shape of the occlusal aspect of the crown alone, in either OES or EDJ, separates *Homo* from both *Australopithecus* and *Paranthropus* very well. The methods here succeed in distinguishing the relatively low-cusped crowns of both *Australopithecus* and *Paranthropus* from the tall-cusped crowns of *Homo*, and also emphasize the differences in development of the trigon with respect to the talon, the latter being reduced in *Homo* (Robinson, 1956, 1967). The talon contributes to a mesio-distal elongation of the crown in *Australopithecus* and *Paranthropus*, while in *Homo* the crown is relatively bucco-lingually elongated. The cervical outline also separates both *Australopithecus* and *Paranthropus* from *Homo*, while the crown outline shows more overlap between them. Both the EDJ and crown outline analyses separate *H. sapiens* from *H. neanderthalensis* (with reference to the crown outline see Bailey and Lynch, 2005; Gómez-Robles et al., 2008; Benazzi et al., 2011a, 2012). Nonetheless, we found no separation between Clarke's two presumptive *Australopithecus* species, nor between *Australopithecus* and *Paranthropus*. The variation of *Australopithecus* and that of *Australopithecus* and *Paranthropus* taken together are lower than that of *H. sapiens* for both OES and EDJ, and are comparable in value for both the crown and cervical outlines (SOM Fig. S3). This confirms that morphological variability (in this case, dental variability) is more (or at least, not less) heterogeneous among some extinct hominins (e.g., Wood, 1991; Grine, 2013), and also that upper molars might not be suitable for discriminating between *Australopithecus* and *Paranthropus*.

None of the analyses carried out on the outer aspect of the crown distinguished between *Paranthropus* and *Australopithecus*. We explain the large scatter of *Paranthropus* OES as owing to the presence of a more variable morphology of the distal aspect of the occlusal crownd*Paranthropus* presents additional cusps on the mesial and distal margins that do not manifest on the EDJ surface (Robinson, 1956). *Paranthropus* and *Australopithecus* have been distinguished on the basis of the morphology of the molar crown (Robinson, 1956; Sperber, 1974; Wood and Abbott, 1983; Wood et al., 1983; Grine, 2004). However, Skinner et al. (2008) found only very subtle morphological variation between the EDJ of the *Au. africanus* (*sensu lato*) and *P. robustus* lower first and second molars, along with great overlap of the two taxa along their PCs. The results of our M^2 EDJ analysis accord with these findings. Since our *Au. africanus* sample for the EDJ analysis is only three specimens, we cannot tell whether *Paranthropus* clusters more tightly with *Au. prometheus* (where two *Au. africanus*, Sts 22 and StW 204, plot farther from the others). Hence, we cannot confirm Clarke's interpretation of *Au. prometheus* molar morphology as affine to *Paranthropus* (Clarke, 1988, 1996, 2008, 2013), as this may just be an accident of small sample size. In accordance with Wood and Engleman (1988), and contra Sperber (1974), we do not find any

shape differences of the crown outline that distinguish between *Australopithecus* and *Paranthropus*.

Crown and cervical outlines seem to be less informative than surface features for the distinctions we pursue in the present study. This can be explained in different ways. First, although these features are collected from a 3D model, they do result in 2D datasets that results in a loss of morphological information. Second, alterations of the original morphology of the crown owing to interproximal wear or damage at the cervical margin might have contributed to signal deterioration. Third, the enamel cap has been regarded as being more variable than the EDJ, which reflects the morphology of the epithelium more closely (e.g., Butler, 1956; Korenhof, 1960; Corruccini, 1987).

Most importantly, the number of *Australopithecus* individuals available to us is tiny and thus represents a severe constraint on any study of that population structure, including our work here. We do not observe any separation within the *Australopithecus* subsample with respect to any of the four dental features we considered. Hence our results cannot be used as evidence to support the presence of multiple species among the fossil hypodigm conventionally attributed to *Au. africanus*. At the same time, we cannot exclude the possibility that a larger sample would provide different results, nor that a clearer grouping would occur if other anatomical regions are considered.

The *Australopithecus* M^2s Clarke attributes to *Au. prometheus* tend to plot at the extremity of the total distribution for *Australopithecus* and *Paranthropus*, possessing the lowest cusps and being bucco-lingually narrower at the occlusal ridge. However, rather than two distinct morphs, the *Australopithecus* sample seem to plot according to a gradient. There is an almost perfect match between Clarke's specimen attribution and the subgroups we just described, with the exception of Sts 52 M^2, which shows a morphological affinity to other *Au. prometheus* specimens (contrary to Clarke, 1988, 2008). On the basis of cranial and dental features, Sts 52 is commonly attributed to *Au. africanus* (e.g., Lockwood and Tobias, 2002, but see also Clarke, 2008, 2013). However, some authors ally Sts 52 to specimens that Clarke attributes to *Au. prometheus* rather than to those he classifies as *Au. africanus* (Kimbel and White, 1988; Schwartz and Tattersall, 2005; Benazzi et al., 2013; Grine et al., 2013). Aguirre (1970) saw similarities of Sts 52b with *Paranthropus*. In terms of Procrustes distances in all morphospaces considered, the three nearest neighbors to Sts 52 are indeed mostly *Au. prometheus* individuals. The mismatch between our findings and Clarke's interpretation suggests that the morphology of the *Australopithecus* specimens will be difficult to interpret authoritatively, independent of the method used.

Our results also show that the StW 151 M^2 presents an admixture of features. The three nearest neighbors calculated for the OES and cervical outline are *Homo* specimens, but those for the crown outline are *Paranthropus* individuals. StW 151 shows affinities to *Homo* in its cusp height and relative expansion of the talon to trigone, the latter expressing on the cervical outline too. The crown outline is intermediate in being rather regular, almost circular. StW 151 and SK 27 M^2s show similar morphology for the features we considered (we could not analyze the EDJ of StW 151 owing to limits on the primary imaging data). This evidence broadly supports Curnoe (2010), who assigned both specimens to the genus *Homo*.

The extent to which results of a PCA based on Procrustes shape or form coordinates can be used to address taxonomic issues is surely differently regarded by different authors (see discussions in Adams et al., 2011; Bookstein, 2014, 2015). In this study we use geometric morphometrics in order to quantify, and possibly characterize, the morphology of the *Australopithecus* M^2 sample. Although our sample underrepresents *Australopithecus* variability, we were able to include several individuals relevant to Clarke's discussion of the second species (such as Sts 52, StW 252, StW 183). In contrast to Clarke (1988, 2008) and Fornai et al. (2010), we do not find a grouping, but rather a morphological gradient that we interpret more cautiously than we did in Fornai et al., 2014. Such a condition does not allow us to state that two distinct *Australopithecus* species are presentdany line we might draw to split the *Australopithecus* sample into two groups would be arbitrary. Three scenarios are possible:

1. Two or more species are present at Sterkfontein Member 4 (and Makapansgat), but M^2 morphology does not discriminate between them.
2. Two species are present at these sites. The morphological gradient we see actually represents two partially overlapping ranges of variability, and in fact a line could be drawn to separate them, but owing to the small sample we cannot tell where.
3. The sites are best accounted for as one single variable species.

If option 2 is the case then we would agree with Kimbel and White (1988) that these two species might be similar in terms of their morphology and therefore difficult to distinguish. Under option 3, we could not exclude the possibility that the variability observed is owed to the time-depth of the fossil assemblage from Sterkfontein.

5. Conclusions

The present study adds to our understanding of *Australopithecus* M^2 variability by providing substantial information on crown morphological variation and correlation of features in *Homo* and South African *Australopithecus* and *Paranthropus* upper molars. Our approaches differentiate well *Homo* from both *Australopithecus* and *Paranthropus*, and Neanderthals from modern humans. We confirmed that *Australopithecus* and *Paranthropus* M^2s cannot be distinguished on the basis of their gross morphology (Wood and Engleman, 1988; Skinner et al., 2008). Our findings are inconclusive with regard to classifications within South African *Australopithecus*. We did not find clearly separated subgroups within the *Australopithecus* sample, but instead a gradient (as suggested earlier by Calcagno et al., 1999; Grine et al., 2013) along which the proposed *Au. prometheus* individuals plot at one extreme, owing to their low cusps and narrow occlusal area, followed by *Au. africanus*. This observation corresponds to some extent to Clarke's description of the molar teeth of the two *Australopithecus* groups he identified (1988, 2008). We have no evidence that the *Australopithecus* distribution represents two distinct groups as Clarke, based on qualitative assessment of a set of dental and cranial features, describes them. Considering that our study indicates Sts 52 is morphologically closer to the supposed *Au. prometheus* individuals, it remains the case that if the M^2s carry a taxonomic signal, a larger dental sample than the one we could consider might disclose this.

Acknowledgments

We are deeply grateful to R.J. Clarke, B.A. Wood, M. Collard, and B. Richmond for very constructive discussions on the subject of our work. We thank J. Moggi-Cecchi for suggesting this project and S. Benazzi for improving this manuscript in its early drafts. The constructive comments of the editor, associate editor, and three anonymous reviewers contributed appreciably to the quality of the manuscript. M. Coquerelle helped with some aspects of the R programming.

We thank the Ditsong National Museum of Natural History and the University of Witwatersrand for granting permission to study the South African specimens, and S. Potze, F. Thackeray, and B. Zipfel for kind assistance with the collections. NECSA, Pelindaba, South Africa, and F. de Beer provided us with the high resolution CT scans of the South African material and NESPOS (www.nespos.org) with the Neanderthal data. M. Dockner scanned the modern human specimens at the Vienna Micro-CT Lab.

This research was supported by A.E.R.S. Dental Medicine Organisations GmbH, Vienna, Austria (FA547013), the Siegfried Ludwig-Rudolf Slavicek Foundation, Vienna, Austria (FA547016), the European Union FP6 Marie Curie Actions MRTN-CT-2005-019564 "EVAN" (FA547004), and the National Science Foundation Physical Anthropology HOMINID program (NSF BCS0725219, 0725183, 0725147, 0725141, 0725136, 0725126, 0725122, 0725078).

Supplementary Online Material

Supplementary online material related to this article can be found at http://dx.doi.org/10.1016/j.jhevol.2015.05.013.

References

Adams, D.C., Cardini, A., Monteiro, L.R., O'Higgins, P., Rohlf, F.J., 2011. Morphometrics and phylogenetics: principal components of shape from cranial modules are neither appropriate nor effective cladistic characters. J. Hum. Evol. 60, 240e243.

Aguirre, E., 1970. Identification de "*Paranthropus*" en Makapansgat. Cronica del XI Congreso Nacional de Arqueologia, Merida, pp. 98e124.

Ahern, J.C., 1998. Underestimating intraspecific variation: the problem with excluding Sts 19 from *Australopithecus africanus*. Am. J. Phys. Anthropol. 105, 461e480.

Anderson, T.W., 1963. Asymptotic Theory for Principal Component Analysis. Ann. Math. Stat. 34, 122e148.

Bailey, S.E., Lynch, J.M., 2005. Diagnostic differences in mandibular P4 shape between neandertals and anatomically modern humans. Am. J. Phys. Anthropol. 126, 268e277.

Benazzi, S., Coquerelle, M., Fiorenza, L., Bookstein, F., Katina, S., Kullmer, O., 2011a. Comparison of dental measurement systems for taxonomic assignment of first molars. Am. J. Phys. Anthropol. 144, 342e354.

Benazzi, S., Fornai, C., Bayle, P., Coquerelle, M., Kullmer, O., Mallegni, F., Weber, G.W., 2011b. Comparison of dental measurement systems for taxonomic assignment of Neanderthal and modern human lower second deciduous molars. J. Hum. Evol. 61, 320e326.

Benazzi, S., Fornai, C., Buti, L., Toussaint, M., Mallegni, F., Ricci, S., Gruppioni, G., Weber, G.W., Condemi, S., Ronchitelli, A., 2012. Cervical and crown outline analysis of worn Neanderthal and modern human lower second deciduous molars. Am. J. Phys. Anthropol. 149, 537e546.

Benazzi, S., Kullmer, O., Schulz, D., Gruppioni, G., Weber, G.W., 2013. Individual tooth macrowear pattern guides the reconstruction of Sts 52 (Australopithecus africanus) dental arches. Am. J. Phys. Anthropol. 150, 324e329.

Boccone, S., Moggi-Cecchi, J., 2005. Dental development and upper molar cusp dimensions of South African australopithecines. T. Roy. Soc. S. Afr. 60, 95e97.

Bookstein, F.L., 1989. Principal warps: thin-plate splines and the decomposition of deformations. IEEE Trans. Pattern Anal. Mach. Intell. 11, 567e585.

Bookstein, F.L., 1997. Landmark methods for forms without landmarks: Morphometrics of group differences in outline shape. Med. Image Anal. 1, 225e243.

Bookstein, F.L., 2002. Creases as morphometric characters. In: MacLeod, N., Forey, P. (Eds.), Morphology, Shape, and Phylogeny, Systematic Association Special Volume Series 64. Taylor and Francis, London, pp. 139e174.

Bookstein, F.L., 2014. Measuring and Reasoning. Numerical Inference in the Sciences. Cambridge University Press, Cambridge.

Bookstein, F.L., 2015. The relation between geometric morphometrics and functional morphology, as explored by Procrustes interpretation of individual shape measures pertinent to function. Anat. Rec. 298, 314e327.

Bookstein, F.L., Ward, P.D., 2013. A modified Procrustes analysis for bilaterally symmetrical outlines, with an application to microevolution in Baculites. Paleobiology 39, 214e234.

Broom, R., 1936. A new fossil anthropoid skull from South Africa. Nature 138, 486e488.

Broom, R., 1938. Further evidence on the structure of the South African Pleistocene anthropoids. Nature 142, 897e899.

Butler, P.M., 1956. The ontogeny of molar pattern. Biol. Rev. 31, 30e69.

Calcagno, J.M., Cope, D.A., Lacy, M.G., Moggi-Cecchi, J., Tobias, P.V., 1999. Reinvestigating the number of hominid species in Sterkfontein Member 4. Am. J. Phys. Anthropol. S28, 101.

Calcagno, J.M., Cope, D.A., Lacy, M.G., Tobias, P.V., 1997. Is *A. africanus* the only hominid species in Sterkfontein Member 4? Am. J. Phys. Anthropol. S24, 86e87.

Clarke, R.J., 1977. A juvenile cranium and some adult teeth of early *Homo* from Swartkrans, Transvaal. S. Afr. J. Sci. 73, 46e49.

Clarke, R.J., 1985a. Early Acheulian with *Homo habilis* at Sterkfontein. In: Tobias, P.V. (Ed.), Hominid Evolution: Past, Present, and Future. Alan R. Liss, New York, pp. 287e298.

Clarke, R.J., 1985b. *Australopithecus* and early *Homo* in southern Africa. In: Delson, E. (Ed.), Ancestors: The Hard Evidence. Alan R. Liss, New York, pp. 171e177.

Clarke, R.J., 1988. A new *Australopithecus* cranium from Sterkfontein and its bearing on the ancestry of *Paranthropus*. In: Grine, F.E. (Ed.), Evolutionary History of the "Robust" Australopithecines. Aldine de Gruyter, New York, pp. 285e292.

Clarke, R.J., 1994a. Advances in understanding the craniofacial anatomy of South African early hominids. In: Ciochon, R.L. (Ed.), Integrative Paths to the Past: Paleoanthropological Advances in Honor of F. Clark Howell. Prentice Hall, Englewood Cliffs, pp. 205e222.

Clarke, R.J., 1994b. On some new interpretations of Sterkfontein stratigraphy. S. Afr. J. Sci. 90, 211e214.

Clarke, R.J., 1996. The genus *Paranthropus*: What's in a name? In: Meikle, W.E., Howell, F.K., Jablonski, N.G. (Eds.), Contemporary Issues in Human Evolution. California Academy of Sciences, San Francisco, California.

Clarke, R.J., 1999. Discovery of complete arm and hand of the 3.3 million-year-old Australopithecus skeleton from Sterkfontein. S. Afr. J. Sci. 95, 477e480.

Clarke, R.J., 2006. A deeper understanding of the stratigraphy of Sterkfontein fossil horninid site. Trans. R. Soc. S. Afr. 61, 111e120.

Clarke, R.J., 2008. Latest information on Sterkfontein's *Australopithecus* skeleton and a new look at *Australopithecus*. S. Afr. J. Sci. 104, 443e449.

Clarke, R.J., 2013. *Australopithecus* from Sterkfontein Caves, South Africa. In: Reed, K.E., Fleagle, J.G., Leakey, R.E. (Eds.), The Paleobiology of *Australopithecus*. Springer, pp. 105e124.

Clarke, R.J., Partridge, T.C., 2002. On the unrealistic 'Revised age estimates' for Sterkfontein. S. Afr. J. Sci. 98, 415e419.

Clarke, R.J., Partridge, T.C., Granger, D.E., Caffe, M.W., Gibbons, A., 2003. Dating the Sterkfontein fossils. Science 301, 596e597.

Clarke, R.J., Tobias, P.V., 1995. Sterkfontein Member 2 foot bones of the oldest South African hominid. Science 269, 521e527.

Coquerelle, M., Bookstein, F.L., Braga, J., Halazonetis, D.J., Weber, G.W., Mitteroecker, P., 2011. Sexual dimorphism of the human mandible and its association with dental development. Am. J. Phys. Anthropol. 145, 192e202.

Corruccini, R.S., 1987. «Relative growth» from the dentino-enamel junction in primate maxillary molars. Hum. Evol. 2, 263e269.

Curnoe, D., 2010. A review of early *Homo* in southern Africa focusing on cranial, mandibular and dental remains, with the description of a new species (*Homo gautengensis* sp. nov.). HOMO 61, 151e177.

Curnoe, D., Tobias, P.V., 2006. Description, new reconstruction, comparative anatomy, and classification of the Sterkfontein Stw 53 cranium, with discussions about the taxonomy of other southern African early *Homo* remains. J. Hum. Evol. 50, 36e77.

Dahlberg, A.A., 1971. Penetrance and expressivity of dental traits. In: Dahlberg, A.A. (Ed.), Dental Morphology and Evolution. University of Chicago Press, Chicago, pp. 257e262.

Dart, R.A., 1925. *Australopithecus africanus*: The man-ape of South Africa. Nature 115, 195e199.

Dart, R.A., 1948. The Makapansgat proto-human *Australopithecus prometheus*. Am. J. Phys. Anthropol. 6, 259e283.

de Beer, F.C., 2005. Characteristics of the neutron/X-ray tomography system at the SANRAD facility in South Africa. Nuclear Instruments and Methods in Physics Research, Section A: Accelerators, Spectrometers, Detectors and Associated Equipment 542, 1e8.

DeSilva, J.M., Proctor, D.J., Zipfel, B., 2012. A complete second metatarsal (StW 89) from Sterkfontein Member 4, South Africa. J. Hum. Evol. 63, 487e496.

Ferguson, W.W., 1989. Reappraisal of the taxonomic status of the cranium Stw 53 from the Plio/Pleistocene of Sterkfontein, in South Africa. Primates 30, 103e109.

Fornai, C., Clarke, R.J., Moggi-Cecchi, J., Hemingway, J., de Beer, F.C., Radebe, M.J., 2010. Testing the "second australopithecine species hypothesis" for Sterkfontein Member 4, South Africa. Am. J. Phys. Anthropol. S50, 105e106.

Fornai, C., Bookstein, F., Weber, G.W., 2014. Geometric morphometrics of second upper australopithecine molars at Sterkfontein Member 4 for taxonomic appraisal. Am. J. Phys. Anthropol. 153, 119.

Gómez-Robles, A., Martinón-Torres, M., Bermúdez de Castro, J.M., Prado, L., Sarmiento, S., Arsuaga, J.L., 2008. Geometric morphometric analysis of the crown morphology of the lower first premolar of hominins, with special attention to Pleistocene *Homo*. J. Hum. Evol. 55, 627e638.

Gower, J.C., 1975. Generalized procrustes analysis. Psychometrika 40, 33e51.

Grine, F.E., 2004. Description and preliminary analysis of new hominid craniodental remains from the Swartkrans Formation. In: Brain, C.K. (Ed.), Swartkrans: a cave's chronicle of early man. Transvaal Museum, Pretoria, pp. 75e116.

Grine, F.E., 2013. The Alpha taxonomy of *Australopithecus africanus*. In: Reed, K.E., Fleagle, J.G., Leakey, R.E. (Eds.), The Paleobiology of *Australopithecus*. Springer, pp. 73e104.

Grine, F.E., Delanty, M.M., Wood, B.A., 2013. Variation in Mandibular Postcanine Dental Morphology and Hominin Species Representation in Member 4, Sterkfontein, South Africa. In: Reed, K.E., Fleagle, J.G., Leakey, R.E. (Eds.), The Paleobiology of *Australopithecus*. Springer, pp. 125e146.

Gunz, P., Mitteroecker, P., 2013. Semilandmarks: a method for quantifying curves and surfaces. Hystrix 24, 103e109.

Gunz, P., Mitteroecker, P., Bookstein, F.L., 2005. Semilandmarks in three dimensions. In: Slice, D.E. (Ed.), Modern Morphometrics in Physical Anthropology. Kluwer Academic/Plenum Publisher, New York.

Herries, A.I.R., Curnoe, D., Adams, J.W., 2009. A multi-disciplinary seriation of early *Homo* and *Paranthropus* bearing palaeocaves in southern Africa. Quatern. Int. 202, 14e28.

Howell, F.C., 1978. Hominidae. In: Maglio, V.J., Cooke, H.B.S. (Eds.), Evolution of African Mammals. Harvard University Press, Cambridge, pp. 154e248.

Hughes, A.R., Tobias, P.V., 1977. A fossil skull probably of the genus *Homo* from Sterkfontein, Transvaal. Nature 265, 310e312.

Kimbel, W.H., Rak, Y., 1993. The importance of species in paleoanthropology and an argument for the phylogenetic concept of the species category. In: Kimbeland, W.H., Martin, L.B. (Eds.), Species, Species Concepts, and Primate Evolution. Plenum, New York, pp. 461e484.

Kimbel, W.H., White, T.D., 1988. Variation, sexual dimorphism and the taxonomy of *Australopithecus*. In: Grine, F.E. (Ed.), Evolutionary History of the "Robust" Australopithecines. Aldine de Gruyter, New York, pp. 259e268.

Kuman, K., Clarke, R.J., 2000. Stratigraphy, artefact industries and hominid associations for Sterkfontein, Member 5. J. Hum. Evol. 38, 827e847.

Korenhof, C.A.W., 1960. Morphogenetical aspects of the human upper molar: A comparative study of its enamel and dentine surfaces and their relationship to the crown pattern of fossil and recent primates. Uitgeversmaatschappij, Neerlandia, Utrecht.

Le Gros Clark, W.E., 1955. The Fossil Evidence for Human Evolution: An Introduction to the Study of Paleoanthropology. University of Chicago Press, Chicago.

Lockwood, C.A., Moggi-Cecchi, J., 1998. The systematic position of Stw 183, an adolescent maxilla from Sterkfontein. Am. J. Phys. Anthropol. 105, 151e152.

Lockwood, C.A., Tobias, P.V., 1999. A large male hominin cranium from Sterkfontein, South Africa, and the status of *Australopithecus africanus*. J. Hum. Evol. 36, 637e685.

Lockwood, C.A., Tobias, P.V., 2002. Morphology and affinities of new hominin cranial remains from Member 4 of the Sterkfontein Formation, Gauteng province, South Africa. J. Hum. Evol. 42, 389e450.

Mitteroecker, P., Gunz, P., Bernhard, M., Schaefer, K., Bookstein, F.L., 2004a. Comparison of cranial ontogenetic trajectories among great apes and humans. J. Hum. Evol. 46, 679e698.

Mitteroecker, P., Gunz, P., Bookstein, F.L., 2005. Heterochrony and geometric morphometrics: a comparison of cranial growth in *Pan paniscus* versus *Pan troglodytes*. Evol. Dev. 7, 244e258.

Mitteroecker, P., Gunz, P., Weber, G.W., Bookstein, F.L., 2004b. Regional dissociated heterochrony in multivariate analysis. Ann. Anat. 186, 463e470.

Moggi-Cecchi, J., 2003. The elusive 'second species' in Sterkfontein Member 4: The dental metrical evidence. S. Afr. J. Sci. 99, 268e270.

Moggi-Cecchi, J., Boccone, S., 2007. Maxillary molar cusp morphology of South African australopithecines. In: Bailey, S.E., Hublin, J.-J. (Eds.), Dental Perspectives on Human Evolution. Springer, Dordrecht, pp. 53e64.

Moggi-Cecchi, J., Grine, F.E., Tobias, P.V., 2006. Early hominid dental remains from Members 4 and 5 of the Sterkfontein Formation (1966e1996 excavations): Catalogue, individual associations, morphological descriptions and initial metrical analysis. J. Hum. Evol. 50, 239e328.

Moggi-Cecchi, J., Tobias, P.V., Beynon, A.D., 1998. The mixed dentition and associated skull fragments of a juvenile fossil hominid from Sterkfontein, South Africa. Am. J. Phys. Anthropol. 106, 425e465.

Molnar, S., 1971. Human tooth wear, tooth function and cultural variability. Am. J. Phys. Anthropol. 34, 175e189.

Partridge, T.C., 1978. Re-appraisal of lithostratigraphy of Sterkfontein hominid site. Nature 275, 282e287.

Partridge, T.C., 2000. Hominid-bearing cave and tufa deposits. In: Partridge, T.C., Maud, R.R. (Eds.), The Cenozoic of southern Africa. Oxford University Press, New York, pp. 100e125.

Partridge, T.C., Granger, D.E., Caffee, M.W., Clarke, R.J., 2003. Lower Pliocene hominid remains from Sterkfontein. Science 300, 607e612.

Pickering, R., Kramers, J.D., 2010. Re-appraisal of the stratigraphy and determination of new U-Pb dates for the Sterkfontein hominin site, South Africa. J. Hum. Evol. 59, 70e86.

R Core Team, 2013. R: A language and environment for statistical computing. R Foundation for Statistical Computing, Vienna, Austria.

Rak, Y., 1983. The Australopithecine face. Academic Press, New York.

Robinson, J.T., 1954. The genera and species of the australopithecinae. Am. J. Phys. Anthropol. 12, 181e200.

Robinson, J.T., 1956. The dentition of the Australopithecinae. The Transvaal Museum, Pretoria.

Robinson, J.T., 1965. *Homo 'habilis'* and the Australopithecines. Nature 205, 121e124.

Robinson, J.T., 1967. Variation and taxonomy of the early hominids. In: Steere, W.C. (Ed.), Evolutionary Biology. Appleton-Century-Crofts, New York, pp. 69e100.

Rohlf, F.J., Corti, M., 2000. Use of Two-Block Partial Least-Squares to Study Covariation in Shape. Syst. Biol. 49, 740e753.

Schwartz, J.H., Tattersall, I., 2005. The Human Fossil Record. Craniodental Morphology of Early Hominids (Genera *Australopithecus*, *Paranthropus*, *Orrorin*), and Overview. Wiley-Liss, New York.

Skinner, M.M., Gunz, P., Wood, B.A., Hublin, J.J., 2008. Enamel-dentine junction (EDJ) morphology distinguishes the lower molars of *Australopithecus africanus* and *Paranthropus robustus*. J. Hum. Evol. 55, 979e988.

Skinner, M.M., Gunz, P., Wood, B.A., Boesch, C., Hublin, J.-J., 2009. Discrimination of extant *Pan* species and subspecies using the enameledentine junction morphology of lower molars. Am. J. Phys. Anthropol. 140, 234e243.

Sperber, G., 1974. Morphology of the cheek teeth of early South African hominids. University of Witwatersrand, Johannesburg, South Africa.

Spoor, F., 1993. The Comparative Morphology and Phylogeny of the Human Bony Labyrinth. Utrecht University, The Netherlands.

Spoor, C.F., Zonneveld, F.W., Macho, G.A., 1993. Linear measurements of cortical bone and dental enamel by computed tomography: Applications and problems. Am. J. Phys. Anthropol. 91, 469e484.

Thackeray, J.F., Mdaka, S., Navsa, N., Moshau, R., Singe, S., 2000. Morphometric analyses of conspecific males and females: an exploratory study of extant primate and extinct hominid taxa. S. Afr. J. Sci. 96, 534.

Tobias, P.V., 1965. *Australopithecus, Homo habilis*, Tool-Using and Tool Making. S. Afr. Archaeol. Bull. 20, 167e192.

Tobias, P.V., 1978. The earliest Transvaal members of the genus *Homo* with another look at some problems of hominid taxonomy and systematics. Z. Morphol. Anthropol. 69, 225e265.

Wood, B.A., 1991. A paleontological model for determining the limits of early hominid taxonomic variability. Palaeont. Afr. 28, 71e77.

Wood, B.A., Engleman, C.A.,1988. Analysis of the dental morphology of Plio-Pleistocene hominids. V. Maxillary postcanine tooth morphology. J. Anat. 161, 1e35.

Wood, B.A., Richmond, B.G., 2000. Human evolution: taxonomy and paleobiology. J. Anat. 197, 19e60.

Wood, B.A., Abbott, S.A., 1983. Analysis of the dental morphology of Plio-Pleistocene hominids. I. Mandibular molars: crown area measurements and morphological traits. J. Anat. 136, 197e219.

Wood, B.A., Abbott, S.A., Graham, S.H., 1983. Analysis of the dental morphology of Plio-Pleistocene hominids. II. Mandibular molarsdstudy of cusp areas, fissure pattern and cross sectional shape of the crown. J. Anat. 137, 287e314.

Zipfel, B., Berger, L.R., 2009. A partial hominin tibia (Stw 396) from Sterkfontein, South Africa. Palaeont. Afr. 44, 71e75.

Appendix A. Supplementary Online Material

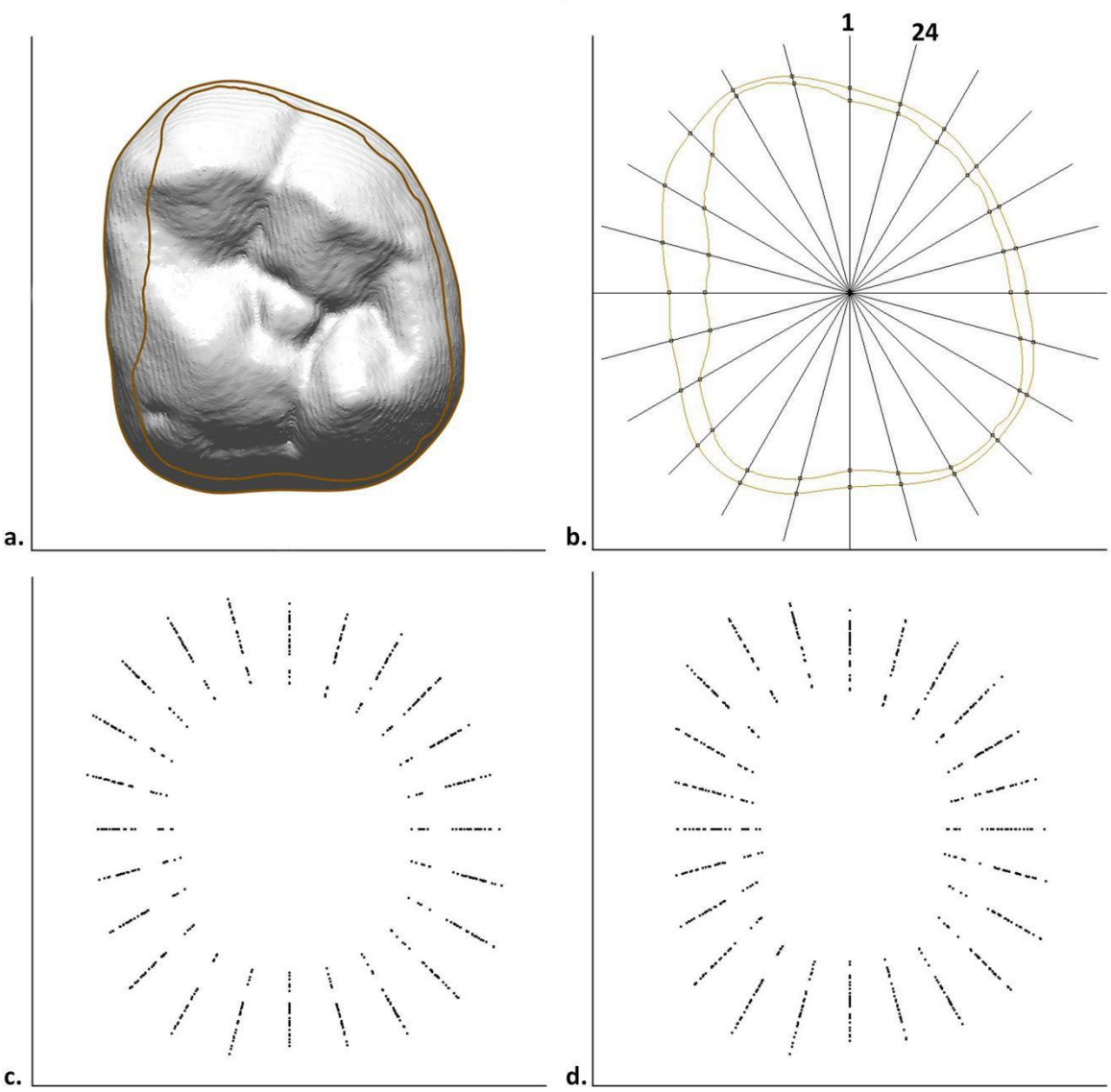

Fig. SM1 – a. crown and cervical outlines are sampled from a pre-oriented dental crown having the cervical plane parallel to the xy plane and the mesial margin parallel to the y-axis; b. the crown and cervical outlines are intersected by a 360° polar array of 24 radii departing from the centroid of their area. The bottom pictures show the set of points collected at the intersection between the polar array and c. all crown outlines, and d. cervical outlines.

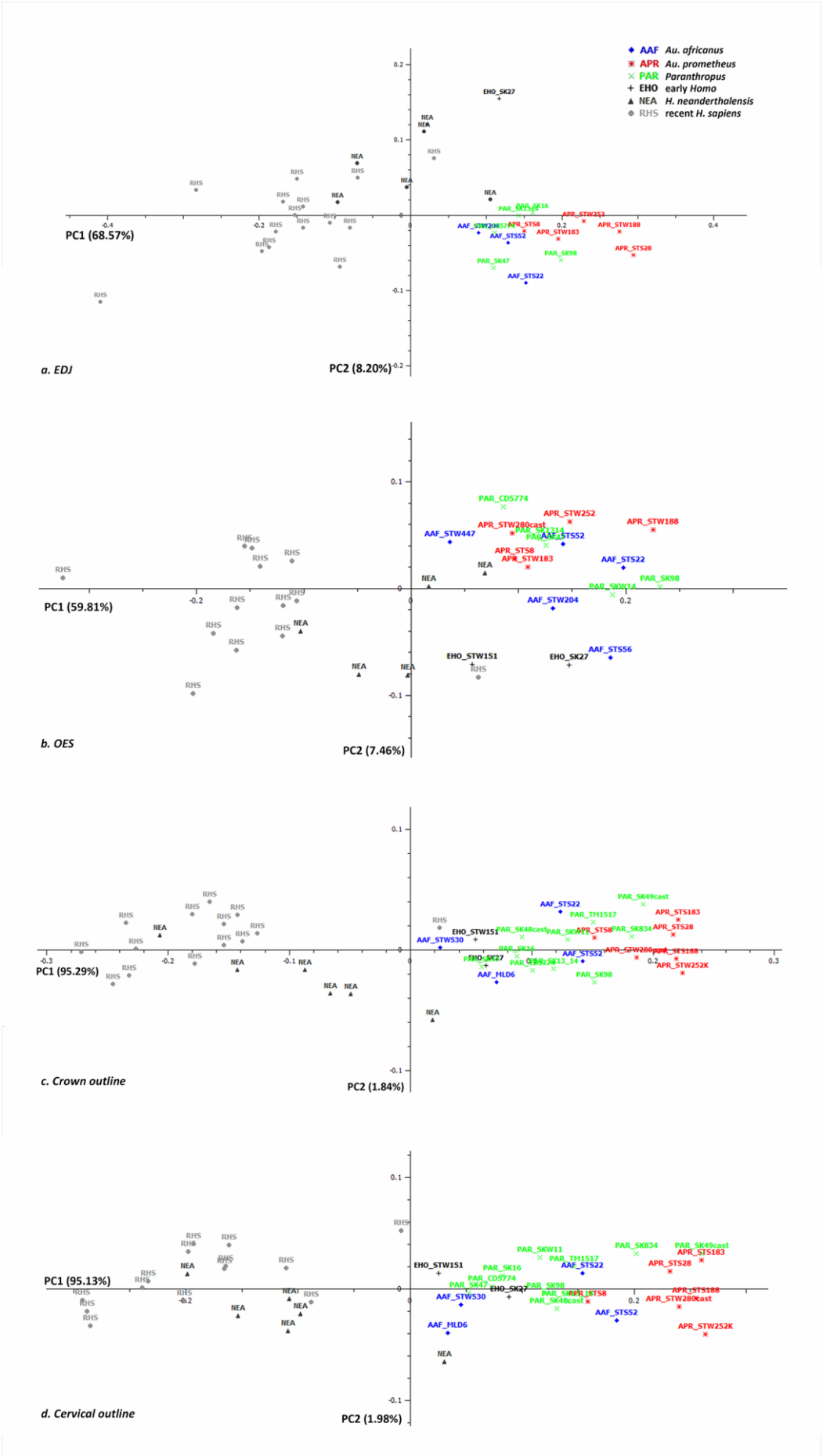

Fig. SM2 – PCA plots for the GM analyses in form space. The distribution of the M^2 specimens is stretched out, increasing the separation between *Homo* and both *Australopithecus* and *Paranthropus*. The *Australopithecus* sample clusters with *Paranthropus* and the subgroups *Au. africanus* and *Au. prometheus* separate better than in the shape analyses (with the exception of the OES landmark configurations).

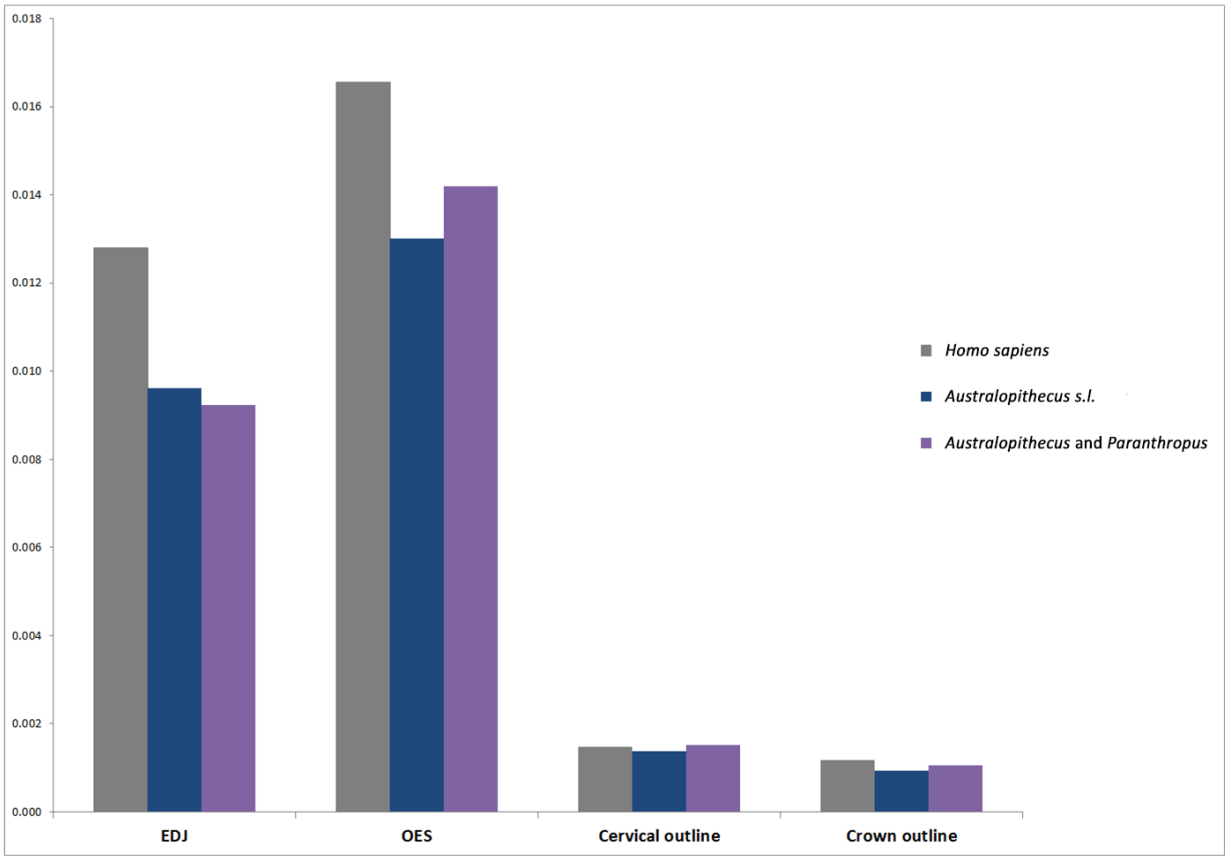

Fig. SM3 – Histogram showing the variation of *Homo sapiens* compared to both *Australopithecus* (*Australopithecus s.l.* = *Au. africanus* and *Au. Prometheus*) and the combined *Australopithecus-Paranthropus* samples for the GM analyses carried out. The *H. sapiens* variation is larger than that of the combined australopithecine sample for OES and EDJ, and is comparable in value to it for both crown and cervical outlines.

2.7. The Qesem Cave hominin material (part 1): A morphometric analysis of the mandibular premolars and molar.

Weber, G. W., Fornai, C., Gopher, A., Barkai, R., Sarig, R., Hershkovitz, I.

Quaternary International (Submitted: 18/05/2015)

Synopsis

This chapter reports a study conducted for the geometric description of three permanent teeth (two lower premolars from one individual, and one lower molar from a second individual) coming from the oldest levels of Qesem Cave, an Acheulo-Yabrudian Middle Pleistocene fossil site in Israel. The taxonomic nature of the Qesem Cave people is not yet understood. In this study we investigated shape and size of the 3D dental crown in a comparative setting considering multiple features, namely the crown and cervical outline and the occlusal aspect of the enamel-dentine junction. Notably, this study contributed to our knowledge of dental variability for a time and place of human evolution for which knowledge is still scant. A classification of these teeth is not yet possible, however we highlighted morphological affinities with Neanderthals, even though the Neanderthal-like features are not markedly expressed. Furthermore, we found an interesting size pattern for the premolars, which, differently from the molar, do not exceed the range of variability of modern humans.

Contribution

Data collection, interpretation of the data, editing of the manuscript.

Research Article for "Quaternary International"

The Qesem Cave hominin material (part 1): A morphometric analysis of the mandibular premolars and molar.

Weber, Gerhard W.[1,2]; Fornai, Cinzia[1]; Gopher, Avi[3]; Barkai, Ran[3]; Sarig, Rachel[4]; Hershkovitz, Israel[4]

[1] University of Vienna, Department of Anthropology, Austria
[2] University of Vienna, Core Facility for Micro-Computed Tomography, Austria
[3] Tel Aviv University, Institute of Archaeology, Israel
[4] Tel Aviv University, Sackler Faculty of Medicine, Department of Anatomy and Anthropology, Israel

Corresponding author:

Univ. Prof. Dr. Gerhard W. Weber

Department of Anthropology & Core Facility for Micro-Computed Tomography, University of Vienna

Althanstr. 14, A-1090 Wien, Austria

Tel: +43-1-4277-54701

Fax: +43-1-4277-9547

Email: gerhard.weber@univie.ac.at

Web: http://www.anthropology.at/people/gweber

Abstract

The Mid-Pleistocene Qesem Cave near Tel Aviv in Israel has yielded several hominin teeth and abundant faunal as well as cultural remains. The geological sequences of the cave fall right into the estimated split time between the populations leading to anatomically modern humans (AMH) and Neanderthals (NEA). In this contribution, we focused on the three lower postcanine teeth because they represent the oldest material from Qesem. We used Geometric Morphometrics and qualitative observations on the outer enamel surface and the enamel-dentine junction to investigate shape and size variation in a sample of geographically diverse modern humans, Neanderthals, and Early to Late Pleistocene fossils (Sangiran, Mauer, Bilzingsleben, Ehringsdorf, Qafzeh, Ohalo). Our approach based on three dental traits from three tooth types is able to distinguish quite well between dental specimens from AMH and NEA. It also confirms a mosaic of features in Mid-Pleistocene specimens in general, and the close proximity of Ehringsdorf to NEA. The Qesem premolars display an intermediate shape between NEA and AMH, similar to Mauer, but their size is definitely modern-like.
The Qesem molar features a morphology and size nearer to NEA. One possibility for an explanation is the dissociation of size and shape in premolars, and molars that are morphologically closer to NEA than premolars. With the current data, however, we cannot confidently assign the Qesem teeth to any existing taxon, nor exclude that it is an autochthonous phenomenon in the Levant.

Keywords

Qesem Cave; Dental Morphometrics; Middle Pleistocene; Late Pleistocene; Neanderthals, Anatomically Modern Humans, Shape and Form Analysis; Virtual Anthropology

Introduction

According to morphological and genetic data, the split between the populations leading to modern humans and Neanderthals can roughly be assumed between 440,000-270,000 years ago (Green et al. 2010; Endicott et al. 2010). The fossil record in the Middle Pleistocene delivers a rather confusing picture. Specimens from all three continents (e.g., Bodo, Elandsfontein or Ndutu in Africa; Dali, Jinniushan or Yunxian in eastern Asia; Mauer, Petralona or Arago in Europe) are difficult to assess taxonomically and it remains questionable if they can be lumped into one taxonomical container. An accurate definition of the species *Homo heidelbergensis* is lacking, but this heterogenous group is nevertheless one possible candidate for representing the last common ancestor of the two lineages leading to modern humans and Neanderthals. As Stringer (2012) laid it out, reclassifying the Sima de los Huesos (SH) material as an early form of *H. neanderthalensis* would remove most of the data

supporting a European chronospecies of *H. heidelbergensis-H.neanderthalensis*. Others also supported a view seeing the SH population as quite close to Neanderthals (Martinon-Torres et al. 2012).

While it remains still unclear whether *H. heidelbergensis*' roots might be found in Africa, Europe, or Asia (Rightmire 2008; Martinon-Torres et al. 2011; Stringer 2012; Meyer et al. 2012), the Levant – located at the crossroads between the three continents – is geographically a potential habitat of the last common ancestor of modern humans and Neanderthals. Doubts have nevertheless been raised (Martinon-Torres et al. 2011) if a passage from sub-Saharan Africa to the Levant might have been possible in the time frame between 500-300 thousand years ago (kya) due to the large desert areas in north-east Africa. Still, the unique geographical position of the Levant could even have allowed admixture of longitudinally migrating population streams between Europe and Asia, or yet Africa, if a passage was possible. To complicate the picture further, we have recently welcomed another hominin group in Asia, the Denisovans (Reich et al. 2010). They exist rather as a genetic construct than as a morphologically evident taxon but they seem to be closer related to Neanderthals than to modern humans. Geneticists calculated a split time between Denisovans and Neanderthals roughly at 380kya (Prüfer et al. 2014), which would be only a bit earlier than the dating of the first Qesem hominins (350kya). Their origin is as unknown as that one of *H. heidelbergensis* but we cannot exclude that Denisovans, or their immediate precursors, inhabited the Levant. The region is also interesting from another, much later, perspective: It is the home of some of the first anatomically modern humans which were found outside Africa (Skhul, Qafzeh), and at the same time it is the home of those Neanderthals (Tabun, Kebara, Amud) that were found geographically closest to Africa (which they never reached according to our fossil record).

Hominin fossils dated around the genetically expected split time are very rare. The Mid-Pleistocene Qesem Cave (QC) near Tel Aviv in Israel has so far yielded several hominin teeth and abundant faunal, as well as cultural remains. The geological sequences present at the cave could be dated between 420,000 to 200,000 years (Gopher et al. 2010; Mercier et al. 2013). They are thus falling exactly into the crucial time frame mentioned above. The hominins at Qesem Cave were associated with the Acheulo-Yabrudian Cultural Complex (Barkai et al. 2009; Barkai and Gopher 2013). A first description of eight teeth has been published by Hershkovitz and colleagues (2011). Based on qualitative assessments and traditional linear measurements they pointed already out the ambiguous morphological affinities of the Qesem population to anatomically modern humans (AMH) and Neanderthals (NEA). Since then, some more isolated teeth have emerged from the cave. These teeth are described in Hershkovitz et al. (2015, this volume), and one of them below in this contribution (right lower second molar).

The present paper focuses on the mandibular third and fourth premolar (P_3 and P_4, respectively) from the same individual (Hershkovitz et al. 2011), dated to roughly 350kya, and the recently discovered lower second molar (M_2), which at least post-dates 300kya (Fig. 2), because they represent some of the oldest material from the cave. In contrast to earlier attempts, we mainly use 3D geometric morphometric methods which capture the external and internal geometry of the teeth, and easily allow analyses of shape and size independent from each other. Our goal is to put the morphology of the Qesem premolars and molar into a quantitative comparative context with other Pleistocene and Holocene material.

Materials and Methods

- Insert Tab. 1

The sample (Tab. 1) consists of the three Qesem Cave teeth P_3-QC9, P_4-QC10, and M_2-QC12, several Neanderthals from Europe and the Levant, Late Pleistocene (~ 127-10kya[1]) anatomically modern humans from the Levant, epipaleolithic Natufians, and a quite diverse sample of recent modern human populations from various geographic regions, among them Khoesan, Papuans, Europeans, Avars (7^{th}-8^{th} century Euro-Asian nomads), and recent Bedouins from Israel. The accessibility of high-resolution 3D data of well-preserved teeth from the Middle Pleistocene (~ 781-127kya[1]) is unfortunately very low. Teeth are either missing, or broken, too worn, of the wrong tooth type, or simply not accessible to us or for scanning in general. Nevertheless, we could collect a small, but subtle and crucial sample of Early (> 781kya[1]) to Middle Pleistocene lower premolars and molars that includes the type specimen of *Homo heidelbergensis* (Mauer), another potential European member of the same taxon, or even of *Homo erectus* (Bilzingsleben E6; see Vlcek et al. 2002, Stringer 2012), some of the oldest Neanderthal-affine European fossils (Ehringsdorf F and G) [we call it *Proto-Neanderthal* here due to its old age (Grün et al. 1988; van Asperen 2012) and its near-Neanderthal or transitional morphology, see e.g. Vlcek 1993, Smith 1984], and some Javanese *Homo erectus* specimens from Sangiran (S7). The Bilzingsleben E6 specimen is still partly embedded in a stone matrix and not extensively described. It was only classified as “lower P1-2 sin.” by Vlcek (2011). Looking at its morphology after virtual removal from the stone matrix, we assess the specimen as a left lower P_4.

[1] http://quaternary.stratigraphy.org/definitions/pleistocenesubdivision/

All QC teeth and most of the comparable material were µCT-scanned at the Core Facility for Micro-Computed Tomography at University of Vienna with a custom built VISCOM X8060 (Germany) µCT scanner with slightly differing scan parameters: 140-160kV, 300-400µA, 1400-2000msec, diamond high performance transmission target, 0.75mm copper filter, isometric voxel sizes between 9 - 44µm. X-ray images were taken from 1440 different angles. Using filtered back-projection in VISCOM XVR-CT 1.07 software, these data were reconstructed as 3D volumes with a colour depth of 16,384 grey values. Other comparable material was obtained from existing collections and data bases (Thüringisches Landesamt für Denkmalpflege und Archäologie Weimar, Ruprecht Karls Universität Heidelberg, NESPOS Data Base, Senckenberg Research Institute Frankfurt, the Croatian Natural History Museum Zagreb, the Muséum National d'Histoire Naturelle Paris, the Max-Planck Institute Leipzig). All teeth were standardized to left ones, i.e. right ones were mirrored. If both antimeres were present in specimens, the better preserved one was chosen. The post-processing of the image stack was performed in AMIRA 5.6 (Mercury Computer Systems, Chelmsford, USA), and surface models of the outer enamel surface (OES) and enamel-dentine junction (EDJ) were produced after segmentation of the volume data. All operations follow in principle the guidelines described in the textbook “Virtual Anthropology” (Weber & Bookstein 2011, see also summary in Weber 2015).

If the teeth were affected by wear up to grade 3 of Molnar’s classification (1971), some minimally affected dentine horn tips were virtually reconstructed in order to include them into the analysis of the EDJ. Specimens with heavier wear were not considered for this investigation. The quality of scans of the Sangiran material unfortunately did not allow any separation of the enamel from the dentine. They were thus excluded from the EDJ analysis (see Tab. 1). Landmark data were collected from 3D virtual models of the dental crowns. We used Geometric Morphometric methods based on landmarks and semilandmarks to examine shape and form (Weber & Bookstein 2011, Weber 2015) of three different dental traits:

1) the enamel-dentine-junction (EDJ),
2) the cervical outline, and
3) the crown outline.

This allows gathering much of the morphological information carried by dental crowns. Moreover, the use of cervical and crown outlines permits the inclusion of those teeth that showed strongly affected occlusal surfaces by dental wear or damage.

- Insert Fig. 1

For the landmark-based analyses of the EDJ, the following protocol was used (Fig. 1): Four landmarks were identified on P_3s and P_4s: protoconid horn tip, metaconid horn tip, deepest point of the mesial fossa, deepest point of the distal fossa. Eight semilandmarks were identified on the mesial marginal ridge, 13 semilandmarks on the distal marginal ridge. For M_2s, seven landmarks were used: The horn tips of the protoconid, metaconid, hyponid, entoconid, the deepest point of the central fossa, and of the buccal and lingual fissure. In addition, 22 semilandmarks were identified along the whole occlusal ridge of the EDJ. Landmarks and curves were created in the Templand partition of the EVAN Toolbox 1.71 (ET; http://evan-society.org), where the sliding of the semilandmarks is based on the minimum bending energy approach (Bookstein 1989; Gunz 2005; Gunz & Mitteroecker 2013).

For cervical and crown outline analyses, we followed the instruction published in Benazzi et al. 2012, with some modifications (Fig. S1). The surface data of the dental crowns (OES and EDJ) were imported into RapidForm XOR2 (INUS Technology) and realigned so that the best fit plane at the cervical margins was parallel to the XY plane. Premolars were subsequently rotated in such a way that the buccal ridge of the EDJ was aligned parallel with the X-axis, molars were rotated to align the lingual margins parallel to the X-axis (Fig. S1 a&b). The crown and cervical outlines of each tooth were collected and projected onto the respective cervical plane. The crown outline thus corresponds to the silhouette of the oriented tooth, as seen in occlusal view. The cervical outline represents the perimeter of the dental crown at the intersection with the cervical plane. The outlines were then transferred to Rhinoceros 4.0 Beta CAD environment (Robert McNeel & Associates, Seattle, WA). The centroid for each outline area was calculated and 24 equiangularly (15^o) spaced radii were drawn counter-clockwise. At the intersection of these radii with the outline there resulted 24 pseudolandmarks (in contrast to 16 in Benazzi et al. 2012).

The landmark configurations from cervical and crown outlines, and the EDJ surface, were treated separately in the GM analyses. A combination of EDJ with cervical outline, which would in principle be useful to include information about the base of the crown in relation to the occlusal surface, would have further reduced the applicable data set because some interesting specimens, such as Sangiran, feature only outline data. Conversion of the Cartesian coordinates into shape variables, which means to eliminate variation in orientation, location, and size, was done by means of a Generalized Procrustes Analysis (GPA; Gower 1975; Marcus et al. 1996), which also separates shape from size. Shape variables (or form variables, if size is brought back, Mitteröcker et al. 2004) were then subjected to Principal Component Analysis (PCA) for reducing dimensions, and then shape/form changes were visualized by Thin Plate Spline warping (TPS; Bookstein 1978; 1991). These tasks were performed in the EVAN Toolbox 1.71. For MANOVA permutation tests the software PAST (Hammer et al. 2001) was used, other statistics were done in IBM SPSS Statistics 22 (IBM Corporation). Two-block Partial Least Squares analysis (PLS) was performed in the EVAN Toolbox 1.71. It is based on a singular

value decomposition of the matrix of covariances between the two sets of variables. The results are pairs of linear combinations that successively maximize the covariance between the sets of variables, while being mutually uncorrelated across sets. Linear Discriminant Analysis (LDA) using the first ten principal components of PCA (accounting for roughly 90% of shape variance, or more) was performed in IBM SPSS Statistics 22 (IBM Corporation) to assess the predicted group membership of those specimens that were not clearly assigned to either “AMH” or “NEA”, and to determine the percentage of correctly classified cases for the defined groups. The leave-one-out approach was applied to those specimens in the Tab. 2 that we considered clearly attributable to one of these two groups (Amud 1, Qafzeh 9, Qafzeh 11, Ohalo 1) .

Results

A qualitative description of the two lower premolars from QC can be found in Hershkovitz et al. (2011). A brief description of M_2-QC12 can be found in Hershkovitz et al. (this volume). As this tooth is otherwise unpublished, we also provide a description below.

The right lower second molar M_2-QC12

- Insert Fig. 2

M_2-QC12 (also referred to as QC_J15_540-550) was found in 2011 in quadrant J/15, depth 540-550. It originates from an Amudian blade-dominated context and dates to c. 300kya. The tooth is complete (Fig. 2), the apices of the roots are fused. The grooves and pits of the occlusal surface are partly covered by sedimentary concretion, as are parts of the roots, especially at the root bifurcation. These concretions were removed virtually prior to the morphological description. There are several delicate cracks visible on the mesial, lingual, and distal side walls of the crown, but there is only one actually severe crack on the buccal side, leading down from the buccal fissure to the cervical margin. The crown shows a rectangular outline (Fig. 2), its distal portion is not pointed. The cusp tips of the protoconid and hypoconid show wear, without exposure of the dentine (stage 2; Molnar 1971). The metaconid and the entoconid show also wear facets. The distal slope of the entoconid exhibits a deep enamel pit. The crown has only four cusps, a hypoconulid is not present (Fig2; see also Fig. 6 left for dentine surface). The sequence of cusp size is protoconid > hypoconid > metaconid > entoconid. No protostylid is visible. The mesial fossa is deep and anteriorly bounded by a continuous mesial marginal ridge. The longitudinal fissure is interrupted mesially shortly after leaving the central fossa by a strong middle trigonid crest on the enamel (ASUDAS 1B, Turner et al. 1991). The distal

fossa is shallow and large, delimited by a sharp distal marginal ridge. Both interproximal contact facets (IPCF) are well developed, the mesial IPCF being fairly large in transverse direction and clearly inclined upwards (~116^{o} in relation to the anterior occlusal surface). The mesial roots are fused, as are the distal ones. There are two root canals mesially, but only a fused one distally. All roots are slightly curved distally and approximately of equal length. The bifurcation is rather high (43% of root length from cementoenamel junction, only visible on the electronically cleaned specimen), the pulp chamber is unremarkably small. A proper diagnosis of taurodontism would need further quantitative investigation, but if any is present, it would only be of a mild degree. Mesio-distal (M/D) diameter of the crown is 12.3mm (uncorrected for IPCF), the bucco-lingual (B/L) diameter is 11.3mm, crown height at the protoconid 7.4mm, root length on the buccal aspect ~ 14.0mm.

Although there is no absolute argument ruling out the possibility of a lower M_1 (a lower M_3 can be ruled out with high confidence based on the presence of mesial and distal IPCFs), we consider M_2-QC12 being a lower M_2 based on the following morphological evidence: there are only four cusps present; the tooth has a rectangular outline with no triangular distal extension; a Y5 pattern is missing; the tooth was markedly inclined forward when in place, as denoted by the angulation of the mesial IPCF, and the wear is mainly located mesially and distally rather than on the central basin, both as it would be expected for an M_2 in a normal functional dental relationship.

Geometric morphometric analyses

The GM analyses cover the geometry of the three traits mentioned (cervical and crown outline, EDJ occlusal surface). Owing to the preservational status of the individual specimens, not all of them could be included in all analyses (Tab. 1. provides an overview of the maximum sample for each tooth type), for instance, when there was enamel chipping on the lateral crown walls so that crown outline had to be excluded, or dentine and enamel could not be separated because the border could not be detected in the µCT scans.

Form, shape, and size for three traits and three tooth types were analyzed separately, leading to 3x3x3 results. Accounting for the space limitations of this article, we cannot show all of them but we focus on the most significant findings, respectively on summaries of them. The sample focuses on AMH and NEA variation to shed light on the possible similarities/differences of the Qesem and other teeth.

Starting with size, we observe that AMH and NEA separate quite clearly in all traits and tooth types. Highly significant differences in size (represented as lnCS in permutation tests, 10.000 samples) of P_3s for cervical outlines ($p<0.001$), crown outlines ($p<0.001$), and EDJ ($p<0.001$) between AMH and NEA were found, where NEAs are constantly larger than AMHs. The same highly significant size

differences between AMH and NEA apply to P_4s (cervical outlines p<0.001; crown outlines p=0.002; EDJ p<0.001), and M_2s (cervical outlines p<0.001; crown outlines p<0.001; EDJ p<0.001). Sizes for the three traits within a tooth type are significantly correlated (P_3 between 0.84 and 0.92, highest between cervical and crown outline; P_4 between 0.86 and 0.90, highest between crown outline and EDJ; M_2 between 0.81 and 0.90, highest between cervical and crown outline).

- Insert Fig. 3

lnCS is hence a very distinctive parameter characterizing the lower premolars and the second molar of anatomically modern humans on the one hand, and Neanderthals on the other hand. We observe in all analyses quite small Qesem premolars in comparison to NEA (Fig. 3). They are almost always within the middle 50% (interquartile range - IQR) of anatomically modern humans (with the only exception of P_3 EDJ). Qesem premolars are also always smaller than the Early to Middle Pleistocene material from Sangiran, Mauer, and Ehringsdorf. Only the P_4 EDJ of Bilzingsleben is smaller. Sangiran, Ehringsdorf, and Bilzingsleben (here only cervical outline) are generally intermediate in size between AMH and NEA. The Qesem lower molar, in contrast to the premolars, is quite large, ranging within the IQR of NEA in all three traits. Mauer is large too in all aspects, thus in the size range of NEA, Ehringsdorf is again intermediate between NEA and AMH.

While size is giving us a very clear signal with regard to an AMH/NEA distinction, results from shape space are far more ambiguous. Some of the nine analyses show a very neat separation in the plots of the first two Principal Components (PCs) of the Procrustes shape coordinates, others do not (Fig. 4B. and 4C. show two extreme examples for the former and the latter). Tab. S1 summarizes a non-parametric MANOVA to test for significant shape differences between AMH and NEA (only specimens of these groups were used). Crown outlines of P_3 and P_4, and EDJ surfaces of P_4 deliver only weak results. All other differences of the permutation tests are highly significant. This, however, does not imply that each individual specimen clusters clearly with its group (see, for instance, NEA_Kr-d26 in Fig. 4B.). We can state that lower P_4 shape is a less powerful candidate to reliably distinguish between NEA and AMH, and the same is true for lower premolar crown outlines in general (but cf. Bailey & Lynch 2005; Gomez-Robles et al. 2008).

While P_3 crown, and P_4 crown and EDJ shape plots deliver generally rather unclear pictures, in the other analyses Qesem teeth are often found at the fringes of the AMH and NEA shape distributions. Only for P_4 cervical outline and M_2 EDJ surface Qesem is right within the NEA cluster. In the former case, however, Qesem establishes a separate cluster with Mauer and Bilzingsleben that is located at the extreme end of PC1, even beyond the NEA shape trend. The Qesem premolars are generally

often in the vicinity of the Mauer premolars. The Qesem molar, in contrast, is far apart from Mauer. The oldest material in the sample, Sangiran, is very clearly in the modern human shape distribution (but only P_3s were available). Ehringsdorf is always near the Neanderthals, Bilzingsleben and Mauer are rather intermediate. These PC plots, however, only capture the situation for the first two principal components, which explain, by definition, most of the variance but curtail the total information available.

- Insert Fig. 4

The associated shape changes can be visualized by warping the average shape along PC1 and PC2, respectively relevant combinations of them. Starting with P_3 EDJ surface, we can exemplify NEA lower third premolars (Fig. 4 A.) as having a more rhomboid and asymmetric silhouette (from occlusal view), a truncation of the mesiolingual aspect, and a protoconid slightly more placed towards the center. These observations roughly agree with those made by Gomez-Robles et al. 2008 for *H. heidelbergensis* and *H. neanderthalensis* (including Sima des los Huesos) using a different approach (orientated 2D photographs) to study lower P_3 OES. We observe in addition on the EDJ a relatively larger mesial fossa, and low lingual horn tips (the highest elevation of the EDJ underneath an enamel cusp tip). AMH lower third premolars, in contrast to NEA, present an oval and more symmetric silhouette (as do the Sangiran specimens), and a more buccally placed protoconid, which is also in agreement with Gomez-Robles and colleagues' findings on the OES (2008), except that they find circular outlines as being typical for *H. sapiens*. On EDJ, we find also a relatively smaller mesial fossa for AMH, but, similarly to NEA and generally differing from lower P_4s, also quite low lingual horn tips. The Qesem third premolar features only a mildly rhomboid and asymmetric silhouette, a fairly truncated mesiolingual portion of the tooth, a rather centrally placed protoconid, a large mesial fossa, and a low lingual horn tip. This composition of features places Qesem at the border of the NEA distribution, near Mauer, Qafzeh 11, and modern humans. Qafzeh 9 is very different to Qafzeh 11, and Ehringsdorf G shows the whole set of NEA features in an extreme form.

Looking at P_4 EDJ surface (Fig. 4 B.) we can describe NEA lower fourth premolars as having a more subequal (i.e., a relatively shorter B/L diameter) but asymmetric silhouette owing to a mesiolingual truncation of the lingual lobe (also observed by Bailey & Lynch 2005, as well as by Martinon-Torres et al. 2006 on the OES, using again 2D photographic approaches). In addition, we find on the EDJ a markedly smaller mesial fossa (which seems to be associated to the mesiolingual truncation), and a more equal height of buccal and lingual horn tips (the latter still being a bit lower than the buccal one). AMH lower fourth premolars show quite a lot of variation but the trend for shape can be

described as an almost perfect oval (i.e., a relatively elongated B/L diameter) and symmetric silhouette, which confirms the OES findings of Bailey & Lynch (2005) and Martinon-Torres et al. (2006). AMH have rather a larger mesial fossa, and a relatively low lingual horn tip. The early anatomical modern humans Qafzeh 9 and 11 are, again, quite different from each other with regard to the silhouette (Qafzeh 9 imperfectly oval, Qafzeh 11 subequal with mesiolingual truncation), but both feature small mesial fossae. Bilzingsleben is almost oval in shape and within the modern human distribution. Mauer, against it, is much less oval. Qesem has a moderately relative B/L length, a small mesial fossa, a relatively high lingual horn tip - compared to the buccal one, and definitely a mesiolingual truncation of the lingual lobe. Together with Mauer, it is found at the border of the distributions of NEA and AMH. Ehringsdorf G is close to Qafzeh 11 and again on the extreme of the NEA cluster, thus showing all features mentioned above in an extreme expression.

The shape of the M_2 EDJ surface (Fig. 4 C.) of NEA and also Qesem is characterized by a more rectangular silhouette that is mesiodistally larger, has a buccolingually wider talonid, and relatively higher buccal horn tips (protoconid and hypoconid). This is contrasting with AMH which features a less elongated silhouette, exhibiting a conspicuous convexity of the lingual marginal ridge between the metaconid and entoconid. In extreme cases, such as Qafzeh 9, the marginal ridge can adopt a heart-shaped rather than a rectangular outline (Fig. 4 C.). The talonid appears buccolingually narrower due to this convexity in the middle of the tooth on the one hand, and a more inwardly positioned entoconid on the other hand. Generally, the entoconid is reduced, and the hypoconid and entoconid are placed slightly more distally. Qesem also exhibits this more distal placement of the distal cusps but lacks the marked convexity of the lingual margin, the narrow talonid, and particularly the inwardly positioned entoconid. Alltogether, it is quite NEA-shaped and, like Ehringsdorf G, clearly in their shape distribution. On the other hand, its hypoconulid is absent. Four cusped M_2s were not detected in Neanderthals and other archaic hominins in a study by Bailey (2006). The two Qafzeh specimens are not close to each other but perfectly in the AMH cluster, far from NEA.

- Insert Fig. 5

The PLS analysis shows how P_3 and P_4 EDJs covary with each other (the sample is even further limited because the EDJ for both teeth had to be preserved, only 32 specimens featuring both tooth types could be included). The plot for the left and right first singular warps (percentage of total squared covariance for pair 1 = 59.1%, pairwise correlation between singular warp 1 left and singular warp 1 right $r_1 = 0.637$), and the actual shape changes correlated with each other are visualized in Fig. 5. They can be understood as shape changes in P_3 that best explain shape changes in P_4, and vice versa.

The distribution of the sample is elliptical, running from the left lower -/- quadrant to the right upper +/+ quadrant. Although there were only very few NEA specimens qualifying for this analysis, the shape changes look very similar to the results of the isolated analyses for P_3 and P_4. That means rhomboid and asymmetric P_3 silhouette showing a truncation of the mesiolingual aspect, a small P_4 mesial fossa, and also a mesiolingual truncation of the lingual P_4 lobe on the side of NEA. On the opposite side of AMH, there are more oval and symmetric P_3 and P_4 silhouettes with relatively smaller P_3 and larger P_4 mesial fossae. These matching trends in two tooth types and the fairly high correlation between singular warps left and right are a first hint on functional constraints that might be behind a concerted shape change, rather than documenting random fluctuations. However, there is not much known about these relationships and we will have to await further studies on whole dentitions. The two Qafzeh individuals are again quite divergent – Qafzeh 9 perfectly in the AMH distribution, and Qafzeh 11 on the NEA end.

In addition to these relative warps and PLS analysis we looked at other statistics to interpret the relations between groups and the tentative associations of individual specimens. Firstly, we calculated the five nearest neighbors of Qesem and some other individuals for all three traits and tooth types in shape space (Tab. 2). These data are based on the full Procrustes distances (the square root of the sum of squared distances between corresponding points), and thus have not the same information content as the first two PCs. Secondly, we performed linear discriminant analyses (LDA) using the individual scores of the first ten PCs in shape space which explain between 87.3% to 98.8% of the total variance. Only specimens that we clearly assigned to either AMH or NEA (see Tab. 1) were used to establish the two groups. We did not put the Early to Mid-Pleistocene fossils into a third group because they are too heterogenous from various points of view, and sample size would still be too small. Tab. 2 provides the percentage of correctly classified AMH and NEA specimens in the linear discriminant analyses, and the predicted group memberships for all Early to Late Pleistocene specimens, as well as the probabilities for this classification (Ppost). The pictures drawn by the five nearest neighbors on the one hand, and the linear discriminant analyses on the other, can be consistent, but do not have to be. This is because LDA is a multivariate approach considering the covariance structures of the groups, whereas Procrustes distance does not. In particular, if the difference between the established groups in LDA is heavily weighted on high-numbered PCs (which it often is), then the discrimination will likely deviate from the simple optimization based on Procrustes distance. In other words, LDA might focus on small scale features represented in, e.g. PC6 or PC9, and Procrustes distance is an added distance across the full multidimensional space.

We included also the Late Pleistocene hominins Amud 1, Qafzeh 9, Qafzeh 11, and Ohalo 1 into this comparison, although their taxonomic affiliation to NEA, respectively to AMH, is out of question from our point of view. The reason was to see how they would perform in this approach. Sangiran,

Bilzingsleben E6, and Ohalo 1 just appear in one tooth type, simply because only this material was available for the study. Some of the EDJ analyses (also for Amud 1) had to be left out because the µCT scans, respectively the preservational status, did not allow for inclusion.

- Insert Tab. 2

Out of the nine Early to Late Pleistocene specimens, three show an entirely unambiguous picture. Sangiran (in fact all three of them in the sample, but only S7-25 shown in Tab. 3), Qafzeh 9, and Qafzeh 11 have only or almost only AMH as nearest neighbors, and the LDA puts them in this group in *all* analyses. This, of course, does not mean that Sangiran is modern human, but the outline shapes of these Early Pleistocene premolars are virtually indistinguishable from moderns. Interestingly, Qafzeh 9 and 11 show a quite high frequency of nearest neighbors from the Levantine Natufian and Bedouin sample, sometimes also affinities to a Neanderthal. The question of a local shape signal probably persisting through 100 Millennia is certainly worth to be pursued in a further study. Although the two Qafzeh specimens are everything else than similar in shape, our discriminant analysis has no problem assigning them both unequivocally to the modern human group in all cases. A relationship of Qafzeh 9 or 11 to Qesem is not inferable from these data.

The picture drawn by Ehringsdorf G is a bit more ambiguous but the predominant signal is that nearest shape neighbors are mainly Neanderthals (and in some cases also Qesem and Mauer), and nine out of nine LDA results lead to a grouping with NEA. This is supporting the view that Ehringsdorf represents indeed an early form of Neanderthals, one that probably has not yet developed the full suite of classical NEA traits. For Amud 1 we could just study outlines since the EDJ is too much affected by heavy wear. It has almost no nearest neighbor from the Mid-Pleistocene (except Ehringsdorf G for P_4 crown outline), but its premolar outlines are quite near modern humans with an astonishingly high frequency of Levantine Natufians and Bedouins. The discriminant analyses, however, group it five out of six times with Neanderthals. Ohalo 1 is only represented with M_2 outlines here. Its nearest neighbors are almost exclusively modern humans, but the LDA is indecisive with one classification in each possible group.

Bilzingsleben could only be included with one premolar. Depending on the trait studied, its shape is intermediate between AMH and NEA, and strongly resembling Qesem and Mauer for the outlines. It is particularly the base of the P_4 (cervical outline) that features a more Neanderthal-like shape, the crown outline is much more modern-like. Two out of three LDA results, however, put Bilzingsleben into NEA.

Mauer, the type specimen for *H. heidelbergensis*, and Qesem are represented by all three teeth in our study. They are both intermediate in shape, as we saw already on the limited picture provided by the PC-plots. Their nearest neighbors switch between AMH, NEA, and the other Mid-Pleistocene hominins. Six out of nine LDA results put both into NEA, three into AMH (though sometimes with a quite low Ppost). As we observed in Bilzingsleben, the P_4 cervical outline is particularly resembling Neanderthals and quite similar among these three Mid-Pleistocene specimens. The Qesem M_2 cervical outline is also overwhelmingly NEA-like.

If we merge shape and size, we observe highly significant differences between our two groups AMH and NEA in *each* trait for *each* tooth type (see Tab. S1). Fig. S2 shows two examples in this form space. In each of the six plots for the premolars, Qesem lies within the AMH cluster or near the border between AMH/NEA because of the small size, which is the dominating factor for PC1. For the molar, this picture is reversed, i.e. Qesem is always located within the NEA distribution. Yet, also Mauer, Qafzeh, and one Sangiran specimen are found there, again due to their big size. Evolutionary allometry (across phylogenetically related species) is rather low, i.e. only 4.5% of P_3, 8.7% of P_4, and 11.5% of M_2 EDJ shape variance can be explained by lnCS. Other authors have suggested a negligible influence of size on shape in lower hominin premolars (Bailey & Lynch 2005). Martinon-Torres and colleagues (2006) found a similar allometry (7.5%) than we did for P_4s, and Gomez-Robles et al. 2008 calculated a higher 17.3% allometric effect for lower P_3s, however, both in samples that comprised hominin taxa from Australopithecines to modern humans, and thus embracing a much greater variation in shape and size than our study. In a larger sample of geographically diverse modern humans, we obtained also similar values for allometry around 5% for lower premolars (Krenn 2015). Since size and shape are rather loosely connected, at least in the lower postcanine dentition from the Mid-Pleistocene to the Holocene, we put less weight on form space results and rather focus at size and shape results separately.

- Insert Fig. 6

The virtual representation of the EDJ allows observing qualitative characteristics too. Looking on the Qesem molar EDJ surface (Fig. 6 left), we observe a strong “grade 3” trigonid crest (Bailey et al. 2011), described as being the most frequent grade in NEA, but completely absent in a sample of modern humans. Ehringsdorf G features exactly the same type of middle trigonid crest (see Fig. 6 middle). Mauer (see Fig. 6 right) and Qafzeh 9, in contrast, present only a weak distal crests, and Jebel Irhoud 3 lacks it completely, according to the aforementioned authors. In Qesem and Ehringsdorf, the crest originates at the protoconid and metaconid and connects them in a straight

line. A discontinuous distal trigonid crest is visible. According to Martinez de Pinillos et al. (2014), the Qesem trigonid crest on the EDJ would correspond to a "Type 12" continuous middle trigonid crest with discontinuous distal trigonid crest, which in M_2s appears never in *H. sapiens* and NEA, but in 18.2% of the SH sample. According to the same author's scheme, Qesem features a "Type A" trigonid crest on the OES, which has a frequency of 87.5% in NEA, 100% in SH, but only 25% in *H. sapiens.* Completely opposite to the crest finding is another qualitative observation, namely the absence of a hypoconulid in the Qesem lower M_2, which had a frequency of zero in a sample of 39 Neanderthals in a study by Bailey (2006).

There was an additional tooth found at Qesem cave, a lower third molar (M_3-Q13), which is not included in this geometric morphometric analysis here because we consider the intra-species shape variability of M_3s as generally too high to use it successfully in our approach (but see Bailey 2006 for a different opinion, using a different approach). M_3-Q13 is described in this volume in detail (Hershkovitz et al. 2015). The tooth comes from a layer dated to >300kya and is thus of similar chronological age as the other mandibulary teeth in this study. A strongly expressed trigonid crest is visible on the OES. Looking at the segmented data of the EDJ, we also find a markedly expressed middle trigonid crest on this M_3. It is continuously running from protoconid to metaconid in a straight line. Its height dips slightly more towards the midline than those crests of the above mentioned M_2s of Qesem or Ehringsdorf G, but we would still see it in correspondence with a grade 3 in Bailey et al. (2011) scoring system (see image in Hershkovitz et al. 2015, this volume).

The EDJ trigonid crest expression on Qesem specimens and Ehringsdorf G hence points to strong similarities with Neanderthals. Mauer and Qafzeh 9, in contrast, feature weakly expressed crests as they can be found frequently in modern humans (Bailey et al. 2011).

Discussion

The fossil record of well-preserved lower premolars and molars from Middle Pleistocene specimens is very restricted. While the approach employed here produced a detailed view on the external, and particularly, the internal shape and size variation of the Qesem specimens, our sample does not permit a definite classification of the Qesem material. This is, however, not unique if we compare the situation to other approaches or to other osteological material because the assignment of Middle Pleistocene specimens is per se rather difficult due to their often ambiguous "mosaic of features", sometimes referred to as the "muddle in the middle" (Buck & Stringer 2014).

Qesem Cave, with regard to hominins, delivered only isolated teeth. Not one single tooth type in the sample is represented by more than one specimen, and they come from different layers that might comprise a period of roughly 150kya. To reduce some of these difficulties, we focused on the three

lower postcanine teeth in this study because they represent the oldest material from Qesem (which reduces the time difference to roughly 50kya), and two of them (P_3, P_4) belonged to the same individual. Concordant results from these latter two could at least show morphological tendencies clearer than results from just one specimen; nevertheless, the population variation covered here remains the smallest possible random snapshot.

Anatomically modern humans and Neanderthals represent the endpoints of two hominin lineages. Our quantitative approach using three traits on three types of teeth is able to characterize them quite well. 24 out of the 27 analyses led to highly significant shape or form differences between those groups. The discriminant analyses were able to correctly classify members of these two groups in 87.5-100%. With regard to the Early to Mid-Pleistocene specimens, we can confirm that Qesem features an intermediate morphology between NEA and AMH, or “a mosaic of traits”. This statement is not surprising for a population living around the split time of those two lineages, and it is also applying to other Mid-Pleistocene fossils in the sample such as Mauer and Bilzingsleben. Qesem often clusters with these fossils in the analyses. The P_4 cervical outline is the trait where Qesem, Mauer, and Bilzingsleben are most similar to each other, and all three are very near to the Krapina Neanderthals.

The picture that can be drawn is yet more differentiated than only confirming an intermediate position. Regarding the metrics of the shape, the Qesem molar is somewhat more similar to NEA than the Mauer molar. This is also confirmed by a qualitative observation, the expression of the mid-trigonid crest. The Qesem premolars are as intermediate between NEA and AMH in shape as those from Mauer. In terms of size they are quite modern-like, outside the range of NEA, and smaller than Mauer. The Qesem molar in contrast is large (almost outside the range of AMH).

Taking all results together, Qesem, Bilzingsleben and Mauer deliver the most heterogenous pictures. The three much older Sangiran teeth do not show such ambiguity and are quite similar to AMH (but only P_3 outlines could be tested). Ehringsdorf, in contrast, is by all means more developed into the NEA direction than any other Mid-Pleistocene hominin in our sample. Yet, it is also chronologically younger than those, and from another geographical region.

Mauer was recently dated to ~ 609kya (Wagner et al. 2010) and is the type specimen of a taxon who’s origin is uncertain (Stringer 2012). We assume that there was a split somewhere around 440-270kya (see introduction) leading finally to Neanderthals and anatomically modern humans (even if genetics suggested that this was not a full speciation event, thus interbreeding was possible, and occurred). The Sima de los Huesos sample (recently re-dated to 427kya, Arnold et al. 2014) falls in this period and shows that many Neanderthal traits were already present at this time in Western Europe. Ehringsdorf, from Central Europe, is likely younger than the lower border of the estimated

split period, and very much Neanderthal-like in our study. Qesem and Bilzingsleben originate from different geographical regions, also fall right into the split period, and both feature intermediate morphologies, like Mauer does. Their morphology definitely does not show this strong resemblance with Neanderthals as Ehringsdorf does. We cannot exclude that Qesem, Mauer, and Bilzingsleben could, in principle, be members of the same taxon, which would make it incidentally very unlikely that they represent Denisovans (but this is morphologically impossible to answer since there are so few anatomical elements known from Denisovans). Given the large geographical distance to German sites and the still existing differences to specimens from there, the Qesem population could be a variant of an archaic population that developed a Levantine version of Neanderthal similarities. Qesem could be a local phenomenon which raises an interesting question: did these people leave traces in later populations? We cannot answer this question, but some nearest shape neighbours of Qesem were Qafzeh 9, Qafzeh 11, Amud 1, Kebara 2, and Tabun 2. Two of the Qafzeh specimens appear also in Mauer's neighbourhood list, but no Levantine Neanderthals. Bilzingsleben has no Pleistocene Levantine neighbours other than Qesem.

Evolutionary changes can affect both the shape of a structure, as well as its size. Steven J. Gould, and many researchers before and after him, argued for this (1977, 234f). Basal was the insight that ontogeny and evolution are interrelated because changes in the developmental processes are producing morphological variation which in turn is the basis for evolutionary processes such as natural selection. In this event, growth (the increase in size) and development (any change in shape during ontogeny) can be dissociated, respectively can be affected by different factors. The Qesem premolars are intermediate in shape between NEA and AMH, their size is quite small, i.e. in the middle to lower range of AMH. The divergence of shape and size is also remarkable looking at other Levantine cases, for instance Qafzeh 9, which often appears within a cluster of NEA in form space due to its very large size, at the same time featuring definitely a modern shape. Qafzeh 11 on the other hand is quite small and mostly in the range of AMH for shape. Amud 1, described as featuring a more progressive morphology (Suzuki & Takai 1970), is a microdont Neanderthal (Trinkaus 1984). It comes close or is in the cluster of AMH in form space due to this small tooth size in the range of AMH. The fact that we find such cases in the fossil record calls for caution, especially the large size range of the Qafzeh individuals.

Diverging trends for shape and size of dental elements in our small sample could reflect just random variation. However, one actual factor allowing for size reduction without losing fitness appeared around the time of our Qesem population. Cooking changes the physical properties of food quite radically, and dramatically reduces the work of the dentition and masticatory apparatus (Lucas 2004). There is a lively discussion about this. Some authors claimed a very early appearance of cooking, even in the Early Pleistocene (e.g. Wrangham 2009), while others suggested that ubiquitous cooking,

at least in Eurasia, started later around 400-300,000 years ago (Roebroeks & Vill 2011; Shahack-Gros et al. 2014), and the diet in the Levant might have changed around the same time (Ben-Dor et al. 2011). Dental dimensions remained relatively stable in *H. erectus* populations, but declined gradually since about 300kya (Lucas 2004). Changing size along an evolutionary pathway is not necessarily coupled with changing shape. Martinon-Torres and colleagues (2013) found shape variables of the Sima de los Huesos upper M^1s to match the *H. neanderthalensis* pattern, while size related measures were similar to *H. sapiens*. Studying cusp areas, Quam et al. (2009) found a general size reduction of upper M^1s in the genus *Homo*, and shifts between relative cusp sizes. Bermudez de Castro et al. (1999) suggested an imbalance of the sizes for I_1-P_3 on the one hand, and P_4-M_3 on the other for *H. heidelbergensis* which would point to different evolutionary trends for anterior and posterior dentitions (they suggested to place the boundary between anterior and posterior dentition after P_3 rather than after C). We cannot confirm this different pattern for P_3 and P_4 of Qesem (it does, however, apply to Mauer), but their results remind us to keep dissociated size developments in mind. The conspicuous size-shape relationships of the Qesem teeth suggest three different hypotheses:

- H^1: The different patterns seen in the premolars and in the molar is due to mere individual variation and has no further meaning.
- H^2: The premolars and the molar originate from different populations inhabiting Qesem Cave at different times (corresponding roughly to a maximum difference of 50kya).
- H^3: The premolars and the molar are from the same population and represent a typical pattern. Premolars show a clear tendency towards size reduction, at the same time featuring an intermediate shape between NEA and AMH. Molars are closer to NEA in size and shape.

The random case formulated in H^1 cannot be excluded, as in all other cases of isolated fossil findings.

H^2 does not seem to be likely since culturally [concerning the habitual use of fire; lithic economy, technology, typology and recycling patterns; faunal composition and hunting and butchering patterns (Karkanas et al. 2007; Shahack-Gross et al. 2014; Shimelmitz et al. 2011, 2015 this volume; Parush et al. 2015; Stiner et al. 2009, 2011; Blasco et al. 2014)] the Qesem Cave context provides no reason to support the hypothesis of two different populations. However, this line of argumentation is based on the assumption that evolutionary changes of human body parts (teeth in this case) would “instantly” (i.e., within several tens of thousands of years) result in a recognizable behavioural change, which is certainly problematic. Still, if we assume that the chronologically younger molar originates from a Qesem population that was more developed along a Neanderthal pathway, we are still left with the unique size-shape pattern of the premolars.

H^3 gains some importance if we are willing to accept the rejection of H^1 and H^2. We are facing an interesting scenario suggesting dissociating size and shape trends in the Mid-Pleistocene in the

Levant. This exemplifies a pattern of form in postcanine dentition that is neither NEA, nor AMH, nor *H. heidelbergensis*, as they are covered in this sample. As the low amount of allometry (5-12%) suggests, size and shape are not strongly related to each other, at least for premolars and molars.

Conclusions

The two lower premolars and the lower molar investigated in this study are among the oldest material (> 300kya) recovered so far from Qesem Cave. Yet, the premolars and the molar were not found in the same strata, therefore there could still be considerable time difference between them. Our geometric morphometric approach is able to distinguish quite well between dental specimens from the two endpoints of Pleistocene hominin evolution, anatomically modern humans and Neanderthals. It also confirms in general the intermediate position of Mid-Pleistocene specimens, respectively a closer similarity of some with regard to AMH or NEA. The Qesem premolars in particular display an intermediate shape between NEA and AMH, but their size is definitely modern-like. The Qesem molar features a shape and size nearer to NEA. This suggests three different hypotheses for explanation. The most interesting one advocates a dissociation of size and shape in premolars, and molars that are morphologically closer to Neanderthals than premolars.

With the current data, we cannot assign the Qesem teeth to any existing taxon nor exclude that it is a new taxon appearing in the Levant. Qesem is not a Neanderthal, but could potentially be near this evolutionary development. However, it is not as close to Neanderthals as Ehringsdorf is, and the reduced size of premolars contradicts this view fundamentally. Size reduction would put Qesem rather closer to AMH, but the molar morphology is suggesting differently. Finally, because Qesem shows such ambiguous trends, it could be a local phenomenon.

The Qesem lower premolars and molars are characterized quite comprehensively with this study. For a definite taxonomic assessment of the Qesem population, however, more complete specimens from the cave are needed, as well as the inclusion of additional specimens from the Mid-Pleistocene.

Acknowledgements

We thank Martin Dockner for support during µCT scanning, Roman Ginner for taking photographs, and Vivian Slon, Hila May, and Aviad Agam for helping with the transport of the Israeli material. We thank the Tel Aviv University Anthropological Collection, the Croatian Natural History Museum in Zagreb, the Muséum National d'Histoire Naturelle in Paris, the Ruprecht Karls Universität Heidelberg, the Max-Planck Institute Leipzig, the Thüringisches Landesamt für Denkmalpflege und Archäologie Weimar, and NESPOS for access to fossils, respectively for scanning fossils. We are grateful to Maria

Martinón-Torrez, José Maria Bermúdez de Castro, Tim Schüler, Inga Stolbovaya, and Rudolf Slavicek for discussion and comments. This research was supported by the Department of Anthropology at University of Vienna, A.E.R.S. Dental Medicine Organisations GmbH, Vienna, Austria, and the Siegfried Ludwig - Rudolf Slavicek Stipendienstiftung. The anthropological study of the Qesem hominids is supported by the Dan David Foundation.

References

Arnold, L.J., Demuro, M., Parés, J.M., Arsuaga, J.L., Aranburu, A., Bermúdez de Castro, J.M., Carbonell, E., 2014. Luminescence dating and palaeomagnetic age constraint on hominins from Sima de los Huesos, Atapuerca, Spain. Journal of Human Evolution 67, 85-107.

Bailey, S., 2006. Beyond shovel-shaped incisors: Neandertal dental morphology in a comparative context. Periodicum Biologorum 108, 253-267.

Bailey, S.E., Lynch, J.M., 2005. Diagnostic differences in mandibular P4 shape between neandertals and anatomically modern humans. American Journal of Physical Anthropology 126, 268-277.

Bailey SE, Skinner MM, and Hublin JJ. 2011. What lies beneath? An evaluation of lower molar trigonid crest patterns based on both dentine and enamel expression. American Journal of Physical Anthropology 145(4):505-518.

Barkai, R. and Gopher. 2013. Cultural and biological transformations in the Middle Pleistocene Levant: A view from Qesem Cave, Israel. The Replacement of Neanderthals by Modern Humans series ('RNMH series'). Springer. Pp. 115-137.

Barkai R, Lemorini C, Shimelmitz R, Lev Z, Stiner MC, Gopher A (2009) A blade for all seasons? Making and using Amudian blades at Qesem Cave, Israel. Human Evolution 24(1):57-75

Barkai R, Gopher A, Solodenko N, Lemorini C (2013) An amudian oddity: A giant biface from late lower palaeolithic Qesem Cave. Tel Aviv 40(2):176-186

Benazzi, S., Fornai, C., Buti, L., Toussaint, M., Mallegni, F., Ricci, S., Gruppioni, G., Weber, G.W., Condemi, S., Ronchitelli, A., 2012. Cervical and crown outline analysis of worn Neanderthal and modern human lower second deciduous molars. Am J Phys Anthrop 149, 537-546.

Ben-Dor, M., Gopher, A., Hershkovitz, I., Barkai, R., 2011. Man the fat hunter: The demise of homo erectus and the emergence of a new hominin lineage in the middle pleistocene (ca. 400 kyr) Levant. PLoS ONE 6.

Bermúdez de Castro, J.M., Rosas, A., Nicolás, M.E., 1999. Dental remains from Atapuerca-TD6 (Gran Dolina site, Burgos, Spain). Journal of Human Evolution 37, 523-566.

Blasco, R., Rosell, J., Gopher, A. and Barkai, R. 2014. Subsistence economy and social life: A zooarchaeological view from the 300 kya central hearth at Qesem Cave, Israel. Journal of Anthropological Archaeology 35, 248–268.

Bookstein, F.L., 1978. The Measurement of Biological Shape and Shape Change. Lecture Notes in Biomathematics Vol. 24. Springer-Verlag., New York.

Bookstein, F.L., 1989. Principal warps: Thin plate splines and the decomposition of deformations. IEEE Trans. Pattern Anal. Machine Intelligence 11, 567-585.

Bookstein, F.L., 1991. Morphometric tools for landmark data: geometry and biology. [Orange Book]. Cambridge University Press., Cambridge, New York.

Buck, L.T., Stringer, C.B., 2014. Homo heidelbergensis. Current Biology 24, R214-R215.

Endicott, P., Ho, S.Y.W., Stringer, C., 2010. Using genetic evidence to evaluate four palaeoanthropological hypotheses for the timing of Neanderthal and modern human origins. Journal of Human Evolution 59, 87-95.

Gopher A, Ayalon A, Bar-Matthews M, Barkai R, Frumkin A, Karkanas P, Shahack-Gross R (2010) The chronology of the late Lower Paleolithic in the Levant based on U-Th ages of speleothems from Qesem Cave, Israel. Quaternary Geochronology 5(6):644-656

Gower, J.C., 1975. Generalized procrustes analysis. Psychometrika 40, 33-51.

Green, R.E., Krause, J., Briggs, A.W., Maricic, T., Stenzel, U., Kircher, M., Patterson, N., Li, H., Zhai, W., Fritz, M.H.Y., Hansen, N.F., Durand, E.Y., Malaspinas, A.S., Jensen, J.D., Marques-Bonet, T., Alkan, C., Prüfer, K., Meyer, M., Burbano, H.A., Good, J.M., Schultz, R., Aximu-Petri, A., Butthof, A., Höber, B., Höffner, B., Siegemund, M., Weihmann, A., Nusbaum, C., Lander, E.S., Russ, C., Novod, N., Affourtit, J., Egholm, M., Verna, C., Rudan, P., Brajkovic, D., Kucan, Ž., Gušic, I., Doronichev, V.B., Golovanova, L.V., Lalueza-Fox, C., De La Rasilla, M., Fortea, J., Rosas, A., Schmitz, R.W., Johnson,

P.L.F., Eichler, E.E., Falush, D., Birney, E., Mullikin, J.C., Slatkin, M., Nielsen, R., Kelso, J., Lachmann, M., Reich, D., Pääbo, S., 2010. A draft sequence of the neandertal genome. Science 328, 710-722.

Gómez-Robles, A., Martinón-Torres, M., Bermúdez de Castro, J.M., Prado, L., Sarmiento, S., Arsuaga, J.L., 2008. Geometric morphometric analysis of the crown morphology of the lower first premolar of hominins, with special attention to Pleistocene Homo. Journal of Human Evolution 55, 627-638.

Gould, S.J., 1977. Ontogeny and Phylogeny. Harvard University Press, Cambridge, MA.

Grün, R., Schwarcz, H.P., Ford, D.C., Hentzsch, B., 1988. ESR dating of spring deposited travertines. Quaternary Science Reviews 7, 429-432.

Gunz, P., Mitteroecker, P., Bookstein, F.L., 2005. Semilandmarks in three dimensions, in: Slice, D.E. (Ed.), Modern Morphometrics in Physical Anthropology. Kluwer Press, New York, pp. 73-98.

Gunz, P., Mitteroecker, P., 2013. Semilandmarks: A method for quantifying curves and surfaces. Hystrix 24.

Hammer, O., Harper, D.A.T., Ryan, P.D., 2001. PAST: Paleontological Statistics software package for education and data analysis. Palaeontologia Electronica 4, 9.

Hershkovitz, I., Smith, P., Sarig, R., Quam, R., Rodríguez, L., García, R., Arsuaga, J.L., Barkai, R., Gopher, A., 2011. Middle pleistocene dental remains from Qesem Cave (Israel). American Journal of Physical Anthropology 144, 575-592.

Hershkovitz, I., Weber, G.W., Fornai, C., Gopher, A., Barkai, R., Sloan, V., Quam, R., Yankel, G., Sarig, R., 2015. New Middle Pleistocene dental remains from Qesem cave (Israel). Quaternary International.

Karkanas, P., Shahack-Gross, R., Ayalon, A., Bar-Matthews, M., Barkai, R., Frumkin, A., Gopher, A. and Stiner, M.C. 2007. Evidence for Habitual Use of Fire at the End of the Lower Paleolithic: Site Formation Processes at Qesem Cave, Israel. Journal of Human Evolution 53, 197-212.

Krenn, V., 2015. Variation of 3D outer and inner crown morphology of lower premolars in modern humans. Masterthesis at the University of Vienna, Vienna.

Lucas, P.W., 2004. Dental Functional Morphology - How Teeth Work. Cambridge University Press, Cambridge.

Marcus, L.F., Corti, M., Loy, A., Naylor, G., Slice, D.E., 1996. Advances in morphometrics. [White Book]. Plenum Press, New York.

Martínez de Pinillos, M., Martinón-Torres, M., Skinner, M.M., Arsuaga, J.L., Gracia-Téllez, A., Martínez, I., Martín-Francés, L., Bermúdez de Castro, J.M., 2014. Trigonid crests expression in Atapuerca-Sima de los Huesos lower molars: Internal and external morphological expression and evolutionary inferences. Comptes Rendus - Palevol 13, 205-221.

Martinón-Torres, M., Bastir, M., Bermudez de Castro, J.M., Gomez, A., Sarmiento, S., Muela, A., Arsuaga, J.L., 2006. Hominin lower second premolar morphology: evolutionary inferences through geometric morphometric analysis. Journal of Human Evolution 50, 523-533.

Martinón-Torres, M., Dennell, R., Bermudez de Castro, J.M., 2011. The Denisova hominin need not be an out of Africa story. Journal of Human Evolution 60, 251-255.

Martinon-Torres M, Bermudez De Castro JM, Gomez-Robles A, Prado-Simon L, Arsuaga JL (2012) Morphological description and comparison of the dental remains from Atapuerca-Sima de los Huesos site (Spain). Journal of Human Evolution 62(1):7-58

Martinón-Torres M, Spěváčková P, Gracia-Téllez A, Martínez I, Bruner E, Arsuaga JL, and Bermúdez de Castro JM. 2013. Morphometric analysis of molars in a Middle Pleistocene population shows a mosaic of 'modern' and Neanderthal features. Journal of Anatomy 223(4):353-363.

Mercier N, Valladas H, FalguÃ¨res C, Shao Q, Gopher A, Barkai R, Bahain JJ, Vialettes L, Joron JL, Reyss JL (2013) New datings of Amudian layers at Qesem Cave (Israel): Results of TL applied to burnt flints and ESR/U-series to teeth. Journal of Archaeological Science 40(7):3011-3020

Meyer, M., Kircher, M., Gansauge, M.T., Li, H., Racimo, F., Mallick, S., Schraiber, J.G., Jay, F., Prüfer, K., De Filippo, C., Sudmant, P.H., Alkan, C., Fu, Q., Do, R., Rohland, N., Tandon, A., Siebauer, M., Green, R.E., Bryc, K., Briggs, A.W., Stenzel, U., Dabney, J., Shendure, J., Kitzman, J., Hammer, M.F., Shunkov, M.V., Derevianko, A.P., Patterson, N., Andrés, A.M., Eichler, E.E., Slatkin, M., Reich, D., Kelso, J., Pääbo, S., 2012. A high-coverage genome sequence from an archaic Denisovan individual. Science 338, 222-226.

Mitteroecker, P., Gunz, P., Bernhard, M., Schaefer, K., Bookstein, F.L., 2004. Comparison of cranial ontogenetic trajectories among great apes and humans. J Hum Evol 46, 679-697.

Molnar, S., 1971. Human tooth wear, tooth function and cultural variability. Am J Phys Anthrop 34, 175-189.

Parush, Y., Assaf, E., Slon, V., Gopher, A. and Barkai, R. 2015. Looking for Sharp Edges: Modes of Flint Recycling at Qesem Cave, Israel: Report on Work-in-Progress. Quaternary International. This volume.

Prüfer, K., Racimo, F., Patterson, N., Jay, F., Sankararaman, S., Sawyer, S., Heinze, A., Renaud, G., Sudmant, P.H., De Filippo, C., Li, H., Mallick, S., Dannemann, M., Fu, Q., Kircher, M., Kuhlwilm, M., Lachmann, M., Meyer, M., Ongyerth, M., Siebauer, M., Theunert, C., Tandon, A., Moorjani, P., Pickrell, J., Mullikin, J.C., Vohr, S.H., Green, R.E., Hellmann, I., Johnson, P.L.F., Blanche, H., Cann, H., Kitzman, J.O., Shendure, J., Eichler, E.E., Lein, E.S., Bakken, T.E., Golovanova, L.V., Doronichev, V.B., Shunkov, M.V., Derevianko, A.P., Viola, B., Slatkin, M., Reich, D., Kelso, J., Pääbo, S., 2014. The complete genome sequence of a Neanderthal from the Altai Mountains. Nature 505, 43-49.

Quam, R., Bailey, S., Wood, B., 2009. Evolution of M1 crown size and cusp proportions in the genus Homo. Journal of Anatomy 214, 655-670.

Reich, D., Green, R.E., Kircher, M., Krause, J., Patterson, N., Durand, E.Y., Viola, B., Briggs, A.W., Stenzel, U., Johnson, P.L.F., Maricic, T., Good, J.M., Marques-Bonet, T., Alkan, C., Fu, Q., Mallick, S., Li, H., Meyer, M., Eichler, E.E., Stoneking, M., Richards, M., Talamo, S., Shunkov, M.V., Derevianko, A.P., Hublin, J.J., Kelso, J., Slatkin, M., Pääbo, S., 2010. Genetic history of an archaic hominin group from Denisova cave in Siberia. Nature 468, 1053-1060.

Rightmire GP (2008) Homo in the middle pleistocene: Hypodigms, variation, and species recognition. Evolutionary Anthropology 17(1):8-21

Roebroeks W, Vill P (2011) On the earliest evidence for habitual use of fire in Europe. Proceedings of the National Academy of Sciences of the United States of America 108(13):5209-5214

Shahack-Gross R, Berna F, Karkanas P, Lemorini C, Gopher A, Barkai R (2014) Evidence for the repeated use of a central hearth at Middle Pleistocene (300ky ago) Qesem Cave, Israel. Journal of Archaeological Science 44(1):12-21

Shimelmitz, R., Barkai, R. and Gopher, A. 2011.Systematic blade production at late Lower Paleolithic (400-200 kyr) Qesem Cave, Israel. Journal of Human Evolution 61, 458-479.

Shimelmitz, R., Barkai, R. and Gopher, A. 2015. Regional Variability in Late Lower Paleolithic Amudian Blade Technology: Analyzing New Data from Qesem, Tabun and Yabrud I. Quaternary International. This volume.

Smith, F., 1984. Fossil hominids from the Upper Pleistocene of central Europe and the Origin of Modern Europeans., in: Smith, F., Spencer, F. (Eds.), The Origins of Modern Humans. Alan R. Liss, New York, pp. 137-209.

Stiner, M., Gopher, A. and Barkai, R. 2009.Cooperative Hunting and Meat Sharing 400-200 kya at Qesem Cave, Israel. Proceedings of the National Academy of Sciences U.S.A. 106, 13207-13212.

Stiner, M., Gopher, A. and Barkai, R. 2011.Hearth-Side Socioeconomics, Hunting and Paleoecology during the Late Lower Paleolithic at Qesem Cave, Israel. Journal of Human Evolution 60, 213-233.

Stringer, C., 2012. The status of Homo heidelbergensis (Schoetensack 1908). Evolutionary Anthropology 21, 101-107.

Suzuki, H., Takai, F., 1970. The Amud Man and his His Cave Site. University of Tokyo Press, Tokyo.

Trinkaus, E., 1984. Western Asia., in: Smith, F., Spencer, F. (Eds.), The Origins of Modern Humans. Alan R. Liss, New York, pp. 251-325.

Turner, C.G., R., N.C., Scott, G.R., 1991. Scoring procedures for key morphological traits of the permanent dentition: The Arizona State University Dental Anthropology System., in: Kelley, M., Larsen, C. (Eds.), Advances in dental anthropology. Wiley-Liss., New York, pp. 13-31.

van Asperen, E.N., 2012. Late Middle Pleistocene horse fossils from northwestern Europe as biostratigraphic indicators. Journal of Archaeological Science 39, 1974-1983.

Vlcek, E., 1993. Fossile Menschenfunde von Weimar-Ehringsdorf. Kommissionsverlag Konrad Theiss Verlag, Stuttgart.

Vlcek, E., Mania, D., Mania, U., 2002. Der fossile Mensch von Bilzingsleben. Beier & Beran, Weissbach.

Vlcek, E., 2011. Die Zähne des fossilen Menschen von Bilzingsleben. Praehistoria Thuringica. Langenweißbach: Beier und Beran 13, 80-122.

Wagner, G.A., Krbetschek, M., Degering, D., Bahain, J.J., Shao, Q., Falguères, C., Voinchet, P., Dolo, J.M., Garcia, T., Rightmire, G.P., 2010. Radiometric dating of the type-site for Homo heidelbergensis at Mauer, Germany. Proceedings of the National Academy of Sciences of the United States of America 107, 19726-19730.

Weber, G.W., 2015. Virtual Anthropology. Yearbook of Physical Anthropology DOI: 10.1002/ajpa.22658.

Weber, G.W., Bookstein, F.L., 2011. Virtual Anthropology - A Guide to a New Interdisciplinary Field. Springer Verlag. ISBN 978-3-211-48647-4, Wien, New York.

Wrangham, R., 2009. Catching Fire: How Cooking Made Us Human. Basic Books, New York.

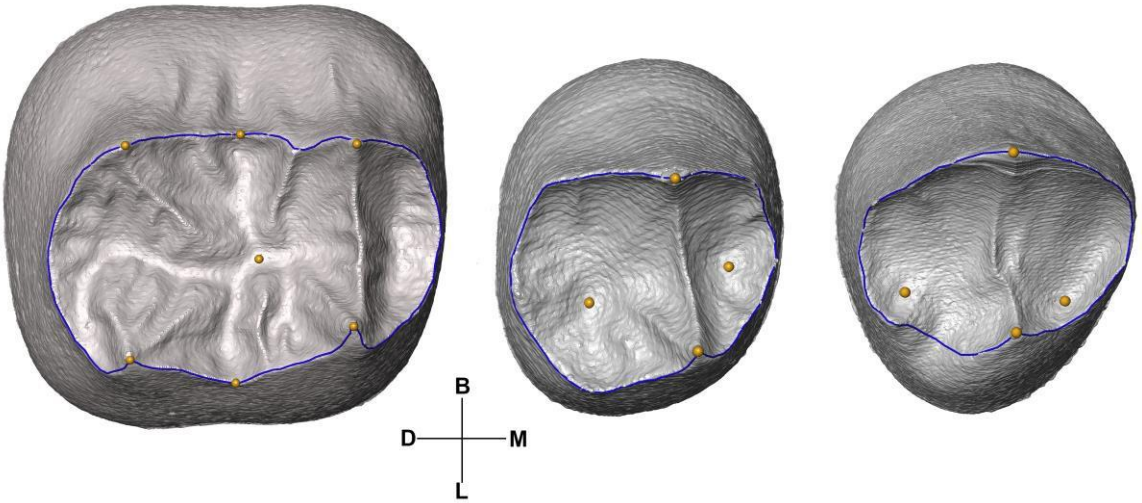

Fig. 1: Landmarks (yellow spheres) and curves (blue) on the EDJ of lower P_3s (right), P_4s (middle), and M_2s (left). All specimens represent the actual Qesem specimens, the right molar was mirrored to be a left one.
B – buccal; M – mesial; L – lingual; D - distal

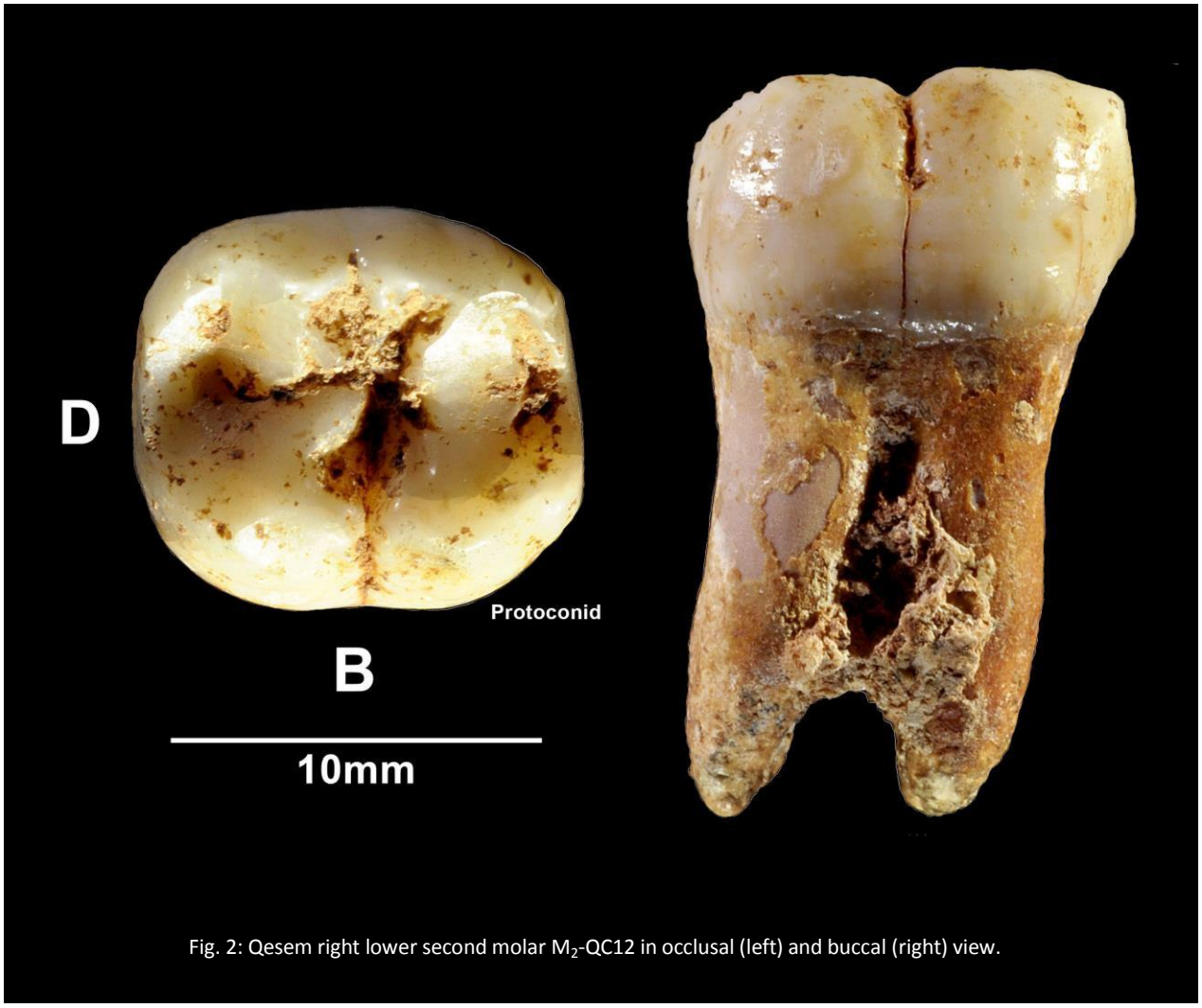

Fig. 2: Qesem right lower second molar M_2-QC12 in occlusal (left) and buccal (right) view.

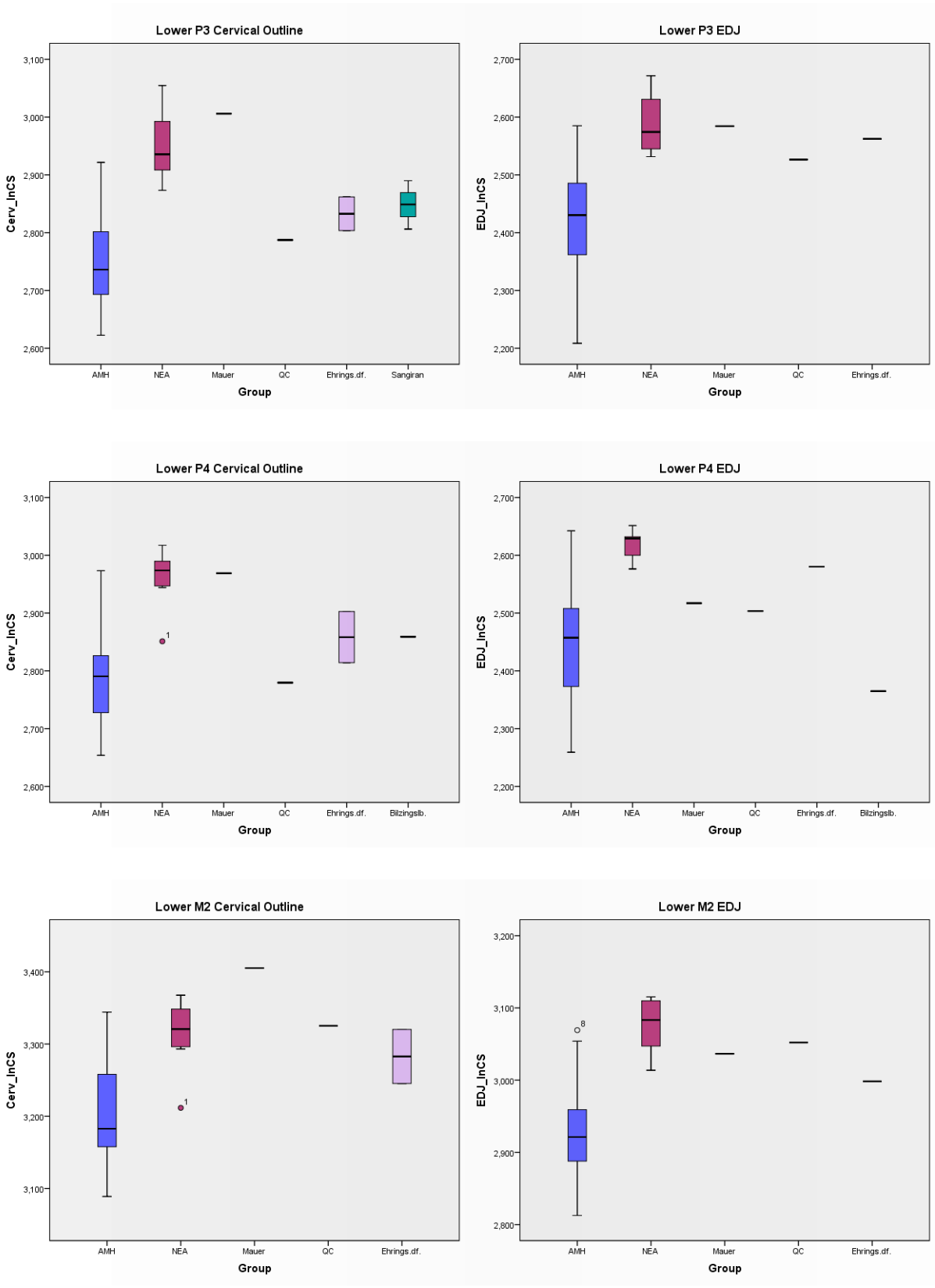

Fig. 3: ln Centroid Size for the three tooth types for cervical outlines and EDJ surface (crown outlines are not plotted here, but results are very similar to cervical outlines). No. 1 = Amud; no. 8 = Qafzeh 9

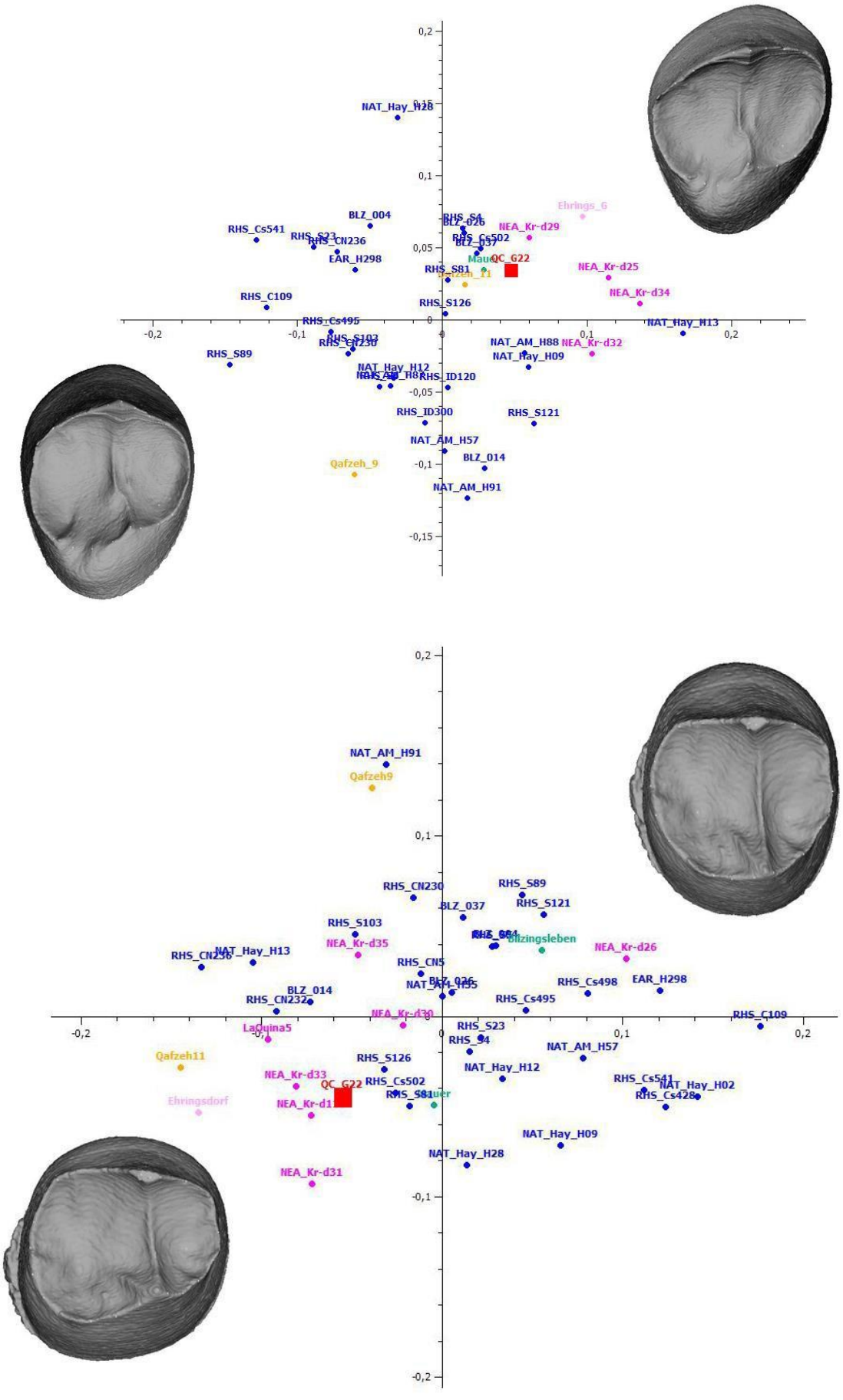

Fig. 4: PCA in shape space. Warped shapes (in each case the surface of a Qesem specimen) for PC -/- and PC+/+ (in panel A. and B.), respectively for PC-/+ and PC +/- (in panel C.) shown.

A. P_3 EDJ surface showing a neat but imperfect separation between AMH and NEA. Qesem and Mauer are at the fringes of the two groups.

B. P_4 EDJ surface showing a quite weak separation between AMH and NEA (see also NP-MANOVA Tab. 2).

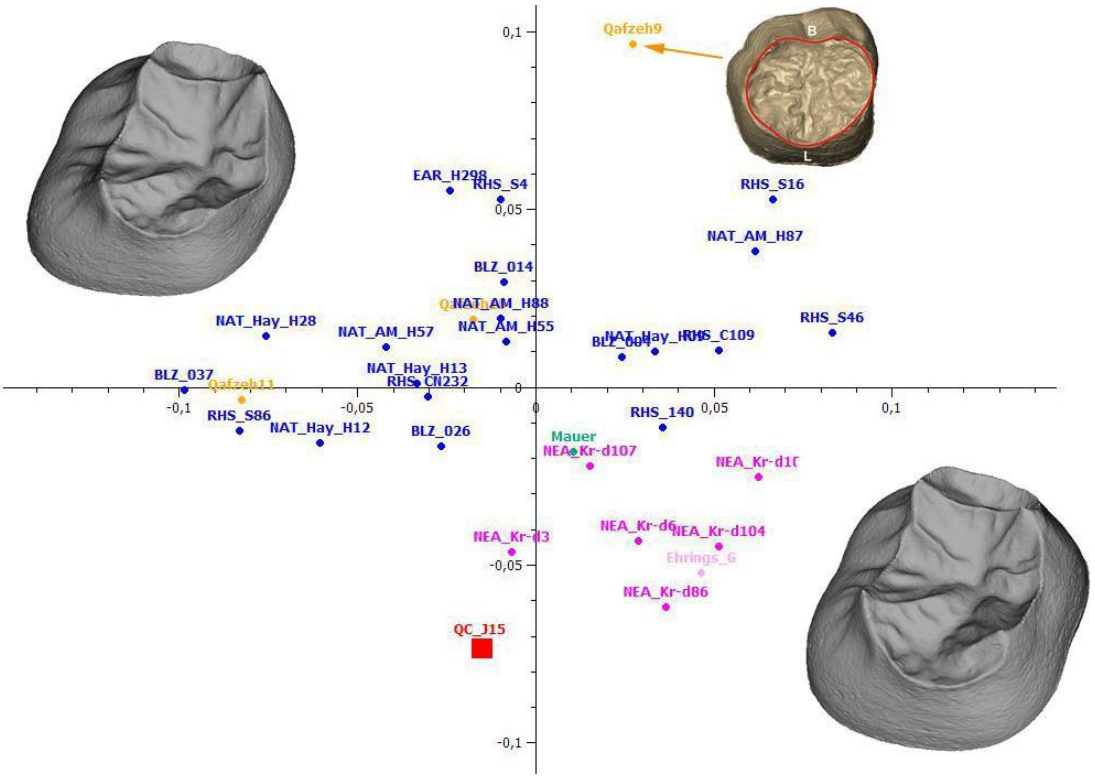

Fig 4C. M_2 EDJ shape with a perfect separation between AMH and NEA. Note the heart-shaped marginal ridge of Qafzeh 9.

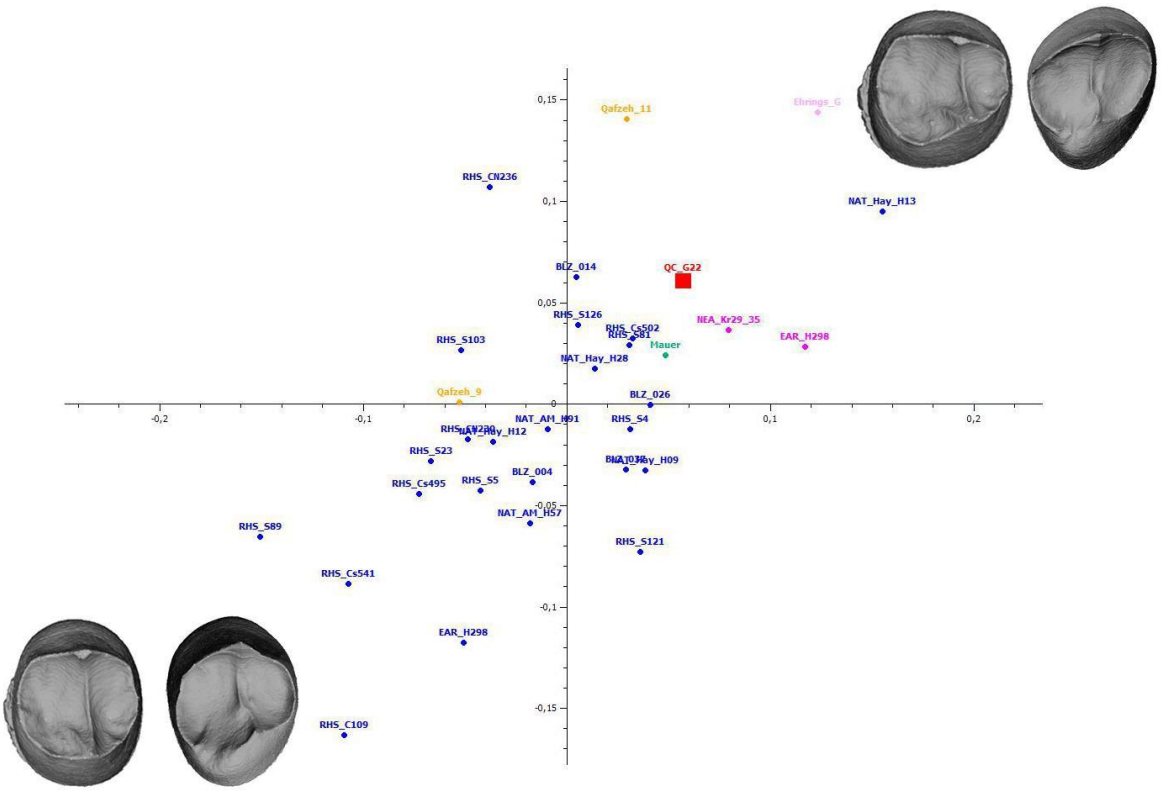

Fig. 5: PLS of EDJ shapes for P_3 (right of the each pair) and P_4 (left of each pair).

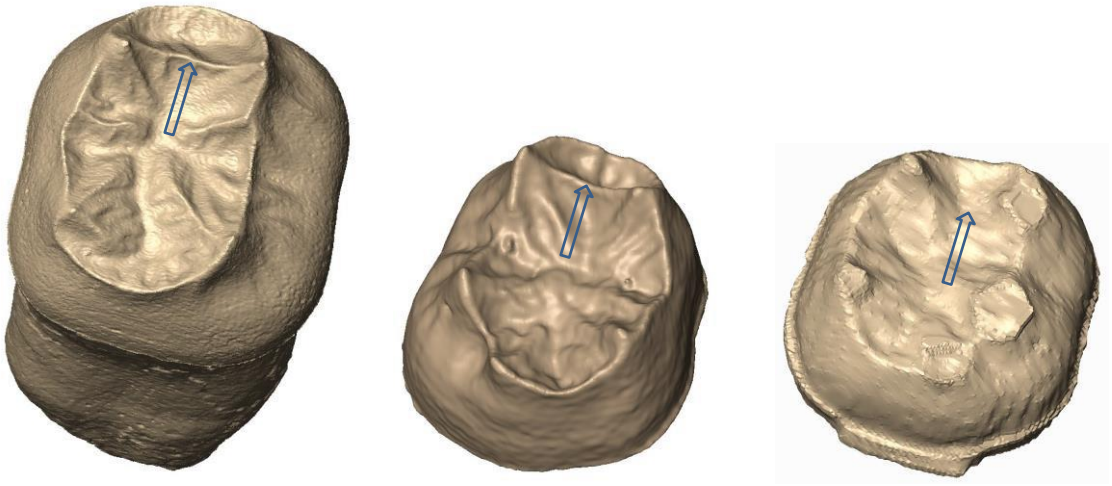

Fig. 6: The M_2 trigonid crest in Qesem (left), Ehringsdorf G (middle), and Mauer (right). Not to scale.

Tab.1: Sample composition Qesem Cave

Lower P3						Lower P4						Lower M2					
Abbrev.	Specimen	Taxon	Cerv	Crown	EDJ	Abbrev.	Specimen	Taxon	Cerv	Crown	EDJ	Abbrev.	Specimen	Taxon	Cerv	Crown	EDJ
Early and Middle Pleistocene																	
QC_G22	P3-QC9	Indetermined	x	x	x	QC_G22	P4-QC10	Indetermined	x	x	x	QC_J15	M2-QC12	Indetermined	x	x	x
Mauer	Mauer Heidelberg	*H. heidelbergensis*	x	x	x	Mauer	Mauer Heidelberg	*H. heidelbergensis*	x	x	x	Mauer	Mauer Heidelberg	*H. heidelbergensis*	x	x	x
SMF-S7-25	Sangiran S7-25	*H. erectus*	x	x		Bilzingslb	Bilzingsleben E6	*?H. heidelbergensis*	x	x	x						
SMF-S7-26	Sangiran S7-26	*H. erectus*	x	x													
SMF-S7-69	Sangiran S7-69	*H. erectus*	x	x													
Ehrings_F	Ehringsdorf F	*?Proto-Neanderthal*	x	x		Ehrings_F	Ehringsdorf F	*?Proto-Neanderthal*	x			Ehrings_F	Ehringsdorf F	*?Proto-Neanderthal*	x		
Ehrings_G	Ehringsdorf G	*?Proto-Neanderthal*	x	x	x	Ehrings_G	Ehringsdorf G	*?Proto-Neanderthal*	x	x	x	Ehrings_G	Ehringsdorf G	*?Proto-Neanderthal*	x	x	x
Late Pleistocene and Holocene																	
Amud1	Amud 1	*H. neanderthalensis*	x	x		Amud1	Amud 1	*H. neanderthalensis*	x	x		Amud1	Amud 1	*H. neanderthalensis*	x	x	
LaQuina5	La Quina H5	*H. neanderthalensis*	x	x		LaQuina5	La Quina H5	*H. neanderthalensis*	x	x	x	Kebara2	Kebara 2	*H. neanderthalensis*	x	x	
NEA_Kr-d25	Krapina 25	*H. neanderthalensis*	x	x	x	NEA_Kr-d26	Krapina 26	*H. neanderthalensis*	x	x	x	LaQuina5	La Quina H5	*H. neanderthalensis*	x	x	
NEA_Kr-d27	Krapina 27	*H. neanderthalensis*	x	x		NEA_Kr-d30	Krapina 30	*H. neanderthalensis*	x	x	x	Tabun2	Tabun 2	*H. neanderthalensis*	x		
NEA_Kr-d28	Krapina 28	*H. neanderthalensis*	x	x		NEA_Kr-d31	Krapina 31	*H. neanderthalensis*	x	x	x	NEA_Kr-d2	Krapina 2	*H. neanderthalensis*	x	x	
NEA_Kr-d29	Krapina 29	*H. neanderthalensis*	x	x	x	NEA_Kr-d33	Krapina 33	*H. neanderthalensis*	x	x	x	NEA_Kr-d3	Krapina 3	*H. neanderthalensis*	x		x
NEA_Kr-d32	Krapina 32	*H. neanderthalensis*	x	x	x	NEA_Kr-d35	Krapina 35	*H. neanderthalensis*	x	x	x	NEA_Kr-d6	Krapina 6	*H. neanderthalensis*	x	x	x
NEA_Kr-d34	Krapina 34	*H. neanderthalensis*	x	x	x	NEA_Kr-d113	Krapina 113	*H. neanderthalensis*	x	x	x	NEA_Kr-d10	Krapina 10	*H. neanderthalensis*	x	x	x
Qafzeh9	Qafzeh 9	Anat. Modern *Homo*	x	x	x	Qafzeh9	Qafzeh 9	Anat. Modern *Homo*	x	x	x	NEA_Kr-d86	Krapina 86	*H. neanderthalensis*	x	x	x
Qafzeh11	Qafzeh 11	Anat. Modern *Homo*	x	x	x	Qafzeh11	Qafzeh 11	Anat. Modern *Homo*	x	x	x	NEA_Kr-d104	Krapina 104	*H. neanderthalensis*	x	x	x
NAT_AM57	Ain Mallaha 57	*Natufian, Israel*	x	x	x	NAT_AM55	Ain Mallaha 55	*Natufian, Israel*	x	x	x	NEA_Kr-d107	Krapina 107	*H. neanderthalensis*	x	x	x
NAT_AM87	Ain Mallaha 87	*Natufian, Israel*	x	x	x	NAT_AM57	Ain Mallaha 57	*Natufian, Israel*	x	x	x	Ohalo1	Ohalo 1	Anat. Modern *Homo*	x		
NAT_AM88	Ain Mallaha 88	*Natufian, Israel*			x	NAT_AM91	Ain Mallaha 91	*Natufian, Israel*	x		x	Ohalo2	Ohalo 2	Anat. Modern *Homo*	x	x	
NAT_AM91	Ain Mallaha 91	*Natufian, Israel*	x	x	x	NAT_Hay02	Hayonim 02	*Natufian, Israel*	x	x	x	Qafzeh9	Qafzeh 9	Anat. Modern *Homo*	x	x	x
NAT_Hay02	Hayonim 02	*Natufian, Israel*	x	x		NAT_Hay09	Hayonim 09	*Natufian, Israel*	x	x	x	Qafzeh11	Qafzeh 11	Anat. Modern *Homo*	x	x	x
NAT_Hay09	Hayonim 09	*Natufian, Israel*	x	x	x	NAT_Hay12	Hayonim 12	*Natufian, Israel*	x	x	x	Qafzeh15	Qafzeh 15	Anat. Modern *Homo*	x	x	x
NAT_Hay12	Hayonim 12	*Natufian, Israel*	x	x	x	NAT_Hay13	Hayonim 13	*Natufian, Israel*	x	x	x	NAT_AM55	Ain Mallaha 55	*Natufian, Israel*	x	x	x
NAT_Hay13	Hayonim 13	*Natufian, Israel*	x	x	x	NAT_Hay28	Hayonim 28	*Natufian, Israel*	x	x	x	NAT_AM57	Ain Mallaha 57	*Natufian, Israel*	x	x	x
NAT_Hay28	Hayonim 28	*Natufian, Israel*	x	x	x	RHS_C109	Modern Homo	Recent, Australia	x	x	x	NAT_AM87	Ain Mallaha 87	*Natufian, Israel*	x	x	x
RHS_C109	Modern Homo	Recent, Australia	x	x	x	RHS_CN5	Modern Homo	Recent, Papua-NG	x	x	x	NAT_AM88	Ain Mallaha 88	*Natufian, Israel*			x
RHS_CN5	Modern Homo	Recent, Papua-NG	x	x		RHS_CN230	Modern Homo	Recent, Papua-NG	x	x	x	NAT_AM91	Ain Mallaha 91	*Natufian, Israel*	x	x	
RHS_CN230	Modern Homo	Recent, Papua-NG	x	x	x	RHS_CN232	Modern Homo	Recent, Papua-NG	x	x	x	NAT_Hay02	Hayonim 02	*Natufian, Israel*	x	x	
RHS_CN232	Modern Homo	Recent, Papua-NG	x	x		RHS_CN236	Modern Homo	Recent, Papua-NG	x	x	x	NAT_Hay09	Hayonim 09	*Natufian, Israel*			x
RHS_CN236	Modern Homo	Recent, Papua-NG	x	x	x	RHS_Cs428	Modern Homo	Historic, Europe	x	x	x	NAT_Hay12	Hayonim 12	*Natufian, Israel*	x	x	x
RHS_Cs428	Modern Homo	Historic, Europe	x	x		RHS_Cs495	Modern Homo	Historic, Europe	x	x	x	NAT_Hay13	Hayonim 13	*Natufian, Israel*	x	x	x
RHS_Cs495	Modern Homo	Historic, Europe	x	x	x	RHS_Cs498	Modern Homo	Historic, Europe	x	x	x	NAT_Hay28	Hayonim 28	*Natufian, Israel*	x	x	x
RHS_Cs498	Modern Homo	Historic, Europe	x	x		RHS_Cs502	Modern Homo	Historic, Europe	x	x	x	RHS_C109	Modern Homo	Recent, Australia	x	x	x
RHS_Cs502	Modern Homo	Historic, Europe	x	x	x	RHS_Cs541	Modern Homo	Historic, Europe	x	x	x	RHS_CN232	Modern Homo	Recent, Papua-NG	x	x	x
RHS_Cs541	Modern Homo	Historic, Europe	x	x	x	RHS_S4	Modern Homo	Recent, Africa	x	x	x	RHS_140	Modern Homo	Recent, Europe	x	x	x
RHS_ID120	Modern Homo	Recent, Europe	x	x	x	RHS_S5	Modern Homo	Recent, Africa	x	x	x	RHS_S4	Modern Homo	Recent, Africa	x	x	x
RHS_ID300	Modern Homo	Recent, Europe	x	x	x	RHS_S23	Modern Homo	Recent, Africa	x	x	x	RHS_S16	Modern Homo	Recent, Africa	x	x	x
RHS_S4	Modern Homo	Recent, Africa	x	x	x	RHS_S81	Modern Homo	Recent, Africa	x	x	x	RHS_S46	Modern Homo	Recent, Africa	x	x	x
RHS_S5	Modern Homo	Recent, Africa	x	x	x	RHS_S89	Modern Homo	Recent, Africa	x	x	x	RHS_S86	Modern Homo	Recent, Africa	x	x	x
RHS_S23	Modern Homo	Recent, Africa	x	x	x	RHS_S103	Modern Homo	Recent, Africa	x	x	x	RHS_S126	Modern Homo	Recent, Africa	x	x	
RHS_S81	Modern Homo	Recent, Africa	x	x	x	RHS_S121	Modern Homo	Recent, Africa	x	x	x	BLZ_004	Modern Homo	Recent, Bedouin	x	x	x
RHS_S89	Modern Homo	Recent, Africa	x	x	x	RHS_S126	Modern Homo	Recent, Africa	x	x	x	BLZ_014	Modern Homo	Recent, Bedouin	x	x	x
RHS_S103	Modern Homo	Recent, Africa	x	x	x	BLZ_004	Modern Homo	Recent, Bedouin	x	x	x	BLZ_026	Modern Homo	Recent, Bedouin	x	x	x
RHS_S121	Modern Homo	Recent, Africa	x	x	x	BLZ_014	Modern Homo	Recent, Bedouin	x	x	x	BLZ_037	Modern Homo	Recent, Bedouin	x	x	x
RHS_S126	Modern Homo	Recent, Africa	x	x	x	BLZ_026	Modern Homo	Recent, Bedouin	x	x	x	EAR_H298	Modern Homo	Recent, Bedouin	x	x	x
BLZ_004	Modern Homo	Recent, Bedouin	x	x	x	BLZ_037	Modern Homo	Recent, Bedouin	x	x	x						
BLZ_014	Modern Homo	Recent, Bedouin	x	x	x	EAR_H298	Modern Homo	Recent, Bedouin	x	x	x						
BLZ_026	Modern Homo	Recent, Bedouin	x	x	x												
BLZ_037	Modern Homo	Recent, Bedouin	x	x	x												
EAR_H298	Modern Homo	Recent, Bedouin	x	x	x												

Table 2 – Results for the three traits of all three tooth types for QC and some selected Early, Mid, and Late Pleistocene specimens. The first five nearest neighbors (based on full Procrustes distances in shape space) of specimens (blue – AMH, pink – NEA, green – Early to Mid Pleistocene hominins) and the results of the linear discriminant analysis (LDA; % of correct classifications for AMH and NEA, classification for the respective specimen, probability for classification Ppost) are given.

P3 Cervical OL	QC	Mauer	Sangiran S7-25	Qafzeh 9	Qafzeh 11	Amud 1	Ehringsdorf G
	RHS_S121	NEA_Kr-d27	RHS_S23	NAT_AM_H57	RHS_Cs498	NAT_AM_H57	NEA_Kr-d28
	RHS_Cs541	Ehrings_F	SMF-S7-26	BLZ_014	BLZ_014	BLZ_004	NEA_Kr-d27
	EAR_H298	RHS_S121	RHS_S4	NAT_AM_H91	RHS_CN230	RHS_S89	Ehrings_F
	NAT_Hay_H02	NEA_Kr-d32	RHS_S5	RHS_S81	RHS_S103	RHS_S81	SMF-S7-25
	NEA_Kr-d29	RHS_S4_LP3	RHS_S126	Amud1	RHS_ID_300	EAR_H298	RHS_S121
Classif. LDA (100.0%, 87,5%)	AMH (Ppost=0.999)	NEA (Ppost=0.723)	AMH (Ppost=0.996)	AMH (Ppost=1.000)	AMH (Ppost=1.000)	AMH (Ppost=0.611)	NEA (Ppost=0.768)
P3 Crown OL	QC	Mauer	Sangiran S7-25	Qafzeh 9	Qafzeh 11	Amud 1	Ehringsdorf G
	RHS_S89	RHS_Cs498	SMF-S7-26	NAT_AM_H87	NAT_Hay_H02	Qafzeh_11	RHS_CN232
	NAT_AM_H87	NEA_Kr-d27	RHS_Cs541	NAT_Hay_H02	RHS_S5	NAT_AM_H91	RHS_S4
	Qafzeh9	NAT_HayH13	NAT_Hay_H09	RHS_S89	RHS_Cs502	NAT_Hay_H02	BLZ_026
	Amud1	NEA_Kr-d25	RHS_S23	NAT_AM_H57	Amud1	NAT_AM_H87	NEA_Kr-d29
	NAT_Hay_H02	BLZ_004	BLZ_037	RHS_ID_120	RHS_S103	RHS_CN230	NEA_Kr-d28
Classif. LDA (97.1%, 100.0%)	NEA (Ppost=0.519)	NEA (Ppost=0.943)	AMH (Ppost=1.000)	AMH (Ppost=1.000)	AMH (Ppost=0.739)	NEA (Ppost=0.930)	NEA (Ppost=0.535)
P3 EDJ	QC	Mauer	Sangiran S7-25	Qafzeh 9	Qafzeh 11	Amud 1	Ehringsdorf G
	RHS_S126	RHS_S81	-	RHS_CN230	BLZ_037	-	NEA_Kr-d29
	NEA_Kr-d29	BLZ_037	-	RHS_S5	RHS_S4	-	NEA_Kr-d25
	RHS_Cs502	NEA_Kr-d29	-	RHS_ID300	RHS_Cs502	-	NEA_Kr-d34
	NEA_Kr-d32	Qafzeh_11	-	NAT_AM_H57	RHS_S81	-	BLZ_026
	Ehrings_G	BLZ_026	-	NAT_AM_H91	BLZ_004	-	NEA_Kr-d32
Classif. LDA (96.8%, 100.0%)	AMH (Ppost=0.559)	AMH (Ppost=0.983)	-	AMH (Ppost=1.000)	AMH (Ppost=1.000)	-	NEA (Ppost=1.000)
P4 Cervical OL	QC	Mauer	Bilzingsleben E6	Qafzeh 9	Qafzeh 11	Amud 1	Ehringsdorf G
	Mauer	Bilzingsleben	Mauer	BLZ_014	NAT_AM_H57	RHS_S4	Ehrings_F
	Bilzingsleben	NEA_Kr-d26	QC_G22	BLZ_037	BLZ_014	NAT_Hay_H13	NEA_Kr-d113
	NEA_Kr-d30	NEA_Kr-d33	NEA_Kr-d33	RHS_CN232	NAT_AM_H55	NAT_Hay_H02	RHS_S89
	NEA_Kr-d33	QC_G22	NEA_Kr-d26	RHS_Cs428	LaQuina5	LaQuina5	NAT_Hay_H13
	NEA_Kr-d113	NEA_Kr-d113	NEA_Kr-d113	NAT_AM_H91	RHS_S23	NAT_Hay_H28	NEA_Kr-d33
Classif. LDA (93.8%, 100.0%)	NEA (Ppost=0.997)	NEA (Ppost=0.986)	NEA (Ppost=0.993)	AMH (Ppost=1.000)	AMH (Ppost=1.000)	NEA (Ppost=0.921)	NEA (Ppost=0.996)
P4 Crown OL	QC	Mauer	Bilzingsleben E6	Qafzeh 9	Qafzeh 11	Amud 1	Ehringsdorf G
	NAT_Hay_H28	NAT_HayH13	NEA_Kr-d33	RHS_S23	LaQuina5	Ehrings_G	Amud1
	BLZ_026	RHS_S103	EAR_H298	RHS_Cs495	NAT_AM_H57	NAT_Hay_H12	NEA_Kr-d113
	RHS_C109	NEA_Kr-d33	Mauer	BLZ_037	BLZ_004	Qafzeh_11	LaQuina5
	RHS_Cs541	RHS_S4	NAT_Hay_H13	RHS_Cs541	RHS_Cs498	RHS_Cs498	RHS_Cs498
	NAT_AM_H55	NAT_HayH28	RHS_S4	BLZ_004	NAT_Hay_H12	LaQuina5	Qafzeh_11
Classif. LDA (93.8%, 100.0%)	NEA (Ppost=0.914)	AMH (Ppost=0.598)	AMH (Ppost=0.991)	AMH (Ppost=0.976)	AMH (Ppost=0.981)	NEA (Ppost=0.894)	NEA (Ppost=1.000)
P4 EDJ	QC	Mauer	Bilzingsleben E6	Qafzeh 9	Qafzeh 11	Amud 1	Ehringsdorf G
	RHS_Cs502	NAT_HayH12	NAT_AM_H57	RHS_CN5	Ehrings_G	-	NEA_Kr-d33
	RHS_S81	RHS_S81	RHS_S5	BLZ_004	BLZ_014	-	NEA_Kr-d113
	NEA_Kr-d33	RHS_Cs502	NAT_Hay_H12	RHS_S89	NEA_Kr-d33	-	Qafzeh11
	Mauer	QC_G22	BLZ_026	NEA_Kr-d35	RHS_CN232	-	RHS_CN232
	BLZ_014	NEA_Kr-d33	RHS_Cs498	BLZ_037	RHS_CN236	-	QC_G22
Classif. LDA (97.0%, 100.0%)	AMH (Ppost=0.832)	NEA (Ppost=0.997)	NEA (Ppost=0.827)	AMH (Ppost=1.000)	AMH (Ppost=0.980)	-	NEA (Ppost=0.570)
M2 Cervical OL	QC	Mauer	Ohalo 1	Qafzeh 9	Qafzeh 11	Amud 1	Ehringsdorf G
	Tabun2	NEA_Kr-d86	NAT_Hay_H28	BLZ_014	Qafzeh_15	LaQuina5	NEA_Kr-d86

	NEA_Kr-d10	NEA_Kr-d3	RHS_S4	RHS_140	RHS_S86	RHS_S46	Ehrings_F
	NEA_Kr-d104	BLZ_026	Qafzeh11	RHS_S46	RHS_S4	Qafzeh_15	Tabun2
	NEA_Kr-d2	Ehrings_F	NEA_Kr-d107	RHS_S86	BLZ_014	NEA_Kr-d107	QC_J15
	NEA_Kr-d6	NAT_HayH13	EAR_H298	Qafzeh11	NAT_AM_H55	RHS_S4	Kebara2
Classif. LDA (96.2%, 90.9%)	NEA (Ppost=0.984)	NEA (Ppost=1.000)	NEA (Ppost=0.862)	AMH (Ppost=1.000)	AMH (Ppost=0.997)	NEA (Ppost=0.970)	NEA (Ppost=0.991)
M2 Crown OL	QC	Mauer	Ohalo 1	Qafzeh 9	Qafzeh 11	Amud 1	Ehringsdorf G
	NEA_Kr-d6	NEA_Kr-d104	Qafzeh11	RHS_140	RHS_S86	RHS_S4	NEA_Kr-d86
	RHS_S86	NEA_Kr-d10	NAT_AM_H55	Qafzeh11	NAT_AM_H55	LaQuina5	Mauer
	NEA_Kr-d2	BLZ_026	RHS_S86	NAT_AM_H55	Kebara2	BLZ_026	Qafzeh15
	Kebara2	NEA_Kr-d6	EAR_H298	Kebara2	BLZ_014	Kebara2	NAT_Hay_H28
	Qafzeh11	RHS_S16	BLZ_014	RHS_S86	RHS_S126	BLZ_037	NEA_Kr-d104
Classif. LDA (92.0%, 88.9%)	NEA (Ppost=0.994)	NEA (Ppost=0.968)	AMH (Ppost=1.000)	AMH (Ppost=0.961)	AMH (Ppost=0.982)	NEA (Ppost=0.773)	NEA (Ppost=0.989)
M2 EDJ	QC	Mauer	Ohalo 1	Qafzeh 9	Qafzeh 11	Amud 1	Ehringsdorf G
	NEA_Kr-d3	NAT_HayH13	-	RHS_S16	RHS_S86	-	NEA_Kr-d86
	NEA_Kr-d86	QC_J15	-	BLZ_014	NAT_Hay_H13	-	NEA_Kr-d104
	Ehrings_G	Qafzeh15	-	EAR_H298	BLZ_026	-	NEA_Kr-d6
	NAT_Hay_H13	NEA_Kr-d86	-	RHS_S4	NAT_Hay_H12	-	QC_J15
	BLZ_026	Ehrings_G	-	NAT_AM_H87	NAT_AM_H55	-	NEA_Kr-d10
Classif. LDA (100.0%, 100.0%)	NEA (Ppost=1.000)	AMH (Ppost=1.000)	-	AMH (Ppost=1.000)	AMH (Ppost=1.000)	-	NEA (Ppost=1.000)

Research Article for "Quaternary International"

The Qesem Cave hominin material (part 1): A morphometric analysis of the mandibular premolars and molar.

Supplementary Information

a)

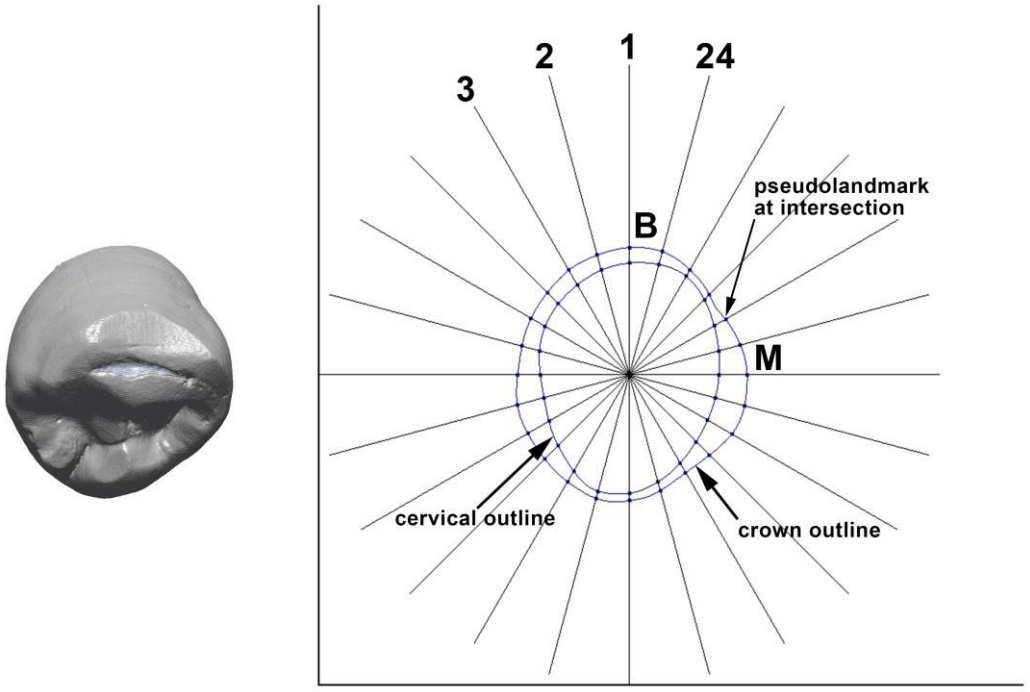

b)

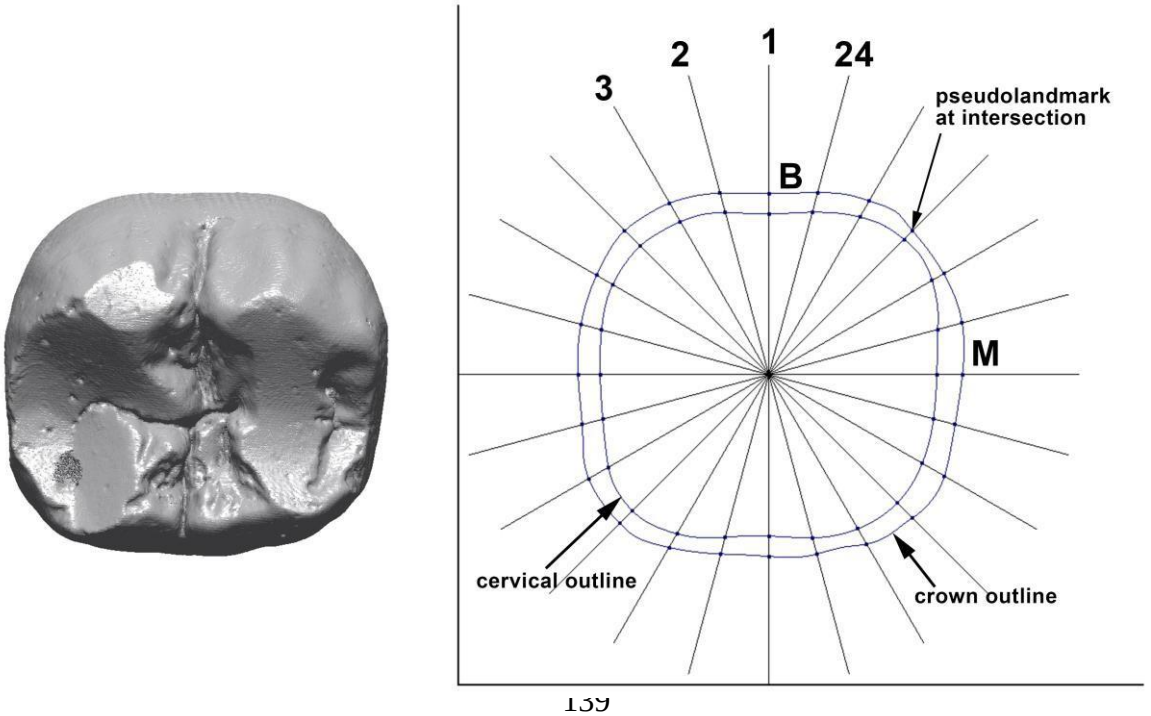

139

Fig. S1: 24 pseudolandmarks of the cervical and crown oulines for a) premolars (here Qesem P_3) and b) molars (here Qesem M_2). The procedure follows Benazzi et al. 2012, with the modification of digitizing 24 instead of 16 points per outline.

Tab. S1: Non-parametric Manova, Euclidean distance, significant differences AMH vs. NEA (9999 permutations, p-values above the 1% level in grey)						
P3	**Shape**	**F**	**p**	**Form**	**F**	**p**
	Cervical	9.962	0.0001	Cervical	37.230	0.0001
	Crown	3.378	0.0119	Crown	24.91	0.0001
	EDJ	4.645	0.0004	EDJ	7.949	0.0001
P4	**Shape**	**F**	**p**	**Form**	**F**	**p**
	Cervical	9.900	0.0001	Cervical	31.760	0.0001
	Crown	3.324	0.0128	Crown	12.35	0.0007
	EDJ	2.394	0.0328	EDJ	9.289	0.0001
M2	**Shape**	**F**	**p**	**Form**	**F**	**p**
	Cervical	6.992	0.0001	Cervical	21.180	0.0001
	Crown	3.064	0.0085	Crown	19.520	0.0003
	EDJ	3.824	0.0006	EDJ	11.530	0.0001

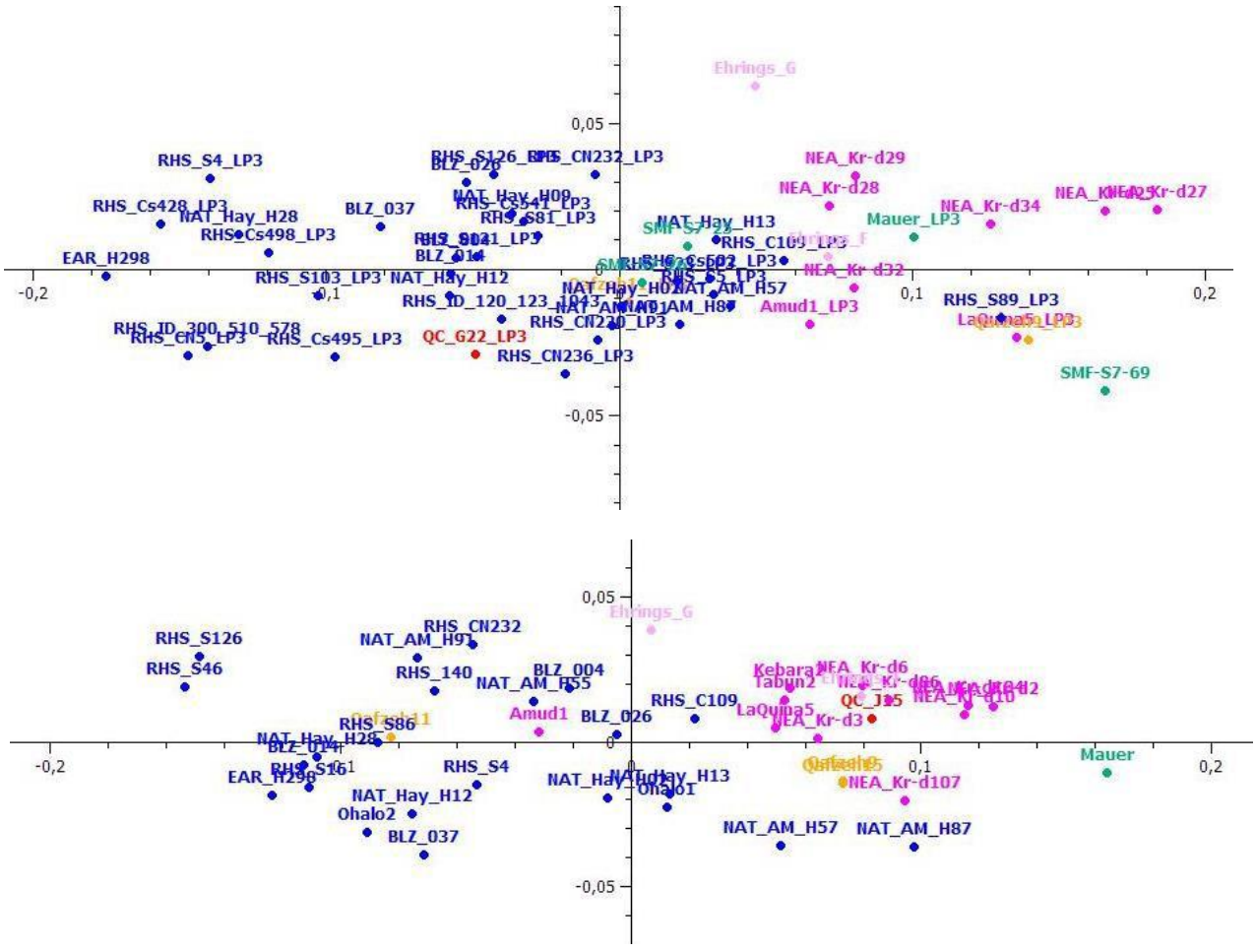

Fig.S2: Two examples of form space: P3 crown outline (top) with Qesem perfectly in the AMH distribution, and M2 cervical outline (below) where Qesem, Mauer, and Qafzeh cluster with Neanderthals due to their large size.

2.8. Dental stigmata and enamel thickness in a probable case of congenital syphilis from XVI century Croatia.

Lauc T., Fornai C., Premužić Z., Vodanović M., Weber, G. W., Mašić B., Rajić Šikanjić P.

Archives of Oral Biology In revision (Submitted: 04/02/2015, accepted: 03/07/2015)

Synopsis

The current chapter focuses on an archeological case showing dental stigmata for congenital syphilis. It reports the qualitative description of the dental remains aided by the acquisition of µCT images, and the analysis of the enamel thickness of both first molars (showing alteration of the enamel cap) and second molars (normally developed). The protocols used for the investigation of dental tissues were designed for taxonomic purposes as described in chapters 2.4 and 2.5. In this case, the exploration of the enamel thickness was carried out to quantify for the first time the effects of the treponemal infection on the first (mulberry) molars in comparison to non-pathological individuals.

Contribution

Contribution to the study design, data collection, interpretation of the data, drafting and editing of the manuscript.

Elsevier Editorial System(tm) for Archives of Oral Biology
Manuscript Draft

Manuscript Number: AOB-D-15-00054R1

Title: Dental stigmata and enamel thickness in a probable case of congenital syphilis from XVI century Croatia

Article Type: Original Paper

Keywords: enamel defects; Fournier canine; hypoplasia; mulberry molars; micro-CT

Corresponding Author: Dr. Petra Rajić Šikanjić,

Corresponding Author's Institution: Institute for Anthropological Research

First Author: Tomislav Lauc

Order of Authors: Tomislav Lauc; Cinzia Fornai; Zrinka Premužić; Marin Vodanović; Gerhard Weber; Boris Mašić; Petra Rajić Šikanjić

Abstract: Objective: To analyse the dental remains of an individual with signs of congenital syphilis by using macroscopic observation, CBCT and micro-CT images, and the analysis of the enamel thickness.
Design: Anthropological analysis of human skeletal remains from the 16th century archaeological site Park Grič in Zagreb, Croatia discovered a female, 17 to 20 years old at the time of death, with dental signs supportive of congenital syphilis: mulberry molars and canine defects, as well as non-specific hypoplastic changes on incisors. The focus of the analysis was on three aspects: gross morphology; hypoplastic defects of the molars, canines and incisors, as well as enamel thickness of the upper first and second molars.
Results: The observed morphology of the first molars corresponds to the typical aspect of mulberry molars, while that of the canines is characterised by hypomineralization. Hypoplastic grooves were observed on the incisal edges of all incisors. The enamel of the first molars is underdeveloped while in the second molars a thick-enamelled condition is observed.
Conclusions: Our observations for the dental and skeletal evidence are supportive to a diagnosis of congenital syphilis for this specimen from XVI century Croatia. The use of CT imaging helped documenting the diagnostic features and quantifying the effect of the dental stigmata on first molars.

Suggested Reviewers:

***Conflict of Interest Form**

Journal:	**Author name**:
Archives of Oral Biology	Tomislav Lauc etal

Declarations

The following additional information is required for submission. Please note that failure to respond to these questions/statements will mean your submission will be returned to you. If you have nothing to declare in any of these categories then this should be stated.

Please state any conflict of interests. A conflict of interest exists when an author or the author's institution has financial or personal relationships with other people or organisations that inappropriately influence (bias) his or her actions. Financial relationships are easily identifiable, but conflicts can also occur because of personal relationships, academic competition, or intellectual passion. A conflict can be actual or potential, and full disclosure to The Editor is the safest course.

There are no conflicts of interest to declare

Please state any sources of funding for your research

Research was supported by the Ministry of Science, Education and Sport of the Republic of Croatia (Project no. 196-1962766-2740), AERS Dental Medical Organizations, Vienna, Austria, and the Sigfried Ludwig - Rudolf Slavicek Foundation, Vienna, Austria.

Please state whether Ethical Approval was given, by whom and the relevant Judgement's reference number

No Ethical Approval was needed giving that presented material is from an archaeological site.

If you are submitting a Randomized Controlled Trial, please state the International Standard Randomised Controlled Trial Number **(ISRCTN)**

Authors contribution (if count of Authors =>4)

All authors have made substantial contributions to the manuscript as follows:

Tomislav Lauc - the conception and design of the study, interpretation of data

Cinzia Fornai - CBCT and micro-CT scanning and analyses and enamel thickness, interpretation of data, drafting and editing the manuscript

Zrinka Premužić – anthropological analysis, drafting and revising of the manuscript

Marin Vodanović - performed morphological analysis of the dental remains

Gerhard W. Weber - CBCT and micro-CT scanning images analysis

Boris Mašić - archaeological context of the site and grave, provided dating

Petra Rajić Šikanjić - anthropological analysis, drafting and revising of the manuscript

Dental stigmata and enamel thickness in a probable case of congenital syphilis from XVI century Croatia

Tomislav Lauc[a,b], Cinzia Fornai[c], Zrinka Premužić[d], Marin Vodanović[e], Gerhard W. Weber[c], Boris Mašić[f] and Petra Rajić Šikanjić[d,*]

[a]*Department for Anthropology, Faculty of Humanities and Social Sciences, University of Zagreb, Zagreb 10000, Croatia*

[b]*Department for Dental Medicine, Faculty of Medicine, University of Osijek, Osijek 31000, Croatia*

[c]*Department of Anthropology, University of Vienna, Vienna A-1090, Austria*

[d]*Institute for Anthropological Research, Zagreb 10000, Croatia*

[e]*Department for Dental Anthropology, School of Dental Medicine, University of Zagreb, Zagreb 10000, Croatia*

[f]*Zagreb City Museum, Zagreb 10000, Croatia*

Corresponding author:

Petra Rajić Šikanjić

Institute for Anthropological Research, Gajeva 32, 10000 Zagreb, Croatia

Phone: + 385 1 5535126

Fax: + 385 1 5535105

e-mail: petra@inantro.hr

Running title: Dental characteristics in congenital syphilis

ABSTRACT

Objective: To analyse the dental remains of an individual with signs of congenital syphilis by using macroscopic observation, CBCT and micro-CT images, and the analysis of the enamel thickness.

Design: Anthropological analysis of human skeletal remains from the 16th century archaeological site Park Grič in Zagreb, Croatia discovered a female, 17 to 20 years old at the time of death, with dental signs supportive of congenital syphilis: mulberry molars and canine defects, as well as non-specific hypoplastic changes on incisors. The focus of the analysis was on three aspects: gross morphology; hypoplastic defects of the molars, canines and incisors, as well as enamel thickness of the upper first and second molars.

Results: The observed morphology of the first molars corresponds to the typical aspect of mulberry molars, while that of the canines is characterised by hypomineralization. Hypoplastic grooves were observed on the incisal edges of all incisors. The enamel of the first molars is underdeveloped while in the second molars a thick-enamelled condition is observed.

Conclusions: Our observations for the dental and skeletal evidence are supportive to a diagnosis of congenital syphilis for this specimen from XVI century Croatia. The use of CT imaging helped documenting the diagnostic features and quantifying the effect of the dental stigmata on first molars.

Key words: enamel defects; Fournier canine; hypoplasia; mulberry molars; micro-CT

1. Introduction

Syphilis is a chronic disease that belongs to the group of treponematoses caused by the spirochetal bacterium *Treponema pallidum*. Based on mode of transmission it can be divided into two types: acquired, transmitted through sexual contact, and congenital, transmitted transplacentally to the developing foetus by an infected mother.[1]

Dental anomalies in patients with congenital syphilis have long been the subject of research[2,3,4,5,6,7,8,9], but in general, affected dental specimens are rare findings in archaeological contexts.[10,11] Dental signs of congenital syphilis include defects of permanent teeth or dental stigmata: Hutchinson‟s incisors, Fournier‟s canines, Moon‟s molars, mulberry molars.[7] All of them have their origin in the process of amelogenesis. Although amelogenesis is genetically controlled, it is very sensitive to different environmental disturbances.[12] Treponemal infection of enamel organs damages or destroys the ameloblasts and disrupts the formation of tooth germs.[7] Burket[13] considered also metaplasia and aplasia of the ameloblasts as possible conditions caused by the treponematosis. Inflammation around the tooth germ can alter enamel formation in two main ways[7,10]: a) as minor or moderate hypoplastic defects and b) as hypoplastic disturbance with morphological distortions. The former can occur in many teeth and in any period of enamel formation resulting in non-specific hypoplastic defects, while the latter can occur due to stronger pressure on the early tooth bud and during tooth morpho-differentiation resulting in the alteration of its shape. The inflammation around the tooth germ caused by congenital syphilis decreases with time, so the hypoplastic abnormalities affect only specific teeth at characteristic locations.

Hypoplastic changes caused by congenital syphilis can be divided into three main groups. The first group includes hypoplastic changes with clear and well-defined morphological features that are specific to congenital syphilis. These are Hutchinson‟s incisors and Moon‟s molars and

they should be considered pathognomonic of this disease.[2,3,4,10,14-16] The inflammation due to *T. pallidum* during the morphological differentiation of the permanent teeth causes a disturbance in the formation of the enamel-dentine junction[17], which results in a typical appearance of the affected teeth. However, Hutchinson‟s incisors and Moon‟s molars occur only in a low percentage of subjects affected by congenital syphilis[8] and with various degree of expression[4] .

The second group of hypoplasy includes Fournier‟s canines and mulberry molars that occur mostly, but not uniquely in congenital syphilis.[4,18,10] Therefore, Fournier‟s canines and mulberry molars are not defined as pathognomonic to congenital syphilis even though highly suggestive of this condition.[11]

These two groups of dental defects present a distinct morphology and are exclusively or mostly found in association to congenital syphilis. Therefore, Hutchinson‟s incisors, Fournier‟s canines, Moon‟s molars and mulberry molars are widely known as dental stigmata.[19,10] Importantly, the aforementioned dental stigmata are typical of permanent teeth, and manifestation on deciduous teeth were observed albeit more rarely than in permanent dentition.[4,20-22] In such cases, circular grooves around the root and just below the crown of the second deciduous molars have been typically detected.[23] Fournier[4] mentioned also the possible occurrence of notched deciduous incisors.

Finally, the third group of hypoplastic defects collectively designated as general enamel hypoplasia can be caused by syphilis as well as other environmental factors.[21] They are widely used as non-specific health indicators reflecting general health, diet, and, more broadly, living conditions. While in congenital syphilis hypoplastic changes appear on the structures that calcify up to the first year of life, the disruptions causing general enamel hypoplasia often affect dental formation for a limited period of time.[24,25] Hypoplastic defects may appear as linear grooves,

depressions (especially labially) or pits visible on the outer surface. The enamel is hard but deficient in amount. Among the hypoplastic manifestations darker and greyish colour of the enamel should be taken into account. The presence of systemic disorders such as the anhidrotic form of hereditary ectodermal dysplasia, dental dysplasia, linear enamel hypoplasia and molar-incisor hypomineralization (MIH) might lead to a wrong diagnosis of congenital syphilis. However, if single manifestations may be misleading, the observations carried out on more teeth and the estimation of the time of appearance of the disturbance can be considered altogether for a correct diagnosis. Disturbances in amelogenesis due to congenital syphilis mostly appear around birth and decrease throughout time. This locates enamel defects on the first molars and permanent incisors whose crown mineralization starts around birth. Time and location specificity distinguishes hypoplastic defects in congenital syphilis from most other environmental disturbances that appear throughout a longer period of life.

Congenital syphilis in past populations is difficult to confidently diagnose due to several reasons. This is firstly affected by the 50% fatality rate of affected foetuses.[26,27] Additionally, degree of skeletal and dental preservation, age at death, and recognition of specific pathological changes influence the diagnosis.[27] Bone deformities and dental stigmata are currently the main way in which congenital syphilis can be diagnosed in archaeological human remains. Teeth are usually better preserved than bones therefore dental changes are more often used for diagnosis.

Frequency of congenital syphilis in archaeological populations is hard to estimate owing to several reasons. The first are high rates of foetal death caused by the infection. Secondly, infected children may not display any sign of the disease, especially on the skeleton. Thirdly, even if symptoms occur, dental stigmata are observed in only 30% of individuals with congenital syphilis.[26,28] Cook and Powell[29] reported only 5.1% frequency of congenital syphilis in juveniles.

The authors stated that the lesions used to identify the disease were less specific than those for adults. Rothschild and Rothschild[30] concluded that only 5% of syphilitic children showed evidence of dental or osseous involvement. This rate is explained by quick remodelling of new bone that leaves no visible trace on the skeleton. In a study by Putkonen[24], Hutchinson‟s incisors and Moon‟s molars were present, in 45% and 22% respectively of children born with syphilis, compared to only 12% that showed skeletal evidence of the disease. However, during the life span, teeth can be lost owing to dental and periodontal diseases, and in any case, the dental stigmata can be obliterated by wear and attrition, which in hypoplastic teeth would occur even at a higher rate. Although they possess very specific morphological characteristics, syphilitic teeth are quite sporadic findings in archaeological samples. However, the analysis of human skeletal remains from the 16th century archaeological site Park Grič in Zagreb, Croatia revealed the presence of five individuals with skeletal changes indicative of syphilis. [31,32] Additionally, individual from grave 55, thereafter PG55, had dental signs supportive of congenital syphilis.[33,34]

The first aim of this paper is to provide a detailed description of PG55 dental remains and discuss the gross morphology and appearance of the affected teeth taking into account their outer enamel surface. Although it is known that the disturbance of the ameloblasts during the secretory phase may cause a reduction in enamel thickness[12] the enamel hypoplasia typical of teeth affected by congenital syphilis has been described in the literature only qualitatively, while no quantitative analyses have been performed up to now on syphilitic dental specimens. Also, little is known about enamel thickness and morphology of the dentine crown in symptomatic teeth of individuals affected by congenital syphilis. Therefore, we aim to investigate the 2D and 3D relative enamel thickness and dental tissue proportions in PG55 affected and unaffected maxillary molars in comparison to non-pathological molar teeth from recent modern humans.

2. Materials and methods

PG55 was a female aged 17 to 20 years at death based on morphological characteristics of the skeleton and dentition.[35,36] The skeleton was very well preserved, with only some of the small bones and teeth missing owing to post-mortem damage (Fig. 1, right individual). Apart from the dental changes, there were additional lesions visible on the skeleton. Significant endocranial lesions were present on the frontal and on both parietals and occipital bones. The right orbital roof showed healed *cribra orbitalia.* Periosteal changes in the form of striation and woven bone were observed on both tibiae.

The analysed dental remains come from a fragmented maxilla and a very well preserved mandible (Figs. 2 and 3). Most of the upper teeth are present except for the left first incisor (LI^1) and the third molars (M^3s). In the lower jaw both fourth premolars (P_4s), the left first molar (LM_1), and the third molars are missing (M_3s). The right second deciduous molar is still present (Rdm_2).

The morphological description of the outer aspect of dental remains was carried out with the aid of a table lamp and Olympus SZX10 Research Stereo Microscope.

Radiological examination of the specimen was first done by means of a CBCT scanner Scanora 3D, Soredex, Finland, (isotropic voxel size 250 µm) at Zubni rendgen Dr. Lauc Laboratory, Zagreb, Croatia. High resolution 3D image data of the dental remains were obtained at the Vienna micro-CT Laboratory, University of Vienna, Austria, through a Viscom X8060 micro-CT scanner, Hannover, Germany (130 kV, 100 mA) at an isotropic voxel size of 24 µm.

Of the teeth preserved, we considered the RM^1 (less worn than the LM^1) and both M^2s for the enamel thickness analysis and dental tissue proportions. Therefore, micro-CT data were

produced also for a comparative recent *Homo sapiens* sample (12 M^1s and 20 M^2s; in four cases both M^1 and M^2 were from the same individual). These individuals were from different geographical areas, as detailed in Table 1. The teeth included in the study presented the same degree of wear as PG55 molars, namely, Molnar"s stage 4 for the M^1s, and stage 1-2 for the M^2s[16] and had a complete and well preserved crown. The image data for all teeth considered were segmented using the software package Amira 5.5 (FEI, http://www.vsg3d.com/) and following the indications by Spoor et al.[37], in order to virtually separate the dental tissues and generate 3D surface models of enamel and dentine. The 3D analysis of the enamel thickness for M^1s and M^2s was carried out following the protocol described in great detail in Benazzi et al.[38] In particular, we used their protocol "3D-a" for molar teeth where the crown is separated from the roots at the cervical plane, namely the plane interpolating the cervical line of the tooth. According to Olejniczak et al.[39] the following measurements were gathered from the virtual model of each molar crown: the volume of the enamel cap (mm^3); the volume of the dentine core (including the coronal pulp – mm^3); the area of the enamel-dentine junction (EDJ; mm^2). These measurements were used for the computation of the 3D average enamel thickness index (3D AET = volume of enamel divided by the EDJ surface; index in mm). The 2D analysis of enamel thickness was carried out on mesial sections of the M^1 crowns, following Benazzi et al.[38] This protocol consists in setting the cervical plane of the molar crown as for the 3D analysis which serves as a reference for identifying the mesial section using a plane perpendicular to the cervical plane and passing through the protocone and paracone horn tips. Since these guidelines are conceived for unworn teeth (or at least for teeth in which the dentine horn tips are not affected by wear), we had to establish a protocol for the identification of alternative points to horn tips through which the section should pass. Similarly to Fornai et al.[40], using a spline curve (namely, a continuous and

smooth curve) we prolonged virtually the occlusal ridges on the exposed dentine patch; the mid-point of the spline trait crossing the exposed dentine patch was used for the identification of the section (see Fornai et al.[40] for more details).

From the virtual section of each molar crown the following values were gathered[36]: the area of the enamel cap (mm^2); the area of the dentine core (including the coronal pulp – mm^2); the length of the enamel-dentine junction (mm), for the computation of the 2D AET (enamel area divided by the EDJ length; index in mm).

3. Results

3.1. Description of the dental remains

The dental remains of PG55 are well preserved. Some of the missing teeth were lost post mortem (LI^1 and RP_3), while the LM_1 was lost ante mortem, since the alveolar bone showed clear signs of resorption. The P_4s and all four M3s were agenetic or aplastic, in fact no dental germs or non-erupted teeth were visible in the micro-CT images. The only tooth with carious lesion is the lower right second deciduous molar (Rdm_2).

PG55 occlusal condition is described below according to the indications given in Corruccini[41]. On the right side the M^1 paracone overlaps with the M_1 buccal groove so the buccal segment relation (BSR) was in Angle Class I. On the left side sagittal discrepancy of BSR with distal displacement of the lower dental arch was noted on the canines (Angle Class II). On the left side posterior crossbite was found on the second molars (M2s). The RP^4 was rotated about 140° and upper and lower midline discrepancy was 3 mm. The PAR index was 25, which implies greater occlusal disbalance, partially due to the lack of both P_4s. Panoramic reconstruction from the 3D data is presented in Figure 4.

First molars. All first molars (M1s) present significant enamel defects. The RM^1 is reduced in all crown dimensions with respect to the M^2s (Figs. 5 and 6). The RM^1 presents a Molnar‟s wear stage 4[16], but the tip of the paracone does not show any wear facets. This cusp is underdeveloped and much reduced in the bucco-lingual dimension presenting a peculiar spoon shape. The paracone is marked by deep grooves exposing small patches of dentine at the base of its lingual aspect. The paracone is characterized by multiple rounded rudimentary enamel nodules. In general, the whole occlusal enamel shows heavy hypoplastic defects in the form of deep grooves. The cusps forming the trigone are characterized by marked hypoplastic defects visible on the central fovea and along the trigone periphery. A hypoplastic ring of deep pits marks the dental crown deeply on all its lateral aspect along the occlusal third. The mesial side is heavily affected especially in correspondence to the paracone.

The LM^1 (Figs. 6 and 7) is heavily worn showing a Molnar‟s wear stage 5.[16] It presents the same size of the M^2 at the base of the crown. The enamel that is still visible on the occlusal surface is highly hypoplastic. The enamel at the paracone is thin with infolded yellow hypoplastic nodule on the tip of the cusp. The paracone is characterized by hypoplastic pitting. The paracone presents a similar spoon shape as in the antimere but less pronounced. Hypoplastic defects are visible in the form of grooves and pits, especially at the palatal aspect of occlusal surface and at the central basin. A ring of hypoplastic pitting surrounds the crown at the base of the cusps and it is more visible on the mesial and palatal aspects than on the distal and buccal sides. On the palatal surface hypoplastic grooves outline protocone and hypocone to the first third of palatal surface and split to the mesial and distal side.

The RM_1 (Figs. 8 and 9) is lightly smaller than the lower second molar. Even under the caveat of wear affecting this tooth (Molnar‟s wear stage 4[16]), it still seemed to possess a rather

flat occlusal aspect with markedly reduced cusps. The occlusal surface is characterised by deep grooves on all preserved occlusal enamel, and the central basin is highly crenulated. The thin enamel is infolded in all cusps. The outer surface shows multiple rounded enamel nodules on the occlusal surface and crests of enamel on a base of hypoplastic deposits. The lateral aspects of the crown are marked by a ring of grooves and pits. This is more evident on the mesial, distal and lingual sides and shallower on the buccal side.

Incisors. All incisors (Is) present are normal in size (Figs. 2 and 3), but show hypoplastic enamel alterations. They are worn to stage 4 of Molnar.[16] In spite of wear, it is possible to observe hypoplastic grooves marking the incisal edges of all Is. The upper Is show a rather smooth labial surface and irregular deep pitting on the lingual aspects. The labial aspect of the lower Is is rather smooth, but a very deep and large pit appears on both right I_1 and I_2. On the lingual side of the lower incisors, a sharp horizontal linear groove is present between the first and the second third of the crown possibly at the same developmental level up to the first year of life in all the Is.

Canines. Upper and lower canines (Cs) are worn to Molnar‟s wear stage 3.[16] Most of the hypoplastic defects in the Cs are located at the apical aspect of the crown. In spite of wear, sharp circular grooves are visible around the tips on both lingual and buccal surfaces of upper and lower Cs. The tip of the C cusp is partially hypoplastic in the form of circular defect around the tip of the crown. The upper Cs exhibited irregular pit hypoplastic defects on the buccal surfaces. Upper Cs exhibit no mesial canine ridge, distal accessory ridge or *tuberculum dentale*.

Premolars and second molars. All third and fourth premolars (P3s and P4s) as well as the M2s do not show any morphological or depositional deficiency. The RM^2 is the only second molar in this individual characterized by a paracone parastyle (stage 4 according to the ASUDAS). Although the left M_1 is absent, we can still observe that the M2s are visibly larger than the M1s.

Lower deciduous second molar. A large carious lesion obliterated almost completely the occlusal aspect of the dm_2 reaching the pulp chamber in its bucco-distal portion. Only the paraconid is still preserved and does not show signs of hypoplasia. The roots are well preserved in the cervical portion and do not present the circular hypoplastic groove described by Karnosh.[23]

3.2. 2D and 3D enamel thickness analyses and dental tissues proportions

The results of the 2D and 3D enamel thickness analyses for M^1s and M^2s are shown in Table 1 and visualized by means of box plots in Figures 10-13. The results of the 3D relative tissue proportions analysis are shown in Figure 14. The mesial sections of PG55 right and left M^1s and the results for the M^1 dental tissue proportions are shown in Figure 15.

The RM^1 delivered low values of the enamel thickness components. Dentine volume and EDJ surface are among the lowest values of the sample, but the enamel volume is the lowest at all, and falls outside the range of variability of the comparative sample considered. Hence, the 3D AET for PG55 RM^1 is the lowest scored, and is outside the range of variability for the comparative sample.

On the contrary, both PG55 right and left M^2 have the highest enamel volume spread on a rather small dentine crown. As a result, both PG55 M^2s provide the highest 3D AET values within the sample considered.

As it can be observed on the mesial sections in Figure 14, PG55 M^1s present defective enamel on both sides (on the middle and occlusal thirds), but especially on the occlusal area, in the portion of the section crossing the central fovea. The dentine portion of the section does not show alterations. PG 55 RM^1 provided the lowest 2D AET value within our sample (Fig. 16).

4. Discussion

Among 180 individuals from the 16th century cemetery Park Grič, Zagreb, Croatia, five of them have been reliably diagnosed with syphilis based on skeletal changes.[42] The individual from grave 55, analysed in this study, is the only one presenting dental changes supportive of congenital syphilis. Since syphilis spread throughout Europe in the 16th century and had all the characteristics of an epidemic, it can be expected that the number of syphilitic individuals recovered at this site reflect the morbidity of syphilis in the urban populations of that time. The ratio of 6/180 is in accordance to 3-4% of syphilis morbidity for the 16th century populations in Central Europe.[43]

We analysed the dental remains of PG55 focusing on three aspects, namely 1) gross morphology of the M1s, 2) hypoplastic defects of the M1s, Cs and Is, 3) enamel thickness of the M^1s in comparison to that of M^2s, and integrated them all. In addition, we discussed observed skeletal lesions.

A confident diagnosis of congenital syphilis should be based on pathognomonic manifestations (i.e., Moon‟s molars or Hutchinson‟s incisors), which are however not ubiquitous.[8,44] Alternatively a molecular detection of treponemal DNA should be carried out, but this procedure is destructive and not yet standardized for archaeological cases.[11]

In archaeological settings, strong support for congenital syphilis comes from other dental manifestations such as mulberry molars described by Fournier[4] and regarded by Jacobi et al.[18] and Mayes et al.[45] as distinctive signs, especially in pre-antibiotic cases. A circular groove around the C‟ tip (also described by Fournier[4]) is interpreted by some as one of the possible manifestations of congenital syphilis.[24,44,46,47] Non-specific enamel hypoplasia is as well indicative of growth disruption associated to congenital syphilis and affecting dental

morphogenesis up to the second year of life.[20,23,48] In addition, particular skeletal changes are supportive of congenital syphilis if taken in conjunction to specific dental manifestations.[1,20]

Hereafter, we consider observed dental and skeletal changes in the context of presenting a diagnosis of congenital syphilis in individual from Park Grič.

Mulberry molars. PG55 M1s are characterized by multiple rounded rudimentary enamel cusps and nodules of the enamel surrounding the cusps with agglomeration of masses of globules giving them the appearance of a mulberry. The plane-form hypoplastic defect affecting the basal area of the M1s‟ cusps corresponds to the classical aspect of a mulberry molar and distinguishes them from cuspal enamel hypoplasia as described by Ogden et al.[49] Importantly, all of the three M1s in PG55 present the same pathological aspect.

Karnosh‟s description of mulberry molars fits well to PG55 M1s: “Occlusal surface is rough, pigmented and pinched, with the exception of two or three nodules of good enamel huddled together which represents the poorly developed cusps. All around this occlusal deformity, the enamel of sound formation wells out in the form of a broad collar to the normal size of the crown at the neck of the tooth. […] The true mulberry molar of syphilis is a first permanent molar characterized by enamel cusps showing crests of sound enamel on a base of hypoplastic deposits. These cusps are generally crowded together on a crown surface of dwarfed dimensions.”[23]

The condition seen in PG55 cannot be attributed only to minor hypoplastic defects and consecutive tooth wear. PG55 M1s would be hardly worn away to that extent before adolescence, if the enamel had developed properly and fully, especially considering that in the same individual the M2s are only slightly worn.

Mulberry molars have been described in other cases of congenital syphilis from archaeological sites. In particular, we can directly compare PG55 M1s to the specimens shown in Mayes et al.[45], Nystrom[50] and Gaul and Grossschmidt[11] despite the different degree of dental wear of these teeth, while we are not able to compare PG55 M1s to the putative mulberry molar shown in Erdal.[51]

General enamel hypoplasia. PG55 presents general hypoplasia clearly expressed on the Is, Cs and M1s in the form of linear grooves (Is), circular groove (Cs) and a combination of grooves and pitting in the occlusal third of the M1 crowns.

While the mulberry defects are mostly located on aspects of the crown that develop up to the first year of life, this generalized hypoplastic defects formed later and possibly simultaneously at an age ranging between about 1 and 1.6 years of age (according to the mean estimate of enamel formation by Reid and Dean).[52] Importantly, teeth that form later, i.e. premolars and second molars do not present any enamel alteration.

Putkonen[24,25] stated that in congenital syphilis the hypoplastic changes appear on the structures that calcify up to the first year of life, and Hutchinson‟s incisors originate in the first three months after birth. According to Stones[53], instead, the treponematosis might affect dental morphogenesis up to the age of two. Whether these hypoplastic changes must be considered as a response to the primary infection acting on the tooth bud, or as a result of a second disturbance might be debated. In any case congenital syphilis is generally regarded as a factor increasing severity of enamel hypoplasia, since affected children usually suffer with concurrent nutritional disorders.[18,20,23,48]

In particular, the diagnostic value of the circular grooves marking the Cs‟ tips, usually defined as Fournier‟s canines[4], has been variously interpreted by different authors. For example,

some authors[10,46,47,54] listed it as one of the dental stigmata typical of congenital syphilis, while others[6,24,44] considered this feature of scarce or none diagnostic value. Whether of the two views is correct, the same kind of enamel alteration has been described in several reports of congenital syphilis in archaeological settings.[11,45,50]

Skeletal changes. The systemic inflammation occurring in congenital syphilis might cause different kinds of lesions. These might be specific, such as sabre shin tibia appearing also in acquired syphilis. However, most changes are general and unspecific, including periostitis, osteitis, and metaphyseal changes.[26,30,55]

The analysed individual presents several cranial and postcranial lesions. Endocranial lesions can be observed on all cranial bones. On frontal and both parietal bones they appear as capillary changes, while on the occipital bone „hair-on-end" lesions are visible. They may be caused by inflammation and/or haemorrhage of the meningeal vessels. These conditions can be the result of several diseases, such as chronic meningitis, trauma, metabolic disorders and tuberculosis.[56] Meningitis can be caused by syphilis, but in those cases the base of the skull is usually affected, causing hydrocephalus and distension of the scalp veins, and spastic paralysis, mental defects, fits and pituitary disorders can occur.[56] Research of possible cases of congenital syphilis by Cook and Buikstra associated presence of these lesions with periostitis, dental defects and a lower expectation of life.[57]

Localized periostitis visible as striation and woven bone is observed on both tibiae. Periostitis is new bone deposition that forms as a result of injury of infection.[56] Rothschild and Rothschild stated that new bone formation can appear in various forms of treponemal diseases and but is not specific only for congenital syphilis.[30] In congenital syphilis periostitis appears, although rarely, and also remodels quickly often leaving no visible signs.[30]

In conclusion to the presence of observed skeletal lesions, it has to be stressed that only 5% of children with syphilis will exhibit skeletal or dental changes.[30] Also, Cook and Powell verified that the lesions used in diagnosing syphilis in children were less specific than in adults.[29]

Additional evidence. Here we include further occurrences which are not typical of congenital syphilis, but are either found in association to it or are otherwise supportive of this diagnosis. In particular, this individual shows a mild malocclusion consisting in a cross-bite. Malocclusion, although not characteristic of congenital syphilis, occurs frequently in affected individuals.[58]

The total of the morphological evidence described in PG55 can be coupled with the presence of syphilis at site, as testified by other skeletal remains showing distinct signs of acquired syphilis, to corroborate a diagnosis of congenital syphilis.[42]

Alternative diagnosis. The most probable aetiology for the enamel defects observed in PG55, can be determined by evaluating the type and expression of defects, their location, and estimating time of appearance of the disturbance. The time of appearance of the hypoplastic changes in conjunction with the fact that Ps and M2s are unaltered made us exclude many conditions that mimic congenital syphilis in their manifestations in the face and mouth of living persons such as the anhidrotic form of hereditary ectodermal dysplasia or dental dysplasia with ectodermal involvement. Gargoylism and achondroplasia that can also have similar manifestations were rejected due to lack of skeletal abnormalities typical for these disorders. Dental defects, as the non-specific health indicators can be seen as different hypoplastic forms, among which the linear enamel hypoplasia, furrow shaped defects, darker and greyish colour, liableness for decay, depression on the labial surface and MIH should be taken into account. Linear enamel hypoplasia and furrow shaped defects cannot explain specific morphological feature of the first permanent molars and difference between enamel thickness of first and second molars. As previously

noticed, none of the present permanent teeth in PG55 have carious lesions and all of them show a normal colour. As expected, M1s present a higher degree of wear compared to M2s. However, it can be assumed that the presence of thinner and irregular occlusal enamel can cause the M1s to wear down at a faster rate. In fact, M1s present a degree of wear ranging from 4 to 5[16], while M2s are unworn or slightly worn. In MIH the enamel defects are usually asymmetric with well-demarcated white/opaque, yellow or brown discoloration affecting cuspal areas and sparing the cervical areas. In many cases the incisor enamel is affected, but often minimally.[59]

Fagrell et al.[60] examined ground radial and sagittal sections from teeth diagnosed with MIH using the same method as in this study, X-ray micro-computed tomography, to estimate the onset and timing of the MIH and to relate the hypomineralized enamel to the incremental lines. Their findings indicate that the ameloblasts in the MIH are capable of forming enamel of normal thickness, but with a substantial reduction of their capacity for maturation of enamel.[60] In our specimen the enamel thickness of M1 is significantly thinner and this condition cannot be attributed to MIH. The assumption that the MIH could explain these findings of the enamel defects was therefore rejected.

Enamel thickness. The enamel thickness components for PG55 M^1s and M^2s show an interesting pattern, since for both tooth types the dentine crown is rather small with respect to the comparative sample, but the enamel cap is absolutely and relatively scarce in the mulberry M^1s while the M^2s have a thick enamel cap. The M^1s' enamel underdevelopment finds an immediate explanation in the treponemal infection that in this individual must have acted on the dental germs perinatally.[7] Obviously, the conditions that gave origin to the mulberry M^1s had ceased at the time of M^2s crown formation; nonetheless, the thick-enamelled condition observed in M^2s is rather surprising. A possible explanation for it could be found in the context of the inhibitory

cascade model.[61] Owing to M1s‟ abnormal development, the M2s would have activated earlier resulting in big-crowned teeth. The dentine crowns of the molars seem to not be affected and present a normal morphology. Although wear affects the dentinal crown at the incisal edges of the Is and in lower degree those of the Cs, such observation can be done for the anterior teeth too.

5. Conclusions

The individual from grave 55 buried at the 16th century cemetery Park Grič in Zagreb, Croatia shows several dental and skeletal manifestations strongly supportive of congenital syphilis. The diagnosis is supported by the following: 1) mulberry molars; 2) enamel hypoplasia marking the lingual aspect of the Is, the Cs‟ tips, and the occlusal third of the M1s, and possibly formed simultaneously; 3) endocranial lesions and tibial periostitis; 4) drastically reduced enamel thickness at the M1s, and normal M2s; 5) presence of malocclusion of M2s; 6) presence of acquired syphilis in several other individuals from the cemetery [42]. The diagnosis of congenital syphilis in this individual would make it the oldest case of this disease in the post-Colombian Europe.[11,62]

Since teeth affected by congenital syphilis are relatively rare in the archaeological records, this individual is of particular relevance for the understanding of the variability in the expression of the symptoms of this pathology and the influence it might have on dental development.[30,62]

The CT images are a suitable means for the analysis of dental remains and in cases of congenital syphilis can inform about the hidden changes on dentine incisal edge under the enamel cap. The analysis of the enamel thickness and dental tissue proportions we carried out on upper first and second molars is the first qualitative assessment of this sort on a individual affected by

congenital syphilis. It provided more insight into development of enamel in cases of congenital syphilis and might serve as comparative reference for future studies.

Acknowledgement

Research was supported by the Ministry of Science, Education and Sport of the Republic of Croatia (Project no. 196-1962766-2740), AERS Dental Medical Organizations, Vienna, Austria, and the Siegfried Ludwig - Rudolf Slavicek Foundation, Vienna, Austria. Authors are thankful to S. Benazzi for his suggestions as well as to the editor and reviewers for their comments that significantly improved the manuscript.

REFERENCES

1. Ortner DJ. Identification of pathological conditions in human skeletal remains. Amsterdam: Academic Press; 2003.
2. Hutchinson J. On the influence of hereditary syphilis on the teeth. Trans Odontol Soc Great Britain1857;2:95-106.
3. Hutchinson J. Report on the effects of infantile syphilis in marring the development of teeth. Trans Pathol Soc London1858;9:449-456.
4. Fournier A. Syphilitic teeth. Dent Cosmos1884;26:12-25,81-91,141-155.
5. Bauer BH. Uber Befunde am Zahnkeim und Kieferknochen bei angeborener Syphilis. Wien Klin Wochenschr1931;44:879-882.
6. Sarnat BG, Shaw NG. Dental development in congenital syphilis. Am J Dis Child1942;64:771-788.
7. Bauer BH. Tooth buds and jaws in patients with congenital syphilis: Correlation between distribution of *Treponema pallidum* and tissue reaction. Am J Pathol1944;20:297-319.
8. Putkonen T, Paatero YV. X-ray photography of unerupted permanent teeth in congenital syphilis. Brit J Vener Dis1961;37:190.
9. Bernfeld WK. Hutchinson's teeth and early treatment of congenital syphilis. Br J Vener Dis1971;47:54-56.
10. Hillson S, Grigson C, Bond S. Dental defects of congenital syphilis. Am J Phys Anthropol1998;107:25-40.
11. Gaul JS, Grossschmidt K. A probable case of congenital syphilis from 18th century Vienna. Int J Paleopathol2014;6:34-43.

12. Souza JF, Jeremias F, Costa-Silva CM, Santos-Pinto L, Zuanon ACC, Cordeiro RCL. Aetiology of molar–incisor hypomineralisation (MIH) in Brazilian children. Eur Arch Paediatr Dent2013;14:233-238.
13. Burket LW. Histopathologic studies in congenital syphilis. Int J Orthod Oral Surg1937; 23:1016-1031.
14. Moon H. On irregular and defective tooth development. Trans Odontol Soc Great Britain1877;9:223-243.
15. Pflüger H. Eine für Lues congenital charakteristische Formveränderung (Knospenform) an dem ersten Molaren. Munch Med Wochenschr1924;71:605-607.
16. Molnar S. Human tooth wear, tooth function and cultural variability. Am J Phys Anthropol1971;34:175-189.
17. Sarnat BG, Schour I. Enamel hypoplasias (chronologic enamel aplasia) in relation to systemic disease: a chronologic, morphologic and etiologic classification. J Am Dent Ass1941;28:1989-2000.
18. Jacobi KP, Cook DC, Corruccini RS, Handler JS. Congenital syphilis in the past: Slaves at Newton Plantation, Barbados, West Indies. Am J Phys Anthropol1992;89:145-158.
19. Condon K, Becker J, Condon C, Hoffman JR. Dental and skeletal indicators of a congenital treponematosis. Am J Phys Anthropol Suppl1994;18:70.
20. Steinbock RT. Paleopathological Diagnosis and Interpretation. Charles C. Thomas RT, IL;1976
21. Curtin AJ. Prehistoric treponematosis in thePacifc Northwest: a review of the skeletal evidence. In: Powell ML and Cook DC (eds). The myth of syphilis: the natural history of treponematosis inNorth America. Gainesville: University of FloridaPress; 2005:306-330.

22. Hutchinson DL, Richman R. Regional, social, and evolutionary perspectives on treponemal infection in the Southeastern United States. Am J Phys Anthropol2006;129;544-558.
23. Karnosh LJ. Histopathology of syphilitic hypoplasia of the teeth. Arch Derm Syphilol1926;13:25-42.
24. Putkonen T. Dental changes in congenital syphilis. Relationship to other syphilitic stigmata. Acta Derm Venereol1962;42:44-62.
25. Putkonen T. Does early treatment prevent dental changes in congenital syphilis? Acta Derm Venereol1963;43:240-249.
26. Aufderheide AC, Rodríguez-Martín C. The Cambridge encyclopedia of human paleopathology. Cambridge: Cambridge University Press; 2011.
27. Roberts C. Manchester K. The archaeology of disease. Ithaca: Cornell University Press; 2005.
28. Larsen CS. Bioarchaeology. Cambridge: Cambridge University Press; 1997.
29. Cook D, Powell M. The myths of syphilis: The natural history of treponematosis in North America. Gainesville: University of Florida Press; 2005.
30. Rothschild BM, Rothschild C. Congenital syphilis in the archaeological record: Diagnostic insensitivity of osseous lesions. Int J Osteoarchaeol1997;7:39-42.
31. Mašić B, Pantlik B. Zagreb – park Grič. In: Wiewegh Z (ed). Hrvatski arheološki godišnjak 4/2007. Zagreb: Ministarstvo kulture; 2008:204-206.
32. Mašić B, Pantlik B. O nalazu novca iz groba 74 u Parku Grič na zagrebačkom Gornjem gradu. VAMZ2008;41:331-342.

33. Vodanović M, Lauc T, Premužić Z, Rajić Šikanjić P. Orthodontic analysis of the 16th century skull with congenital syphilis. Abstracts of the first Congress of the Croatian Society of Orthodontics of Croatian Medical Association. Acta Stomatol Croat2013;47:88.
34. Lauc T, Rajić Šikanjić P, Premužić Z, Fornai C, Mašić B, Vodanović M. Dental morphology of individual with congenital syphilis from 16th century. In: Vodanović M, editor. 16th International Symposium on Dental Morphology 1st Congress of the International Association for Paleodontology, Programme & Book of abstracts. Zagreb: International Association for Paleodontology. 2014:120.
35. Buikstra JE, Ubelaker DH. Standards for data collection from human skeletal remains. Fayetteville: Arkansas Archaeological Survey; 1994.
36. Scheuer L, Black S. The juvenile skeleton. London: Elsevier Academic Press; 2004.
37. Spoor CF, Zonneveld FW, Macho GA. Linear measurements of cortical bone and dental enamel by computed tomography: Applications and problems. Am J Phys Anthropol1993;91:469-484.
38. Benazzi S, Panetta D, Fornai C, Toussaint M, Gruppioni G, Hublin JJ. Technical note: Guidelines for the digital computation of 2D and 3D enamel thickness in hominoid teeth. Am J Phys Anthropol2014;153:305-313.
39. Olejniczak AJ, Smith TM, Feeney RN, Macchiarelli R, Mazurier A, Bondioli L, et al. Dental tissue proportions and enamel thickness in Neandertal and modern human molars. J Hum Evol 2008;55:12-23.
40. Fornai C, Benazzi S, Svoboda J, Pap I, Harvati K, Weber GW. Enamel thickness variation of deciduous first and second upper molars in modern humans and Neanderthals. J Hum Evol2014;76:83-91.

41. Corruccini RS. How anthropology informs the orthodontic diagnosis of malocclusion‟s causes. New York: Edwin Mellen Press; 1999.
42. Premužić Z, Rajić Šikanjić P, Mašić B. Foreign soldiers and syphilis in 16th century Zagreb. 19th European Meeting of the Paleopathology Association, August 27-29; Lille, France, 2012.
43. Sabbatani S. Il contagio luetico a Bologna nel Cinquecento. L‟assistenza sanitaria e sociale (seconda parte). Infez Med2006;14:102-110.
44. Cruickshank LG. The dental stigmata of congenital syphilis. Proc R Soc Med1939;32:343-348.
45. Mayes AT, Melmed A, Barber S. Stigmata of congenital syphilis on a highstatus juvenile at Yugue, Oaxaca, Mexico. Dent Anthropol2009;22:73-84.
46. Colyer JF. Dental Surgery and Pathology London;1923.
47. Bradlaw, RV. The dental stigmata of prenatal syphilis. Oral Surgery, Oral Medicine, Oral Pathology1953;6:147-158
48. De Wilde H. Stigmata of congenital syphilis in the deciduous dentition. Am J Orthodont Oral Surg1943;23:368-376.
49. Ogden AR, Pinhasi R, White WJ. Gross enamel hypoplasia in molars from subadults in a 16th–18th century London graveyard. Am J Phys Anthropol2007;133;957-966.
50. Nystrom KC. Dental evidence of congenital syphilis in a 19th century cemetery from the Mid-Hudson Valley. Int. J. Osteoarchaeol2011;21:371-378.
51. Erdal YS. A pre-Columbian case of congenital syphilis from Anatolia. Int J Osteoarchaeol2006;6:16-33.

52. Reid DJ, Dean MC. Variation in modern human enamel formation times. J Hum Evol2006;50:329-346.
53. Stones HH. Oral and Dental Diseases, second ed. E.&S. Livingstone Ltd., Edinburgh;1951.
54. Stoll HF. The clinical diagnosis of heredosyphilis. J. Am. Med. Assoc1921;77:919-925.
55. Rasool MN, Govender S. The skeletal manifestations of congenital syphilis. Journal of Bone and Joint Surgery1989;71B:752-755.
56. Lewis M. The Bioarchaeology of Children: Perspectives from Biological and Forensic Anthropology. Cambridge: Cambridge University Press; 2007.
57. Cook D, Buikstra J. Health and differential survival in prehistoric populations: prenatal dental defects. Am J Phys Anthropol1979;51;649-664.
58. Stathers F R. Congenital syphilis and malocclusions of the teeth. Am J Orthodontics and Oral Surgery1942;28:138-151.
59. Farah RA, Monk BC, Swain MV, Drummond BK. Protein content of molar-incisor hypomineralisation enamel. J Dent2010;38:591-596.
60. Fagrell TG, Salmon P, Melin L, Noren JG. Onset of molar incisor hypomineralization (MIH). Swed Dent J2013,37:61-70.
61. Kavanagh KD, Evans AR, Jernvall J. Predicting evolutionary patterns of mammalian teeth from development. Nature2007;449:427-432.
62. Harper KN, Zuckerman MK, Harper ML, Kingston JD, Armelagos GJ. The origin and antiquity of syphilis revisited: An Appraisal of Old World pre-Columbian evidence for treponemal infection. Ybk Phys Anthropol2011;146:99-133.

Figure captions

Fig. 1 Grave 55 *in situ* (right individual).

Fig. 2 Upper dental arch.

Fig. 3 Lower dental arch.

Fig. 4 Panoramic reconstruction from CBCT data.

Fig. 5 The first right upper molar (RM^1).

Fig. 6 The first left and right upper molars (LM^1 and RM^1).

Fig. 7 The first left upper molar (LM^1).

Fig. 8 The first right lower molar (RM_1).

Fig 9 The first right lower molar (RM_1).

Fig. 10 Box plots for the enamel volume for PG55 left M^1 (PG55LM1) and PG55 left and right M^2s (PG55LM2 and PG55RM2) compared to the non-pathological M^1 and M^2 samples (UM1s and UM2s).

Fig. 11 Box plots for the dentine volume for PG55 left M^1 (PG55LM1) and PG55 left and right M^2s (PG55LM2 and PG55RM2) compared to the non-pathological M^1 and M^2 samples (UM1s and UM2s).

Fig. 12 Box plots for the enamel dentine junction (EDJ) area for PG55 left M^1 (PG55LM1) and PG55 left and right M^2s (PG55LM2 and PG55RM2) compared to the non-pathological M^1 and M^2 samples (UM1s and UM2s).

Fig. 13 Box plots for the 3D average enamel thickness (3D AET) for PG55 left M^1 (PG55LM1) and PG55 left and right M^2s (PG55LM2 and PG55RM2) compared to the non-pathological M^1 and M^2 samples (UM1s and UM2s).

Fig. 14 Box plots for the proportion of the dentine volume (including the pulp chamber) on the total crown volume. PG55 right M^1 (PG55RM1) and M^2s (PG55M2s) are compared to the rest of the M^1 and M^2 non pathological samples.

Fig. 15 Mesial sections from PG55 right (a) and left (b) M^1s. The left section was flipped horizontally to ease visual comparison. Only PG55 RM^1 was included in the 2D AET analysis.

Fig. 16 Box plots for the 2D average enamel thickness for PG55 right M^1 (PG55RM1) and the non-pathological M^1 sample (UM1s).

Tables

Table 1 Enamel thickness components and relative tissue proportions (both in 3D and 2D) for the maxillary first molars (M^1s) and maxillary second molars (M^2s; in 3D).

Table 1 - Enamel thickness components and relative tissue proportions (both in 3D and 2D) for the maxillary first molars (M^1s) and maxillary second molars (M^2s; in 3D). For the comparative sample the averages and standard deviations (in brackets) are reported

	Specimens	Provenience and number of individuals	Wear stage[16]	Enamel volume	Dentine (and pulp chamber) volume	EDJ area	3D AET	Dentine volume on total crown volume (%)
M^1 crowns	**Park Grič 55, L**	**Croatia**	4	**118,04**	**223,64**	**172,61**	**0,68**	**65,45**
	Park Grič 55, R	**Croatia**	5	**86,37**	**206,96**	**139,89**	**0,62**	**70,56**
	Comparative sample	Australia = 3 Central Europe = 3 Southern Africa = 6	4	195.98 (40.59)	268.11 (60.09)	193.75 (28.55)	1.01 (0.10)	57.70 (2.67)
M^2 crowns	**Park Grič 55, L**	**Croatia**	2	**277,95**	**210,82**	**164,16**	**1,6931652**	**43,13276183**
	Park Grič 55, R	**Croatia**	1	**292,71**	**223,23**	**171,59**	**1,7058686**	**43,26665891**
	Comparative sample	Australia = 3 Central Europe = 5 Eastern Africa = 1 Papua New Guinea = 4 Southern Africa = 6	1-2	234.05 (63.58)	233.39 (56.09)	173.68 (26.07)	1.34 (0.20)	50.05 (3.52)
				Enamel area	Dentine (and pulp chamber) area	EDJ length	2D AET	Dentine area on total crown area (%)
M^1 mesial sections	**Park Grič 55, L**	**Croatia**	4	**11,20**	**38,77**	**18,30**	**0,61**	**77,59**
	Park Grič 55, R	**Croatia**	5	**12,42**	**37,05**	**17,52**	**0,71**	**74,89**
	Comparative sample	Australia = 3 Central Europe = 3 Southern Africa = 6	4	14.57 (2.29)	36.28 (5.72)	16.97 (1.68)	0.86 (0.08)	71.32 (2.03)

EDJ = enamel-dentine junction; AET = average enamel thickness

Figure 1
Click here to download high resolution image

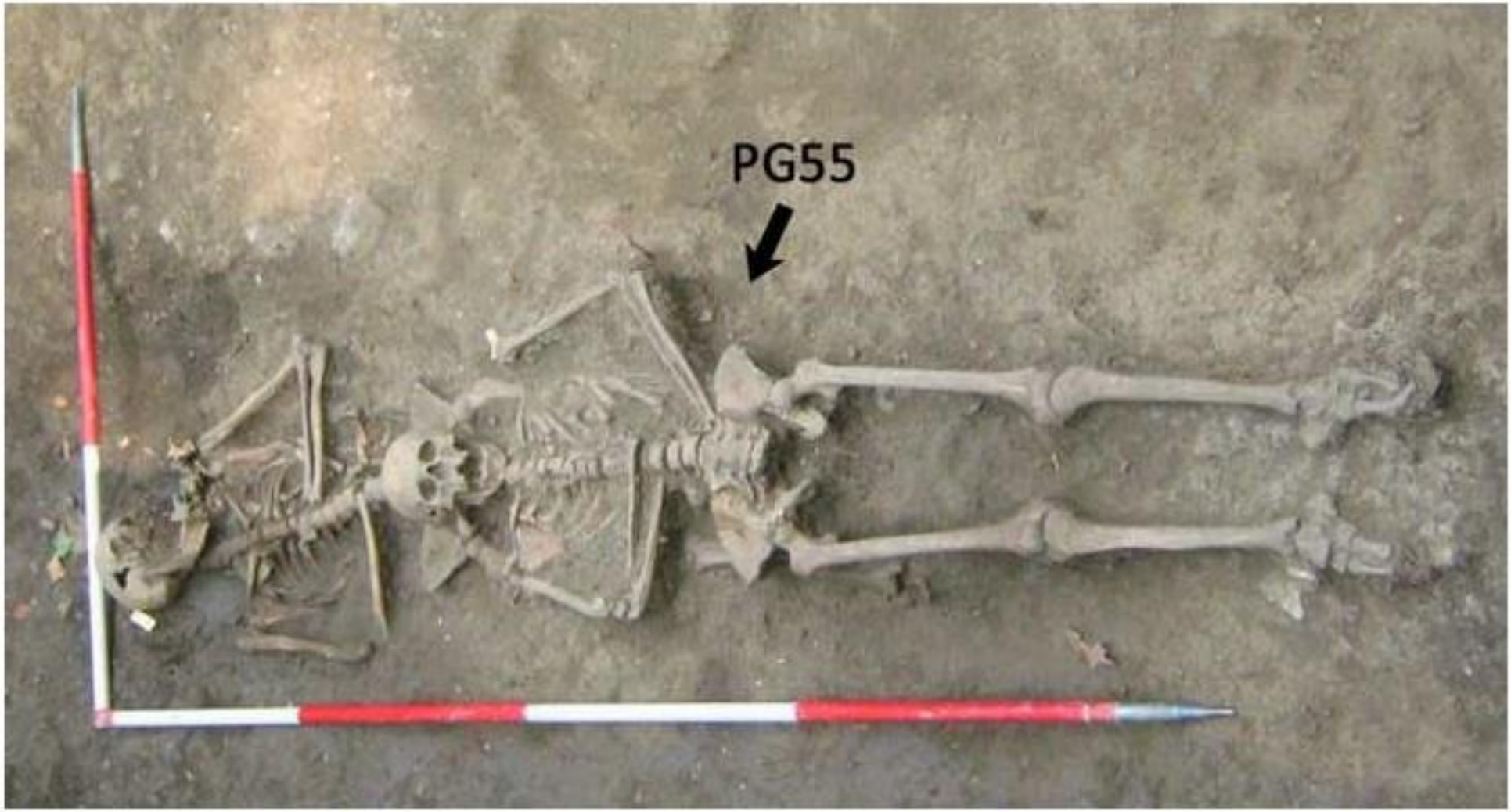

Figure 2
Click here to download high resolution image

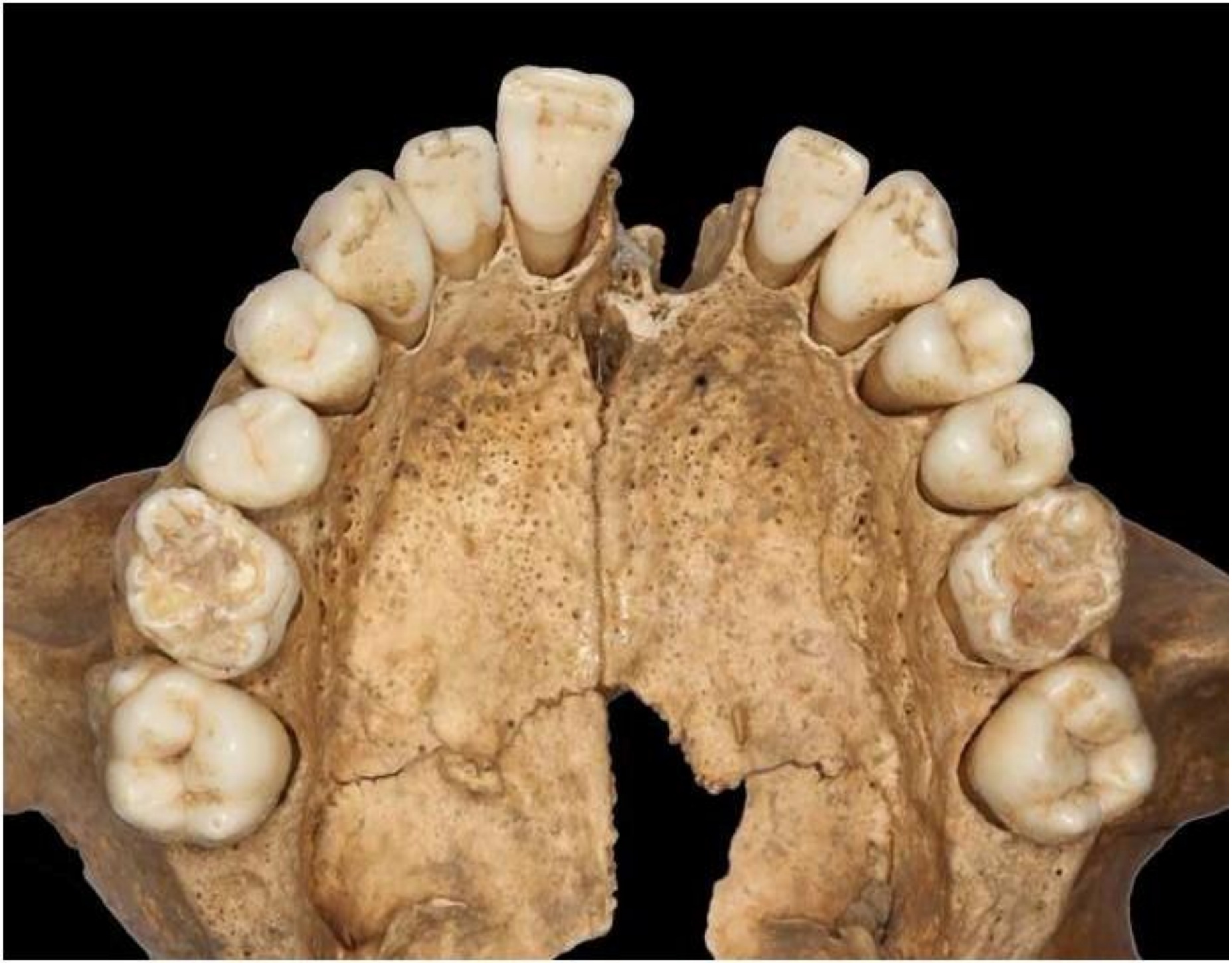

Figure 3
Click here to download high resolution image

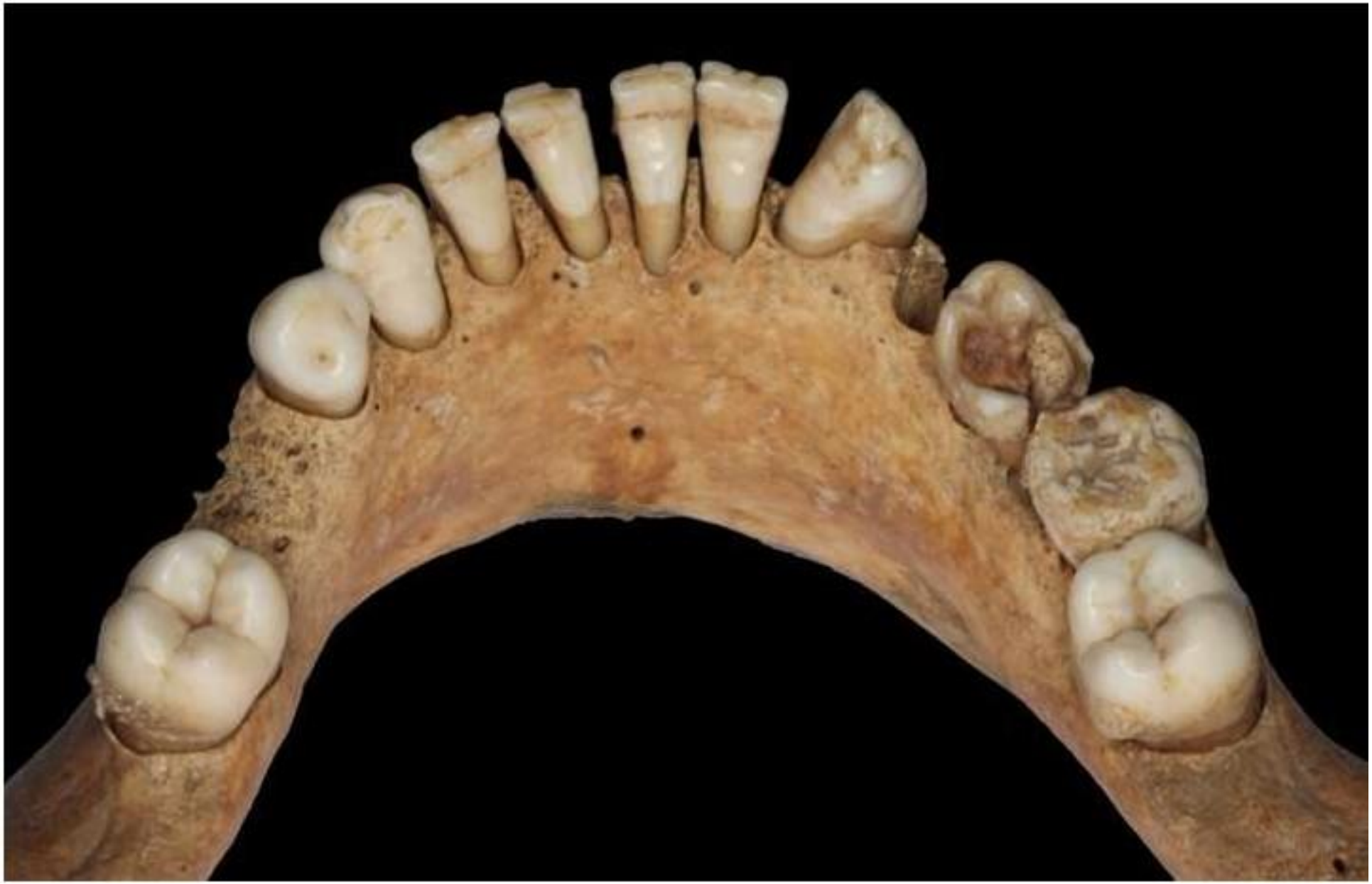

Figure 4
Click here to download high resolution image

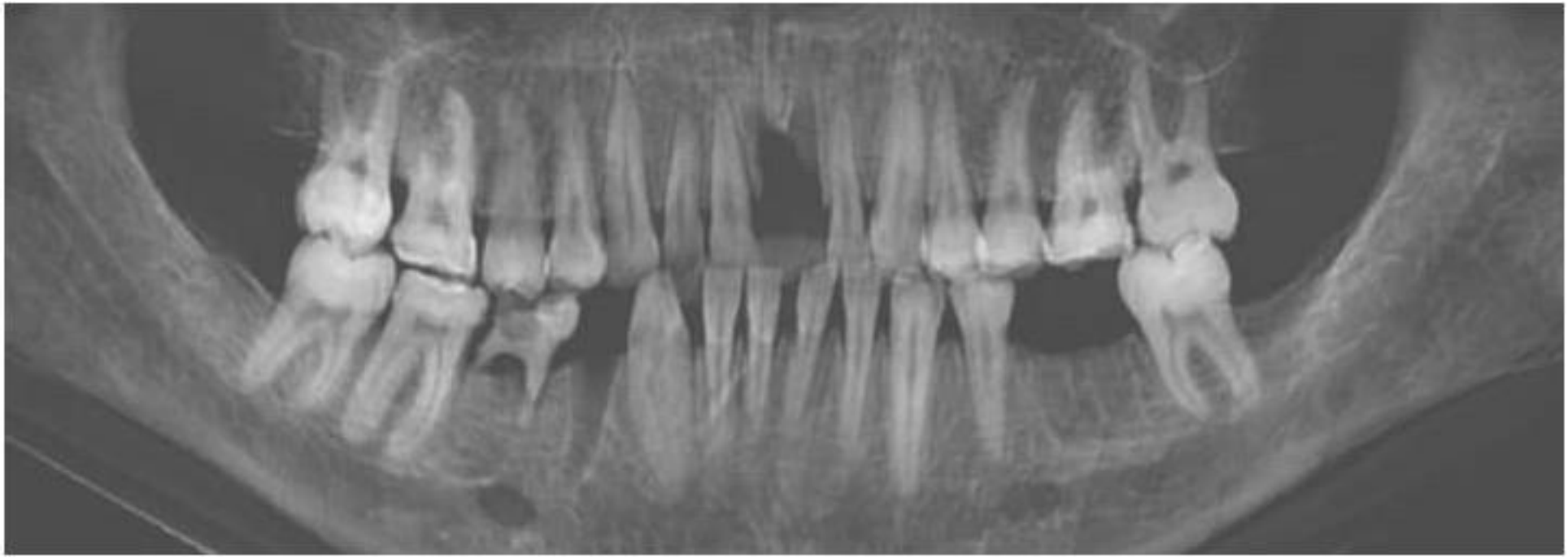

Figure 5
Click here to download high resolution image

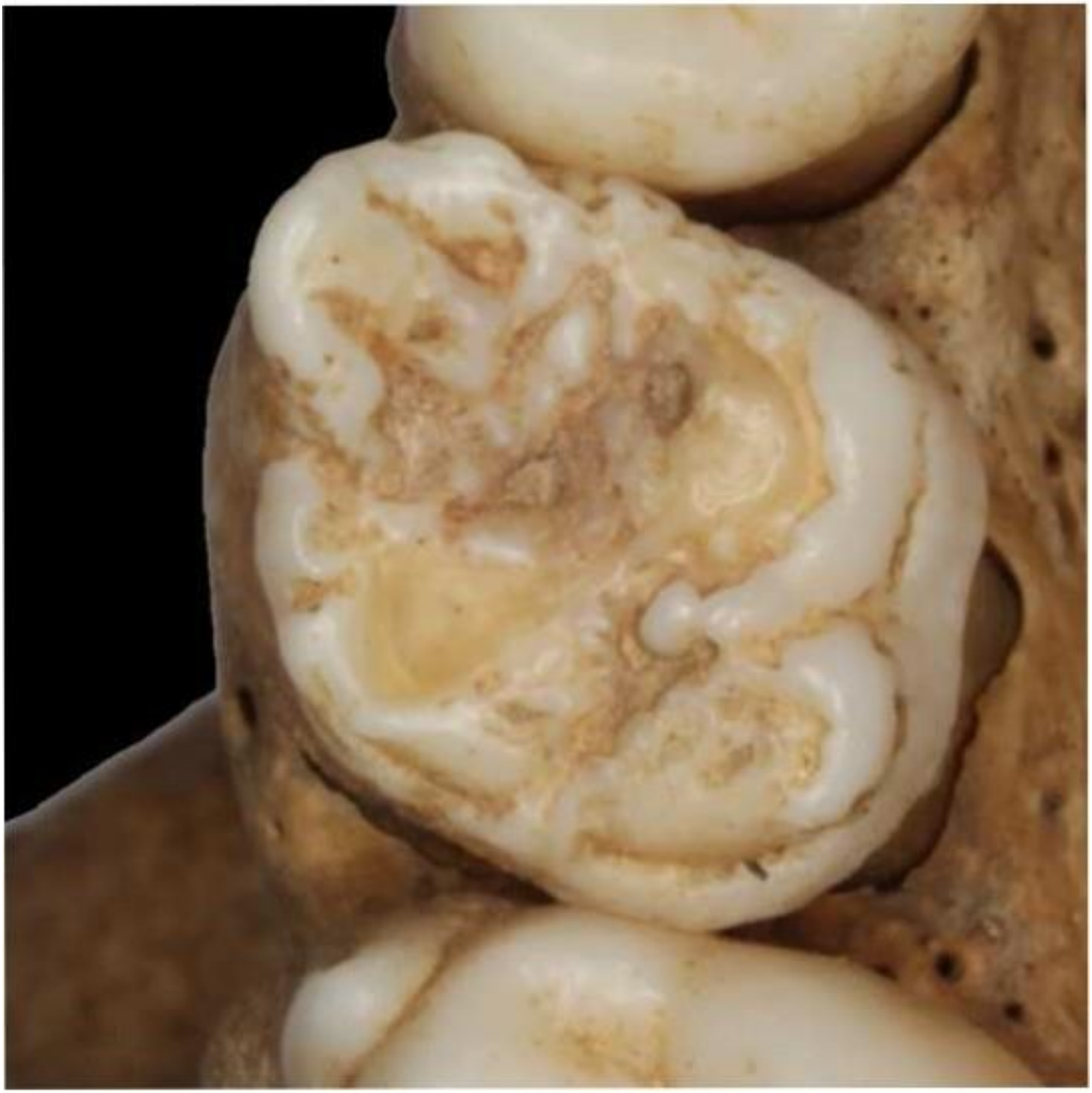

Figure 6
Click here to download high resolution image

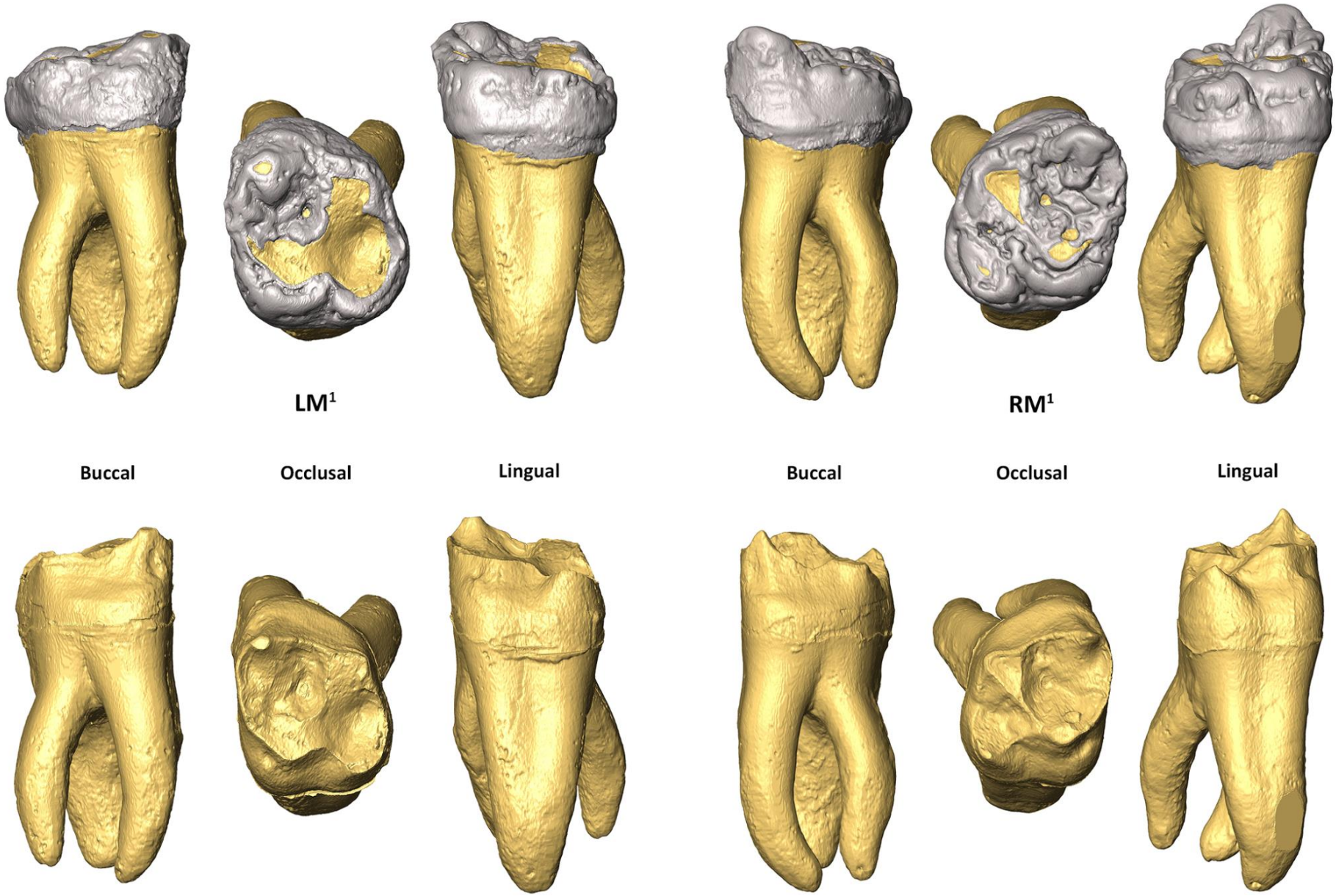

Figure 7
Click here to download high resolution image

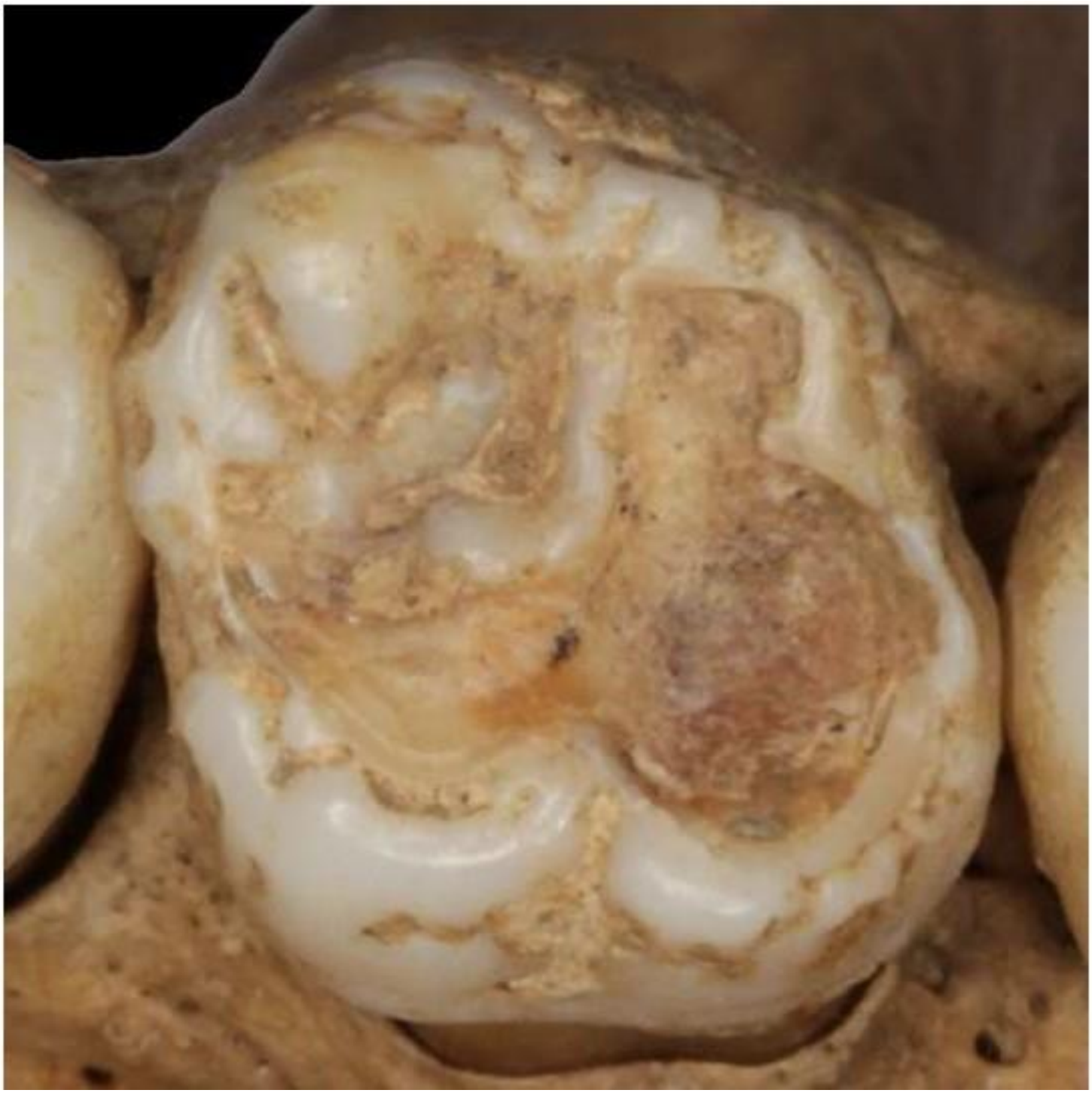

Figure 8

Click here to download high resolution image

Figure 9

Click here to download high resolution image

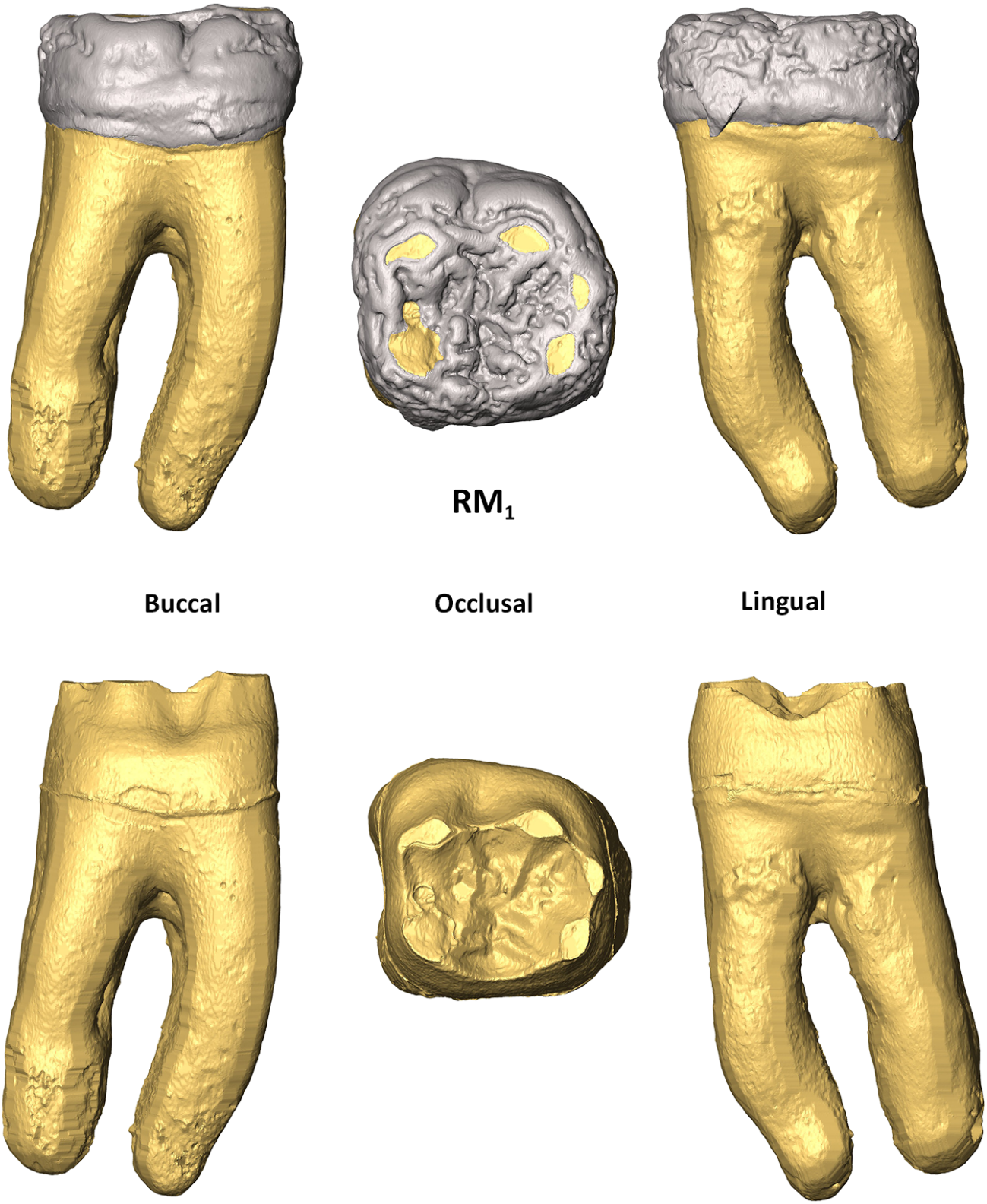

Figure 10
Click here to download high resolution image

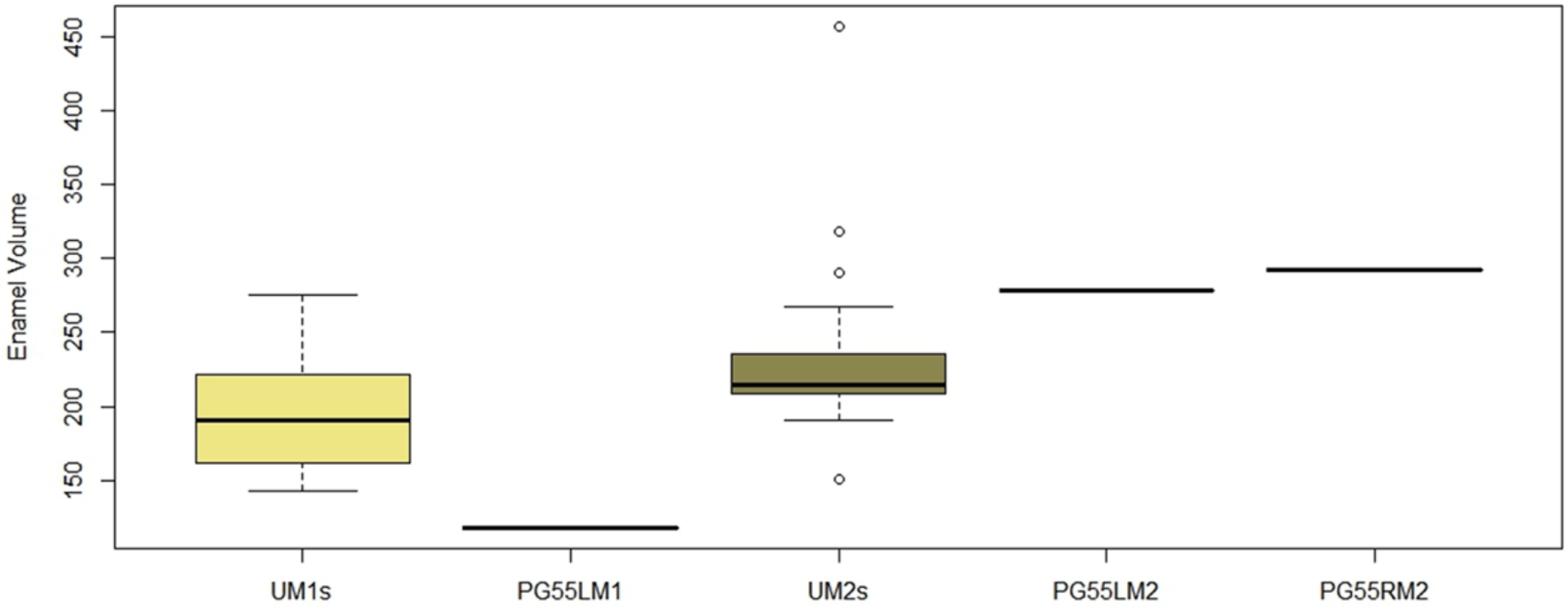

Figure 11
Click here to download high resolution image

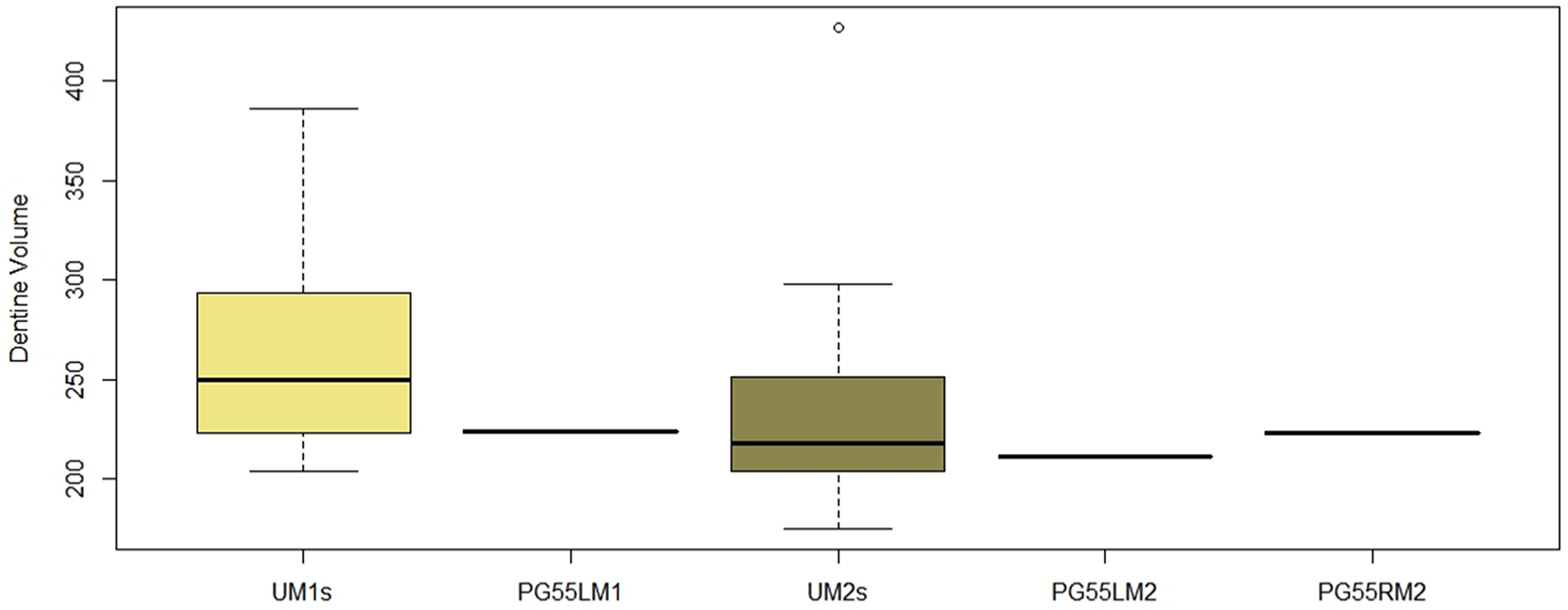

gure 12
lick here to download high resolution image

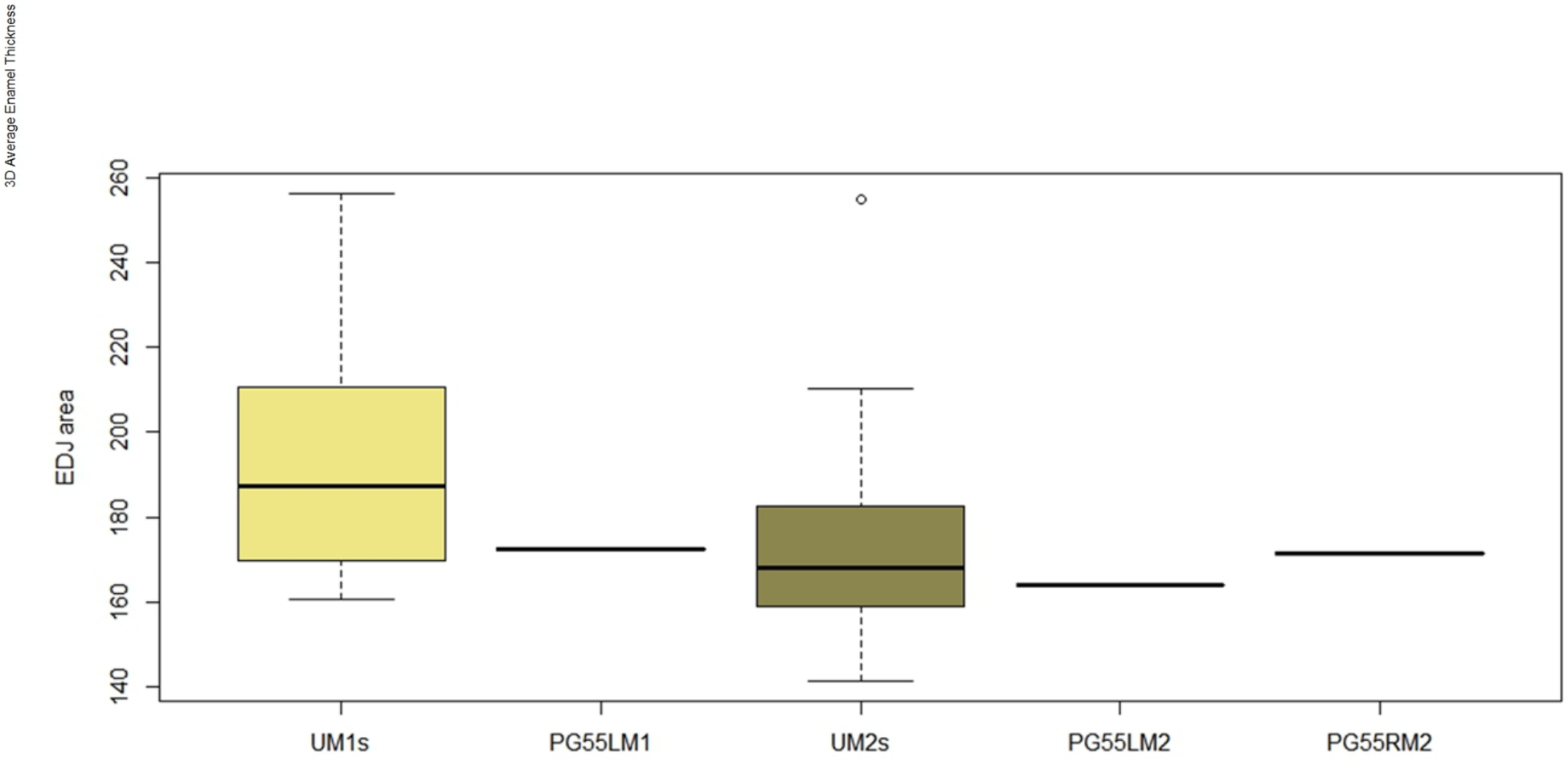

Figure 13
Click here to download high resolution image

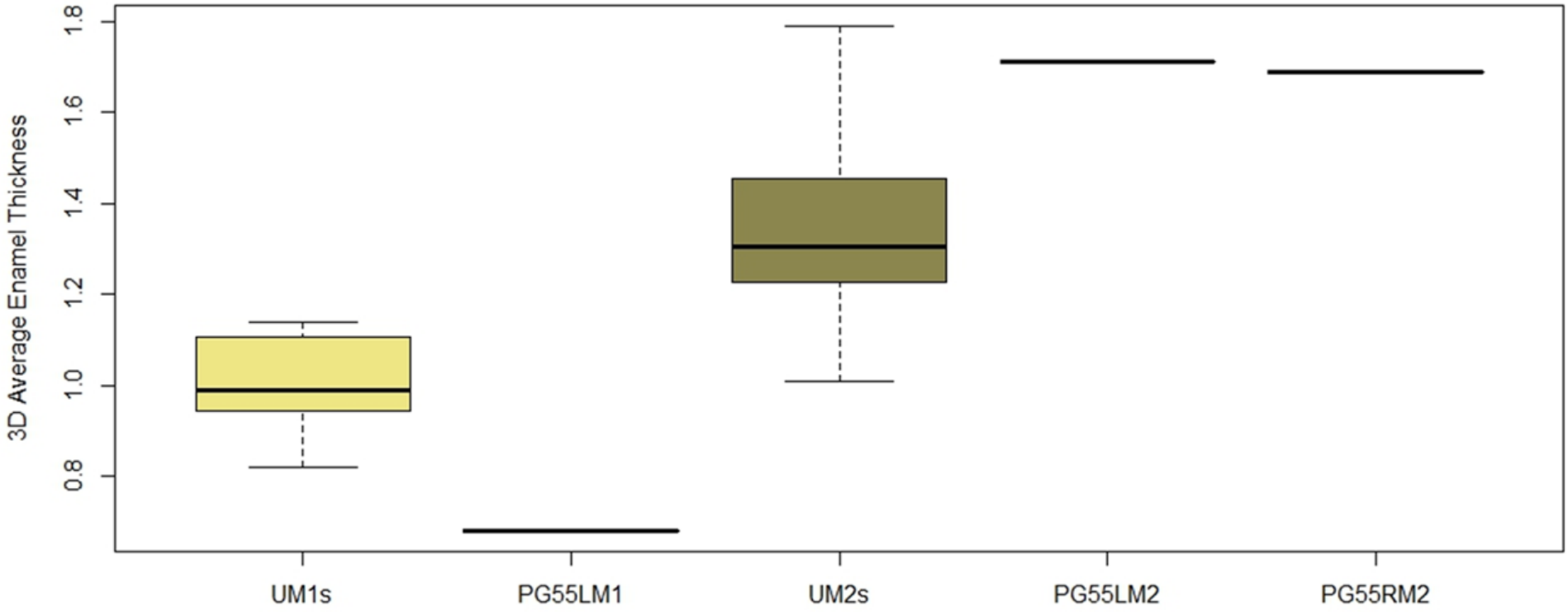

l4

ere to download high resolution image

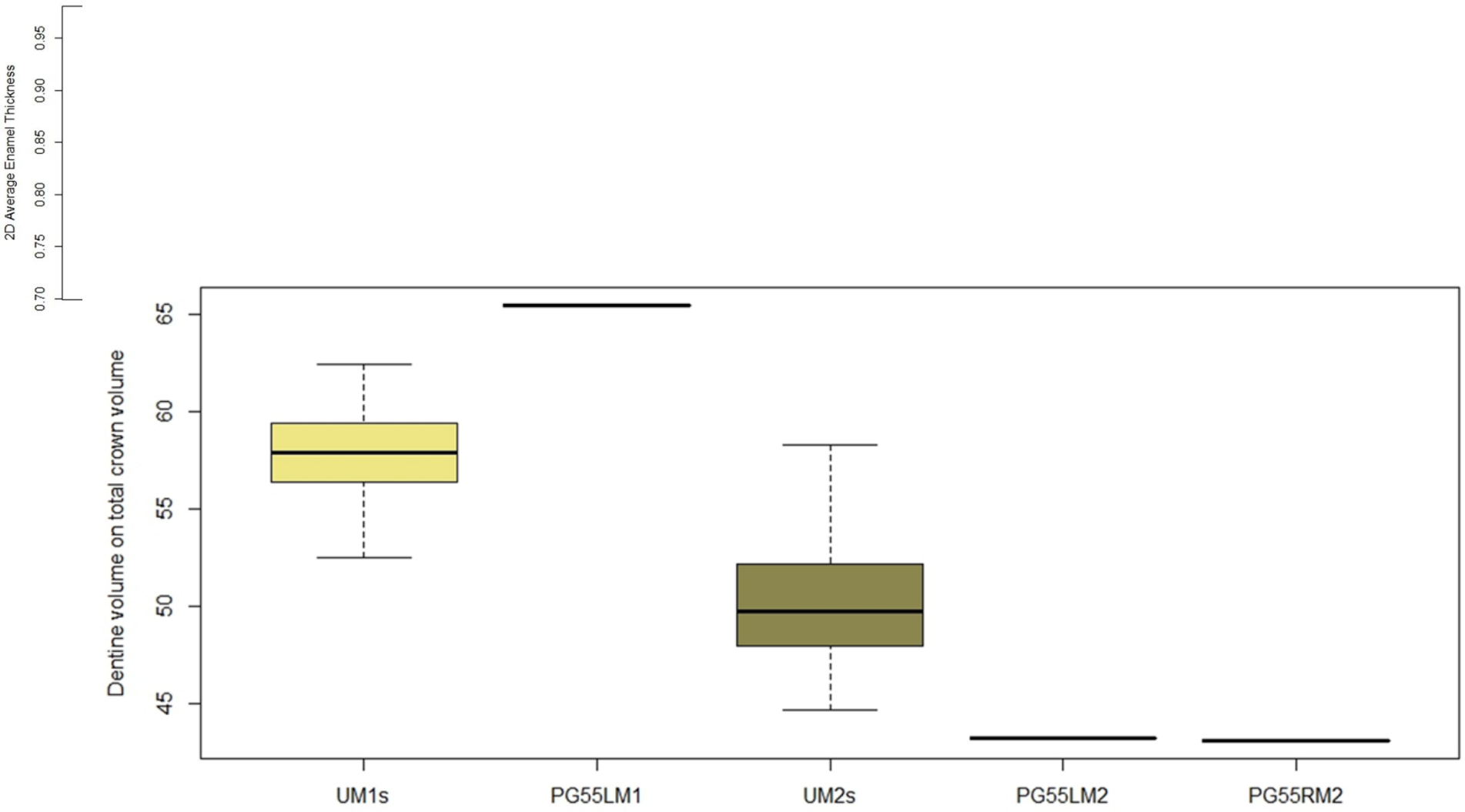

Figure 15
Click here to download high resolution image

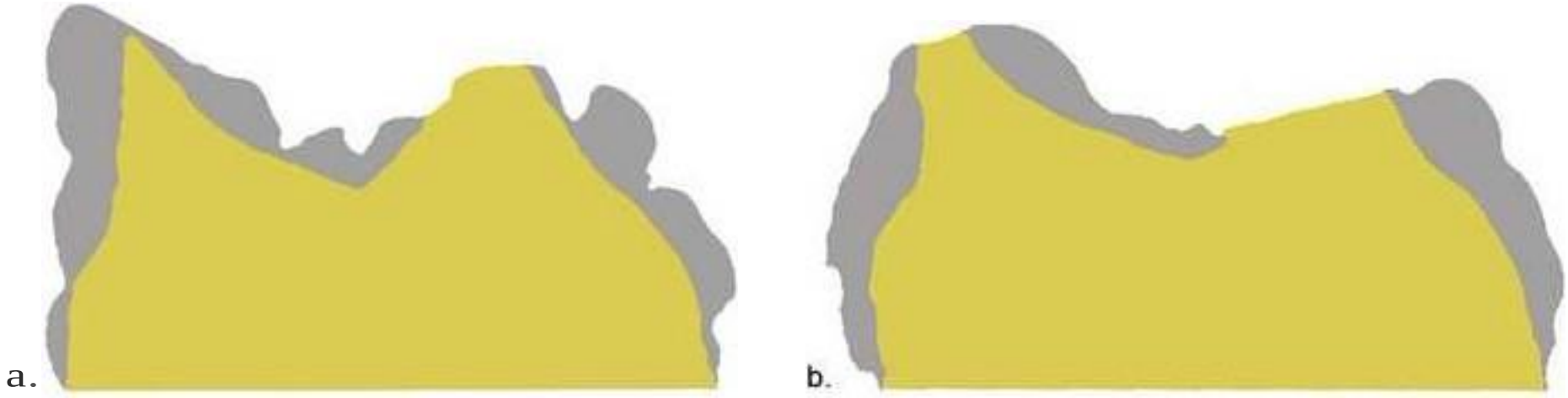

Figure 16
Click here to download high resolution image

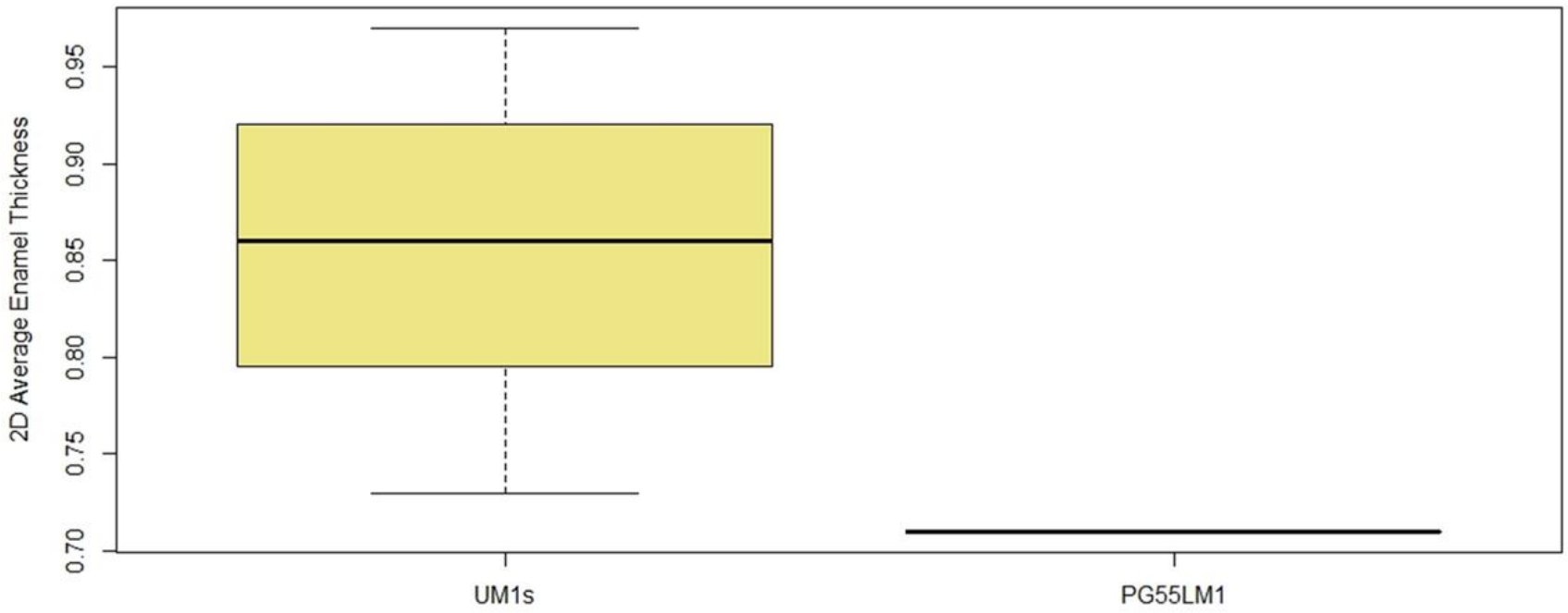

3. Conclusions

3.1. Why labelling individuals matters: The cases of Qesem Cave, Israel, and Grotta del Cavallo, Italy

Our view on human evolution changes and widens as the fossil evidence accumulates and new information is gathered. Despite the recent advancement in our understanding of the human past, the scenario we have reconstructed is still patchy. In this perspective each finding is of crucial relevance, and its morphology, function, and taxonomic identification has important implications for our understanding of human evolution and the history of the human population.

The research reported in chapters 2.2 and 2.7, used various virtual techniques for the investigation of the enamel thickness and crown morphology by means of GM methods. Focusing on deciduous and permanent teeth, respectively, they were conceived for the morphological characterization of the dental specimens in order to gather hints about the nature of the human clade to which they belonged.

The work on the deciduous teeth from Grotta del Cavallo, Apulia, Italy presented in chapter 2.2 illustrates how the application of new techniques and approaches to already known findings might change our view on the nature and timing of human evolution. The taxonomic reassessment of these deciduous molars to modern humans has radically changed our interpretation of the makers of the Uluzzian, a “transitional” culture previously attributed to Neanderthals. Moreover, a new dating of the teeth pushed the modern human settlement of southern Italy to at least 43,000-45,000 years ago, suggesting that modern humans entered Europe also from a southern route, possibly from the Levant (Soares et al., 2010; Hershkovitz et al., 2015). The success of the morphological assessment for these dental specimens owes to several factors. First, even if Neanderthals and modern humans are phylogenetically very close (Wall et al., 2009; Green et al., 2010; Prüfer et al., 2014), Neanderthals accumulated derived features that possess a high diagnostic value, as detailed in section 3.2. Second, the research protocols designed were able to capture and assess those features. Third, our knowledge of Neanderthal and modern human dental variability is based on numerous studies (Bailey, 2002; Macchiarelli et al., 2006; Smith et al., 2010), which have contributed to the definition of the diagnostic features and new approaches for their assessment (Bailey and Lynch, 2005; Benazzi et al., 2011a; Gómez-Robles et al., 2012; Bauer et al., 2015), and to the evaluation of their frequencies and degree of expression (e.g., Kupczik and Hublin, 2010; Bailey et al., 2011).

Chapter 2.7 (and Fornai et al., in preparation), which focuses on some of the dental remains from Qesem Cave (QC) Middle Pleistocene teeth (Hershkovitz et al., 2011; Hershkovitz et al., submitted), demonstrated once more that the methods used were effective in distinguishing between modern humans and Neanderthals. The 3D imaging techniques combined with GM methods provided an accurate quantitative description of the QC specimens, using several dental traits of crown shape and form. Even though the QC teeth cannot yet be classified on the basis of the evidence still available, the analyses carried out provided an accurate description of the dental specimen in comparison to a large sample of Neanderthal, modern human, and *Homo heidelbergensis* specimens. For the Levantine Lower and Middle Pleistocene, the only hard evidence available consists of skull fragments and isolated teeth, and a femoral shaft (Turville-Petre, 1927; McCown and Keith, 1939; Tobias, 1966; Anati and Haas, 1967; Geraads and Tchernov, 1983; Jagher et al., 1997; Belmaker et al., 2002). Moreover, since the teeth are the only human remains at the QC site, it is crucial to carry out studies for a comprehensive investigation of the dental morphology. Thus, our study provided important information for this place and time of

human evolution for which human history must be reconstructed from scarce and discontinuous evidence.

The case studies mentioned above illustrate that two key points need to be addressed to enable the identification of unknown specimens and to attempt reconstructing human history. These are:

- the exploration of intra- and inter-specific variations in both extinct and living species, and

- the creation of new methods and protocols for the morphological and morphometric investigation of dental remains.

3.2. Exploration of intra- and inter-specific variation

Our scientific contributions have added to the understanding of the intra- and inter-specific variability with the exploration of the variation in teeth from different species.

We have confirmed through several studies that even closely related taxa might deviate morphologically on the bases of specific diagnostic features, as in the case of Neanderthals and modern humans. As seen throughout chapters 2.1-2.3, and 2.5-2.7, these taxa can be distinguished on the basis of several features of the dental crown, e.g., the shape of their cervical and crown outlines (see also, Bailey and Lynch, 2005; Benazzi et al., 2011a; Gómez-Robles et al., 2012; Bauer et al., 2015; Fornai et al., in preparation), the shape of the EDJ marginal ridge (see also, Bauer et al., 2015; Fornai et al., in preparation). Additionally, it has been demonstrated that significant differences can be found also in the relative thickness of the enamel, measured on the whole crown or at specific sections (Zilberman and Smith, 1992; Macchiarelli et al., 2006; Olejniczak et al., 2008a), as well as in other dental aspects, for example the morphology of the dental roots (Kupczik and Hublin, 2010). Similar morphological distinctions were observed on the basis of the deciduous dentition as shown in chapters 2.2, 2.3, and 2.5 (but see also Zilberman et al., 1992, Bailey et al., 2014, Fornai et al., in preparation). The fact that Neanderthals and modern humans almost certainly interbred (see the latest Fu et al., 2015) introduces additional challenges in the interpretation of the phenotypic manifestations of these *Homo* groups. The ranges of variability of Neanderthals and modern humans in the various diagnostic features is still to be fully explored, but considering the challenges proper of paleosciences, we need to accumulate knowledge from various studies. With this aim, in chapter 2.5, we provided information about the range of variability for the enamel thickness in upper deciduous molars from both Neanderthals and modern humans, while in chapter 2.3 the variability of the dental crown was investigated in terms of crown and cervical outlines.

In fact, we have seen above (section 1.3) how challenging it might be to assess variation in extinct species, and define the boundaries between individual, age related, sexual or specific differences. Moreover, it is difficult to distinguish between homology and homoplasy, thus establishing the presence of monophyly or parallelism (Gould, 2002) (the thin-enamel condition in both *Pongo* and *Homo* represents an example). The case of *Australopithecus africanus* (*sensu latu*) discussed in chapter 2.6 is emblematic. Many possible sources of variation have been advocated to explain the variability observed within its hypodigm, including individual variation (Kimbel and White, 1988; Lockwood and Tobias, 1999; Wood, 1991; Zipfel and Berger, 2009; Grine et al., 2013), sexual-dimorphism (Broom, 1947; Lockwood, 1999), and inter-specific variation (Clarke, 1988, 2008). Although hints suggesting the presence of two or more distinct species arose from investigations focused on different anatomical regions, including teeth, cranial and postcranial remains (e.g., Clarke, 1988, 2008; Kimbel and White, 1988; Calcagno et al., 1997; Lockwood and Moggi-Cecchi, 1998; Lockwood and Tobias, 1999, 2002; Schwartz and Tattersall, 2005;

Moggi-Cecchi and Boccone, 2007; Zipfel and Berger, 2009), none of these studies have provided a definitive and unequivocal answer. Our study based on multiple, state-of-the-art geometric morphometric approaches has not resolved the issue either, but has demonstrated that, if some of the *Au. africanus* specimens belonged to a different species, factors other than the morphology of maxillary second molar crown need to be considered to address the issue. Remarkably, the morphological features measured from these teeth cannot be used to distinguish between *Australopithecus* and *Paranthropus*, but their separation into two different hominin genera is widely accepted.

This suggests also that intra-specific variability can easily be underestimated, given that our view of paleodiversity is certainly biased by incomplete and sparse fossil evidence. The very few fortunate cases of relatively complete individuals and abundant assemblages, representing one population, or at least a few close populations (e.g., Sima de los Huesos, Tbilisi), exemplifies a notable warning to paleoanthropologists: the dental remains might show such a degree of variability and admixture of traits that, if we had found few teeth in isolation, we would have never concluded they belonged to individuals of the same species (see discussion in White, 2014). In this regard, further evidence comes from additional studies on modern human lower premolars reported in Krenn (2015; Krenn et al., in preparation; but see also Buchegger et al., 2015 for upper premolars). These works have provided evidence of a very high variability within recent modern populations, with a complete overlap in the distribution of premolars from geographically and behaviorally very diverse populations. This has important implication for studies using recent modern humans for comparative purposes, because it implies that the population used does not influence the outcome.

3.3. Establishing virtual imaging approaches for the investigation of teeth

Considering the rarity of fossils and the central role of their morphology in paleoanthropology, it is important to establish approaches suitable to gather the most information from each specimen (Weber, 2015). The introduction of virtual imaging techniques in anthropology has created new ways of studying teeth. Virtual techniques enable non-destructive access to the internal structure of teeth, allow investigation of small and complex objects, and could lead to higher accuracy than traditional approaches. Throughout the research work presented in this thesis, new protocols for the investigation of dental morphology and morphometry were established, and their efficacy along with their accuracy in comparison to other approaches were assessed. There is no general rule about which kind of approach should be preferred in GM studies. Whether in 2D or 3D, on the outer or the inner aspect of teeth, using only landmarks or adding also semilandmarks, the research protocol must be designed on the basis of the research question to be addressed, the anatomical region to study, the sample size, and the technical resources available. For example, the dentine marginal edge of lower molars is better described using semilandmarks along the marginal edge, rather than few points on and between the horn tips (Fornai, unpublished data); however, relatively few points suffice to assess the relative position of teeth in the dental arch (e.g., Kieser et al., 2007; Banabilh et al., 2009; Čelar et al., 2014). As seen in chapters 2.2, 2.3, 2.6, and 2.7 either the EDJ marginal edge or the cervical and crown outlines can be used for the taxonomic discrimination between Neanderthal and modern human molars (see also Benazzi et al., 2011a; Bailey et al., 2014; Fornai et al., in preparation). Therefore, 3D models of the outer crown can be considered in case the EDJ cannot be represented.

The power and flexibility of virtual techniques make them useful for applications involving various objects and diverse purposes. Obviously, an adaptation of the protocols is needed to better suit the morphology of the item under study and the purposes of the study. For example, the protocols designed

in chapter 2.4 for unworn permanent molars were successfully used on deciduous molars, and adapted to suit the investigation of worn specimens in chapters 2.5 (and in Fornai et al., in preparation). Reproducibility and standardization of procedures are key requisites of scientific methods that should guarantee the reliability of the study and ease the comparison of the outcomes from different studies, as discussed in chapter 2.4. For example, the same protocol defined in chapter 2.4 for the investigation of hominin molar relative enamel thickness was applied to an individual affected by congenital syphilis (chapter 2.8) for the quantification of the expression of the dental stigmata (i.e., mulberry molars). We used the same techniques to design a new protocol for the assessment of enamel thickness in genetically modified mice in the investigation of amelogenesis (fig. 9; Eckstein et al., 2015; work in progress coordinated by Lacruz R.)

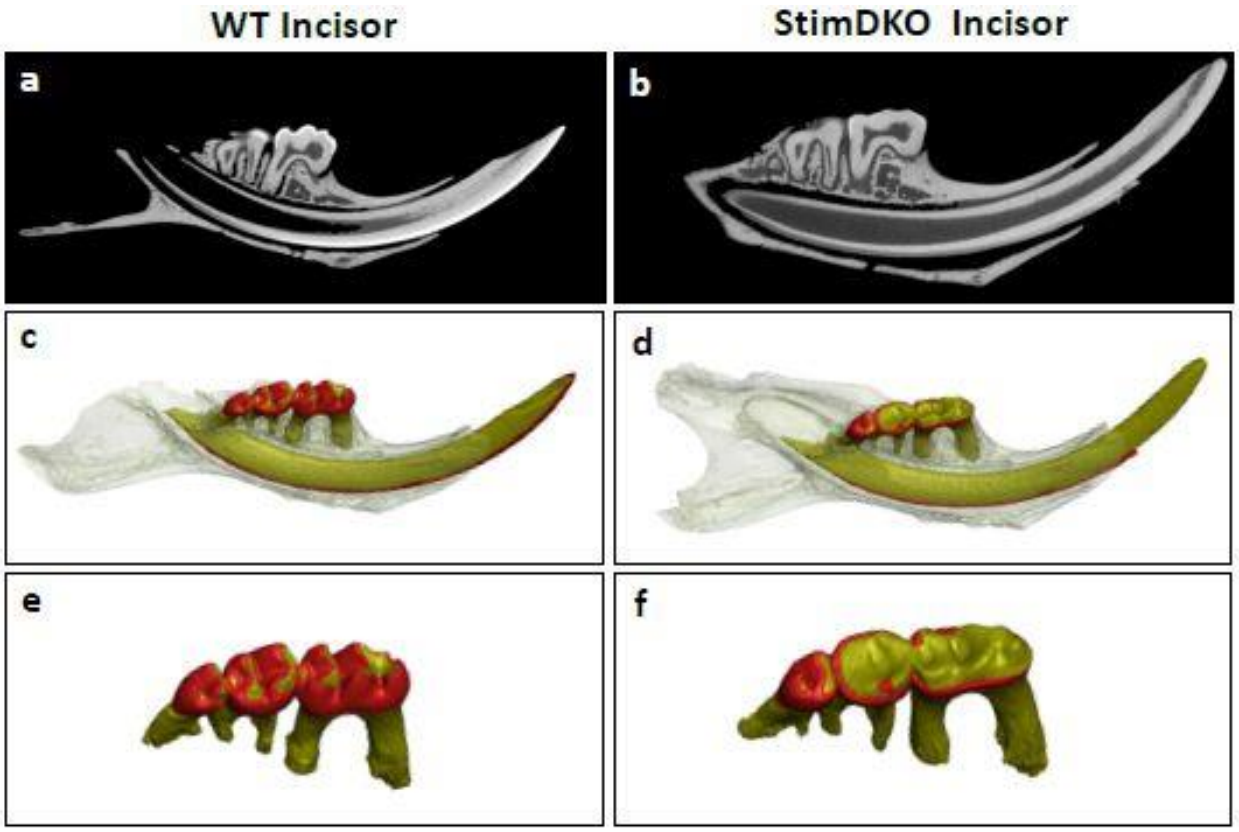

Fig. 9 – Comparison of incisor and molar teeth from individuals at the same age. The knockout (StimDKO), with a conditional deletion of Stim1 and Stim2 specifically in ameloblasts, presents a reduced amount of enamel than the control mouse (WT) (from Eckstein et al., 2015.)

These techniques can be effectively used for exploring the thickness of structures other than dental tissues, as in the research we are carrying out on human mandibles for the assessment of the thickness of the cortical bone in relation to different degrees of dental wear, and in subjects showing different patterns of nocturnal bruxism (fig. 10; Badreddin D., work in progress coordinated by Rausch-Fan X. and Fornai C.).

Similarly, the protocols for the acquisition of crown and cervical outlines described in chapters 2.1 and 2.3, conceived for the investigation of molar dental crowns of Neanderthals and modern humans, have found application to other dental classes and taxa (chapters 2.6, 2.7). Intuitively, one might envisage the

use of the similar techniques to objects other than teeth, where the acquisition of outlines might be convenient (i.e., if the structure lacks anatomical landmarks) and adequately capture the morphology of the features of interest. Broadly speaking, GMM is a tool suited for the study of covariances of biological form (Bookstein, 1991), and can be successfully used to assess the effect of known biological factors on morphology. This means that the morphometric tools presented here can be applied in diverse disciplines, as in forensic anthropology for the investigation of the effects of pathological conditions on skeletal remains (e.g., Baab et al., 2013; Milella et al., 2015) or in medicine for understanding the effects of pathological conditions in patients (e.g., Singh et al., 2004). GMM can be successfully applied in growth and development studies (e.g., O'Higgins and Jones, 1998; Coquerelle et al., 2013; Mitteroecker et al., 2005) and biomechanical research (O'Higgins et al., 2011; Smith et al., 2015).

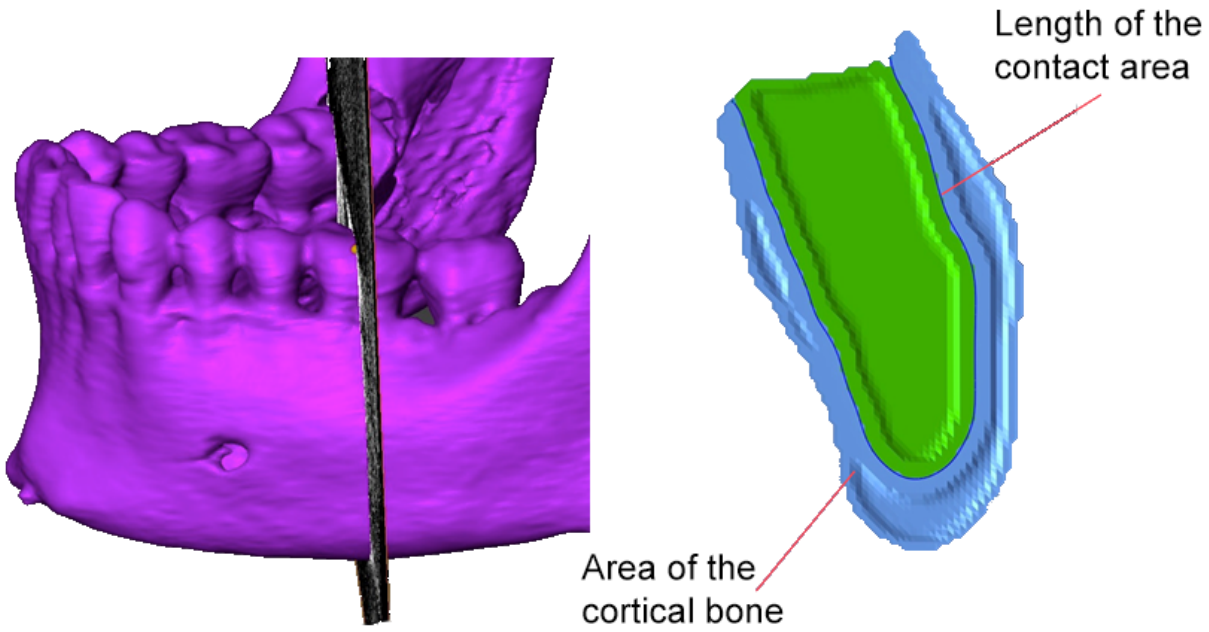

Fig. 10 – Section at the lower first molar where the average cortical thickness is evaluated (= Area of the cortical bone / Length of the contact area between cortical and trabecular bone) (images courtesy of D. Badreddin, modified).

In conclusion, the approaches used in the research works presented in this thesis, combining virtual imaging techniques and GMM, have allowed us to accurately and comprehensively describe the dental specimens investigated. The high reproducibility of the methods applied allow for the comparison of the outcomes from other studies. The tools and protocols we used are particularly flexible and can be adapted to suit the purposes of different kinds of morphological investigations for various biological objects.

4. Acknowledgments

As in any long-term and challenging project, there are many people to thank for their contribution and support.

First of the list is my supervisor Gerhard W. Weber who gave me the possibility to pursue this aim of mine and supported me in many important ways. Without Gerhard, I would have not been part of any of the projects presented in this thesis. Beside him, along the way I met great mentors: Stefano Benazzi, who taught me most of what I know about virtual techniques; Fred L. Bookstein who lavished me with his knowledge, genius, power, and enthusiasm throughout these years; Rudolf Slavicek who is gifted with contagious passion, curiosity, and endless energy, and a deep knowledge of the masticatory apparatus. All of them are kind human beings before been brilliant minds and talented scholars, and instilled trust and enthusiasm in me.

The scientific papers presented here are the outcomes of team works and I am grateful to all co-authors who involved me in their research or participated to mine in such a productive way. I want to thank also my colleagues Diana and Dzhuliana Badreddin, Előd Úry, Inga Stolbovaya, and Peter Currie for the interesting projects they are carrying out and through which I was introduced to a variety of clinical aspects of dentistry, orthodontics and periodontology. During these years, I met many other brilliant researchers, who I do not mention here but I thank for the interesting discussions or for the help they might have provided.

At the Department of Anthropology almost everyone has helped me at some point in some way, so I thank each professor, student, administrator, secretary, cleaning lady. In particular, I want to acknowledge Martin Dockner and Fabian Siegle who are always kind and supportive and eased my working life tremendously.

Matthew DiFranco improved the English language of this dissertation.

Many friends have sustained me throughout these years, encouraging me or looking after my boy when I needed an “emergency childcare”. Norbert and his family, Anita and Denis, Eva and Lebon, Monika and Thomas, Yvette and Norbert, and their kids have been my Austrian family.

My son Niccolò comes as last, but he is always the first in my heart and thoughts. He is my favorite motivator.

My research and my stay at the Department of Anthropology were financed by: the Siegfried Ludwig-Rudolf Slavicek Foundation, Vienna, Austria (FA547016), A.E.R.S. Dental Medicine Organisations GmbH, Vienna, Austria (FA547013), and NSF 01-120 Hominid Grant 2007, and the European Union FP6 Marie Curie Actions MRTN-CT-2005-019564 Q4 “EVAN” (FA547004).

I am deeply grateful to Rudolf Slavicek and Gerhard W. Weber for making it possible.

5. References

Abbott, S.A., 1984. A comparative study of tooth root morphology in the great apes, modern man and early hominids. University of London.

Adams, D.C., Cardini, A., Monteiro, L.R., O'Higgins, P., Rohlf, F.J., 2011. Morphometrics and phylogenetics: principal components of shape from cranial modules are neither appropriate nor effective cladistic characters. J Hum Evol 60, 240-243.

Adams, D.C., Rohlf, F.J., Slice, D.E., 2004. Geometric morphometrics: Ten years of progress following the 'revolution'. Ital J Zool 71, 5-16.

Adams, D.C., Rosenberg, M.S., 1998. Partial warps, phylogeny, and ontogeny: a comment on Fink and Zelditch (1995). Syst Biol 47, 168-173.

Aiello, L.C., Dean, M.C., 2002. An Introduction to Human Evolutionary Anatomy. Elsevier.

Anati, E., Haas, N., 1967. The Hazorea Pleistocene site: A Preliminary Report. Man 2, 454-456.

Baab, K.L., McNulty, K.P., Harvati, K., 2013. *Homo floresiensis* Contextualized: A Geometric Morphometric Comparative Analysis of Fossil and Pathological Human Samples. PLoS One 8, e69119.

Bailey, S.E., 2002. A closer look at Neanderthal postcanine dental morphology: The mandibular dentition. Anat Rec 269, 148-156.

Bailey, S.E., 2004. A morphometric analysis of maxillary molar crowns of Middle-Late Pleistocene hominins. J Hum Evol 47, 183-198.

Bailey, S.E., Benazzi, S., Souday, C., Astorino, C., Paul, K., Hublin, J.-J., 2014. Taxonomic differences in deciduous upper second molar crown outlines of *Homo sapiens*, *Homo neanderthalensis* and *Homo erectus*. J Hum Evol 72, 1-9.

Bailey, S.E., Hublin, J.-J., 2007. Dental Perspectives on Human Evolution. Springer, Dordrecht, The Netherlands.

Bailey, S.E., Lynch, J.M., 2005. Diagnostic differences in mandibular P4 shape between neandertals and anatomically modern humans. Am J Phys Anthropol 126, 268-277.

Bailey, S.E., Skinner, M.M., Hublin, J.-J., 2011. What lies beneath? An evaluation of lower molar trigonid crest patterns based on both dentine and enamel expression. Am J Phys Anthropol 145, 505-518.

Banabilh, S.M., Suzina, A.H., Dinsuhaimi, S., Samsudin, A.R., Singh, G.D., 2009. Dental arch morphology in south-east Asian adults with obstructive sleep apnoea: geometric morphometrics. J Oral Rehabil 36, 184-192.

Bauer, C.C., Benazzi, S., Harvati, K., 2015. Geometric morphometric analysis and internal structure measurements of Neanderthal and modern human lower second premolars. 2015 156 p. 80.

Bayes, M., Hartung, A.J., Ezer, S., Pispa, J., Thesleff, I., Srivastava, A.K., Kere, J., 1998. The anhidrotic ectodermal dysplasia gene (EDA) undergoes alternative splicing and encodes ectodysplasin-A with deletion mutations in collagenous repeats. Hum Mol Genet 7, 1661-1669.

Bei, M., 2009. Molecular genetics of tooth development. Curr Opin Genet Dev 19, 504-510.

Bei, M., Maas, R., 1998. FGFs and BMP4 induce both Msx1-independent and Msx1-dependent signaling pathways in early tooth development. Development 125, 4325-4333.

Belmaker, M., Tchernov, E., Condemi, S., Bar-Yosef, O., 2002. New evidence for hominid presence in the Lower Pleistocene of the Southern Levant. J Hum Evol 43, 43-56.

Benazzi, S., 2007. Image analysis in the morphological and morphometric study of teeth. University of Bologna, Bologna.

Benazzi, S., Coquerelle, M., Fiorenza, L., Bookstein, F.L., Katina, S., Kullmer, O., 2011a. Comparison of dental measurement systems for taxonomic assignment of first molars. Am J Phys Anthropol 144, 342-354.

Benazzi, S., Douka, K., Fornai, C., Bauer, C.C., Kullmer, O., Svoboda, J., Pap, I., Mallegni, F., Bayle, P., Coquerelle, M., Condemi, S., Ronchitelli, A., Harvati, K., Weber, G.W., 2011b. Early dispersal of modern humans in Europe and implications for Neanderthal behaviour. Nature 479, 525-528.

Benazzi, S., Fornai, C., Bayle, P., Coquerelle, M., Kullmer, O., Mallegni, F., Weber, G.W., 2011c. Comparison of dental measurement systems for taxonomic assignment of Neanderthal and modern human lower second deciduous molars. J Hum Evol 61, 320-326

Benazzi, S., Fornai, C., Buti, L., Toussaint, M., Mallegni, F., Ricci, S., Gruppioni, G., Weber, G.W., Condemi, S., Ronchitelli, A., 2012. Cervical and crown outline analysis of worn Neanderthal and modern human lower second deciduous molars. Am J Phys Anthropol 149, 537-546.

Benazzi, S., Kullmer, O., Grosse, I.R., Weber, G.W., 2011c. Using occlusal wear information and finite element analysis to investigate stress distributions in human molars. J Anat 219, 259-272.
Benazzi, S., Nguyen, H.N., Kullmer, O., Hublin, J.-J., 2013a. Unravelling the Functional Biomechanics of Dental Features and Tooth Wear. PLoS One 8, e69990.
Benazzi, S., Nguyen, H.N., Kullmer, O., Hublin, J.-J., 2015. Exploring the biomechanics of taurodontism. J Anat 226, 180-188.
Benazzi, S., Nguyen, H.N., Schulz, D., Grosse, I.R., Gruppioni, G., Hublin, J.J., Kullmer, O., 2013b. The evolutionary paradox of tooth wear: simply destruction or inevitable adaptation? PLoS One 8, e62263.
Bernal, V., 2007. Size and shape analysis of human molars: comparing traditional and geometric morphometric techniques. Homo 58, 279-296.
Beutel, R., Friedrich, F., Leschen, R.B., 2009. Charles Darwin, beetles and phylogenetics. Naturwissenschaften 96, 1293-1312.
Beynon, A.D., Dean, M.C., Reid, D.J., 1991. On thick and thin enamel in hominoids. Am J Phys Anthropol 86, 295-309.
Beynon, A.D., Wood, B.A., 1986. Variations in enamel thickness and structure in East African hominids. Am J Phys Anthropol 70, 177-193.
Bookstein, F.L., 1980. When One Form Is between Two Others: An Application of Biorthogonal Analysis. Amer Zool 20, 627-641.
Bookstein, F.L., 1986. Size and Shape Spaces for Landmark Data in Two Dimensions. 181-222.
Bookstein, F.L., 1989. Principal warps: thin-plate splines and the decomposition of deformations. Pattern Analysis and Machine Intelligence, IEEE Transactions on 11, 567-585.
Bookstein, F.L., 1991. Morphometric tools for landmark data: Geometry and biology. Cambridge University Press, New York.
Bookstein, F.L., 1994. Can biometrical shape be a homologous character?, in: Hall, B.K. (Ed.), Homology: The hierarchical basis of comparative biology. Academic Press, New York, pp. 197–227.
Bookstein, F.L., 1996. Biometrics, biomathematics and the morphometric synthesis. Bull Math Biol 58, 313-365.
Bookstein, F.L., 1998. A hundred years of morphometrics. Acta Zool Hung 44, 7–59.
Bookstein, F.L., 2013. Reasoning and measuring. Cambridge University Press, Cambridge.
Bookstein, F.L., 2015. The Relation Between Geometric Morphometrics and Functional Morphology, as Explored by Procrustes Interpretation of Individual Shape Measures Pertinent to Function. Anat Rec 298, 314-327.
Bookstein, F.L., Chernoff, B., Elder, R.L., Humphries, J.M.J., Smith, G.R., Strauss, R.E., 1985. Morphometrics in Evolutionary Biology. The Academy of Natural Sciences of Philadelphia, Special Publication No. 15.
Broom, R., 1947. Discovery of a New Skull of the South African Ape-man, *Plesianthropus*. Nature 159, 672.
Buchegger, L., 2015. Variation of 3D outer and inner crown morphology of upper premolars in modern humans. Master Thesis, Faculty of Life Sciences, University of Vienna.
Butler, P.M., 1956. The ontogeny of molar patterns. Biol Rev 31, 30–70.
Butler, P.M., 1967. The prenatal development of the human first upper permanent molar. Arch Oral Biol 12, 551-563.
Butler, P.M., 1971. Growth of human tooth germs, in: Dahlberg, A.A. (Ed.), Dental Morphology and Evolution. University of Chicago Press, Chicago, pp. 3-13.
Butler, P.M., 1986. Primate dental evolution, in: Wood, B., Martin, L., Andrews, P. (Eds.), Major topics in primate and human evolution. Cambridge University Press, Cambridge, pp. 89-106.
Calcagno, J.M., Cope, D.A., Lacy, M.G., Moggi-Cecchi, J., Tobias, P.V., 1999. Reinvestigating the number of hominid species in Sterkfontein Member 4. Am J Phys Anthropol S28, 101.
Calcagno, J.M., Cope, D.A., Lacy, M.G., Tobias, P.V., 1997. Is A. africanus the only hominid species in Sterkfontein Member 4? Am J Phys Anthropol S24, 86-87.
Carstens, B.C., Pelletier, T.A., Reid, N.M., Satler, J.D., 2013. How to fail at species delimitation. Mol Ecol 22, 4369-4383.
Carter, K., Worthington, S., Smith, T.M., 2014. News and views: Non-metric dental traits and hominin phylogeny. J Hum Evol 69, 123-128.
Čelar, A.G., Onodera, K., Bertl, M.H., Astl, E., Bantleon, H.P., Sato, S., Mitteroecker, P., 2014. Geometric morphometric evaluations of a randomized prospective split-mouth study on modes of ligation and reverse-curve mechanics. Orthod Craniofac Res 17, 158-169.
Chai, Y., Jiang, X., Ito, Y., Bringas, P., Jr., Han, J., Rowitch, D.H., Soriano, P., McMahon, A.P., Sucov, H.M., 2000. Fate of the mammalian cranial neural crest during tooth and mandibular morphogenesis. Development 127, 1671-1679.

Chaimanee, Y., Jolly, D., Benammi, M., Tafforeau, P., Duzer, D., Moussa, I., Jaeger, J.-J., 2003. A Middle Miocene hominoid from Thailand and orangutan origins. Nature 422, 61-65.

Chaimanee, Y., Lebrun, R., Yamee, C., Jaeger, J.J., 2011. A new Middle Miocene tarsier from Thailand and the reconstruction of its orbital morphology using a geometric-morphometric method. Proc Biol Sci 278, 1956-1963.

Clarke, R.J., 1988. A new *Australopithecus* cranium from Sterkfontein and its bearing on the ancestry of *Paranthropus*, in: Grine, F.E. (Ed.), Evolutionary History of the "Robust" Australopithecines. Aldine de Gruyter, New York, pp. 285-292.

Clarke, R.J., 2008. Latest information on Sterkfontein's *Australopithecus* skeleton and a new look at *Australopithecus*. S Afr J Sci 104, 443-449.

Constant, D.A., Grine, F.E., 2001. A review of taurodontism with new data on indigenous southern African populations. Arch Oral Biol 46, 1021-1029.

Cope, D.A., 1993. Measures of Dental Variation as Indicators of Multiple Taxa in Samples of Sympatric Cercopithecus Species, in: Kimbel, W.H., Martin, L.B. (Eds.), Species, Species Concepts and Primate Evolution. Springer US, pp. 211-237.

Cope, D.A., Lacy, M.G., 1992. Falsification of a single species hypothesis using the coefficient of variation: a simulation approach. Am J Phys Anthropol 89, 359-378.

Coquerelle, M., Prados-Frutos, J.C., Benazzi, S., Bookstein, F.L., Senck, S., Mitteroecker, P., Weber, G.W., 2013. Infant growth patterns of the mandible in modern humans: a closer exploration of the developmental interactions between the symphyseal bone, the teeth, and the suprahyoid and tongue muscle insertion sites. J Anat 222, 178-192.

Corruccini, R.S., 1987. The dentinoenamel junction in primates. Int J Primatol 8, 99-114.

Corti, M., 1993. Geometric morphometrics: An extension of the revolution. Trends Ecol Evol 8, 302-303.

Cracraft, J., 1989. Speciation and its ontology: The empirical consequences of alternative species concepts for understanding the patterns and processes of differentiation, in: Otte, D., Endler, J.A. (Eds.), Speciation and its Consequences. Sinauer Associates, Sunderland, MA, pp. 28-59.

Dahlberg, A.A., 1971. Penetrance and expressivity of dental traits, in: Dahlberg, A.A. (Ed.), Dental Morphology and Evolution. University of Chicago Press, Chicago, pp. 3-13.

Dryden, I.L., Mardia, K.V., 1998. Statistical Shape Analysis. John Wiley, London.

Eckstein, M., Vaeth, M., Fornai, C., Nurbaeva, M., Kakar, L., Atria, P., Tovar, N., Coelho, P., Bromage, T., Feske, S., Lacruz, R.S., 2015. CRAC Channels Are Essential For Amelogenesis. The NYU Center for Skeletal and Craniofacial Biology Biannual Retreat, 17 April 2015. Poster Session.

Eldredge, N., Cracraft, J., 1980. Phylogenetic patterns and the evolutionary process. Columbia University Press, New York.

Emonet, E.-G., Tafforeau, P., Chaimanee, Y., Guy, F., de Bonis, L., Koufos, G., Jaeger, J.-J., 2012. Three-dimensional analysis of mandibular dental root morphology in hominoids. J Hum Evol 62, 146-154.

Feeney, R.N.M., Zermeno, J.P., Reid, D.J., Nakashima, S., Sano, H., Bahar, A., Hublin, J.-J., Smith, T.M., 2010a. Enamel thickness in Asian human canines and premolars. Anthropol Sci 118.

Feeney, R.N.M., Zermeno, J.P., Reid, D.J., Nakashima, S., Sano, H., Bahar, A., Hublin, J.-J., Smith, T.M., 2010b. Enamel thickness in Asian human canines and premolars. Anthropol Sci 118, 191-198.

Fink, W.L., Zelditch, M.L., 1995. Phylogenetic Analysis of Ontogenetic Shape Transformations: A Reassessment of the Piranha Genus Pygocentrus (Teleostei). Syst Biol 44, 343-360.

Fornai, C., Bauer, C.C., Benazzi, S., Harvati, K., Weber, G.W., 2011. Enamel thickness and dental tissue proportions in modern human upper first deciduous molars. Poster presentation, European Society for the study of Human Evolution - ESHE, Leipzig, Germany.

Fornai, C., Benazzi, S., Bayle, P., Pap, I., Svoboda, J., Harvati, K., Weber, G.W., 2012. Enamel thickness and dental tissue proportions in Neanderthal and modern human upper deciduous molars. Am J Phys Anthropol 147, 145.

Fornai, C., Benazzi, S., Gopher, A., Barkai, R., Sarig, R., Hershkovitz, I., Weber, G.W. (submitted). The Qesem Cave hominin material (part 2): A morphometric analysis of dm2-QC2 deciduous lower second molar. Quatern Int.

Fornai, C., Benazzi, S., Svoboda, J., Pap, I., Harvati, K., Weber, G.W., 2014. Enamel thickness variation of deciduous first and second upper molars in modern humans and Neanderthals. J Hum Evol 76, 83-91.

Fu, Q., Hajdinjak, M., Moldovan, O.T., Constantin, S., Mallick, S., Skoglung, P., Patterson, N, Rohland, N., Lazaridis, I., Nickel, B., Viola, T.B., Prüfer, K., Meyer, M., Kelso, J., Reich, D., Pääbo, S., 2015. An early modern human from Romania with a recent Neanderthal ancestor. Nature doi:10.1038/nature14558

Fu, Q., Li, H., Moorjani, P., Jay, F., Slepchenko, S.M., Bondarev, A.A., Johnson, P.L.F., Aximu-Petri, A., Prüfer, K., de Filippo, C., Meyer, M., Zwyns, N., Salazar-Garcia, D.C., Kuzmin, Y.V., Keates, S.G., Kosintsev, P.A., Razhev, D.I., Richards, M.P., Peristov, N.V., Lachmann, M., Douka, K., Higham, T.F.G., Slatkin, M., Hublin, J.-J., Reich, D., Kelso, J., Viola, T.B., Pääbo, S., 2014. Genome sequence of a 45,000-year-old modern human from western Siberia. Nature 514, 445-449.

Gantt, D.G., 1983. The enamel of Neogene hominoids: Structural and phyletic implications, in: Ciochon, R.L., Corruccini, R.S. (Eds.), New Interpretations of Ape and Human Ancestry. Springer US, pp. 249-298.

Gantt, D.G., Rafter, J.A., 1998. Evolutionary and functional significance of hominoid tooth enamel. Connective Tissue Research 39, 195-206; discussion 221.

Garn, S.M., Lewis, A.B., Kerewsky, R.S., 1966. Sexual Dimorphism in the Buccolingual Tooth Diameter. J Dent Res 45, 1819.

Geraads, D., Tchernov, E., 1983. Fémurs Humains du Pleistocene Moyen de Gesher Benot Ya'aqov (Israel). L'Anthropologie 87, 138-141.

Ghiselin, M.T., 1974. A Radical Solution to the Species Problem. Syst Biol 23, 536-544.

Gingerich, P.D., Schoeninger, M.J., 1979. Patterns of tooth size variability in the dentition of primates. Am J Phys Anthropol 51, 457-465.

Gómez-Robles, A., de Castro, J.M.B., Martinón-Torres, M., Prado-Simón, L., Arsuaga, J.L., 2012. A geometric morphometric analysis of hominin upper second and third molars, with particular emphasis on European Pleistocene populations. J Hum Evol 63, 512-526.

Gómez-Robles, A., Martinón-Torres, M., De Castro, J.B., Margvelashvili, A., Bastir, M., Arsuaga, J.L., Pérez-Pérez, A., Estebaranz, F., Martínez, L.M., 2007. A geometric morphometric analysis of hominin upper first molar shape. J Hum Evol 53, 272-285.

Gómez-Robles, A., Martinón-Torres, M., de Castro, J.M.B., Prado-Simón, L., Arsuaga, J.L., 2011. A geometric morphometric analysis of hominin upper premolars. Shape variation and morphological integration. J Hum Evol 61, 688-702.

Gomez-Robles, A., Martinon-Torres, M., de Castro, J.M.B., Prado, L., Sarmiento, S., Arsuaga, J.L., 2008. Geometric morphometric analysis of the crown morphology of the lower first premolar of hominins, with special attention to Pleistocene *Homo*. J Hum Evol 55, 627-638.

González-José, R., Escapa, I., Neves, W.A., Cúneo, R., Pucciarelli, H.M., 2008. Cladistic analysis of continuous modularized traits provides phylogenetic signals in *Homo* evolution. Nature 453, 775-778.

Gould, S.J., 2002. The structure of evolutionary theory. Harvard University Press, Cambridge.

Gower, J.C., 1975. Generalized procrustes analysis. Psychometrika 40, 33-51.

Green, R.E., Krause, J., Briggs, A.W., Maricic, T., Stenzel, U., Kircher, M., Patterson, N., Li, H., Zhai, W., Fritz, M.H.-Y., Hansen, N.F., Durand, E.Y., Malaspinas, A.-S., Jensen, J.D., Marques-Bonet, T., Alkan, C., Prüfer, K., Meyer, M., Burbano, H.A., Good, J.M., Schultz, R., Aximu-Petri, A., Butthof, A., Höber, B., Höffner, B., Siegemund, M., Weihmann, A., Nusbaum, C., Lander, E.S., Russ, C., Novod, N., Affourtit, J., Egholm, M., Verna, C., Rudan, P., Brajkovic, D., Kucan, Ž., Gušic, I., Doronichev, V.B., Golovanova, L.V., Lalueza-Fox, C., de la Rasilla, M., Fortea, J., Rosas, A., Schmitz, R.W., Johnson, P.L.F., Eichler, E.E., Falush, D., Birney, E., Mullikin, J.C., Slatkin, M., Nielsen, R., Kelso, J., Lachmann, M., Reich, D., Pääbo, S., 2010. A Draft Sequence of the Neandertal Genome. Science 328, 710-722.

Green, R.E., Krause, J., Ptak, S.E., Briggs, A.W., Ronan, M.T., Simons, J.F., Du, L., Egholm, M., Rothberg, J.M., Paunovic, M., Pääbo, S., 2006. Analysis of one million base pairs of Neanderthal DNA. Nature 444, 330-336.

Grine, F.E., 2002. Scaling of tooth enamel thickness, and molar crown size reduction in modern humans: research letter, pp. 503-509.

Grine, F.E., 2005. Enamel thickness of deciduous and permanent molars in modern *Homo sapiens*. Am J Phys Anthropol 126, 14-31.

Grine, F.E., Delanty, M.M., Wood, B.A., 2013. Variation in Mandibular Postcanine Dental Morphology and Hominin Species Representation in Member 4, Sterkfontein, South Africa, in: Reed, K.E., Fleagle, J.G., Leakey, R.E. (Eds.), The Paleobiology of *Australopithecus*. Springer, pp. 125-146.

Guatelli-Steinberg, D., Stinespring-Harris, A., Reid, D.J., Larsen, C.S., Hutchinson, D.L., Smith, T.M., 2014. Chronology of Linear Enamel Hypoplasia Formation in the Krapina Neanderthals. PaleoAnthropology, 431-445.

Gunz, P., Mitteroecker, P., 2013. Semilandmarks: a method for quantifying curves and surfaces. Hystrix, the Italian Journal of Mammalogy; Volume 24, Issue 1 (2013): Virtual Morphology and Evolutionary Morphometrics in the new millenium.

Gunz, P., Mitteroecker, P., Bookstein, F.L., 2005. Semilandmarks in Three Dimensions, in: Slice, D.E. (Ed.), Modern Morphometrics in Physical Anthropology. Kluwer Academic/Plenum Publishers., New York, pp. 73–98.

Guy, F., Gouvard, F., Boistel, R., Euriat, A., Lazzari, V., 2013. Prospective in (Primate) dental analysis through tooth 3D topographical quantification. PLoS One 8, e66142.

Harris, E.F., 2007. Carabelli's trait and tooth size of human maxillary first molars. Am J Phys Anthropol 132, 238-246.

Hennig, W., 1950. Grundzüge einer Theorie der phylogenetischen Systematik. Deutscher Zentralverlag, Berlin.

Hennig, W., 1966. Phylogenetic systematics. University of Illinois Press, Urbana.

Henry, A.G., Ungar, P.S., Passey, B.H., Sponheimer, M., Rossouw, L., Bamford, M., Sandberg, P., de Ruiter, D.J., Berger, L., 2012. The diet of *Australopithecus sediba*. Nature 487, 90-93.

Hershkovitz, I., Marder, O., Ayalon, A., Bar-Matthews, M., Yasur, G., Boaretto, E., Caracuta, V., Alex, B., Frumkin, A., Goder-Goldberger, M., Gunz, P., Holloway, R.L., Latimer, B., Lavi, R., Matthews, A., Slon, V., Mayer, D.B.-Y., Berna, F., Bar-Oz, G., Yeshurun, R., May, H., Hans, M.G., Weber, G.W., Barzilai, O., 2015. Levantine cranium from Manot Cave (Israel) foreshadows the first European modern humans. Nature advance online publication.

Hershkovitz, I., Smith, P., Sarig, R., Quam, R., Rodríguez, L., García, R., Arsuaga, J.L., Barkai, R., Gopher, A., 2011. Middle pleistocene dental remains from Qesem Cave (Israel). Am J Phys Anthropol 144, 575-592.

Hershkovitz, I., Weber, G.W., Gopher, A., Bar-Matthews, M., Slon, V., Quam, R., Sarig, R., submitted. New Middle Pleistocene dental remains from Qesem Cave (Israel). Quatery Int.

Howells, W.W., 1973. Cranial Variation in Man. A Study by Multivariate Analysis of Patterns of Differences Among Recent Human Populations. Peabody Museum, Cambridge, Mass.

Howells, W.W., 1989. Skull Shapes and the Map. Craniometric Analyses in the Dispersion of Modern *Homo*. Peabody Museum, Cambridge, Mass.

Howells, W.W., 1995. Who's Who in Skulls. Ethnic Identification of Crania from Measurements. Peabody Museum, Cambridge, Mass.

Hull, D.L., 1974. Philosophy of Biological Science. Prentice-Hall, Englewood Cliffs.

Hull, D.L., 1976. Are species really individuals? Syst Zool 25, 174-191.

Hull, D.L., 1978. A matter of individuality. Philos Sci 45, 335-360.

Jafarzadeh, H., Azarpazhooh, A., Mayhall, J.T., 2008. Taurodontism: a review of the condition and endodontic treatment challenges. Int Endod J 41, 375-388.

Jagher, R., Le Tensorer, J.-M., Morel, P., Muhesen, S., Renault-Miskovsky, J., Rentzel, P., Schmid, P., 1997. Découvertes de restes humains dans les niveaux acheuléens de Nadaouiyeh Aïn Askar (El Kowm, Syrie Centrale). Paléorient, 87-93.

James Rohlf, F., Marcus, L.F., 1993. A revolution morphometrics. Trends Ecol Evol 8, 129-132.

Jernvall, J., Aberg, T., Kettunen, P., Keranen, S., Thesleff, I., 1998. The life history of an embryonic signaling center: BMP-4 induces p21 and is associated with apoptosis in the mouse tooth enamel knot. Development 125, 161-169.

Jernvall, J., Kettunen, P., Karavanova, I., Martin, L.B., Thesleff, I., 1994. Evidence for the role of the enamel knot as a control center in mammalian tooth cusp formation: non-dividing cells express growth stimulating Fgf-4 gene. Int J Dev Biol 38, 463-469.

Jernvall, J., Thesleff, I., 2000. Reiterative signaling and patterning during mammalian tooth morphogenesis. Mech Dev 92, 19-29.

Kaidonis, J.A., 2008. Tooth wear: the view of the anthropologist. Clinical Oral Investigations 12, 21-26.

Kaifu, Y., Kasai, K., Townsend, G.C., Richards, L.C., 2003. Tooth wear and the "design" of the human dentition: a perspective from evolutionary medicine. Am J Phys Anthropol Suppl 37, 47-61.

Kangas, A.T., Evans, A.R., Thesleff, I., Jernvall, J., 2004. Nonindependence of mammalian dental characters. Nature 432, 211-214.

Kavanagh, K.D., Evans, A.R., Jernvall, J., 2007. Predicting evolutionary patterns of mammalian teeth from development. Nature 449, 427-432.

Kay, R.F., 1975. The functional adaptations of primate molar teeth. Am J Phys Anthropol 43, 195-215.

Kay, R.F., 1981. The nut-crackers - A new theory of the adaptations of the Ramapithecinae. Am J Phys Anthropol 55, 141-152.

Keeling, R., Berger, L., 2013. Potential soft organic tissue preserved in association with the *Australopithecus sediba* fossils from Malapa cave site, South Africa. Am J Phys Anthropol 150, 163-164.

Keith, A., 1913. Problems relating to the teeth of the earlier forms of prehistorical man. Proc R Soc Med 6, 103-119.

Keller, A., Graefen, A., Ball, M., Matzas, M., Boisguerin, V., Maixner, F., Leidinger, P., Backes, C., Khairat, R., Forster, M., Stade, B., Franke, A., Mayer, J., Spangler, J., McLaughlin, S., Shah, M., Lee, C., Harkins, T.T., Sartori, A., Moreno-Estrada, A., Henn, B., Sikora, M., Semino, O., Chiaroni, J., Rootsi, S., Myres, N.M., Cabrera, V.M., Underhill, P.A., Bustamante, C.D., Vigl, E.E., Samadelli, M., Cipollini, G., Haas, J., Katus, H., O'Connor, B.D., Carlson, M.R.J., Meder, B., Blin, N., Meese, E., Pusch, C.M., Zink, A., 2012. New insights into the Tyrolean Iceman's origin and phenotype as inferred by whole-genome sequencing. Nat Commun 3, 698.

Kelley, J., Plavcan, J.M., 1998. A simulation test of hominoid species number at Lufeng, China: implications for the use of the coefficient of variation in paleotaxonomy. J Hum Evol 35, 577-596.

Kendall, D.G., 1984. Shape Manifolds, Procrustean Metrics and Complex Projective Spaces. Bull London Math Soc 16, 81–121.

Kere, J., Srivastava, A.K., Montonen, O., Zonana, J., Thomas, N., Ferguson, B., Munoz, F., Morgan, D., Clarke, A., Baybayan, P., Chen, E.Y., Ezer, S., Saarialho-Kere, U., de la Chapelle, A., Schlessinger, D., 1996. X-linked anhidrotic (hypohidrotic) ectodermal dysplasia is caused by mutation in a novel transmembrane protein. Nat Genet 13, 409-416.

Kieser, J.A., 1990. Human adult. Odontometrics. Cambridge University Press, Cambridge.

Kieser, J.A., Bernal, V., Neil Waddell, J., Raju, S., 2007. The uniqueness of the human anterior dentition: a geometric morphometric analysis. J Forensic Sci 52, 671-677.

Kimbel, W.H., White, T.D., 1988. Variation, sexual dimorphism and the taxonomy of *Australopithecus*, in: Grine, F.E. (Ed.), Evolutionary History of the "Robust" Australopithecines. Aldine de Gruyter, New York, p. 259−268.

Kono, R.T., 2004. Molar enamel thickness and distribution patterns in extant great apes and humans: new insights based on a 3-dimensional whole crown perspective. Anthropol Sci 112, 121-146.

Kono, R.T., Suwa, G., 2008. Enamel distribution patterns of extant human and hominoid molars: occlusal versus lateral enamel thickness. Bull Nat Mus Natural Sci, Ser. D 34, 1-9.

Kono, R.T., Suwa, G., Tanijiri, T., 2002. A three-dimensional analysis of enamel distribution patterns in human permanent first molars. Arch Oral Biol 47, 867-875.

Kono, R.T., Zhang, Y., Jin, C., Takai, M., Suwa, G., 2014. A 3-dimensional assessment of molar enamel thickness and distribution pattern in Gigantopithecus blacki. Quaternary International 354, 46-51.

Korenhof, C.A.W., 1960. Morphogenetical Aspects of the Human Upper Molar. Utrecht, Uitgeversmaatschappij Neerlandia.

Korenhof, C.A.W., 1961. The enamel-dentine border: a new morphological factor in the study of the (human) molar pattern. Proceedings of the Koninklijke 64B, 639-664.

Kovacs, I., 1967. Contribution to the ontogenetic morphology of roots of human teeth. J Dent Res 46, 865-874.

Kovacs, I., 1971. A systematic description of dental roots, in: Dahlberg, A.A. (Ed.), Dental Morphology and Evolution. University of Chicago Press, Chicago, pp. 3-13.

Krenn, V., 2015. Variation of 3D outer and inner crown morphology of lower premolars in modern humans. Master Thesis, Faculty of Life Sciences, University of Vienna.

Krenn, V.A., Fornai, C., Bookstein F.L., Weber, G.W. (in preparation). Variation of 3D outer and inner crown morphology in modern human lower premolars. Am J Phys Anthropol

Kupczik, K., Dean, M.C., 2008. Comparative observations on the tooth root morphology of *Gigantopithecus blacki*. J Hum Evol 54, 196-204.

Kupczik, K., Hublin, J.-J., 2010. Mandibular molar root morphology in Neanderthals and Late Pleistocene and recent *Homo sapiens*. J Hum Evol 59, 525-541.

Kupczik, K., Spoor, F., Pommert, A., Dean, C., 2005. Premolar root number variation in hominoids: genetic polymorphism vs. functional significance, in: Zadzinska, E. (Ed.), Current Trends in Dental Morphology Research. University of Lodz Press, Lodz, pp. 257-268.

Lari, M., Di Vincenzo, F., Borsato, A., Ghirotto, S., Micheli, M., Balsamo, C., Collina, C., De Bellis, G., Frisia, S., Giacobini, G., Gigli, E., Hellstrom, J.C., Lannino, A., Modi, A., Pietrelli, A., Pilli, E., Profico, A., Ramirez, O., Rizzi, E., Vai, S., Venturo,

D., Piperno, M., Lalueza-Fox, C., Barbujani, G., Caramelli, D., Manzi, G., 2015. The Neanderthal in the karst: First dating, morphometric, and paleogenetic data on the fossil skeleton from Altamura (Italy). J Hum Evol 82, 88-94.
Lavelle, C.L.B., 1977. A study of the taxonomic significance of the dental arch. Am J Phys Anthropol 46, 415-421.
Lawing, A.M., Polly, P.D., 2010. Geometric morphometrics: recent applications to the study of evolution and development. Journal of Zoology 280, 1-7.
Leakey, M.G., Spoor, F., Dean, M.C., Feibel, C.S., Anton, S.C., Kiarie, C., Leakey, L.N., 2012. New fossils from Koobi Fora in northern Kenya confirm taxonomic diversity in early *Homo*. Nature 488, 201-204.
Lele, S.R., Richtsmeier, J.T., 2001. An Invariant Approach To Statistical Analysis Of Shapes. Chapman Hall/CRC, New York.
Liu, H.H., Dung, S.Z., Yang, Y.H., 2000. Crown diameters of the deciduous teeth of Taiwanese. Kaohsiung J Med Sci 16, 299-307.
Liu, W., Clarke, R., Xing, S., 2010. Geometric morphometric analysis of the early Pleistocene hominin teeth from Jianshi, Hubei Province, China. SCI CHINA EARTH SCI 53, 1141-1152.
Lockwood, C.A., 1999. Sexual dimorphism in the face of *Australopithecus africanus*. Am J Phys Anthropol 108, 97-127
Lockwood, C.A., Moggi-Cecchi, J., 1998. The systematic position of Stw 183, an adolescent maxilla from Sterkfontein. Am J Phys Anthropol 105, 151-152.
Lockwood, C.A., Tobias, P.V., 1999. A large male hominin cranium from Sterkfontein, South Africa, and the status of *Australopithecus africanus*. J Hum Evol 36, 637-685.
Lockwood, C.A., Tobias, P.V., 2002. Morphology and affinities of new hominin cranial remains from Member 4 of the Sterkfontein Formation, Gauteng province, South Africa. J Hum Evol 42, 389-450.
Lucas, P.W., 2004. Dental functional morphology: how teeth work. Cambridge University Press, Cambridge.
Lumsden, A.G., 1988. Spatial organization of the epithelium and the role of neural crest cells in the initiation of the mammalian tooth germ. Development 103 Suppl, 155-169.
Macchiarelli, R., Bondioli, L., Debenath, A., Mazurier, A., Tournepiche, J.-F., Birch, W., Dean, M.C., 2006. How Neanderthal molar teeth grew. Nature 444, 748-751.
Macleod, N., Forey, P., 2002. Morphology, Shape And Phylogenetics. Taylor and Francis, London.
Mahoney, P., 2010. Two-dimensional patterns of human enamel thickness on deciduous (dm1, dm2) and permanent first (M1) mandibular molars. Arch Oral Biol 55, 115-126.
Mahoney, P., 2013. Testing functional and morphological interpretations of enamel thickness along the deciduous tooth row in human children. Am J Phys Anthropol 151, 518-525.
Manthi, F.K., Plavcan, J.M., Ward, C.V., 2012. New hominin fossils from Kanapoi, Kenya, and the mosaic evolution of canine teeth in early hominins. S Afr J Sci 108, 00-00.
Martin, L.B., 1985. Significance of enamel thickness in hominoid evolution. Nature 314, 260-263.
Martin, L.B., Olejniczak, A.J., Maas, M.C., 2003. Enamel thickness and microstructure in pitheciin primates, with comments on dietary adaptations of the middle Miocene hominoid Kenyapithecus. J Hum Evol 45, 351-367.
Martin, R., Saller, K., 1957. Lehrbuch der Anthropologie in Systematischer Darstellung. Gustav Fischer Verlag, Stuttgart, Germany.
Martínez de Pinillos, M., Martinón-Torres, M., Skinner, M.M., Arsuaga, J.L., Gracia-Téllez, A., Martínez, I., Martín-Francés, L., Bermúdez de Castro, J.M., 2014. Trigonid crests expression in Atapuerca-Sima de los Huesos lower molars: Internal and external morphological expression and evolutionary inferences. Comptes Rendus Palevol 13, 205-221.
Mayr, E., 1942. Systematics and the Origin of Species, from the Viewpoint of a Zoologist. Harvard University Press, Cambridge.
McCown, T., Keith, A., 1939. The Stone Age of Mount Carmel, Volume 2. The Fossil Human Remains from the Levallois-Mousterian. Clarendon Press, Oxford.
Meyer, M., Fu, Q., Aximu-Petri, A., Glocke, I., Nickel, B., Arsuaga, J.-L., Martinez, I., Gracia, A., de Castro, J.M.B., Carbonell, E., Pääbo, S., 2014. A mitochondrial genome sequence of a hominin from Sima de los Huesos. Nature 505, 403-406.
Milella, M., Zollikofer, C.P.E., Ponce de León, M.S., 2015. Virtual Reconstruction and Geometric Morphometrics as Tools for Paleopathology: A New Approach to Study Rare Developmental Disorders of the Skeleton. Anat Rec 298, 335-345.
Mitteroecker, P., Gunz, P., 2009. Advances in Geometric Morphometrics. Evol Biol 36, 235-247.
Mitteroecker, P., Gunz, P., Bookstein, F.L., 2005. Heterochrony and geometric morphometrics: a comparison of cranial growth in *Pan paniscus* versus *Pan troglodytes*. Evol Dev 7, 244-258.

Moggi-Cecchi, J., 2003. The elusive 'second species' in Sterkfontein Member 4: The dental metrical evidence. S Afr J Sci 99, 268-270.
Moggi-Cecchi, J., Boccone, S., 2007. Maxillary molar cusp morphology of South African australopithecines, in: Bailey, S.E., Hublin, J.-J. (Eds.), Dental Perspectives on Human Evolution. Springer, Dordrecht, The Netherlands, pp. 53-64.
Molnar, S., 1971. Human tooth wear, tooth function and cultural variability. Am J Phys Anthropol 34, 175-189.
Monteiro, L.R., 2000. Why morphometrics is special: the problem with using partial warps as characters for phylogenetic inference. Syst Biol 49, 796-800.
Morita, W., Yano, W., Nagaoka, T., Abe, M., Ohshima, H., Nakatsukasa, M., 2014. Patterns of morphological variation in enamel–dentin junction and outer enamel surface of human molars. J Anat 224, 669-680.
Nieminen, P., 2009. Genetic basis of tooth agenesis. J Exp Zool B Mol Dev Evol 312b, 320-342.
Nixon, K.C., Wheeler, Q.D., 1990. An Amplification of the Phylogenetic Species Concept. Cladistics 6, 211-223.
O'Higgins, P., 2000. The study of morphological variation in the hominid fossil record: biology, landmarks and geometry. J Anat 197, 103-120.
O'Higgins, P., Jones, N., 1998. Facial growth in *Cercocebus torquatus*: an application of three-dimensional geometric morphometric techniques to the study of morphological variation. J Anat 193, 251-272.
Olejniczak, A.J., 2006. Micro-computed tomography of primate molars. Stony Brook University, Stony Brook, NY.
O'Higgins, P., Cobb, S. N., Fitton, L.C., Groening, F., Phillips, R., Liu, J., Fagan, M.J., 2011. Combining geometric morphometrics and functional simulation: an emerging toolkit for virtual functional analyses. J Anat 218, 3-15.
Olejniczak, A.J., Grine, F.E., 2006. Assessment of the accuracy of dental enamel thickness measurements using microfocal X-ray computed tomography. Anat Rec A Discov Mol Cell Evol Biol 288, 263-275.
Olejniczak, A.J., Smith, T.M., Feeney, R.N.M., Macchiarelli, R., Mazurier, A., Bondioli, L., Rosas, A., Fortea, J., de la Rasilla, M., Garcia-Tabernero, A., Radovčić, J., Skinner, M.M., Toussaint, M., Hublin, J.J., 2008a. Dental tissue proportions and enamel thickness in Neandertal and modern human molars. J Hum Evol 55, 12-23.
Olejniczak, A.J., Smith, T.M., Skinner, M.M., Grine, F.E., Feeney, R.N.M., Thackeray, J.F., Hublin, J.J., 2008b. Three-dimensional molar enamel distribution and thickness in *Australopithecus* and *Paranthropus*. Biol Lett 4, 406-410.
Olejniczak, A.J., Smith, T.M., Wang, W., Potts, R., Ciochon, R., Kullmer, O., Schrenk, F., Hublin, J.J., 2008c. Molar enamel thickness and dentine horn height in Gigantopithecus blacki. Am J Phys Anthropol 135, 85-91.
Olejniczak, A.J., Tafforeau, P., Feeney, R.N.M., Martin, L.B., 2008d. Three-dimensional primate molar enamel thickness. J Hum Evol 54, 187-195.
Ortiz, A., Skinner, M.M., Bailey, S.E., Hublin, J.-J., 2012. Carabelli's trait revisited: An examination of mesiolingual features at the enamel–dentine junction and enamel surface of *Pan* and *Homo sapiens* upper molars. J Hum Evol 63, 586-596.
Prado, S.I.M., Oacute, N, L., Martin, Oacute, N-Torres, M.A.R., Iacute, Baca, P., Oacute, Mez-Robles, A., Lapresa, M.A.R., Iacute, Carbonell, E., Berm, Uacute, Dez De Castro, J.O.S., Eacute, Maria, 2012. A morphological study of the tooth roots of the Sima del Elefante mandible (Atapuerca, Spain): a new classification of the teeth—biological and methodological considerations. Anthropol Sci 120, 61-72.
Prüfer, K., Racimo, F., Patterson, N., Jay, F., Sankararaman, S., Sawyer, S., Heinze, A., Renaud, G., Sudmant, P.H., de Filippo, C., Li, H., Mallick, S., Dannemann, M., Fu, Q., Kircher, M., Kuhlwilm, M., Lachmann, M., Meyer, M., Ongyerth, M., Siebauer, M., Theunert, C., Tandon, A., Moorjani, P., Pickrell, J., Mullikin, J.C., Vohr, S.H., Green, R.E., Hellmann, I., Johnson, P.L.F., Blanche, H., Cann, H., Kitzman, J.O., Shendure, J., Eichler, E.E., Lein, E.S., Bakken, T.E., Golovanova, L.V., Doronichev, V.B., Shunkov, M.V., Derevianko, A.P., Viola, B., Slatkin, M., Reich, D., Kelso, J., Pääbo, S., 2014. The complete genome sequence of a Neanderthal from the Altai Mountains. Nature 505, 43-49.
Rightmire, G.P., 1993. The evolution of *Homo erectus*: Comparative anatomical studies of an extinct human species. Cambridge University Press, Cambridge.
Robinson, D.L., Blackwell, P.G., Stillman, E.C., Brook, A.H., 2001. Planar Procrustes analysis of tooth shape. Arch Oral Biol 46, 191-199.
Robinson, J.T., 1956. The dentition of the Australopithecinae. The Transvaal Museum, Pretoria.
Rohlf, F.J., 1998. On applications of geometric morphometrics to studies of ontogeny and phylogeny. Syst Biol 47, 147-158; discussion 159-167.
Rohlf, F.J., Corti, M., 2000. Use of Two-Block Partial Least-Squares to Study Covariation in Shape. Syst Biol 49, 740-753.

Rohlf, F.J., Slice, D., 1990. Extensions of the Procrustes Method for the Optimal Superimposition of Landmarks. Syst Biol 39, 40-59.
Saini, T., Wilson, C.A., 1990. Taurodont molars: Review of literature and radiological features. The Saudi Dental Journal 2, 68-70.
Sakai, T., Hanamura, H., 1971. A Morphological Study of Enamel-Dentin Border on the Japanese Dentition: V. Maxillary Molar. Journal of the Anthropological Society of Nippon 79, 297-322.
Sakai, T., Hanamura, H., 1973a. A Morphological Study of Enamel-Dentin Border on the Japanese Dentition: VI. Mandibular Molar. Journal of the Anthropological Society of Nippon 81, 25-45.
Sakai, T., Hanamura, H., 1973b. A Morphological Study of Enamel-Dentin Border on the Japanese Dentition: VII. General Conclusion. Journal of the Anthropological Society of Nippon 81, 87-102.
Sakai, T., Sasaki, I., Hanamura, H., 1965. A Morphological Study of Enamel-Dentin Border on the Japanese Dentition. Journal of the Anthropological Society of Nippon 73, 91-109.
Sakai, T., Sasaki, I., Hanamura, H., 1967a. A Morphological Study of Enamel-Dentin Border on the Japanese Dentition:II. Maxillary Canine. Journal of the Anthropological Society of Nippon 75, 155-172.
Sakai, T., Sasaki, I., Hanamura, H., 1967b. A Morphological Study of Enamel-Dentin Border on the Japanese Dentition:III. Maxillary Premolar. Journal of the Anthropological Society of Nippon 75, 207-223.
Sakai, T., Sasaki, I., Hanamura, H., 1969. A morphology study of enamel-dentin border on the Japanese dentition. Part IV. Mandibular premolar. Journal of the Anthropological Society of Nippon 77, 71-98.
Sasaki, K., Makiguchi, H., Yoshino, K., Kanazawa, E., 2002. Morphological Study of the Dentino-enamel Junction of the Upper First Deciduous Molar. Anthropol Sci 110, 349-363.
Schroer, K., Wood, B.A., 2013. Evolution of hominin postcanine macromorphology: a comparative meta-analysis, in: Scott, G.R., Irish, J.D. (Eds.), Anthropological Perspectives on Tooth Morphology: Genetics, Evolution, Variation. Cambridge University Press.
Schroer, K., Wood, B.A., 2015. Modeling the dental development of fossil hominins through the inhibitory cascade. J Anat 226, 150-162.
Schwartz, G.T., 2000. Taxonomic and functional aspects of the patterning of enamel thickness distribution in extant large-bodied hominoids. Am J Phys Anthropol 111, 221-244.
Schwartz, J.H., Tattersall, I., 2005. The Human Fossil Record. Craniodental Morphology of Early Hominids (Genera *Australopithecus*, *Paranthropus*, *Orrorin*), and Overview. Wiley-Liss, New York.
Scott, G., Turner, C., 1997. The Anthropology of Modern Human Teeth: Dental Morphology and its Variation in Recent Human Populations. Cambridge University Press, Cambridge.
Scott, J.E., Lockwood, C.A., 2004. Patterns of tooth crown size and shape variation in great apes and humans and species recognition in the hominid fossil record. Am J Phys Anthropol 125, 303-319.
Seidler, H., Bernhard, W., Teschler-Nicola, M., Platzer, W., zur Nedden, D., Henn, R., 1992. Some anthropological aspects of the prehistoric Tyrolean ice man. Science 258, 455-457.
Sharma, J.C., 1985. Evolutionary significance of dental morphology and odontometry, in: Rami Reddy, V. (Ed.), Dental Anthropology: application and methods. Inter-India Publications, New Delhi, India, pp. 251-267.
Shellis, R.P., Beynon, A.D., Reid, D.J., Hiiemae, K.M., 1998. Variations in molar enamel thickness among primates. J Hum Evol 35, 507-522.
Simmer, J.P., Papagerakis, P., Smith, C.E., Fisher, D.C., Rountrey, A.N., Zheng, L., Hu, J.-C., 2010. Regulation of Dental Enamel Shape and Hardness. J Dent Res 89, 1024-1038.
Simpson, G.G., 1945. The Principles of Classification and a Classification of Mammals. Bull Am Mus Nat His 85, 1-350.
Singh, G.D., Rivera-Robles, J., de Jesus-Vinas, J., 2004. Longitudinal craniofacial growth patterns in patients with orofacial clefts: geometric morphometrics. Cleft Palate Craniofac J 41, 136-143.
Skinner, M.M., Gordon, A.D., Collard, N.J., 2006. Mandibular size and shape variation in the hominins at Dmanisi, Republic of Georgia. J Hum Evol 51, 36-49.
Skinner, M.M., Gunz, P., Wood, B.A., Boesch, C., Hublin, J.-J., 2009a. Discrimination of extant *Pan* species and subspecies using the enamel-dentine junction morphology of lower molars. Am J Phys Anthropol 140, 234-243.
Skinner, M.M., Gunz, P., Wood, B.A., Hublin, J.-J., 2008a. Enamel-dentine junction (EDJ) morphology distinguishes the lower molars of *Australopithecus africanus* and *Paranthropus robustus*. J Hum Evol 55, 979-988.

Skinner, M.M., Gunz, P., Wood, B.A., Hublin, J.-J., 2009b. How many landmarks? Assessing the classification accuracy of *Pan* lower molars using a geometric morphometric analysis of the occlusal basin as seen at the enamel-dentine junction. Frontiers of oral biology 13, 23-29.

Skinner, M.M., Wood, B.A., Boesch, C., Olejniczak, A.J., Rosas, A., Smith, T.M., Hublin, J.-J., 2008b. Dental trait expression at the enamel-dentine junction of lower molars in extant and fossil hominoids. J Hum Evol 54, 173-186.

Slice, D.E., 2005. Modern morphometrics in physical anthropology, in: Tuttle, R.H. (Ed.), Developments in Primatology: Progress and Prospects. Kluwer Academic/Plenum Publishers, New York.

Slice, D.E., 2007. Geometric Morphometrics. Annual Review of Anthropology 36, 261-281.

Smith, A.L., Benazzi, S., Ledogar, J.A., Tamvada, K., Pryor Smith, L.C., Weber, G.W., Spencer, M.A., Dechow, P.C., Grosse, I.R., Ross, C.F., Richmond, B.G., Wright, B.W., Wang, Q., Byron, C., Slice, D.E., Strait, D.S., 2015. Biomechanical implications of intraspecific shape variation in chimpanzee crania: moving toward an integration of geometric morphometrics and finite element analysis. Anat Rec (Hoboken) 298, 122-144.

Smith, R., Zaitoun, H., Coxon, T., Karmo, M., Kaur, G., Townsend, G., Harris, E.F., Brook, A., 2009. Defining new dental phenotypes using 3-D image analysis to enhance discrimination and insights into biological processes. Arch Oral Biol 54, S118-S125.

Smith, T.M., 2013. Teeth and human life-history evolution. Annual Review of Anthropology 42, 191-208.

Smith, T.M., Alemseged, Z., 2013. Reconstructing Hominin Life History. Nature Education Knowledge 4, 2.

Smith, T.M., Kupczik, K., Machanda, Z., Skinner, M.M., Zermeno, J.P., 2012a. Enamel thickness in Bornean and Sumatran orangutan dentitions. Am J Phys Anthropol 147, 417-426.

Smith, T.M., Olejniczak, A.J., Martin, L.B., Reid, D.J., 2005. Variation in hominoid molar enamel thickness. J Hum Evol 48, 575-592.

Smith, T.M., Olejniczak, A.J., Zermeno, J.P., Tafforeau, P., Skinner, M.M., Hoffmann, A., Radovčić, J., Toussaint, M., Kruszynski, R., Menter, C., Moggi-Cecchi, J., Glasmacher, U.A., Kullmer, O., Schrenk, F., Stringer, C., Hublin, J.-J., 2012b. Variation in enamel thickness within the genus *Homo*. J Hum Evol 62, 395-411.

Smith, T.M., Reid, D.J., Olejniczak, A.J., Tafforeau, P., Hublin, J.-J., Toussaint, M., 2014. Dental development in and age at death of the Scladina 1-4. A juvenile Neanderthal, in: Toussaint, M., Bonjean, D. (Eds.), The Scladina I-4. A Juvenile Neandertal (Andenne, Belgium) Palaeoanthropology and Context. Études et Recherches Archéologiques de l' Université de Liège, Liège, pp. 155-166.

Smith, T.M., Tafforeau, P., Reid, D.J., Pouech, J., Lazzari, V., Zermeno, J.P., Guatelli-Steinberg, D., Olejniczak, A.J., Hoffman, A., Radovčić, J., Makaremi, M., Toussaint, M., Stringer, C., Hublin, J.-J., 2010. Dental evidence for ontogenetic differences between modern humans and Neanderthals. Proceedings of the National Academy of Sciences 107, 20923-20928.

Soares, P., Achilli, A., Semino, O., Davies, W., Macaulay, V., Bandelt, H.J., Torroni, A., Richards, M.B., 2010. The archaeogenetics of Europe. Curr Biol 20, R174-183.

Sperber, G., 1974. Morphology of the cheek teeth of early South African hominids. University of Witwatersrand, Johannesburg, South Africa.

Stockton, D.W., Das, P., Goldenberg, M., D'Souza, R.N., Patel, P.I., 2000. Mutation of PAX9 is associated with oligodontia. Nat Genet 24, 18-19.

Suwa, G., Kono, R.T., Katoh, S., Asfaw, B., Beyene, Y., 2007. A new species of great ape from the late Miocene epoch in Ethiopia. Nature 448, 921-924.

Suwa, G.E.N., Kono, R.T., 2005. A micro-CT based study of linear enamel thickness in the mesial cusp section of human molars: reevaluation of methodology and assessment of within-tooth, serial, and individual variation. Anthropol Sci 113, 273-289.

Swiderski, D.L., Zelditch, M.L., Fink, W.L., 1998. Why morphometrics is not special: coding quantitative data for phylogenetic analysis. Syst Biol 47, 508-519.

Tafforeau, P., 2004. Phylogenetic and functional aspects of tooth enamel microstructure and three-dimensional structure of modern and fossil primate molars. Université de Montpellier II.

Tafforeau, P., Le Cabec, A., Bonazzi, M., Schünemann, V., Viola, B., Harvati, K., Pääbo, S., Krause, J., Hublin, J.-J., 2014. Assessing the real effects of X-ray imaging on recent fossils: facts vs. speculations. American Journal of Pysical Anthropology 153, 251.

Tafforeau, P., Smith, T.M., 2008. Nondestructive imaging of hominoid dental microstructure using phase contrast X-ray synchrotron microtomography. J Hum Evol 54, 272-278.
Tafforeau, P., Zermeno, J.P., Smith, T.M., 2012. Tracking cellular-level enamel growth and structure in 4D with synchrotron imaging. J Hum Evol 62, 424-428.
Thesleff, I., 2003. Epithelial-mesenchymal signaling regulating tooth morphogenesis. J Cell Sci 116, 1647-1648.
Thesleff, I., Sharpe, P., 1997. Signalling networks regulating dental development. Mech Dev 67, 111-123.
Tobias, P.V., 1966. Fossil hominid remains from Ubeidiya, Israel. Nature 211, 130-133.
Tobias, P.V., 1995. Root number in the maxillary third premolars: a very ancient polymorphism, in: Moggi-Cecchi, J. (Ed.), Aspects of Dental Biology: Palaeontology, Anthropology and Evolution. International Institute for the Study of Man, Florence, pp. 283–290.
Toussaint, M., Olejniczak, A.J., El Zaatari, S., Cattelain, P., Flas, D., Letourneux, C., Pirson, S., 2010. The Neanderthal lower right deciduous second molar from Trou de l'Abîme at Couvin, Belgium. J. Hum. Evol. 58, 56-67.
Tucker, A., Sharpe, P., 2004. The cutting-edge of mammalian development; how the embryo makes teeth. Nat Rev Genet 5, 499-508.
Tummers, M., Thesleff, I., 2009. The importance of signal pathway modulation in all aspects of tooth development. J Exp Zool B Mol Dev Evol 312b, 309-319.
Turner, C.G.I., Nichol, C.R., Scott, G.R., 1991. Scoring procedures for key morphological traits of the permanent dentition: the Arizona State University Dental Anthropology System, in: Kelley, M.A., Larsen, C.S. (Eds.), Advances in dental anthropology. Wiley-Liss, New York, pp. 13–31.
Turville-Petre, F., 1927. Researches in Prehistoric Galilee, 1925-26. Council of the British School of Archaeology in Jerusalem, London.
Ulhaas, L., Kullmer, O., Schrenk, F., 2007. Tooth wear and diversity in early hominid molars: A case study, in: Bailey, S., Hublin, J.-J. (Eds.), Dental Perspectives on Human Evolution: State of the Art Research in Dental Paleoanthropology. Springer Netherlands, pp. 369-390.
Vastardis, H., Karimbux, N., Guthua, S.W., Seidman, J.G., Seidman, C.E., 1996. A human MSX1 homeodomain missense mutation causes selective tooth agenesis. Nat Genet 13, 417-421.
Wall, J.D., Lohmueller, K.E., Plagnol, V., 2009. Detecting Ancient Admixture and Estimating Demographic Parameters in Multiple Human Populations. Mol Biol Evol 26, 1823-1827.
Wang, X.P., O'Connell, D.J., Lund, J.J., Saadi, I., Kuraguchi, M., Turbe-Doan, A., Cavallesco, R., Kim, H., Park, P.J., Harada, H., Kucherlapati, R., Maas, R.L., 2009. Apc inhibition of Wnt signaling regulates supernumerary tooth formation during embryogenesis and throughout adulthood. Development 136, 1939-1949.
Weber, G.W., 2001. Virtual anthropology (VA): a call for glasnost in paleoanthropology. Anat Rec 265, 193-201.
Weber, G.W., 2015. Virtual Anthropology. Am J Phys Anthropol 156, 22-42.
Weber, G.W., Bookstein, F.L., 2011. Virtual Anthropology. A guide to a new interdisciplinary field. Springer, Wien.
White, J., 2009. Geometric morphometric investigation of molar shape diversity in modern lemurs and lorises. Anat Rec (Hoboken) 292, 701-719.
White, T.D., 2014. Delimitating species in paleoanthropology. Evol Anthropol 23, 30-32.
Wiens, J.J., Servedio, M.R., 2000. Species delimitation in systematics: inferring diagnostic differences between species.
Wiley, E.O., Lieberman, B.S., 2011. Phylogenetics: Theory and Practice of Phylogenetic Systematics. Wiley-Blackwell.
Wood, B.A., 1991. A paleontological model for determining the limits of early hominid taxonomic variability. Palaeont Afr 28, 71-77.
Wood, B.A., Abbott, S.A., 1983. Analysis of the dental morphology of Plio-Pleistocene hominids. I. Mandibular molars: crown area measurements and morphological traits. J Anat 136, 197-219.
Wood, B.A., Abbott, S.A., Graham, S.H., 1983. Analysis of the dental morphology of Plio-Pleistocene hominids. II. Mandibular molars - study of cusp areas, fissure pattern and cross sectional shape of the crown. J Anat 137, 287-314.
Wood, B.A., Abbott, S.A., Uytterschaut, H., 1988. Analysis of the dental morphology of Plio-Pleistocene hominids. IV. Mandibular postcanine root morphology. J Anat 156, 107-139.
Wood, B.A., Engleman, C.A., 1988. Analysis of the dental morphology of Plio-Pleistocene hominids. V. Maxillary postcanine tooth morphology. J Anat 161, 1-35.

Wood, B.A., Zuckerman, L., 1981. Tooth Size and Shape and their Relevance to Studies of Hominid Evolution [and Discussion]. Philosophical Transactions of the Royal Society B, London.

Zelditch, M.L., Fink, W.L., Swiderski, D.L., 1995. Morphometrics, Homology, and Phylogenetics: Quantified Characters as Synapomorphies. Syst Biol 44, 179-189.

Zilberman, U., Skinner, M., Smith, P., 1992. Tooth components of mandibular deciduous molars of *Homo sapiens sapiens* and *Homo sapiens neanderthalensis*: A radiographic study. Am J Phys Anthropol 87, 255-262.

Zilberman, U., Smith, P., 1992. A comparison of tooth structure in Neanderthals and early *Homo sapiens sapiens*: a radiographic study. J Anat 180:3, 387-393.

Zipfel, B., Berger, L.R., 2009. A partial hominin tibia (Stw 396) from Sterkfontein, South Africa. Palaeontologia africana 44, 71-75.

6. List of figures

7. Curriculum Vitae

CINZIA FORNAI

COURSE OF STUDIES

- **2015 –** PhD in Biology, through the Department of Anthropology, University of Vienna. Supervisor: Prof. G. Weber.
- **2009 –** MSc by research in Paleoanthropology. School of Anatomical Sciences and Institute for Human Evolution, Faculty of Science, University of the Witwatersrand, Johannesburg, South Africa. Supervisor: Prof. R. J. Clarke (University of Witwatersrand, Johannesburg, South Africa). Title of the project: Testing the second species hypothesis for the South African sites of Sterkfontein and Makapansgat: Geometric morphometric analysis of maxillary molar teeth. Score: distinction
- **2009 -** single course through the Università degli Studi di Firenze: *Taphonomy and Archaeozoology*, score: 30/30 *Cum Laude*
- **2008 –** single courses through the Università degli Studi di Firenze: *Paleoanthropology*, score: 30/30; *Laboratory of Anthropology*, score: 30/30
- **October 2004 – June 2005 –** Certificate in "Technician of archaeological excavation", International University of Arts (U.I.A.) Foundation – Florence. 300 hours: theoretical lessons + 300 hours apprenticeship
- **2002 -** Laurea (Degree) in Natural Sciences (Paleo-biology). University of Rome *La Sapienza*. Thesis title: "Variabilità biologica nei Garamanti. Morfometria multivariata del cranio in popolazioni protostoriche del Sahara Centrale (Fezzan, Libia)", "Biological variability in Garamants. Multivariate analysis of the skull in a proto-historic population of Central Saharan (Fezzan, Libya)". Supervisors Prof. G. Manzi, Prof. P. Passarello, Prof. F. Vecchi. Score: 110/110, *Cum Laude*
- **1993 –** Certificate in Accountancy, Rome. Score: 60/60

WORKING EXPERIENCES AND COLLABORATIONS

- **April 2014 – March 2016 –** Assistant and tutor for the project "Dental wear in historical populations" through the Department of Anthropology, University of Vienna, sponsored by "Siegfried Ludwig - Rudolf Slavicek Stipendienstiftung, Wien". Project number FA547016. Supervisor: Prof G. Weber
- **March 2011 – March 2014 –** Assistant for the project "3D Craniometry for Dentistry" (3d-dentistry.org) through the Department of Anthropology, University of Vienna, sponsored by "A.E.R.S. Dental Medicine Organisations GmbH". Supervisor: Prof G. Weber
- **From September 2011 –** Assistant for the EVAN Society (evan-society.org) for the online support to members and assistant at the workshops on the software for 3D Geometric Morphometrics EVAN Toolbox (ET).
- **January 2010 – April 2010 –** Early stage researcher employment at the Department of Anthropology, University of Vienna, under the NSF project "Collaborative Research: Integrative analysis of hominid feeding biomechanics". Director: Dr D. Strait. Supervisor in Vienna: Prof G. Weber

- **September 2009 – December 2009 –** Early stage researcher employment at the Department of Anthropology, University of Vienna, through the pre-doctoral Marie Curie Research Training fellowship (European Virtual Anthropology Network, EVAN) in quantitative morphology of hominoid teeth. Supervisor: Prof. G. Weber
- **January–June 2004** – Collaboration with the Animal and Human Biology Department, University of Rome *La Sapienza* "Preservation and evaluation of human osteological collections." Supervisors: Prof. G. Manzi and Prof. G. Spedini
- **October-December 2002** – Collaboration with the Animal and Human Biology Department, University of Rome *La Sapienza* in researching and teaching. Supervisors: Prof. G. Manzi and Prof. P. Passarello

LANGUAGES

- **Italian:** mother tongue
- **English:** C1
- **German:** B1

SOFTWARE

- General: Microsoft Office
- Image manipulation: Amira, VGStudioMAX, Rapidform, Rhinoceros, Photoshop, Adobe Illustrator
- Statistics: EVAN Toolbox (and Morphologika), ViewBox, R, PAST, MorphoJ

WORKSHOPS

- **22-23 May and 23-24 June 2014** – R course for beginners and follow up, ZID, University of Vienna
- **18-20, 22 February and 24-26, 28 June 2013** – R software workshop for beginners and follow up (reader: Dr. Michael Coquerelle). University of Vienna, Austria. Sponsored by A.E.R.S. Dental Medicine Organisations GmbH
- **22 October 2010** – EVAN Toolbox (ET) Training day. University of Vienna, Austria
- **1-5 February 2010** – Morphometric Laboratory for Systematics and Evolutionary Researches. Centre for Evolutionary Ecology and University of Molise, Pesche, Isernia, Italy
- **21-22 September 2009** – Evan meeting: Applying EVAN toolkit in VA, medicine, industry. HYMS, University of York, England

TEACHING AND LECTURES

- **2014-2015** – At Department of Anthropology, University of Vienna. SS: "300154 UE - 3D Image data processing, landmarking and template building"; WS: "300318 UE - Virtual Image Manipulation and Segmentation"; "300033 VO Virtuelle Anthropologie - Einführung in digitale 3D-Verfahren", by Prof. Gerhard Weber.
- **July 2014** - Lecturing at the Vienna Summer School, Forum for Science in Interdisciplinary Dentistry (Viesid): "Combining Occlusal Fingerprint Analysis and Finite Element Methods for the investigation of the masticatory apparatus"
- **July 2013** - Lecturing at the Vienna Summer School, Forum for Science in Interdisciplinary Dentistry (Viesid): "Bipedalism in the light of evolution", "Functional aspects of the hominin masticatory apparatus"
- **July 2012** – Lecturing at the Vienna Summer School, Forum for Science in Interdisciplinary Dentistry (Viesid): "Dental Morphometrics"
- **January-February 2005** – Teaching at the Civic University, *Andrea Sacchi*, in Nettuno, Rome: course title "Physical Anthropology and Human Evolution" (theoretical and practical lessons)

SCHOLARSHIPS, GRANTS AND PROFESSIONAL EXPERIENCES

- **August 2009 –** Teaching assistant at GAES, University of the Witwatersrand: data collection for the

Google Earth Project: Mapping South African archaeological sites. Supervisor: Prof. K. Sadr

- **January-June 2009 –** Italian Government Scholarship for South African citizens and Italian citizens resident abroad. Research project "Analysis of mandibular molar tooth cusp areas of Plio-Pleistocene South African australopithecines" through Laboratori di Antropologia, Dipartimento di Biologia Evoluzionistica, Via del Proconsolo 12, 50122 Firenze, Univ. degli Studi di Firenze; supervisor: Prof. Jacopo Moggi-Cecchi 700.00 € per month
- **January-September 2008 –** Italian Government Scholarship for South African citizens and Italian citizens resident abroad. Research project: "Testing the second species hypothesis at Sterkfontein Formation: A comparative analysis of the Plio-Pleistocene South African hominid teeth through geometric morphometric techniques" through Laboratori di Antropologia, Dipartimento di Biologia Evoluzionistica, Via del Proconsolo 12, 50122 Firenze; supervisor: Prof. Jacopo Moggi-Cecchi. 700.00 € per month
- **2008 –** P.A.S.T. – Palaeontological Scientific Trust grant. 40,000 Rand
- **2008 –** Merit Award, Univ. of the Witwatersrand. 17,920 Rand
- **2008 –** J.J.J. Smieszek bursary, School of Anatomical Sciences, Univ. of the Witwatersrand. 5,580 Rand
- **2007 –** J.J.J. Smieszek bursary, School of Anatomical Sciences, Univ. of the Witwatersrand. 12,000 Rand
- **2007 –** P.A.S.T. – Palaeontological Scientific Trust grant. 36,000 Rand
- **September 2004 –** Excavation on the Mediaeval site of Populonia (Tuscany), organized by Univ. of Siena and by University "Cà Foscari" of Venice (Directors of excavation, respectively: Prof. R. Francovich and Prof. S. Gelichi)
- **2001 –** Data collection from African skulls located at the Anthropological Museum *G. Sergi*, Univ. of Rome *La Sapienza* using a Microscribe 3DX (Immersion) to assist in morphometric analysis. Supervisor: Prof. G. Manzi
- **June 2001 –**Excavations on the Ceprano Campogrande site (Field school by Istituto Italiano di Paleontologia Umana. Director of the excavation: Prof. G. Manzi) and Fontana Ranuccio – Anagni site (Director of the excavation: Prof. G. Segre)
- **2000 –** Collaboration Scholarship performed at the *Museum of Anthropology "G. Sergi"*, granted by the University of Rome *La Sapienza*
- **1999 –** Collaboration Scholarship performed at the *Library of Comparative Anatomy*, granted by the University of Rome *La Sapienza*

8. List of publications

PUBLICATIONS

- Krenn, V.A., **Fornai, C.**, Bookstein F.L., Weber, G.W. (in preparation for the Am J Phys Anthropol). Variation of 3D outer and inner crown morphology in modern human lower premolars.
- **Fornai, C.**, Benazzi, S., Gopher, A., Barkai, R., Sarig, R., Hershkovitz, I., Weber, G.W. (submitted). The Qesem Cave hominin material (part 2): A morphometric analysis of dm_2-QC2 deciduous lower second molar. Quatern Int
- Hershkovitz, I., Weber, G. W., **Fornai, C.**, Gopher, A., Barkai, R., Slon, V., Rolf, Q., Sarig, R. (submitted). New Middle Pleistocene dental remains from Qesem cave (Israel). Quatern Int
- Sarig, R., Gopher, A., Barkai, R., Weber, G. W., **Fornai, C.**, Sella-Tunis, T., Hershkovitz, I., (submitted). How Did the Qesem People Use their Teeth? Analysis of Dental Wear Patterns. Quatern Int
- Weber, G. W., **Fornai, C.**, Gopher, A., Barkai, R., Sarig, R., Hershkovitz, I., (submitted). The Qesem Cave hominin material (part 1): A morphometric analysis of the mandibular premolars and molar. Quatern Int
- Lauc T., **Fornai C.**, Premužić Z., Vodanović M., Weber, G. W., Mašić B., Rajić Šikanjić P. (accepted). Dental stigmata and enamel thickness in a probable case of congenital syphilis from XVI century Croatia. Arch Oral Biol
- **Fornai C.**, Bookstein F.L., Weber G.W. (publishes online 07/07/2015) Variability of *Australopithecus* second maxillary molars from Sterkfontein Member 4. J Hum Evol
- **Fornai C.**, Benazzi S., Svoboda J., Pap I., Harvati K., Weber G. W. (2014) Enamel thickness variation of deciduous first and second upper molars in modern humans and Neanderthals. J Hum Evol. 76, 83-91
- Benazzi S., Panetta, D., **Fornai C.**, Toussaint, M., Gruppioni, G., Hublin, J.-J. 2014. Guidelines for the digital computation of 2D and 3D enamel thickness in hominoid teeth. Am J Phys Anthropol 153, 305–313.
- Benazzi S., **Fornai C.**, Buti L., Toussaint M., Mallegni F., Ricci S. Gruppioni G., Weber G.W., Condemi S., Ronchitelli A. 2012. Cervical and crown outline analysis of worn Neanderthal and modern human lower second deciduous molars. Am J Phys Anthropol 149(4):537-46
- Benazzi S., Douka K., **Fornai C.**, Bauer C.C., Kullmer O., Svoboda J., Pap I., Mallegni F., Bayle P., Coquerelle M., Condemi S., Ronchitelli A., Harvati K., Weber G. W. 2011. Early dispersal of modern humans in Europe and implications for Neanderthal behaviour. Nature 479, 525–528
- Benazzi S., **Fornai C.**, Bayle P., Coquerelle M., Kullmer O., Mallegni F., Weber G.W. 2011. Comparison of dental measurement systems for taxonomic assignment of Neanderthal and modern human lower second deciduous molars. J Hum Evol 61: 320-326.
- Ricci F, **Fornai C**, Tiesler Blos V, Rickards O, di Lernia S, Manzi G. 2008. Evidence of artificial cranial deformation from the later prehistory of the Acacus Mts. (southwestern Libya, Central Sahara). *International Journal of Osteoarchaeology* 18(4):372-391
- Fiori O, **Fornai C**, Manzi G. 2004. Ai Confini del Gaudo. Una riconsiderazione dei resti scheletrici umani provenienti dai siti eneolitici di Cantalupo Mandela e Valvisciolo (Lazio meridionale). "To the border of Gaudo. A reconsideration of the human remains from the Eneolithic sites of Cantalupo Mandela and Valvisciolo (Southern Latium)." *Origini* XXVI:121-154
- Ricci F., **Fornai C**., Passarello P., Vecchi F., Manzi G., 2002. Human skeletal remains from Wadi Tanezzuft: inventory, documentation, and description. In S. Di Lernia, G. Manzi (Eds), *Sand, Stones, and Bones. The Archaeology of Death in the Wady Tanezzuft Valley*, p. 217-250. Edizioni All'Insegna del Giglio: Firenze

- Weber, G. W., Krenn, V., Buchegger, L., Teplanova, D., **Fornai, C.**, 2015. Shape variation of in human postcanine dentition. ESHE, London.
- **Fornai C.**, Bookstein F. L., Weber G. W., 2015. Second maxillary molars do not resolve South African australopithecines taxonomy. EAAPP, Dar es Salaam, Tanzania (Podium presentation)
- Eckstein, M., Vaeth, M., **Fornai, C.**, Nurbaeva, M., Kakar, L., Atria, P., Tovar, N., Coelho, P., Bromage, T., Feske, S., Lacruz, R.S., 2015. CRAC Channels Are Essential For Amelogenesis. The NYU Center for Skeletal and Craniofacial Biology Biannual Retreat, 17 April 2015. Poster Session.
- **Fornai, C.**, Benazzi, S., Gopher, A., Barkai, R., Sarig, R., Hershkovitz, I., Weber, G. W. 2015. Comparative morphometric analyses of a lower deciduous second molar from Qesem Cave Middle Pleistocene site (Israel). 84th annual AAPA meeting, St. Lois, USA. In Am J Phys Anthropol, 156(S60), p.136 (Poster presentation)
- Buchegger, L., **Fornai, C.**, Weber, G. W. 2014. Variation of the Enamel-Dentin Junction morphology of upper premolars in modern human populations. ESHE, Florence, Italy (Poster presentation)
- **Fornai, C.**, Benazzi, S., Gopher, A., Barkai, R., Sarig, R., Hershkovitz, I., Weber, G. W. 2014. A morphometric analysis of the hominin deciduous lower second molar (I/12a) from Qesem Cave. ESHE, Florence, Italy (Podium presentation)
- Krenn, V., **Fornai, C.**, Weber, G. W. 2014. Variation of 3D outer and inner crown morphology of lower premolars in modern humans. ESHE, Florence, Italy (Poster presentation)
- **Fornai, C.**, Benazzi, S., Gopher, A., Barkai, R., Sarig, R., Hershkovitz, I., Weber, G. W. 2014. The Qesem Cave hominin material (part 2): A morphometric analysis of I/12a deciduous lower second molar. UISPP, Burgos, Spain (Podium presentation)
- Hershkovitz, I., Weber, G. W., **Fornai, C.**, Gopher, A., Barkai, R., Slon, V., Sarig, R. 2014. Who Lived In the Qesem Cave? The Dental Perspective. UISPP, Burgos, Spain (Podium presentation)
- Weber, G. W., **Fornai, C.**, Gopher, A., Barkai, R., Sarig, R., Hershkovitz, I., 2014. The Qesem Cave hominin material (part 1): A morphometric analysis of the mandibular premolars and molar. UISPP, Burgos, Spain (Podium presentation)
- Lauc T., Rajić Šikanjić P., Premužić Z., **Fornai C.**, Mašić B., Vodanović M. 2014. Dental morphology of individual with congenital syphilis from 16th century. 16th International Symposium on Dental Morphology. 1st Congress of the International Association for Paleodontology (IAPO). Zagreb, Croatia (Poster presentation)
- **Fornai C.**, Bookstein F. L., Weber G. W., 2014. Geometric morphometrics of second upper australopithecine molars at Sterkfontein Member 4 for taxonomic appraisal. AAPA, Calgary, Canada (Podium presentation)
- **Fornai C.**, Bookstein F. L., Weber G. W., 2013. Second maxillary molars confirm a dimorphism of *Australopithecus* at Sterkfontein Member 4. ESHE, Vienna, Austria (Podium presentation)
- Weber G.W., **Fornai C.**, Gopher A., Barkai R., Sarig R., Hershkovitz I., 2013. The Qesem Cave dental material: A first morphometric analysis based on μCT images of mandibular teeth. ESHE, Vienna, Austria (Podium presentation)
- **Fornai C.**, Bookstein F. L., Weber G. W., 2013. Is there a second species at Sterkfontein Member 4? Quantitative approaches using second maxillary molars. "Paleoanthropology Society Meetings Abstracts, Honolulu, HI, 2-3 April 2013" PaleoAnthropology 2013:A11 (Podium presentation)
- **Fornai C.**, Benazzi S., Bauer C.C., Kullmer, O., Svoboda J., Pap I., Bayle P., Harvati K., Weber G.W. 2012. Investigation of 2D dental tissue proportions in deciduous first and second upper molars of modern humans and Neanderthals. ESHE, Bordeaux, France (Poster presentation)
- Benazzi S., **Fornai C.**, Buti L., Toussaint M., Mallegni F., Ricci S. Gruppioni G., Weber G.W., Condemi S., Ronchitelli A. 2012. Outline analyses of Neanderthal and modern human lower second deciduous molars. ESHE, Bordeaux, France (Poster presentation)

- **Fornai C.**, Benazzi S., Bayle P., Pap I., Svoboda J., Harvati K., Weber G.W. 2012. Enamel thickness and dental tissue proportions in Neanderthal and modern human upper deciduous molars. AAPA, Portland, Oregon (Poster presentation)
- **Fornai C.**, Bauer C.C., Benazzi S., Harvati K., Weber G.W. 2011. Enamel thickness and dental tissue proportions in modern human upper first deciduous molars. ESHE, Leipzig, Germany (Poster presentation)
- Benazzi S., **Fornai C.**, Bayle P., Coquerelle M., Kullmer O., Mallegni F., Weber G.W. 2011. Comparison of dental measurement systems for taxonomic assignment of Neanderthal and modern human lower second deciduous molars. ESHE 2011, Leipzig, Germany (Poster presentation)
- **Fornai C**, Clarke RJ, Moggi-Cecchi J, Hemingway J, de Beer FC, Radebe MJ. 2010. Testing the "second australopithecine species hypothesis" for Sterkfontein Member 4, South Africa. AAPA, Albuquerque, New Mexico (Poster presentation)
- R. J. Clarke. 19-20 October 2009. Discussion Meeting of the Royal Society "The first 4 million years of human evolution". "A skeleton of *Australopithecus* and the two *Australopithecus* species of Sterkfontein", London, UK (Oral presentation on behalf of R. J. Clarke)
- **Fornai C**, Clarke RJ, Moggi-Cecchi J, Hemingway J, de Beer FC, Radebe MJ. 2009. Geometric morphometric analysis of three-dimensional images of South African hominid molar teeth. A test for the "second australopithecine species hypothesis" for Sterkfontein and Makapansgat. Associazione Antropologica Italiana (AAI) congress, Firenze, Italy, October 1- 4. (Poster presentation)
- **Fornai C**, Clarke RJ, Moggi-Cecchi J, Hemingway J, de Beer FC, Radebe MJ. 2009. Testing the "second australopithecine species hypothesis" for Sterkfontein and Makapansgat: Geometric morphometric analysis of three-dimensional images of hominid molar teeth. East African Association for Paleoanthropology and Paleontology (EAAPP) congress, Arusha, Tanzania, August 15-21. (Oral presentation)
- **Fornai C**, Hemingway J, de Beer FC, Radebe MJ, Moggi-Cecchi J, Clarke RJ. 2008. A geometric morphometric analysis of virtual images of South African Australopithecine molars. Wits Postgraduate Symposium, 7th-8th November, Johannesburg. (Poster presentation, awarded as an outstanding presentation)
- **Fornai C**, Ricci F, Vecchi F, Manzi G. 2006. Exploratory investigation on the cranial morphology in ancient Libyans. African Genesis Symposium, Johannesburg (Poster presentation)
- Fiori O, **Fornai C**, Manzi G. 2005. Integrazione bio-culturale nel corso dell'Eneolitico in un'area di contatto: il Lazio meridionale. Riconsiderazione critica di una collezione storica del Museo "G. Sergi", Roma. In Atti della XL Riunione Scientifica, Istituto Italiano di Preistoria e Protostoria, Roma (Poster presentation)
- **Fornai C**, Ricci F, Rickards O, di Lernia S, Manzi G. 2003. Crani deformati intenzionalmente in una popolazione Tardo-Pastorale del Tadrart Acacus (Fezzan, Libia): nota preliminare (Poster presentation). In: Atti del XV Congresso degli Antropologi Italiani: Chieti, 28-30 September 2003

Vienna, 11 July 2015